

Lenzinger Berichte

94/2018

Scientific Reports on Wood, Pulp and Regenerated Cellulose

LENZINGER BERICHTE

Scientific Reports on Wood, Pulp and Regenerated Cellulose

Dedicated to Univ.-Prof. Dr. Paul Kosma
on the Occasion of his 65th Birthday

„Älter werden ist wie einen Berg besteigen: Je höher man kommt,
umso mühsamer wird der Weg, aber umso weiter wird der Blick.“

Ingmar Bergmann
(1918 - 2007), schwedischer Drehbuchautor, Film- und Theaterregisseur

AU-ISSN 0024-0907
Published by Lenzing AG
4860 Lenzing, Austria
Phone +43 7672 701-0

Editorial Board

| | |
|--|---|
| Ao. Univ. Prof. Dr. Thomas Bechtold | Universität Innsbruck, Research Institute of Textile Chemistry and Textile Physics, Austria |
| DDr. Haio Harms | Kelheim Fibres GmbH, Germany (retired) |
| Univ. Prof. Dr. Paul Kosma | University of Natural Resources and Applied Life Sciences, Department of Chemistry, Vienna, Austria |
| Univ. Prof. Dr. Herbert Sixta | Aalto University, Department Chemical Pulping Technology, Espoo, Finland |
| Univ. Prof. Dr. Dr. Thomas Rosenau | University of Natural Resources and Applied Life Sciences, Department of Chemistry, Vienna, Austria |

The authors assume full responsibility for the contents.

Editor: Dr. Thomas Röder
Printed in Austria, September 2018

Front page: Copyright Lenzing AG
Fotos: Copyright Lenzing AG
Layout: MMS Werbeagentur

Additional copies can be obtained by contacting the following address:

Dr. Thomas Röder
c/o Lenzing AG, R&D, 4860 Lenzing, Austria
Phone: +43 7672 701-3082, Fax: +43 7672 918-3082
E-mail: t.roeder@lenzing.com

All papers are available online at:
<http://www.lenzing.com>
and
<http://www.lenzinger-berichte.com>

I FOREWORD

SUSTAINABILITY AND BIOREFINERY

- 1 **Basic Indicators for the Sustainability of European Forestry**
Peter Schwarzbauer and Fritz Wittmann
- 15 **Development of an Organosolv Biorefinery Based on Nanolignin as Main Product**
Angela Miltner, Martin Miltner, Stefan Beisl, Walter Wukovits, Michael Harasek, Daniel Koch, Bettina Mihalyi, and Anton Friedl

ANALYTICS

- 27 **FTIR Micro-Spectroscopy for Characterisation of Radial Substituent Diffusion in Cellulose II-Beads**
Danuta Mozdyniewicz, Andreas Schwaighofer, Karin Wieland, Martin Häubl, and Bernhard Lendl

CELLULOSE CHEMISTRY

- 33 **Key Aspects of the Bleaching of Industrially Found Cellulosic Chromophores**
Nele Sophie Zwirchmayr, Ute Henniges, Thomas Röder, Antje Potthast, and Thomas Rosenau
- 43 **Cellulose Carboxylate/Tosylate Mixed Esters: Dependence of their Physicochemical Properties on the Degree of Carboxylate Substitution**
Daniela C. Ferreira, Gustavo S. Bastos, Annett Pfeiffer, Denise F. S. Petri, Thomas Heinze, and Omar A. El Seoud
- 57 **Kinetics of Cellulose Acylation with Carboxylic Anhydrides and N-acylimidazoles in Ionic Liquid/Molecular Solvent Mixtures: Relevance to the Synthesis of Mixed Cellulose Esters**
Thais A. Bioni, Naved I. Malek, and Omar A. El Seoud

FIBERS

- 67 **Lignocellulosic Multicomponent Fibers Spun from Superbase-Based Ionic Liquids**
Michael Hummel, Yibo Ma, Anne Michud, Shirin Asaadi, Annariikka Roselli, Agnes Stepan, Sanna Hellstén, and Herbert Sixta
- 77 **Man-Made Cellulosic Fibers via the Viscose Process – New Opportunities by Cellulose Carbamate**
R. Protz, G. Weidel, and A. Lehmann
- 85 **Influence of Carbonization Aids on the Manufacture of Carbon Fibers based on Cellulosic Precursors**
Johanna M. Spörl, Frank Hermanutz, and Michael R. Buchmeiser

TEXTILE APPLICATIONS

- 95 **Continuous Alkali Treatments of Lyocell. Effects of Alkali Concentration, Temperature and Fabric Construction.**
Ján Šíroký, Avinash P. Manian, Barbora Šíroká, Richard S. Blackburn, and Thomas Bechtold
- 105 **Chitin Coated Cellulosic Textiles as Natural Barrier Materials**
Auriane Freyburger, Yaqing Duan, Cordt Zollfrank, Thomas Röder, and Werner Kunz
- 115 **Improvement of Dyeing Performance of Cellulose Fibers by Pre-treatment with Amino Cellulose**
Thomas Heinze, Thomas Wellhöfer, Kerstin Jedvert, Andreas Koschella, and Hendryk Würfel

RAW MATERIALS

- 123 **Possibilities for Expansion of the Raw Materials Base in Lyocell Applications by Enzymatic Treatment**
Birgit Kosan and Frank Meister

Foreword

The authors of the study “The New Plastics Economy: Rethinking the future of plastics“, which was presented at the World Economic Forum in Davos in 2016, rendered a great service to the society. The results of their work have gone around the world and made millions of people aware of environmental pollution caused by plastic waste. According to the study of the Ellen MacArthur Foundation, without action there will be more plastic than fish in the oceans by 2050.

Many of our major contemporary challenges – such as marine pollution – can only be solved with innovations, a core strength of the Lenzing Group. Regarding this problem, we are conscious of our corporate responsibility and are doing everything possible to make a positive contribution to mankind and to the environment by making sustainability a condition for every new development at Lenzing.

In the 2017 financial year, we invested more than EUR 55 mn in R&D, a top result in the sector both in absolute figures and in relation to revenue. With their outstanding performance, our approx. 190 employees working in process and product development not only ensure the economic success of the Lenzing Group, but they also make a significant contribution to solving many social and ecological problems.

The “Lenzinger Berichte” cover many important issues along the entire value chain, from wood to pulp up to the fiber and beyond. In this edition, you will find reports about sustainable forestry and the efficient use of resources, the further development of the biorefinery concept, the ecologically responsible production and further processing of wood-based fibers as well as new and innovative cellulose-based materials. In accordance of our new brand positioning “Innovative by nature”, I wish you sustainably inspiring reading.

Dr. Stefan Doboczky, MBA

Chief Executive Officer Lenzing AG

Lenzing, September 2018



Vorwort

Die Autoren der Studie „The New Plastics Economy: Rethinking the future of plastics“, die 2016 auf dem Weltwirtschaftsforum in Davos vorgestellt wurde, haben der Gesellschaft einen großen Dienst erwiesen. Die Ergebnisse ihrer Arbeit sind um die Welt gegangen und haben Millionen Menschen für die Verschmutzung der Natur durch Plastikmüll sensibilisiert. Wenn nicht gehandelt wird, so die Studie der Ellen-MacArthur-Foundation, wird es in den Ozeanen 2050 mehr Plastik geben als Fische.

Viele der großen Herausforderungen unserer Zeit wie die der Meeresverschmutzung lassen sich nur mit Innovationen lösen, und diese sind eine zentrale Stärke der Lenzing Gruppe. Wir sind uns dabei unserer unternehmerischen Verantwortung bewusst und setzen alles daran, einen positiven Beitrag für Mensch und Umwelt zu leisten, indem wir Nachhaltigkeit zur Bedingung für jede neue Entwicklung bei Lenzing machen.

Im Geschäftsjahr 2017 haben wir mehr als EUR 55 Mio. in die Forschung & Entwicklung investiert – sowohl in absoluten Zahlen als auch in Relation zum Umsatz ein Spitzenwert in der Branche. Mit ihren hervorragenden Leistungen sichern unsere rund 190 Mitarbeiter/innen in der Prozess- und Produktentwicklung nicht nur den wirtschaftlichen Erfolg der Lenzing Gruppe. Sie leisten eben auch einen wesentlichen Beitrag zur Lösung vieler gesellschaftlicher und ökologischer Probleme.

Die Lenzinger Berichte decken wichtige Fragestellungen entlang der gesamten Wertschöpfungskette vom Holz über Faserzellostoff bis zur Faser und darüber hinaus ab. In dieser Ausgabe finden Sie Berichte über nachhaltige Forstwirtschaft und die effiziente Nutzung von Ressourcen, die Weiterentwicklung des Bioraffinerie-Konzepts, die ökologisch verantwortungsbewusste Erzeugung und Weiterverarbeitung von holzbasierten Fasern sowie innovative neue Materialien auf Cellulosebasis. Im Sinne unserer neuen Markenpositionierung „Innovative by nature“ wünsche ich Ihnen eine nachhaltig inspirierende Lektüre.

Dr. Stefan Doboczky, MBA

Vorstandsvorsitzender Lenzing AG

Lenzing, September 2018

Congratulation to Univ.Prof. Dr. Paul Kosma

This fall, Univ.Prof. Dr. Paul Kosma from BOKU University Vienna, a longstanding co-operation partner of Lenzing AG, turns 65. His birthday is a welcome occasion for a short look back, sincere congratulation, and best wishes for the future.

Paul Kosma studied Technical Chemistry at Vienna University of Technology, followed by a PhD study in Organic Chemistry at the same institution, concluding both educational phases “with excellence”. In 1980 he joined BOKU University as “Universitätsassistent” at the Institute of Chemistry, where he obtained the habilitation (venia docendi) in organic chemistry in 1988. In 1983 and 1999 he stayed as a visiting scientist at the N.D. Zelinsky Institute in Moscow, Russia, and at the Department of Biochemistry, University of Edinburgh, UK, respectively. In 1990, he was appointed full professor at BOKU University Vienna, in which function he stayed until today.



Between 1992-1998 and 2002-2013 Prof. Kosma acted as the head of the Department of Chemistry. He was scientific head of the ASPEX project (Antiviral Spot of Excellence Vienna, 2006-2009) and director of the “Christian Doppler Laboratory of Pulp Reactivity”, which was established and run in close cooperation with Lenzing AG. Since this time, long and fruitful cooperation has continued. This is also reflected by Prof. Kosma’s editorial board membership in “Lenzinger Berichte” – which makes this short retrospect the right place to say a big thank you also for that. Highlights of the “CD-lab” time were the „Japanese-European Workshop on Cellulose and Functional Polysaccharides“, Vienna 2005, and the „9th European Workshop on Lignocellulosics and Pulp“, Vienna 2006, both of which he organized and chaired.

With the establishment of the Christian Doppler Laboratory, he also laid the foundation for the institutionalization of cellulose and polysaccharide science at BOKU, which became one thriving branch of the “Chemistry of renewable resources” field, which he always supported, fostered and nurtured. In 2013, the Division of Chemistry of renewable resources” was founded, the destination of a long path that Prof. Kosma had opened and continuously paved. Also today, the Division of Organic Chemistry and its younger offspring, the Division of Chemistry of Renewable Resources remain connected by tight scientific links – but far more than that: by strong bonds of collegiality and friendship.

Prof. Kosma was BOKU delegate at FWF and head of the European Carbohydrate Society; he has been serving the scientific community as evaluator and peer for an incredibly high number of institutions, journals and research projects, and continues to do so today, also as the Austrian Delegate in the International Carbohydrate Organization (ICO) and European Carbohydrate Organization (ECO), Board Member of the Christian Doppler Research Society, and Member of the Austrian Agency for Scientific Integrity.

Paul Kosma is internationally recognized today as being one of the world-leading figures in carbohydrate chemistry, carbohydrate synthesis and glycochemistry, having published more than 270 scientific papers that were cited more than 5000 times.

The editorial team of “Lenzinger Berichte”, also on behalf of Lenzing AG as a whole and its many collaborators of Prof. Kosma’s, would like to say “Happy birthday!” and “Thank you”.

On behalf of many congratulants,

Dr. Thomas Röder,

Dr. Axel Russler,

Univ.-Prof. Dr. Dr. Thomas Rosenau



In Memoriam Dr. Vasken Kabrelian

Cellulose scientist Dr. Vasken Kabrelian passed away at the 5th EPNOE International Polysaccharide Conference in Jena on September 23rd at the age of 57. He collapsed in front of the Lecture Hall of Jena's Friedrich University, Germany and was dead at once – just one day before he wanted to give his talk on “Preparation of xylan derivatives from hemi-rich alkaline process lye”.

As a young Syrian scientist Kabrelian was part of the group of Prof. Werner Berger at Dresden University, Germany. There he earned a doctorate in organic chemistry entitled “Synthesis, characterization and experiments for applications of new dipolar O-basic organic solvents for cellulose”. He returned to Syria and finally worked as lecturer and researcher at Aleppo University. During a second stay in Germany in 2001 he assisted Prof. Dieter Klemm in his well-known cellulose research group at Jena's Friedrich Schiller University.

After bearing up against the war in Aleppo for more than three years he decided to leave his home country together with his wife and their twins in 2014. His family belongs to the Armenian Christian minority and life had really become a daily struggle. They had to start all over again in Austria after their daring escape. He worked as a project manager at Kompetenzzentrum Holz GmbH for Lenzing AG, where he continued his scientific work. He is author of several patents and scientific publications.

Many appraised his cordiality. After all he still was a warm hearted, optimistic and pleasant person spreading happiness and always ready for a little joke. He saved his family and, thus, could not enjoy the fruits.

With Vasken Kabrelian we lost an experienced scientist, an esteemed colleague and a really good friend.

Team Lenzing R&D
Team Kompetenzzentrum Holz GmbH

Basic Indicators for the Sustainability of European Forestry

Peter Schwarzbauer* and Fritz Wittmann

University of Natural Resources and Life Sciences, Vienna. Institute of Marketing and Innovation, Feistmantelstraße 4, 1180 Wien, Austria, and Wood K plus Market Analysis and Innovation Research Team, Vienna, Austria

* Contact: peter.schwarzbauer@boku.ac.at

Abstract

This study focuses on one important set of indicators regarding the sustainable management of forests (SMF) – forest resources. It is based on the latest internationally and partly nationally published forest inventory data. The developments of overall forest area, growing stock, increment, fellings and felling rates are covered for Europe as a whole (excl. Russian Federation), the EU28 and the total of European countries outside of the EU. In addition, forest resource changes were analyzed for single European countries (Austria, Germany, Czech Republic, Slovakia, Slovenia, Hungary and Belarus) as well as the Russian Federation, including – with limited data availability – also the specific resource developments for Norway spruce and beech. The general time-frame for the study was 1990-2015. Forest area and growing stock are increasing in all regions/countries. Fellings everywhere are below or far below net-annual increment; this underutilization is the main reason for growing stock increasing much more than forest area. In some countries, a shift from coniferous-resources to broadleaved-resources has become visible.

Keywords: European forest resources, sustainability indicators

Background and mandate

Sustainable management of forestry in Europe is guided by stringent forest laws. However, outside of Europe this is not well known. Therefore, the practice of sustainable forest management (SFM) in Europe has to be documented and presented by available and tangible indicators.

One important set of indicators regarding the sustainable management of forests contains forest resources. The goal of this study is to present the development of forest resources (area, growing stock, net-annual-increment (NAI), fellings – including the ratio of increment and fellings [felling rate: fellings in % of NAI]) over time in quantitative terms and – as far as possible given consistent data availability – for the species Norway spruce (*Picea abies*) and beech (*Fagus sylvatica*). Given

that comparable data are available we aim for a longer-term presentation of these developments over the last decades (whenever possible 1990-2015).

This report contains two different sets of data:

1. The development of total forest resources (forest area, growing stock, increment, fellings, felling rate) by the following countries/country groupings:
 - Europe total (excl. Russian Federation)
 - EU 28
 - total of European countries outside the EU
 - single European countries: Austria, Germany, Czech Republic, Slovakia, Slovenia, Hungary, Belarus
 - Russian Federation

2. The development of Norway spruce and beech resources (as far as consistent data are available) for the countries:

- Austria
- Germany
- Czech Republic
- Slovakia
- Slovenia
- Hungary
- Belarus
- Russian Federation

Results and Discussions

The latest international study with largely comparable data on forest resources by European countries including the development over time and the main data source for this study is:

FAO/EFI (2015): State of Europe's Forests 2015,

published by the “Ministerial Conference on the Protection of Forests in Europe – FOREST EUROPE Liaison Unit Madrid”. The data contained in this study are therefore not only comparable for all European countries as well as up-to-date but also official! The general time span covered is from 1990-2015, the last 25 years.

However, there are some limitations. Not for each country all data are available. The regional totals therefore are always limited to the country data available. Another aspect is that the forest inventories in the various countries are not always conducted at the same time period(s). The country results were inter- and extrapolated in order to harmonize these data regarding the time context. Reported are the years: 1990, 2000, 2005, 2010, 2015. However, for some countries the data on resources are not covering the whole time frame (sometimes only 2000-2010).

The specific data on Norway spruce and beech resources are not as consistent as the overall forest resource data. For Austria and Germany we rely on the published results of the national forest inventories (BFW for Austria, the Thünen Institute's database for Germany) as well as on the country reports for the FAO Global Forest Resources Assessment 2015 (FRA). For the other countries we only rely on the respective country reports for the FRA [1].

The data contained in the FAO/EFI report as well as in the country reports for the FRA are transferred into graphs, which form the main part of this study.

Quantitative Basic Indicators for the Sustainability of European Forestry by Regions and Specific Countries

Europe total (excl. Russian Federation)

From 1990-2015 forest resources in Europa have significantly grown; forest area by +9%, growing stock by +40% and net-annual increment (NAI) by +15%. The increase of growing stock, much above the increase of forest area and increment is due to the underutilization of forests, which can also be seen in the third part of figure 1: Fellings are much below NAI, the felling rates are 60-65%, which means that only 2/3 of the sustainable potential is actually used.



Figure 1: Development of Forest Resources in Europe total (excl. Russian Federation).

European Union (28)

From 1990-2015 forest resources in the European Union have significantly grown; forest area by +9%, growing stock by +38% and net-annual increment (NAI) by +17%. The increase of growing stock, much above the increase of forest area and increment is again due to the underutilization of forests, which can also be seen in the third part of figure 2: Fellings are much below NAI, the felling rates are 70-75%, which means that only 3/4 of the sustainable potential is actually used.

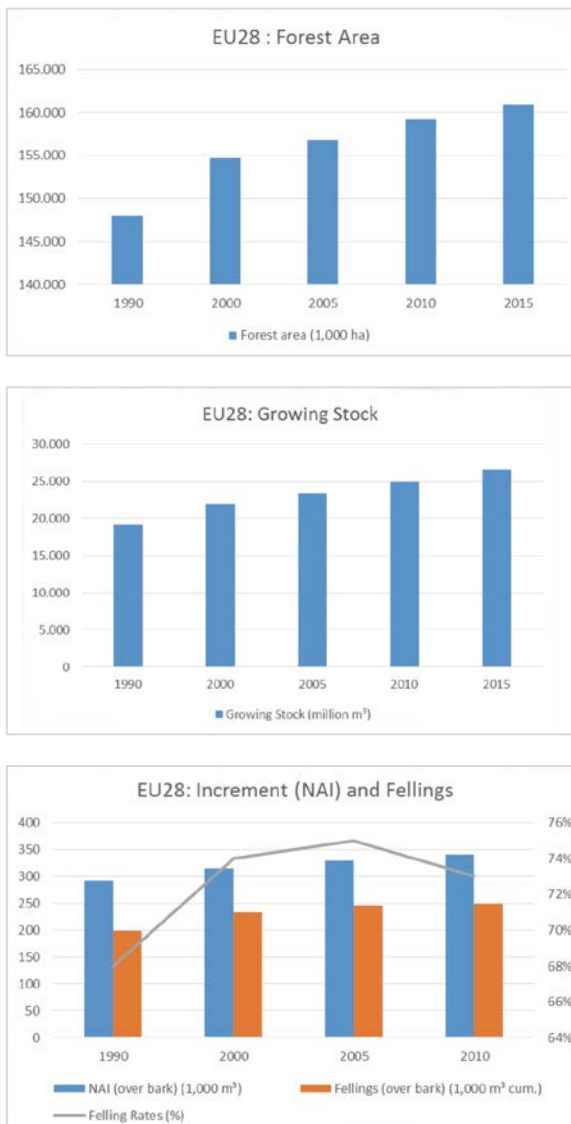


Figure 2: Development of Forest Resources in the European Union (28).

Total of European Countries other than EU28 (excl. Russian Federation)

From 1990-2015 forest resources in Europa outside of the EU have also grown significantly; forest area by +9%, growing stock by +47% and net-annual increment (NAI) by +11%. The increase of growing stock, much above the increase of forest area and increment is again due to the underutilization of forests, which can also be seen in the third part of figure 3: Fellings are much below NAI, the felling rates are only around 20%, and fellings have slightly declined over time.

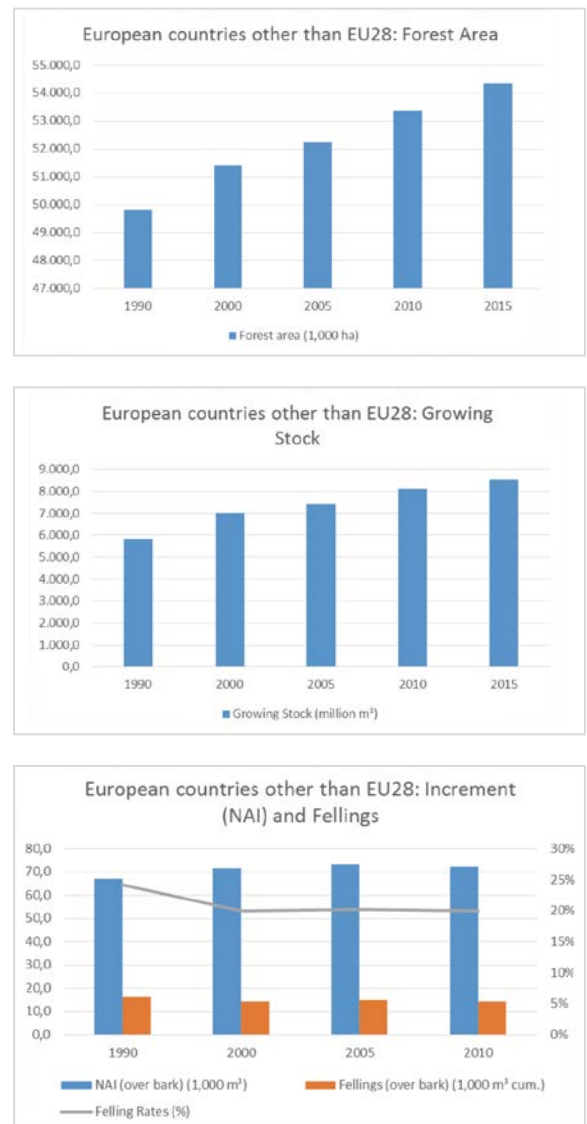


Figure 3: Development of Forest Resources in European countries other than EU28 (excl. Russian Federation).

[1] In case more detailed information on spruce and beech resources are necessary, the country experts and contributors to the FAO FRA 2015 need to be contacted: <http://www.fao.org/forestry/fra/83059/en/>

Austria

Total forest resources

From 1990-2015 forest resources in Austria have significantly grown; forest area by +3%, growing stock by +25% and net-annual increment (NAI) by +6%. The increase of growing stock, much above the increase of forest area and increment is again due to the underutilization of forests, which can also be seen in the third part of figure 4: Felling rates are 60-90%, which means that not all of the sustainable potential is actually used.

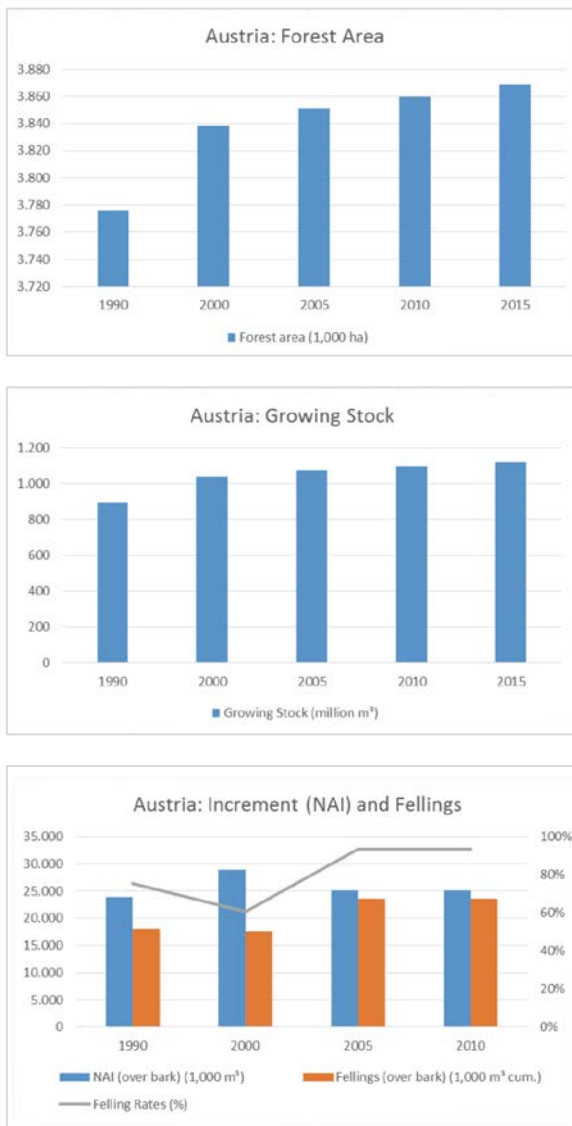


Figure 4: Development of Forest Resources in Austria.

Spruce

Spruce still covers about 51% of the Austrian forest area available for wood supply, although the spruce forest area declined between the 1990ies and 2007-09 by -8%; however, growing stock grew by +15%, net-annual increment (NAI) by +16%. Although the felling rate of spruce increased from 70% to 88%, still less is harvested than annually grows. This is also the main reason that spruce growing stock increased, despite that spruce forest area declined. The decrease in spruce forest area is not caused by overexploitation of spruce resources, but results from increased regeneration of forests by more broadleaved species (see also chapter Beech).

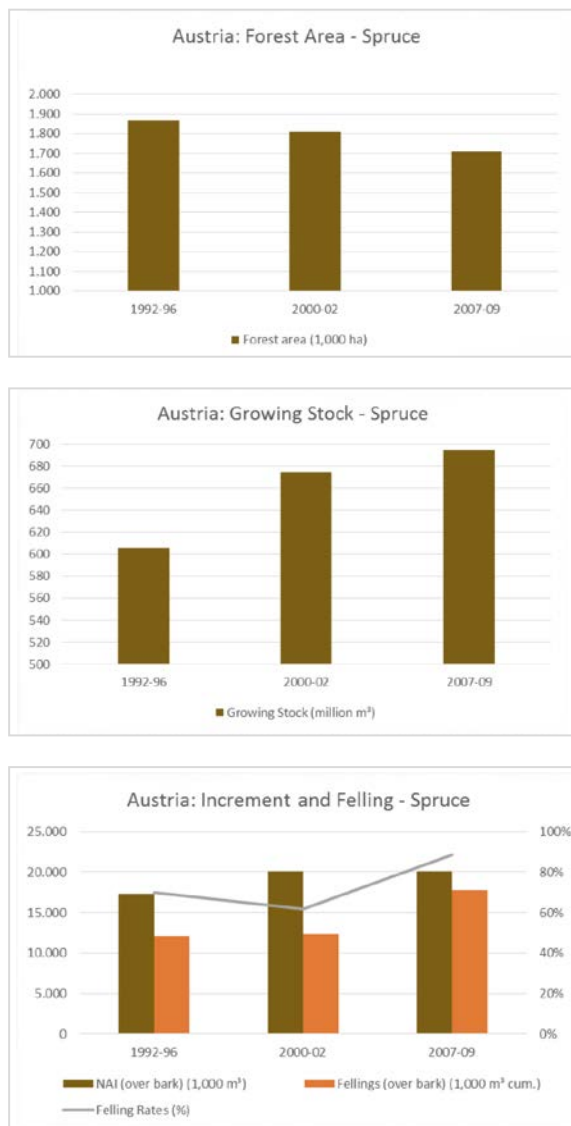


Figure 5: Development of Spruce Forest Resources in Austria.

Beech

Beech covers about 10% of the Austrian forest area available for wood supply. All beech forest resource categories increased between the 90ies and 2007-09; forest area by +8%, growing stock by +20%, net-annual increment (NAI) by +24%. The felling rate of beech around 60% is much lower than for spruce, which is the main reason that growing stock grew at a faster pace than forest area. The increase in beech forest area is mainly caused by increased regeneration of forests by more deciduous species (see also chapter Spruce).

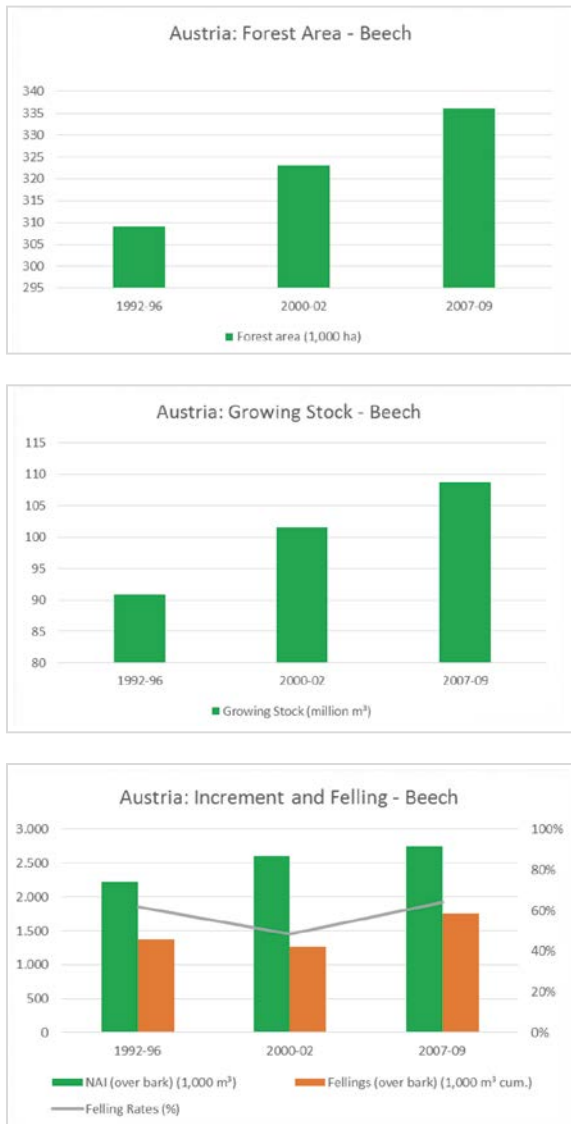


Figure 6: Development of Beech Forest Resources in Austria.

Germany

Total forest resources

From 1990-2015 forest resources in Germany have grown, but at a low pace – increment has slightly decreased; forest area increased by +1%, growing stock by +34% and net-annual increment (NAI) slightly decreased by -0,1% between 2000 and 2010. The increase of growing stock, much above the increase of forest area and increment is again due to the underutilization of forests, which can also be seen in the third part of figure 7: Felling rates are 75-80%, which means that not all of the sustainable potential is actually used. The decrease of increment could be caused by over-aged forests.

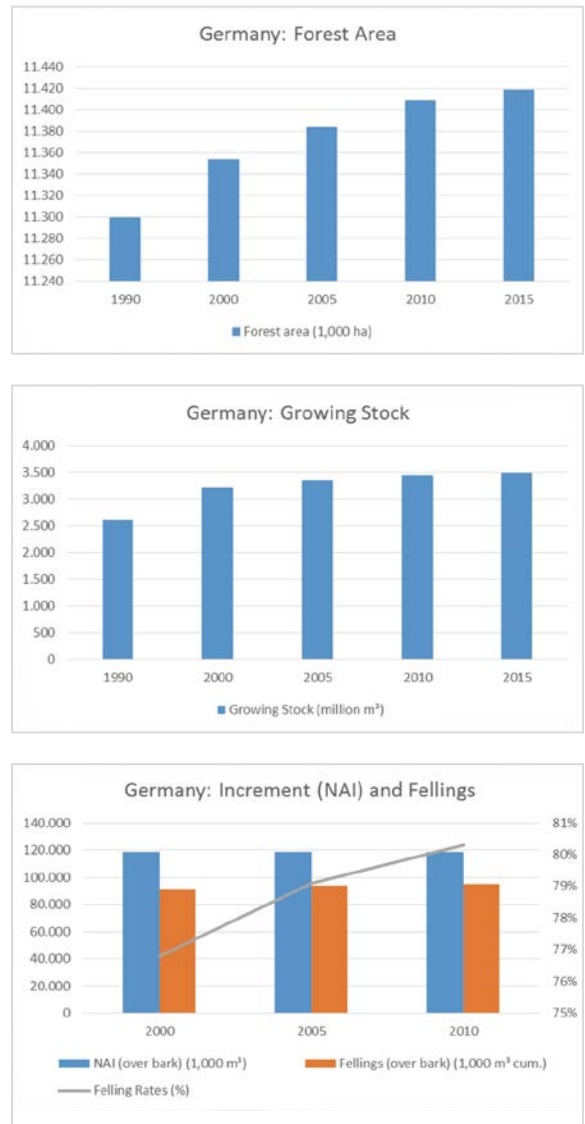


Figure 7: Development of Forest Resources in Germany

After the German reunification in 1990, the first forest inventory including both (former) parts of Germany took place in 2002, therefore, the availability of consistent data is mainly limited to the period 2002 to 2012 (most recent inventory). Growing stock data for spruce and beech are also available for 1990 (total of West and East Germany).

Spruce

Spruce still covers about 25% of the German forest area, but spruce forest area has declined between 2002 and 2012 by -8%; growing stock also declined in that period by -4%. Comparable data on NAI and fellings is only available for 2012 showing a felling rate of about 107%. However, the decline in spruce resources was more than compensated by the increase of broad-leaved resources (see chapter Beech).



Figure 8: Development of Spruce Forest Resources in Germany.

Beech

Beech covers about 15% of the German forest area available for wood supply. All beech forest resource categories increased between 2002 and 2012; forest area by +7%, growing stock by +10%. The felling rate of beech around 70% is much lower than for spruce, which is the main reason that growing stock grew at a faster pace than forest area. The increase in beech forest area is mainly caused by increased regeneration of forests by more deciduous species (see also chapter Spruce).

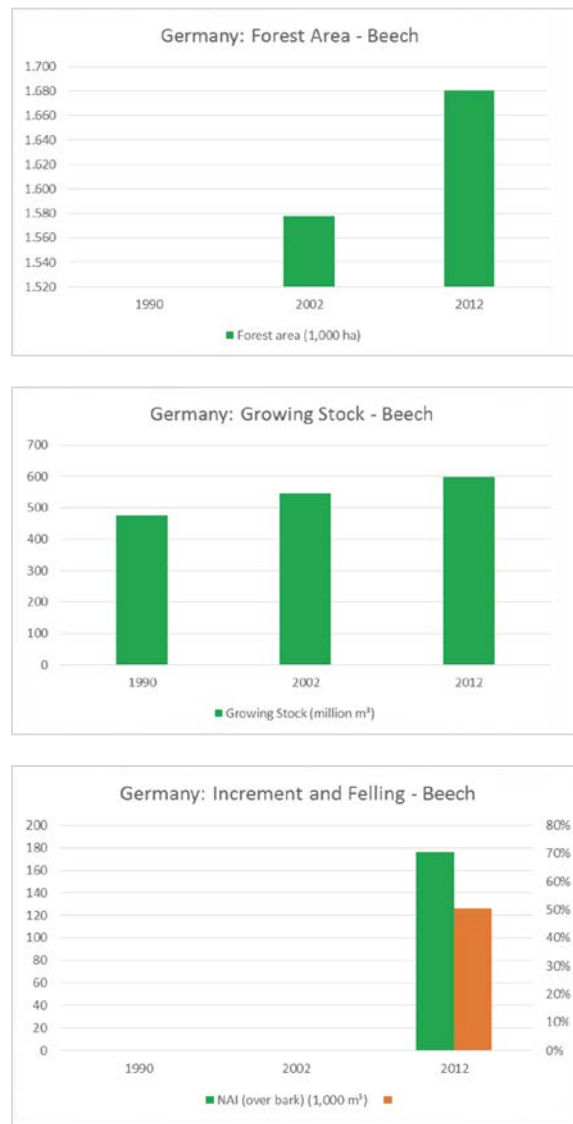


Figure 9: Development of Beech Forest Resources in Germany.

Czech Republic

Total forest resources

From 1990-2015 forest resources in the Czech Republic have grown, but at a moderate pace; forest area by +1%, growing stock by +9% and net-annual increment (NAI) by +9%. Given the fact that felling rates have increased, but are still below 90%, the decrease in increment and growing stock since 2005 might be caused by overaged forests and/or a change in forest inventory methodology.

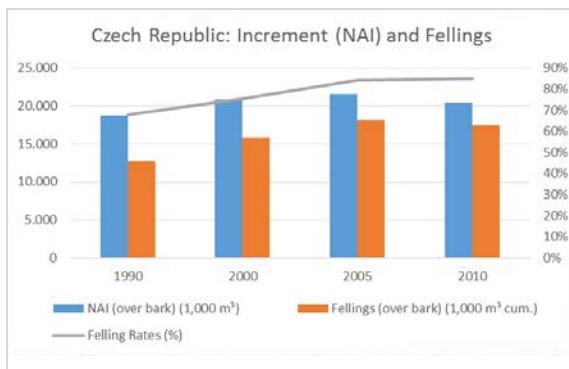
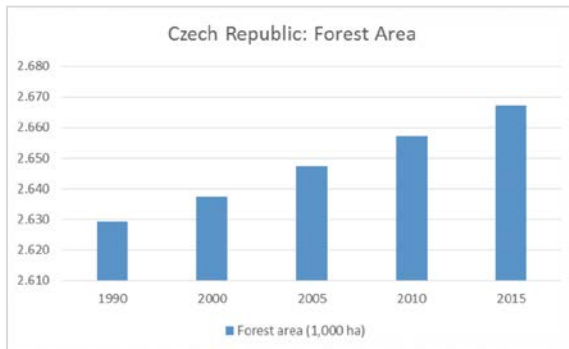


Figure 10: Development of Forest Resources in the Czech Republic.

Regarding spruce and beech resources, consistent data is only available for growing stock.

Spruce

In the Czech Republic about 61% of total growing stock and 75% of coniferous growing stock is spruce, which has increased from 1990 to 2010 by +15%.

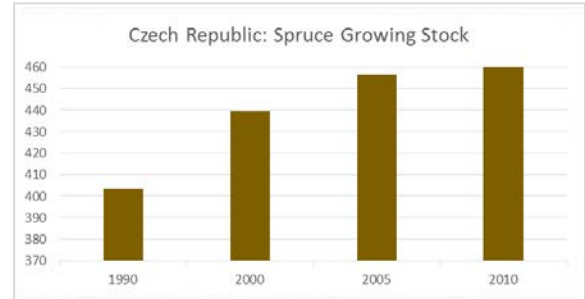


Figure 11: Development of Spruce Growing Stock in the Czech Republic (million m³).

Beech

In the Czech Republic about 7% of total growing stock and 36% of broadleaved growing stock is beech, which has increased from 1990 to 2010 even by +45%.

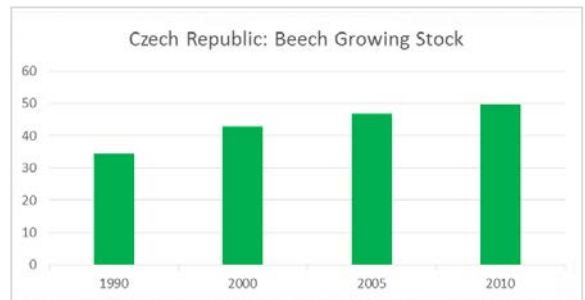


Figure 12: Development of Beech Growing Stock in the Czech Republic (million m³).

Slovakia

Total forest resources

From 1990-2015 forest resources in Slovakia have significantly grown; forest area by +1%, growing stock by +21% and net-annual increment (NAI) by +33%. Although growing stock slightly decreased since 2005, the growth over the entire time period much above the increase of forest area due to the underutilization of forests, which can also be seen in the third part of figure 13: Felling rates are 60-80%, which means that not all of the sustainable potential is actually used. At the same time and different from the countries/regions presented above increment itself increased more than area and growing stock: +33%!

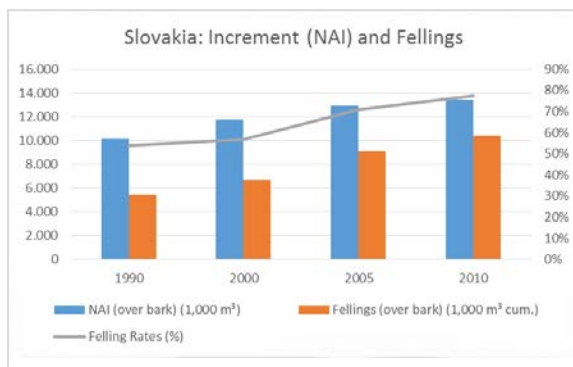
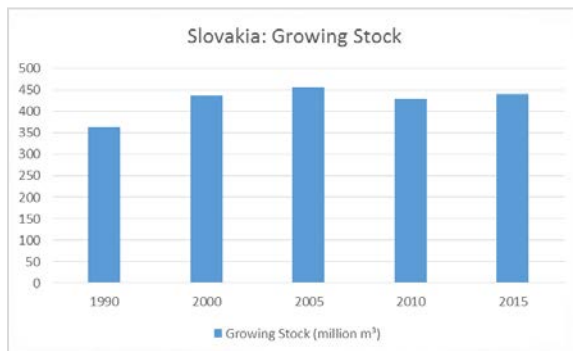


Figure 13: Development of Forest Resources in Slovakia.

Regarding spruce and beech resources, consistent data is only available for growing stock.

Spruce

In Slovakia about 21% of total growing stock and 70% of coniferous growing stock is spruce, which has increased from 1990 to 2010 by +21%.

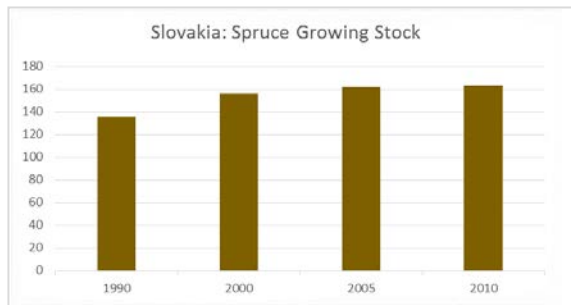


Figure 14: Development of Spruce Growing Stock in Slovakia (million m³).

Beech

In Slovakia about 32% of total growing stock and 59% of broadleaved growing stock is beech, which has increased from 1990 to 2010 even by +48%.

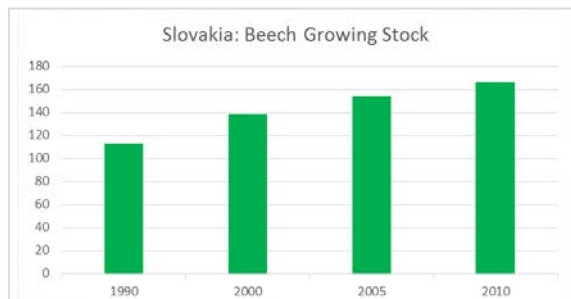


Figure 15: Development of Beech Growing Stock in Slovakia (million m³).

Slovenia

Total forest resources

From 1990-2015 forest resources in Slovenia have significantly grown; forest area by +5%, growing stock by +54% and net-annual increment (NAI) by +53%. The increase of growing stock, much above the increase of forest area is due to the underutilization of forests, which can also be seen in the third part of figure 16: The felling rates are below 40%, which means that about 60% of the sustainable potential is currently not used. At the same time and similar to the Czech Republic increment itself increased more than area and almost as much as growing stock: +53%!

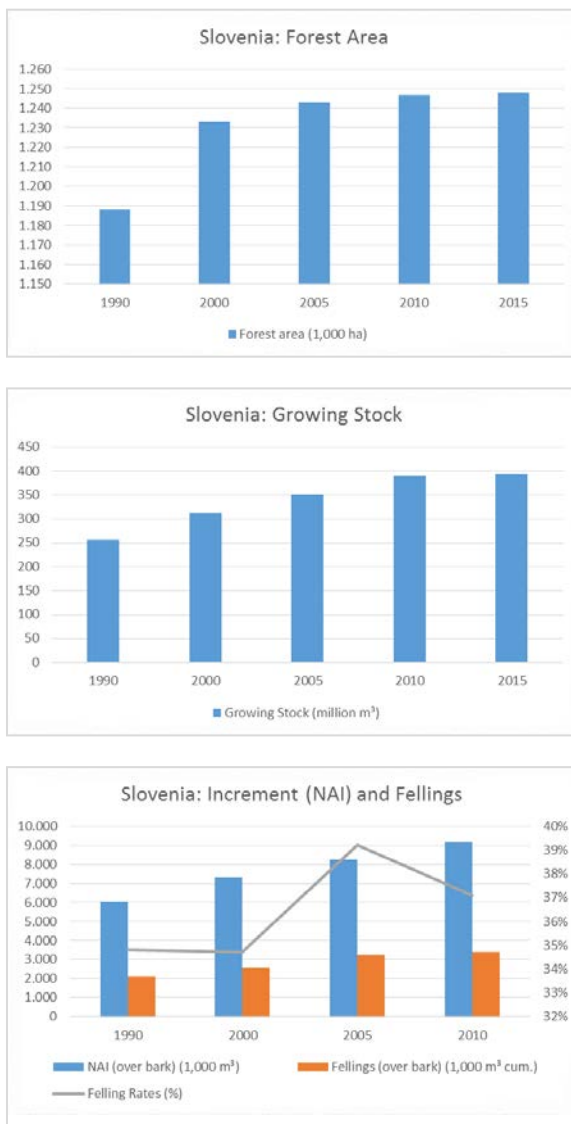


Figure 16: Development of Forest Resources in Slovenia.

Regarding spruce and beech resources, consistent data is only available for growing stock.

Spruce

In Slovenia about 31% of total growing stock and 68% of coniferous growing stock is spruce, which has increased from 1990 to 2015 by +49%.

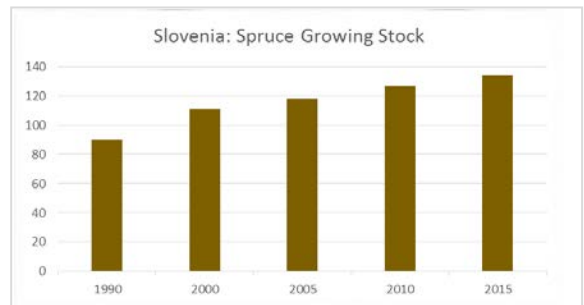


Figure 17: Development of Spruce Growing Stock in Slovenia (million m³).

Beech

In Slovenia about 31% of total growing stock and 68% of broadleaved growing stock is beech, which has increased from 1990 to 2015 by +57%.

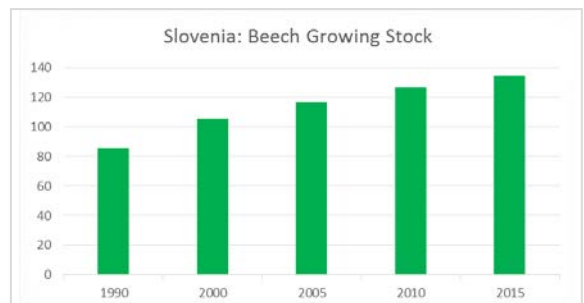


Figure 18: Development of Beech Growing Stock in Slovenia (million m³).

Hungary

Total forest resources

From 1990-2015 forest resources in Hungary have significantly grown; forest area by +15%, growing stock by +28%, and net-annual increment (NAI) has slightly decreased between 1990-2010 by -2%. The increase of growing stock, above the increase of forest area again is due to the underutilization of forests, which can also be seen in the third part of figure 19: Fellings are below NAI, the felling rates are between 70 and 85%, which means that a part of the sustainable potential is not used.

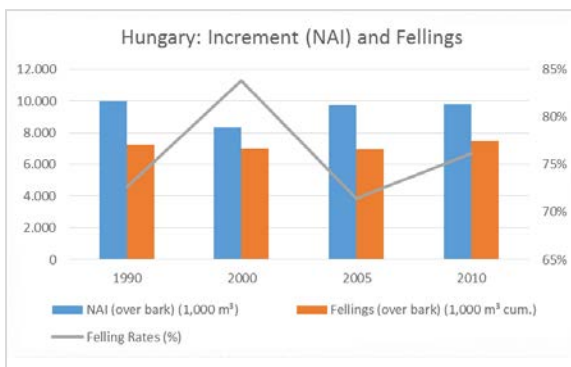
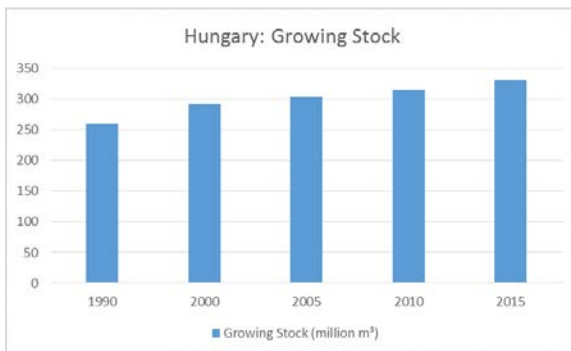
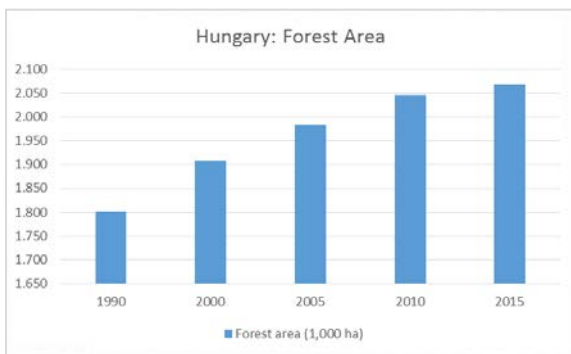


Figure 19: Development of Forest Resources in Hungary.

Because of the minor importance of spruce in Hungary the FRA country report does not explicitly present data on this species. Regarding beech resources, the only available data is for growing stock.

Beech

In Hungary about 11% of total growing stock and 13% of broadleaved growing stock is beech, which has increased from 1990 to 2010 by +7%.



Figure 20: Development of Beech Growing Stock in Hungary (million m³).

Belarus

Total forest resources

From 1990-2015 forest resources in Belarus have significantly grown; forest area by +11%, growing stock by +59% and net-annual increment (NAI) by +29% from 1990 to 2010. No comparable data exist for fellings, but the fact that growing stock increased so strongly shows that no overexploitation of forest resources has taken place in Belarus (Figure 21).

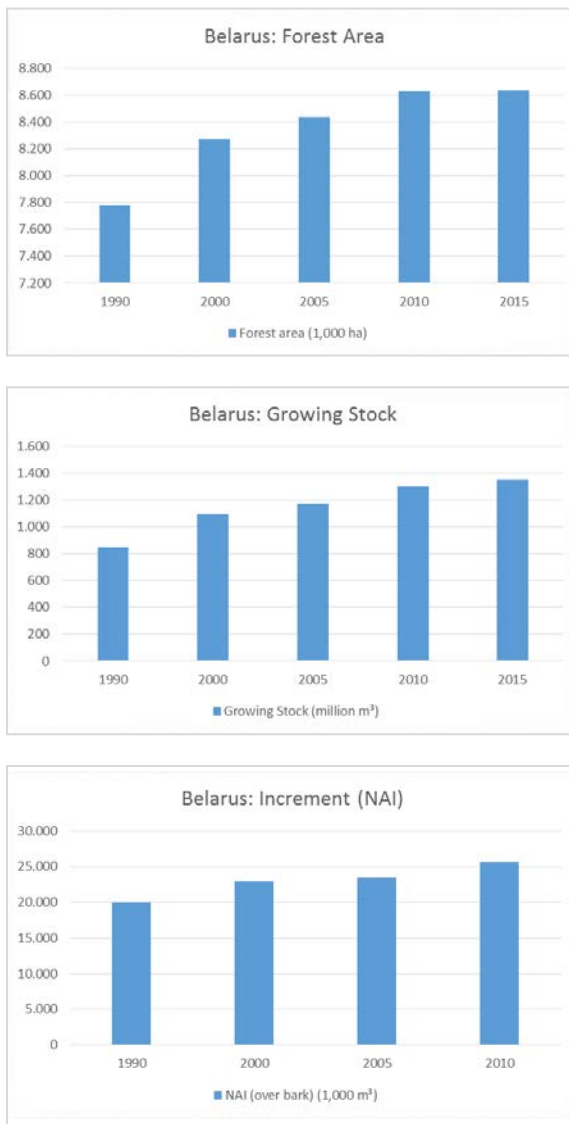


Figure 21: Development of Forest Resources in Belarus.

Because of the minor importance of beech in Belarus the FRA country report does not explicitly present data on this species. Regarding spruce resources, the only available data is for growing stock.

Spruce

In Slovenia about 31% of total growing stock and 68% of coniferous growing stock is spruce, which has increased from 1990 to 2015 by +49%.

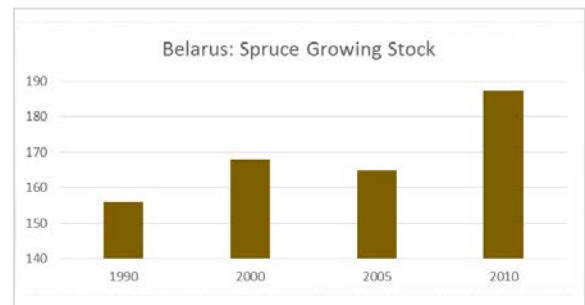


Figure 22: Development of Spruce Growing Stock in Belarus (million m³).

Russian Federation

Total forest resources

From 1990-2015 forest resources in the Russian Federation have remained quite stable; forest area +/-0%, growing stock -1%, net-annual increment (NAI) +2%. Because fellings were reduced by 50% during this period, the felling rate also drastically declined from 40% (1990) to 20% (2015) (Figure 23).

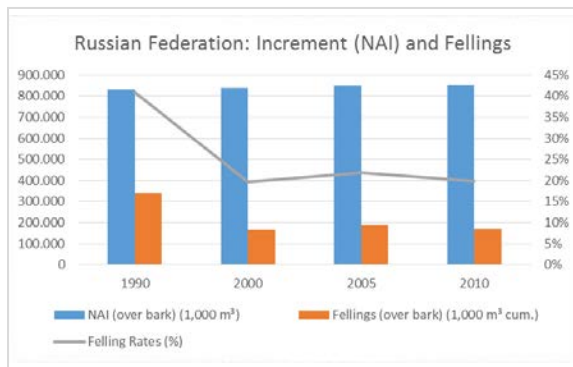
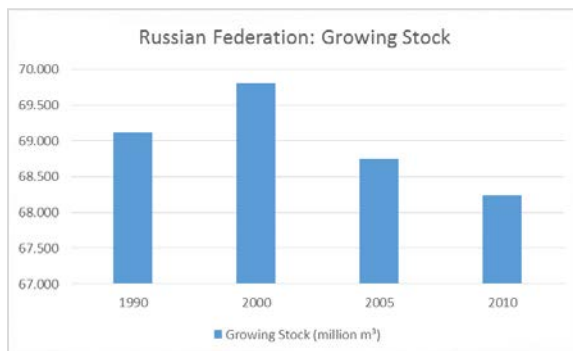
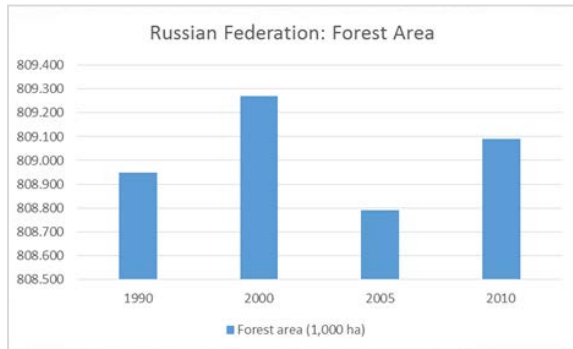


Figure 23: Development of Forest Resources in the Russian Federation.

Regarding spruce and beech resources, consistent data is only available for growing stock.

Spruce

In the Russian Federation about 13% of total growing stock and 19% of coniferous growing stock is spruce, which has increased from 1990 to 2010 by +15%.

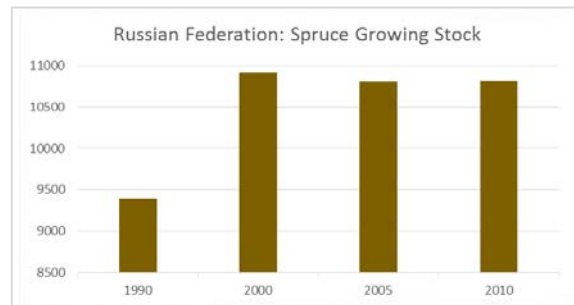


Figure 24: Development of Spruce Growing Stock in the Russian Federation (million m³).

Beech

In the Russian Federation about 0,2% of total growing stock and 0,8% of broadleaved growing stock is beech, which has slightly decreased from 1990 to 2010 by -5%.

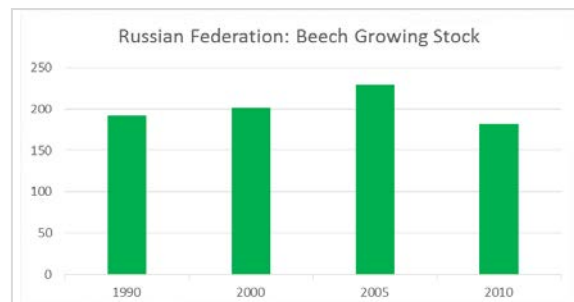


Figure 15: Development of Beech Growing Stock in the Russian Federation (million m³).

Conclusions

Sustainable forest management (SFM) has to keep the balance between three main pillars: ecological, economic and socio-cultural. SFM can be characterized by a broad array of indicators, both quantitative and qualitative. The focus here was on a set of quantitative indicators describing the development of forest resources: forest area, growing stock, increment, fellings and felling-rates.

Other than global forest resources, the forest resources in Europe have significantly grown over the last 25 years. The increase of growing stock is much above the increase of forest area and increment due to the under-utilization of forests – fellings are and have been for a long time significantly below net-annual-increment. In Europe as a whole fellings amount to 60-65% of increment, which means that only 2/3 of the sustainable potential is actually used.

Regarding this specific set of sustainability indicators, the results of this study show that (a) forest management in Europe can be labelled as „sustainable” and (b) that sustainable timber production could be even expanded.

Data Sources

General – European level

FAO/EFI (2015): State of Europe’s Forests 2015. Ministerial Conference on the Protection of Forests in Europe. FOREST EUROPE Liaison Unit Madrid, Madrid. <http://www.foresteurope.org/docs/fullsoef2015.pdf> (last accessed June 7th 2016)

Austria

Bundesforschungs- und Ausbildungszentrum für Wald, Naturgefahren und Landschaft (BFW): Österreichische Waldinventur. <http://bfw.ac.at/rz/wi.home> (last accessed June 7th 2016)

N.N. (2014): Country Report Austria. Global Forest Resource Assessment 2015, Rome

Germany

N.N. (2014): Country Report Germany. Global Forest Resource Assessment 2015, Rome

Thünen Institut: Dritte Bundeswaldinventur (BWI) 2012: Ergebnisdatenbank. <https://bwi.info/> (last accessed June 7th 2016)

Czech Republic

N.N. (2014): Country Report Czech Republic. Global Forest Resource Assessment 2015, Rome

Slovakia

N.N. (2014): Country Report Slovakia. Global Forest Resource Assessment 2015, Rome

Slovenia

N.N. (2014): Country Report Slovenia. Global Forest Resource Assessment 2015, Rome

Hungary

N.N. (2014): Country Report Hungary. Global Forest Resource Assessment 2015, Rome

Belarus

N.N. (2014): Country Report Belarus. Global Forest Resource Assessment 2015, Rome

Russian Federation

N.N. (2014): Country Report Russian Federation. Global Forest Resource Assessment 2015, Rome

Development of an Organosolv Biorefinery Based on Nanolignin as Main Product

Angela Miltner*, Martin Miltner, Stefan Beisl, Walter Wukovits, Michael Harasek, Daniel Koch, Bettina Mihalyi, and Anton Friedl

TU Wien, Institute of Chemical, Environmental and Bioscience Engineering, Getreidemarkt 9/166, A-1060 Vienna, Austria. * Contact: angela.miltner@tuwien.ac.at.

Abstract

Within the presented work the different aspects of the development of an organosolv biorefinery process with the focus on the production of sulphur free Nanolignin as main product are presented. Experimental investigations for the pre-treatment of the raw material using organosolv extraction as well as precipitation of lignin nanoparticles have been carried out. For the experiments wheat straw has been applied as the model substrate. Furthermore, design and analysis tools have been applied to investigate whole Biorefinery concepts using the in-house developed IDEAS-Engine. This toolbox has been applied for investigations on process design and optimisation, detailed optimisation of the extraction reactor, economics and life cycle assessments (LCA). The economic investigations have also been carried out for maize straw, soft and hard wood as raw materials.

The optimized process conditions and equipment lead to Nanolignin with approximately 100 nm size and precipitation yields greater than 65 wt%. Energy integration using Pinch technology resulted in an exergy efficiency of 92%. Within the cost analyses Nanolignin showed the highest contribution to the revenues with a share of around 50% to 80% for hard and softwood, respectively, as well as 34-65% for wheat and maize straw. Within an economic risk analysis it was found that the risks of a negative profit for the Biorefinery concept is only 4-8% for the scenarios with soft wood and hard wood under the assumed conditions.

Keywords: *Biorefinery, organosolv, Nanolignin, process development*

Introduction

Lignocellulosic biomass is abundantly available and offers a wide range of variability with many natural treasures. Nevertheless these large fluctuations also pose a challenge in regard to process development. Especially if a multi-feedstock and multi-product approach is chosen. The main constituents of lignocellulosic materials are cellulose, hemicellulose, also known as polyose, and lignin. However, also other associated components within the lignocellulosic materials (e.g. extractives) are potential sources for value added products. Lignocellulosic biomass is traditionally used as raw material in the pulp and paper industry which combines material and energetic use of the biomass as well as solely energy production from lignocellulosic biomass. But also other Biorefinery concepts can be based on lignocellulosic materials.

The integrated development of lignocellulosic Biorefinery concepts demands the consideration of various aspects. General framework requirements for the process development are appropriate process parameters and conditions for the chosen raw materials leading to a specific set of process streams. A development of applications for all process streams received during the process is necessary with the aim of highest valuable material outputs. Diluted side streams that cannot be utilised economically for material production should be used for energy production with the secondary objective of conserving nutrients which can be returned to the farmers as fertiliser for plant production whereby closing the cycle.

When using an organosolv approach for the treatment of biomass, a wide variety of solvents like alcohols,

organic acids, phenol and cresol as well as esters, ketones and amines can be applied [1]. Many process variants have been investigated and developed to different scales like ALLCELL, NAEM, ASAM and ORGANOCELL processes [1, 2]. All of them have an integrated process development in common with the target of preserving the cellulose as main material product and extracting the other components in order to obtain additional products. In contrast, the approach of the presented research is to extract sulphur free lignin and process it to nanoparticles while utilising the nature of both the nanostructure and the chemical properties of native lignin from the production [3] to the application in various fields [4]. Along with lignin the cellulose stream as well as the mixed sugar stream is investigated to produce high value products. Side streams are dedicated for energy production.

Based on long tradition and knowledge of the group, process development and scale up of process ideas from experimentally proven process steps on laboratory scale into pilot and semi-technical scale are done with the help of various software tools. Process simulation is used to derive substantial material balances. Energy and exergy analyses are used for overall process optimization. Computational fluid dynamics (CFD) is used for detailed optimization of the equipment design. Received process data are used for economic and ecological evaluation of the processes. This strategy leads to a toolbox called IDEAS-Engine equipped with design and analysis tools (e.g. process simulation, CFD, efficiency and cost analysis tools, LCA) applied for the support and speed up the process development.

Materials and Methods

Experiments

At present the organosolv Biorefinery experiments designed for Nanolignin production have all been based on wheat straw as raw material. The wheat straw used was harvested in 2015 in Lower Austria, stored under dry conditions until use and was cut in a cutting mill, equipped with a 5 mm mesh, before pre-treatment. The composition of the straw was 16.1 wt% lignin and 63.1 wt% carbohydrates consisting of Arabinose, Glucose, Mannose, Xylose and Galactose. Ultra-pure water (18 M Ω /cm) and Ethanol (Merck, 96 vol%, undenatured) was used in the organosolv treatment and additionally sulfuric acid (Merck, 98 vol%) in the precipitation steps.

The experimental work is structured in three parts, illustrated in Figure 1. In the “Organosolv Pre-treatment” part, the lignin is extracted from the wheat straw applying an organosolv process and solids are removed

from the extract. In the “Precipitation” different precipitation setups and conditions can be applied and nanoscaled lignin is produced. In the “Downstream Processing”, resulting particles are separated from the suspension via centrifugation, dried and dispersed in water.

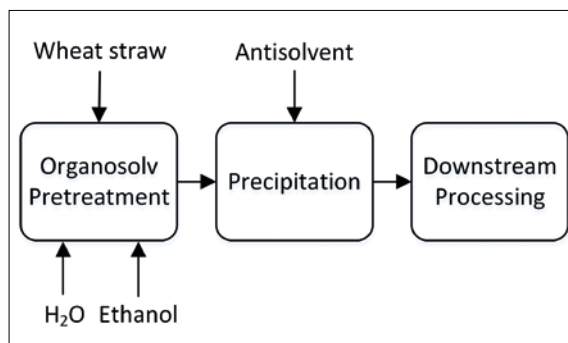


Figure 1: Schematic representation of the experimental procedure

Organosolv pre-treatment

The organosolv pre-treatment can be executed in different apparatuses at the Research Division. For screening experiments as well as kinetic experiments 45 ml stainless steel high pressure reactors (PARR, Model 4716) are applied while detailed process investigations are carried out in a 1 l stirred autoclave (Zirbus, HAD 9/16). In mid 2018 also an Extraction pilot plant will be available (Samtech Extraktionstechnik GmbH, prototype) with a 10 l extractor that can be operated up to 30 bar and 250 °C.

The optimum organosolv pre-treatment conditions are strongly dependent on the kind of biomass used and the desired main product of the pre-treatment step. In the case of wheat straw and Nanolignin as desired product, experiments are typically carried out with 60 wt% aqueous ethanol mixture as solvent. The content of wheat straw in the reactor is set between 8 wt% and 20 wt% based on dry straw. The reactor is heated to temperatures between 120 °C to 220 °C within max. 45 min and held at this temperature for a defined time span between 0 min and 60 min before cooling down to room temperature. The solid and liquid fractions are subsequently separated using a hydraulic press (Hapa, HPH 2.5) at 200 bar and a centrifuge (Sorvall, RC 6+) at 30,074 g for 20 min. The supernatant is analysed and stored at 5 °C.

Precipitation

The precipitation of the lignin dissolved in the organosolv extract is still under intense research. Applied precipitation setups combine the most commonly used methods solvent shifting and pH shifting and reduce the solubility of the lignin by decreasing the solvent

concentration and lowering the pH value [3]. The experiments are conducted at room temperature. The volume ratio of extract to antisolvent is chosen in the range of 1:2 to 1:5, where the antisolvent consists of water set to a pH value of 2 to 7 with sulfuric acid. Up to now three different setups have been investigated at the Research Division:

- a) “Batch” precipitation in a temperature controlled stirred 250 ml beaker; 20 ml extract were placed in the beaker and 100 ml antisolvent were added with a flowrate of 20 ml/min through an immersed anti-diffusion tip using a syringe pump.
- b) “T-Fitting” precipitation consists of a T-Fitting and a 20.4 cm long pipe with inner diameter of 3.7 mm and a metering valve at its end. Extract and antisolvent are pumped into the T-Fitting via two syringe pumps with a flowrate of 4 ml/min (20 ml total volume) and 20 ml/min (100 ml total volume), respectively. The precipitate is collected in a 250 ml beaker without stirring. The whole setup is temperature controlled.
- c) “Static Mixer” precipitation uses the setup (b) but the pipe after the T-Fitting is equipped with static mixing elements (Striko, Helical DN4) that redirect the flow 30 times. Total volume and flowrates were identical to setup (b).

More details on the setups can be found in [5].

Downstream processing

The suspension gained in the precipitation step containing the Nanolignin particles is centrifuged immediately after precipitation to separate the lignin particles. For particle separation a Thermo Scientific, Sorvall RC 6+ centrifuge (typically used with 30,074 g), a Sigma 4k15 centrifuge (typically used with 24,104 g) and a Thermo WX Ultra 80 ultracentrifuge (typically used with 288,000 g) are available. The supernatant is decanted, collected and analysed.

Analytics

The organosolv extract is typically analysed for carbohydrates, lignin and degradation products. Details can be found in [5] and [6]. Dried precipitate is investigated in terms of molecular mass via High Performance Size Exclusion Chromatography (HPSEC) using an Agilent 1200 HPLC system equipped with a UV-Detector. Its chemical composition is analysed via ATR-FTIR absorption obtained with a Bruker Vertex 70 Fourier Spectrometer. The particle size and shape of the lignin particles are investigated in a scanning electron microscope (SEM) (Fei, Quanta 200 FEGSEM). For the investigation of the ζ -Potential as well as the particle size a ZetaPALS (Brookhaven Instruments, USA) is

available. Particle size measurements can be conducted in a Mastersizer 2000E (Malvern Instruments, UK) using laser diffraction in liquid suspensions where two different measurements can be conducted: (1) Centrifuged particles dispersed in supernatant (without drying), (2) Centrifuged and dried particles redispersed in water.

IDEAS-Engine

The design and development of concepts and plants in chemical engineering and related disciplines is performed in strong interconnection between experimental and simulative work. For a powerful and reliable simulative approach, the research division Thermal Process Engineering and Simulation fully relies on a toolbox called the IDEAS-Engine which is an acronym standing for Integrated Design and Analysis System. The exhaustive simulation of every aspect of a novel process concept or an innovative plant layout necessitates the use of very diverse modelling and simulation tools with a high degree of integration and interaction. Thus, the IDEAS-Engine covers a multitude of relevant aspects like material property data, process simulation, process analysis, CFD simulation and cost analysis (Figure 2) which are usually executed in a repetitive and iterative approach. In every aspect, the development and validation of new models and algorithms as well as the gaining of expertise in their application are major tasks.

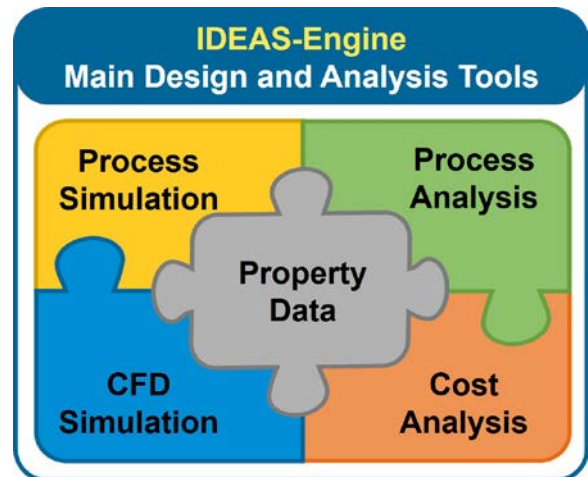


Figure 2: The IDEAS-Engine for design of innovative processes and plants in chemical engineering and related disciplines

The assessment of material property data ranges from simple data extraction from compendia or trustworthy web resources like NIST Chemistry WebBook [7] over well-accepted regression models for engineering purposes and ends with highly predictive methods like molecular dynamics simulation and ab-initio quantum

can be lost due to process irreversibilities. Therefore, exergy analysis gives information of kind and quantity of heat and material losses in the process as well as to justify the products quality.

CFD Simulation

The process efficiency of unit operations along ligno-cellulosic biorefinery concepts is governed strongly by equipment design. Process intensification to improve phase contact, to reduce solvent consumption and to maximize lignin extraction with minimum by-product generation is an important design goal with strong impact on the selection of downstream unit operations for high product purity. The extractive separation of lignin from cellulose and hemicellulose is often carried out in packed beds, where a uniform distribution of the solvent in the packed bed helps to maximize the contact time between solvent and biomass particles or straw fibres and increase the efficiency. Usually, the solvent mixture is passed over the biomass packed bed. CFD simulations can give a very detailed view about the flow behaviour, uniformity and distribution in these packed bed systems.

The analysis of random packings of particles or fibres poses a great challenge on CFD as the creation of the complex, unstructured geometry is usually not possible applying standard CAD tools. A code based on discrete element modelling (DEM) developed at TU Wien using particle clumps to consider non-spherical or fibrous biomass particles was used in combination with the open-source CFD tool OpenFOAM® for the simulation of the flow [13]. The filling of the extractor geometry with arbitrary non-spherical finite geometries representing the biomass pieces was performed by an automated procedure which includes STL file creation (representing the geometry) and the computation of the mesh for the computational domain through SnappyHexMesh.

An example of an extractor geometry filled with fibres (two different sizes) is shown in Figure 4.

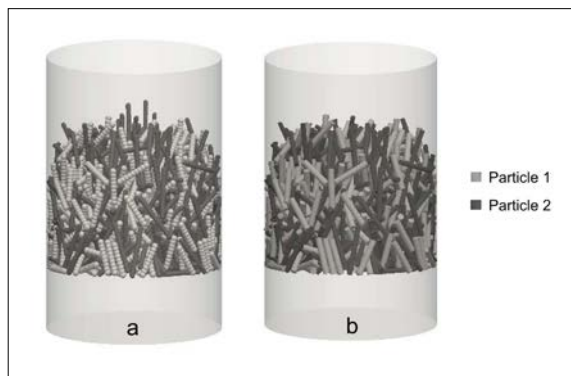


Figure 4: DEM created packing using particle clumps (a, left) – STL file generated from DEM filling (b, right)

Fluid flow through the meshed packed bed was simulated using the open-source CFD package OpenFOAM®. A steady state incompressible solver was selected (simpleFoam) based on the semi-implicit method for pressure linked equations. Residence time distributions were calculated using scalarTransportFoam which solves a scalar transport equation based on the velocity field derived from simpleFoam. The liquid used in the simulations was a 60% volume mixture of ethanol/water entering the bed from bottom (z direction) at 0.01 m/s and exiting from top. In this case, the velocity regime was laminar and the wall-treatment was no-slip; as a start, pressures and temperatures were set to ambient, and the viscosity for the mixture was adapted accordingly.

As shown previously [14], CFD – in combination with laser-based flow measurement and Raman spectroscopy – can also be applied to investigate mixing processes. With regard to organosolv biorefinery, this approach could be used to get more insight into the precipitation of Nanolignin.

Process Analysis via Life Cycle Assessment

Along with the presented design and optimisation of the process using simulation tools, also the environmental impact has to be analysed to obtain a sustainable development. Life Cycle Assessment (LCA) is carried out for different process concepts of the innovative organosolv Biorefinery with Nanolignin as a main product, in order to investigate and minimize its environmental implications. The main objective of this methodical assessment is to provide information on the possible environmental effects connected to alternative process concepts and product qualities within the Biorefinery. Based on the gained impact informations well-founded decisions can be made for the further development of the technology.

The LCA method requires life cycle thinking, including raw material production, upstream and downstream process considerations as well as possible applications, use and end of life scenarios. A hotspot analysis in different impact categories highlights the critical points from an environmental perspective and enables a more holistic process development.

The LCA method is standardized by ISO14040 and ISO14044 and consists of four consecutive stages (see Figure 5) with iterative nature [15, 16]. Goal and scope definition is followed by gathering of the Life Cycle Inventory, leading to the Life Cycle Impact Assessment which is followed by the interpretation phase. Findings in every stage can trigger the need to return to other stages and adapt the chosen scope, goal and methodological decisions.

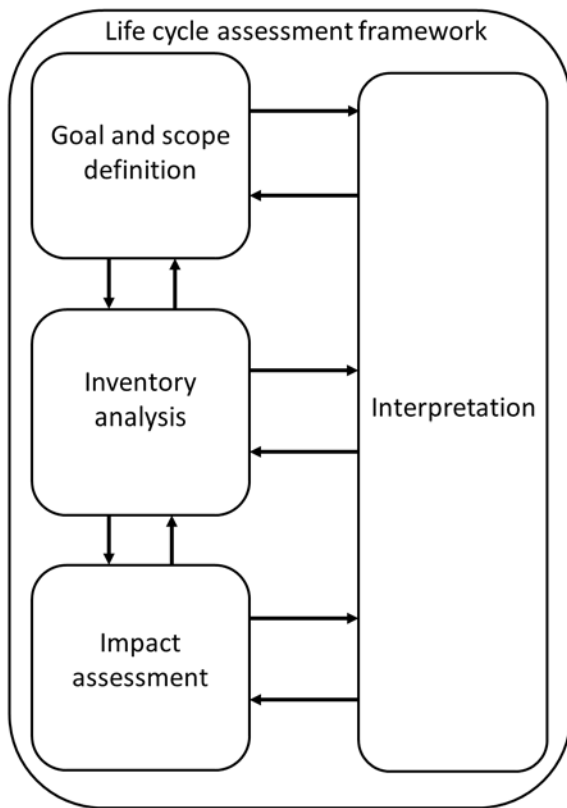


Figure 5: Stages of a life cycle assessment, adapted from ISO14040 [15]

For the life cycle inventory, laboratory experiments and simulation results at first hand, are combined to gather the best possible quality of inventory data at this stage of the technology development. For modelling life cycle inventory the LCA software GaBi is applied. Datasets from commercial databases developed by the company thinkstep (www.gabi-software.com) are used for background data requirements.

Cost Analysis

Costs in economics always play an important role in industry. The best engineered and most sustainable Biorefinery concept will not be implemented if it does not prove to be economic. Therefore all Biorefinery concepts developed within the Research Division are also investigated from an economic point of view. We can carry out these investigations using different tools depending on the problem to be solved. Economic calculations can be implemented in MS Excel® based on standards like VDI 2067. But also the software tools IPSEpro PSEconomy and Aspen Process Economic Analyzer™ are used to carry out profitability calculations. These calculations are applied to identify optimization potentials used as input for experimental optimization and process simulation. They also form the basis to identify the most economic Biorefinery concept within some variants. Moreover the results

from the economic calculations are used to compare the costs of Biorefinery products with prices of commercial products.

Beside this well-known field of application for economic calculations and cost analysis, it is also important to consider economic aspects at an early stage of process development in order to support the identification of promising processes and product scenarios that are still under development. A model has been developed that allows the comparison of different innovative Biorefinery scenarios [17]. Within the model key performance indicators (KPI) for expenses and revenues are calculated and lead to a KPI representing the profit of the scenario.

To identify the expenses KPI, the model of “levelized costs of electricity”, known from the energy production sector [18], that offers the possibility to compare long term investigations for systems with different cost structures, has been adapted. Literature data and market data for investment costs, material costs, personnel costs and other costs have been used together with technical know-how to calibrate the model for the different Biorefinery scenarios. The gained expenses KPI also considers uncertainties as it bases on the weighted average cost of capital (WACC).

The revenue KPI is also based on literature data for revenues for each product or for comparable products if the revenue for the intended innovative product is not yet known. In the latter case it is recommended to use a span for the revenue rather than a single value. This is especially true in the case of Nanolignin as a product as it is not yet known, which final product will be gained from Nanolignin. Thus, the expectable revenues are also unknown at the moment. Revenues for Nanolignin were assumed with values starting from 3.300 EUR/t. The other products of the Biorefinery concepts (cellulose, hemicellulose and normal sized lignin) have also been assigned with revenue ranges [17].

Furthermore, the risks that are connected with innovative developments are considered in the model. This is done by applying distributions (e.g. normal or triangular distribution) to the defined ranges for costs and revenues and by carrying out Monte Carlo Simulations. The results from these simulations lead to probabilities for positive and negative profit KPIs that can be used as basis for decisions.

Results and Discussion

Experiments

Preliminary experiments investigated the influence of the ethanol content during organosolv pre-treatment of wheat straw on the extraction yields of lignin and sugars [19]. The results showed the best lignin yields at ethanol concentrations of 50-60 wt%. In contrast, the sugar yields are maximized when the extraction is carried out with pure hot water and decreases considerably with increasing ethanol content.

Thus, it is evident that the pre-treatment step has to be optimized for the desired biorefinery concept. If both sugars and lignin yields are claimed to be maximized, a staged pre-treatment combining a pure water extraction step with an ethanol organosolv extraction step should be developed.

Recent experiments have focused on the production of lignin particles in micro- to nanoscale. The pre-treatment process has, therefore, been implemented as organosolv process with an aqueous ethanol solution with 60 wt% ethanol. The experiments have been carried out in the 1 l stirred autoclave with 8.3 wt% dry wheat straw content in the reactor and at a temperature of 180 °C that was held constant for 15 min. Details on the experiments are given in [5]. The resulting organosolv extract contains 0.677 g/l total carbohydrates and 6.62 g/l total lignin.

This organosolv extract was used as feed for the three precipitation setups described above. The precipitation experiments were carried out at 25 °C and with a constant volume ratio of extract to antisolvent of 1:5. The antisolvent consisted of water set to a pH of 2 or 5 by adding sulfuric acid.

It could be shown that the precipitation with the “Static Mixer” setup resulted in the smallest particle of 386 to 463 nm (for undried and dried particles, respectively, precipitated with an antisolvent with pH 2) followed by the “T-Fitting” setup and the “Batch” setup [5]. The width of the particle distributions from these measurements on the other hand is smallest for the “Batch” setup followed by the “T-Fitting” setup and the “Static Mixer” setup.

The experiments with the “Static Mixer” setup have also been carried out with an antisolvent with pH 5. The comparison of the results from both “Static Mixer” experiments showed that the antisolvent with pH 5 leads to a significant reduction of the median diameter of the particles to approx. 100 nm [5]. These particle size results measured with the Mastersizer 2000E are supported by SEM images (Figure 6).

The precipitation yields (ratio of mass of precipitate after drying to the lignin amount in the organosolv extract) showed that the precipitation with pH 5 anti-

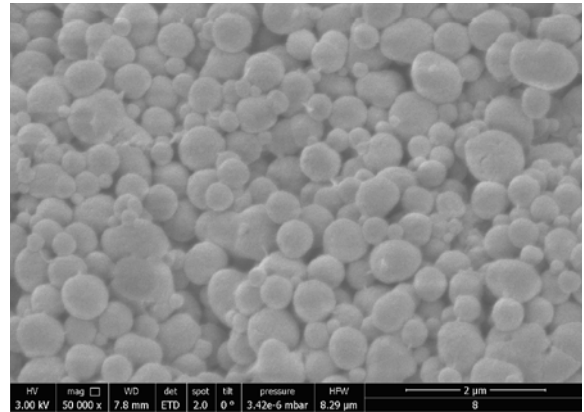


Figure 6: Example of a scanning electron microscopy (SEM) image of dried lignin particles

solvent leads to maximum yields around 50 wt% while pH 2 antisolvent leads to yields greater than 65 wt%.

Determination of the molecular mass of the Nanolignin particles showed that the precipitation setup has only minor influence on the molecular mass of the Nanolignin. The weight average molecular weight for the three investigated precipitation setups lies in the range of 1.600 to 1.800 Da [5].

Process Simulation

Simulation is performed for a constant feedstock flow rate of 12.5 t/h wheat straw. Besides the base case (no pre-concentration via membrane unit) a stage cut of 15%, 50% and 80% is considered for the membrane unit. For ethanol and water, no rejections were observed experimentally, so the split factor was equal to the stage cut. For lignin, ash, and proteins, split factors of 1%, 10%, and 50% of the stage cut were used. For the main sugars xylose, arabinose and glucose, the used split factors were 77.3%, 80.6% and 52.6% of the stage cut. Based on the assumed feedstock input it was possible to obtain around 26.2 t/h wet cellulose/hemicellulose stream as well as 2.5 t/h of wet lignin. Both output streams are containing about 70% water. Following Table 1 a pre-concentration step via nanofiltration (NF) brought some savings in the fresh water and acidified water demand. Furthermore, under the considered process settings pre-concentration prevents ethanol losses. However, detailed experimental investigations are necessary to confirm findings and lignin quality [9].

Table 1: Basic mass balance for all process versions based on 12.5 t/h straw input. Values given in t/h

| | Input | | | |
|-------|-------|--------|-------------|------------|
| | Straw | *Water | Ethanol 95% | Acid water |
| V1 | 12.5 | 28.1 | 1.1 | 167.7 |
| V2_15 | | 25.3 | 0.9 | 142.2 |
| V2_50 | | 21.7 | 0.5 | 86.6 |
| V2_80 | | 18.6 | 0.2 | 37.5 |

| | Output | | |
|-------|---------------|------------|----------------|
| | Wet cellulose | Wet lignin | Hemi-cellulose |
| V1 | 26.2 | 2.5 | 179 |
| V2_15 | | | 154 |
| V2_50 | | | 92.2 |
| V2_80 | | | 40.4 |

Basic energy balances are calculated for original (non-integrated) process designs, including thermal energy for fractionation and solvent recovery, not considering the drying of the final products. Obtained results are in a good agreement with studies reported in the literature (similar process designs, but less process steps considered), determining a specific energy demand for heating of 11.84 MJ/kg dry biomass [20] and 11.6 MJ/kg dry biomass [21]. While base case (V1) and process option V2_15 obtain a considerably higher specific heat demand than reported in literature, cases V2_50 and V2_80 are comparable or lower than reference processes (13.45 and 9.45 MJ/kg dry biomass, respectively; non-integrated) [8]. At this point, it is shown that utilization of NF could bring some advantages in energy savings without implementation of any heat integration. Further investigations show that Pinch analysis and heat integration has a discernible impact on improvement of process energy efficiency. Figure 7 illustrates the optimum HEN design suggested by the TVTHENS software. Version V1 shows lowest capability for heat integration, with minimum number of exchanging units and inability to integrate the column reboiler. Conversely, in V2_80, nanofiltration and its high performance could give a possibility to fully integrate the column reboiler and provide necessary heat from the process streams via HEN, resulting in a specific energy demand of 12.54, 8.16, 6.37 and 2.88 MJ/kg dry biomass for process options V1, V2_15, V2_50 and V2_80, respectively [8].

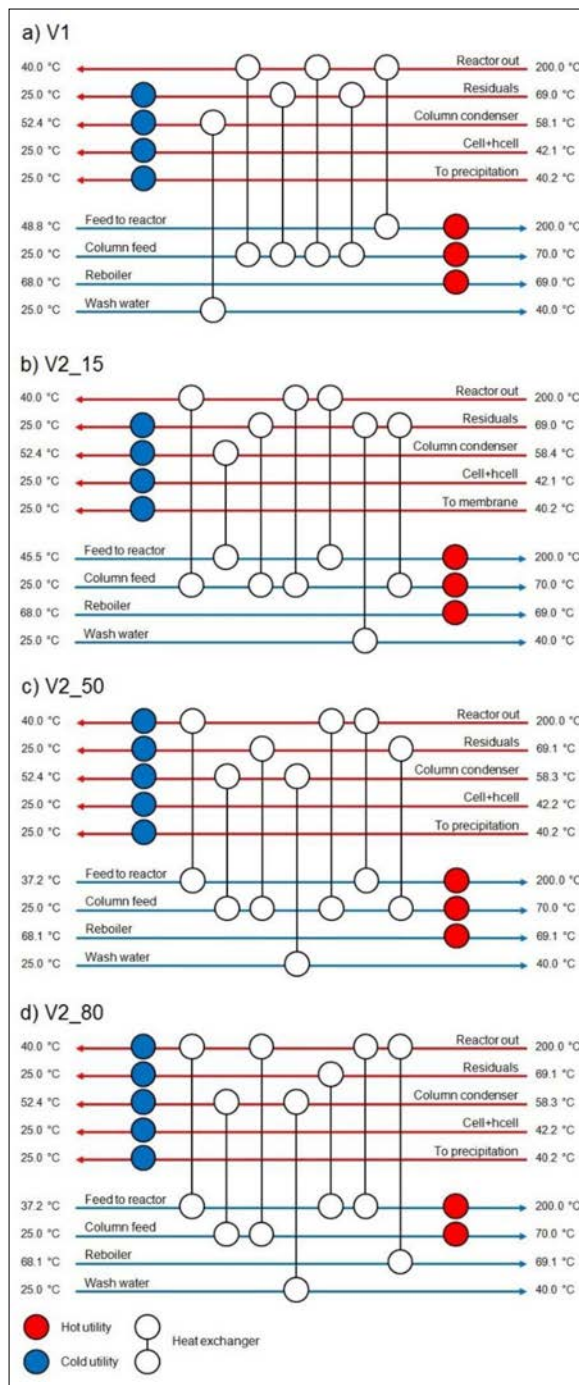


Figure 7: HEN for different process versions obtained from TVTHENS

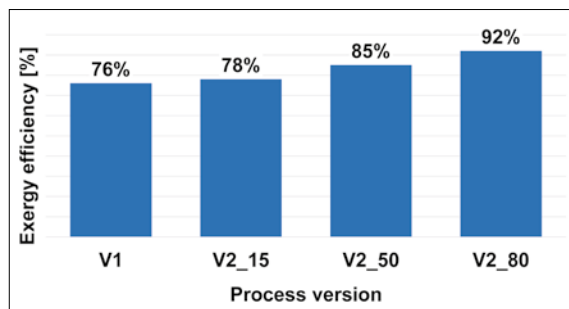


Figure 8: Exergy efficiency=Exergy_out/Exergy_in

Calculated exergy efficiency is presented in Figure 8. V1 has the lowest simple exergy efficiency of 76% due to exergy destruction, most probably in the solvent recovery block. That further leads to a low energy efficiency of the process, since thermal energy available in the process cannot be efficiently exchanged between process streams. Process version V2_80 expresses the highest exergy efficiency due to the minimization of energy consumption in the solvent recovery block. Only 8% of exergy is destroyed in this process version. Exergy loss is a consequence of non-well designed process units (e.g. reactor, washing unit, separation etc.). However, at this point, it was not possible to locate these irregularities. For this purpose, exergy analysis of each process step has to be performed [8].

CFD Simulation

As an example to demonstrate the scope of CFD related methods to investigate organosolv extractors, a straw fibre filled fixed bed extractor vessel was chosen. The investigated cylindrical extractor geometry was approximately 150 mm in diameter and around 100 mm in height. It was filled with 50% fibres of 30 mm length and 5 mm diameter and 50% fibres of 40 mm length and 4 mm diameter. The porosity profiles are a perfect indicator to analyse significant bypassing or channelling. Figure 9 shows the average axial porosity and radial porosity of the bed. The overall average porosity was around 0.61 showing a much lower packing density compared to more spherical particles. The porosity significantly increases towards the wall and towards the top of the extractor vessel. This indicates the risk of wall channelling, however, with low flow velocities typically applied in fixed bed extractors, the channelling effect may be usually less significant. Also, the packing model does not account for fibre softening and re-arrangement effects during a typical organosolv extraction process yet.

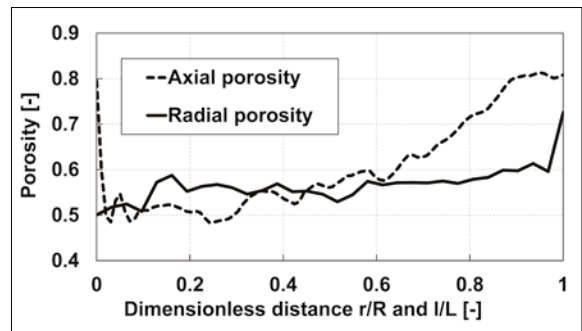


Figure 9: Axial and radial porosity profiles plotted from the bottom to top and from the centre to the wall, respectively

The velocity field was then calculated using an incompressible flow solver of OpenFOAM® at an average inlet velocity of 0.01 m/s. In Figure 10 velocity contour plots at different heights from bottom of the packed bed are shown. Some high velocity spots can be observed close to the walls which show the channelling in the bed – the effect is more pronounced at the top of the extractor where the fibre packing is less compact. Channelling may result in short contact time between straw fibres and liquid and consequently lower extraction performance.

The computation and analysis of the residence time distribution (RTD) is a proper means to further investigate channelling and by-passing effects. By the application of a step function concentration pulse at the inlet the average concentration at the outlet is observed with time. Wide RTDs are a good indication for channelling and/or by-passing. For three different inlet velocities RTD curves were extracted from the flow fields. As shown in Figure 11 (next page), straw fibre packings obviously show a wide RTD which can be narrowed through higher flow rates through the extractor. Further results of this study will be shown in [22].

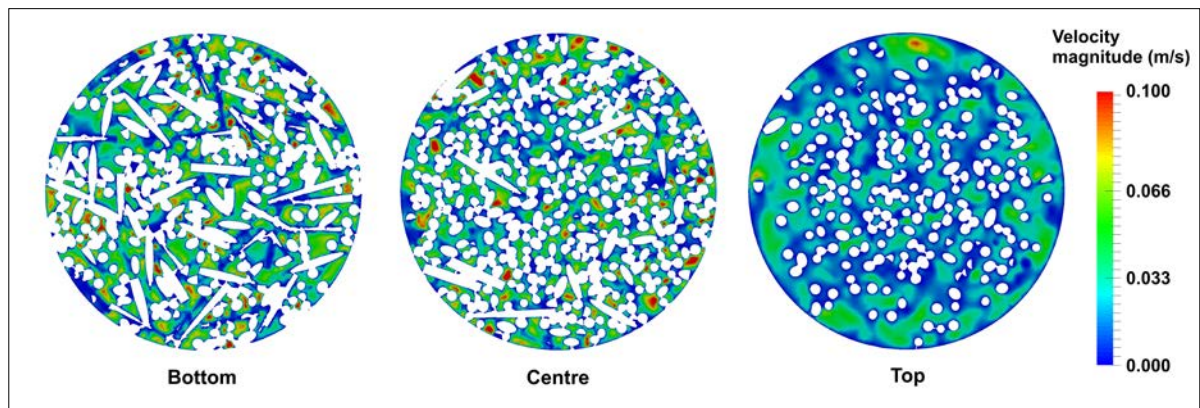


Figure 10: Velocity magnitude contours at the bottom, the centre and the top of the extractor

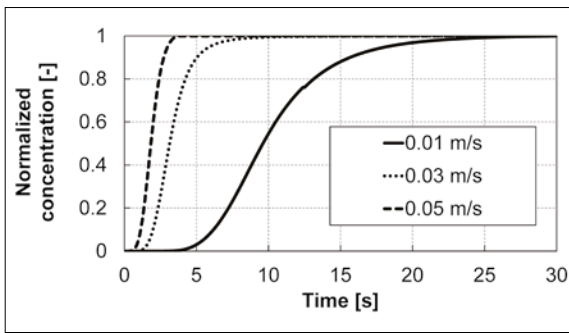


Figure 11: Residence time distribution (RTD) for three different inlet velocities

Process Analysis via Life Cycle Assessment

First results are presented from the methodological perspective of LCA application in the process development.

Supporting the development of the Biorefinery by making the environmental impacts available was found to be the most suitable goal of the assessment. The flexible nature of the LCA method matches the need to adapt to the progress within the process development of the Biorefinery. If new insights are gained from experimental setups or simulation results, they can be incorporated quickly to the developed life cycle model of the Biorefinery.

Burden allocation is an issue at several stages of the Biorefinery. In case more than one product is gained, the question of how to distribute the environmental impacts between these products has to be answered. The wheat straw feedstock is an agrarian byproduct and the environmental impacts from agricultural processes can be accounted between corn and straw with different approaches. Furthermore the intermediate side products of the Biorefinery, cellulose and hemicellulose, have to be handled in a fair way.

All emissions are related to the functional unit, which is defined in the goal and scope stage. For the development phase of the Biorefinery it was considered as sufficient to use a fixed physical parameter of the yielded product Nanolignin as the functional unit. For further assessments of comparative investigations with other products, a functional unit has to be defined that enables a meaningful comparison.

Cost Analysis

The cost analysis to support strategic decisions for the development of a biorefinery process has been carried out for the following concepts (details can be found in [17]):

- organosolv extraction of either hard wood, soft wood, wheat straw or maize straw
- organosolv extraction is carried out with an aqueous ethanol solution with 60 wt% ethanol
- 99% of the ethanol can be recovered within an optimized recovery plant like the process presented in [8]
- products gained in the organosolv extraction are (with varying contents depending on the used raw material):
 - a lignin fraction,
 - a hemicellulose fraction,
 - a cellulose fraction containing some lignin, hemicellulose and other constituents and
 - a residual fraction
- 50% of the lignin fraction can be processed to lignin particles in nano scale
- costs are considered for:
 - investments
 - raw material, ethanol, water
 - heat
 - personnel
 - other costs
 and varied within defined ranges
- revenues are considered for:
 - lignin as nanoscale particles as high prize product
 - lignin in non-nanoscale form used as combustion fuel
 - Hemicellulose fraction used for heat production
 - mixed cellulose fraction used for heat production (worst case) or as input material for pulp and paper industry (best case)
 and varied within defined ranges
- the WACC is analysed with 0%, 6% and 12%

The analysis of the costs KPI showed that the investment costs have a main influence on the levelized costs of production in all scenarios. In the straw based scenarios heat and personnel are the major cost factors within the costs of operation. In the scenarios based on hard and soft wood the raw material costs are the main costs of operation followed by heat and personnel. The total costs for the straw based concepts are significantly lower than the costs for hard wood and soft wood scenarios. This means that from the costs point of view the straw based scenarios are the most promising ones.

The analysis of the revenues for hard wood and soft wood showed that the revenues for Nanolignin as the highest value added product in the concepts have the major share of the total revenues ranging from around 50% to 80% depending on the wood and the revenue scenario. The second largest share has the cellulose fraction with around 15-45%.

For the straw based scenarios the results are more diverse. Wheat straw shows a share of Nanolignin on the revenues of around 44-65% and maize straw a share of approx. 34-61%. This lower share is caused by the much lower ratio of lignin content to cellulose content in the raw materials compared to hard wood and soft wood. Consequently, the share of the cellulose fraction on the revenues is higher with around 26-53% for wheat straw and around 34-61% for maize straw.

Both results can be combined to the profit KPI. This analysis shows that the straw based scenarios have a negative profit for most of the investigated cases. The profit for soft wood is slightly higher than the profit for hard wood. Moreover, the Monte Carlo simulations showed that the risk for a negative profit is around 50% for the wheat straw based scenarios. The maize straw based scenarios have a risk of a negative profit of more than 70%. In contrast, the risks of a negative profit are around 4-6% for soft wood and around 5-8% for hard wood.

Based on the results it can be concluded that the investigated scenarios with wheat and maize straw as raw material are not profitable under the made assumptions. It would, therefore, be necessary to identify higher valued applications for the hemicellulose and cellulose fraction in order to obtain higher revenues and gain positive profits. This could, for example, be achieved by utilizing the hemicellulose fraction as input for chemical or biochemical synthesis or by improving the properties of the cellulose fraction by optimized pre-treatment conditions. Additionally, a reduction of the heat demand by heat integration or a coupling with other industrial plants making use of their waste heat could increase the profitability.

Conclusions

For the valorisation of the main constituents of lignocellulosic materials cellulose, hemicellulose and lignin an organosolv Biorefinery approach using an ethanol/water-mixture has been investigated. As a model substrate wheat straw has been used as raw material. The leading product in the developed concept are sulphur free native lignin micro- and nanoparticles.

In extensive series of experiments in 45 ml and 1 liter high pressure reactors the organosolv pre-treatment conditions have been optimised and will be used in a 10 liter extractor for the production of enough sample material for further application tests. Due to optimized process conditions and equipment optimization for the precipitation of Lignin particles, yields greater than 65 wt% are achieved.

The whole process development is supported by the in-house toolbox IDEAS-Engine which allows for

the handling of a multitude of relevant aspects like material property data, process simulation and process analysis. Process simulation has been applied for investigating the recovery of the used solvents. A nanofiltration process has been simulated as concentration step for a solvent recycle stream with recycle rates of 15, 50 and 80% of the solvent. This recycle stream is led directly back to the extractor without the need of a distillation step. This measure leads to a reduction of energy demand as well as a simplified design of the needed distillation column. CFD simulation has been applied for detailed design and analysis of the core unit within the Biorefinery concept, the extraction vessel. The liquid flow field could be optimised and along with that the maximum utilisation of the extractor volume was ensured.

With the application of the Pinch technology on the Biorefinery concept, an energy optimization has been achieved. On this basis the exergy analyses reveal an exergy efficiency of 92% or 8% loss of exergy.

The cost analysis for Biorefinery concepts with wheat straw and maize straw as substrates showed a share of Nanolignin on the revenues of 44-65% and 34-61%, respectively. The analysis for hard wood and soft wood showed that the revenues for Nanolignin have a share on the total revenues ranging from around 50% to 80%. The second largest share on the revenues has the cellulose fraction with around 15-45%. A risk analysis identified that the straw based scenarios have a high risk of a negative profit and need adaptations of the assumed utilisation scenarios for the cellulose and especially for the hemicellulose fraction. In contrast, the risks of a negative profit for the soft wood and hard wood scenarios are around 4-6% and around 5-8%, respectively, and show high potential under the made assumptions.

The LCA calculations for the developed Biorefinery process are still under investigation but first methodological aspects have been presented.

Acknowledgement

The authors acknowledge the TU Wien University Library for financial support through its Open Access Funding Program. Scanning electron microscopy image acquisition of the lignin particles was carried out using facilities at the University Service Centre for Transmission Electron Microscopy, TU Wien, Austria.

References

- [1] Muurinen E., organosolv pulping – A review and distillation study related to peroxyacid pulping. PhD Thesis 2000, University of Oulu.
- [2] Yawalata D., Catalytic selectivity in alcohol pulping of spruce wood. PhD Thesis 2001, University of British Columbia.
- [3] Beisl, S., Miltner, A., Friedl, A., Lignin from Micro- to Nanosize: Production Methods. *Int. J. Mol. Sci.* 2017. 18(6), 1244.
- [4] Beisl, S., Friedl, A., Miltner, A., Lignin from Micro- to Nanosize: Applications. *Int. J. Mol. Sci.* 2017. 18(11), 2367.
- [5] Beisl, S., Loidolt, P., Miltner, A., Harasek, M., Friedl, A., Production of micro- and nanoscale lignin from wheat straw using different precipitation setups. *Molecules*, 2018. 23(3), 633.
- [6] Beisl, S., Biermair, F., Friedl, A., Mundigler, N., Miltner, A., Sequential Extrusion and organosolv Pre-treatment for Wheat Straw Valorization. *Chemical Engineering Transactions*, 2017. 61: p. 853-858.
- [7] National Institute of Standards, Chemistry WebBook, NIST Standard Reference Database Number 69. <http://webbook.nist.gov/>.
- [8] Drljo, A., Simulation of biorefinery platforms for combined biohydrogen and biogas production from wheat straw, PhD Thesis, 2016, TU Wien.
- [9] Weinwurm, F., Drljo, A., Waldmüller, W., Fiala, B., Niedermayer, J., Friedl, A., Lignin concentration and fractionation from ethanol organosolv liquors by ultra- and nanofiltration, *J. Cleaner Production*, 2016. 136: p. 62-71
- [10] Drljo, A., Liebmann, B., Wukovits, W., Friedl, A., Predicting minimum energy conditions for a distillation column by design of experiments and process simulation, *Chemical Engineering Transactions*, 2012. 29: p. 325-330.
- [11] Drljo, A., Modarresi, A., Weinwurm, F., Wukovits, W., Friedl, A., Integration of an organosolv process applying pinch and exergy analysis, 7th International Conference on Environmental Engineering and Management – ICEEM07, Vienna, Austria, 18.-21.09.2013 in: Conference Abstracts Book, 2013, ISBN: 978-973-621-418-9; S. 197-198.
- [12] Modarresi, A., Kravanja, P., Friedl, A., Pinch and exergy analysis of lignocellulosic ethanol, biomethane, heat and power production from straw, *Applied Thermal Engineering*, 2012. 43: p. 20-28.
- [13] Haddadi, B., Jordan, C., Norouzi, H.R., Harasek M., Investigation of the pressure drop of random packed bed adsorbers, *Chemical Engineering Transactions*, 2016. 52, 439-444.
- [14] Haddadi, B., Gasser, C., Jordan, C., Harasek, M., Lendl, B., Simultaneous Laser Doppler Velocimetry and stand-off Raman spectroscopy as a novel tool to assess flow characteristics of process streams. *Chemical Engineering Journal*, 2018. 334, 123-133.
- [15] European Committee for Standardization CEN, 2006a, Environmental management – Life cycle assessment – Principles and framework (ISO 14040:2006), Brussels, Belgium.
- [16] European Committee for Standardization CEN, 2006b, Environmental management – Life cycle assessment – Requirements and guidelines (ISO 14044:2006), Brussels, Belgium.
- [17] Riepl, S., Economic evaluation of innovative biorefinery scenarios. Master thesis, 2018, TU Wien.
- [18] Branker, K., Pathak, M., Pearce, J., A review of solar photovoltaic levelized cost of electricity. *Renewable and Sustainable Energy Reviews*, 2011, 15: 4470-4482.
- [19] Weinwurm, F., Fractionation and Degradation of Wheat Straw during Liquid Hot Water and Ethanol organosolv Treatments. PhD thesis, 2016, TU Wien.
- [20] García, A., Alriols, M. G., Llano-Ponte, R., Labidi, J., Energy and economic assessment of soda and organosolv biorefinery processes, 20th European Symposium on Computer Aided Process Engineering – ESCAPE 20, Ischia, Naples, Italy, 06.-09.06.2010.
- [21] Viell, J., Harwardt, A., Seiler, J., Marquard, W., Is biomass fractionation by organosolv-like processes economically viable? A conceptual design study. *Bioresource Technology* 2013. 150: p.89-97.
- [22] Harasek, M., Haddadi, B., Jordan, C., Friedl, A. Proceedings of the 28th European Symposium on Computer Aided Process Engineering, 2018, 1583-1588. DOI: 10.1016/B978-0-444-64235-6.50276-X.

FTIR Micro-Spectroscopy for Characterisation of Radial Substituent Diffusion in Cellulose II-Beads

Danuta Mozdyniewicz¹, Andreas Schwaighofer², Karin Wieland², Martin Häubl³,
and Bernhard Lendl²

¹ Kompetenzzentrum Holz GmbH, Altenberger Str.69, 4040 Linz, Austria

² Institute of Chemical Technologies and Analytics, Vienna University of Technology, Vienna, Austria

³ Lenzing AG, Werkstraße 2, 4860 Lenzing, Austria

Contact: d.mozdyniewicz@kplus-wood.at

Abstract

In this paper, a FTIR-based method for localization of substituents along the radius of a cellulosic bead is described. In our experiments, cellulosic beads prepared using the lyocell process are initially functionalized with citric acid (CA) and 1-octenylsuccinylanhydride (OSA), as both reagents contain IR active carboxylic groups. The analysis using FTIR micro-spectroscopy enables the determination of the analyte distribution in a simple way and accordingly reveals the diffusion ability of certain functionalizing agents. The effect of the reagent size and structure as well as reaction conditions on the penetration depth within the spheres is made visible. The maximum diffusion depth of the bulky OSA is around 400 μm whereas CA is found more than twice as deep within the bead. The applied method offers the possibility of tracking the functionalization agents over the cross-section of cellulosic materials and may be applied to other forms, e. g. fibers.

Keywords: Cellulose II beads, functionalization, citric acid, 1-octenylsuccinylanhydride, FTIR Micro-Spectroscopy, radial diffusion

Introduction

The almost unlimited availability of cellulose, the variety of processing possibilities and several advanced applications result in a growing interest in utilization of spherical cellulosic particles in the last few years. Cellulosic particles find application in chemistry, biochemistry, chemical engineering and other related areas [1]. The three free hydroxyl groups of the glucose units making up the cellulose chain are particularly accessible for functionalization, thereby enabling chemical modification and adaptation of the basic material properties. Interest in modification of cellulose surface has existed for a long time, and has even increased in recent years [2-4]. A main disadvantage of cellulose as a raw material is its sensitivity to pH values deviating from neutral. The strong swelling ability due to the hydrophilic character favors the diffusion into the structures and may result in accelera-

ted degradation. Enhancing the surface hydrophobicity may slow down or prevent the corrosion of the cellulosic structure. Another possibility to increase the stability is cross-linking. The formation of intramolecular bonds decreases the swelling ability and as a result increases material strength [5, 6]. Epichlorohydrin is the most common agent for the purpose. However, a substitution of the chemical is desired, due to its toxic and cancerogenic properties. Many other suitable chemicals show similar problematic properties, e. g. glutardialdehyde or glycoldiglycidyl ether. The use of citric acid as an alternative cross-linking agent proves ideal, due to its nontoxicity and availability [7, 8].

For bead production, direct bead formation and simultaneous cellulose regeneration analogous to fiber spinning appears most advantageous. In this approach,

continuous production is possible and additionally the properties may be changed at any given moment. Therefore, procedures can be easily adapted that are already used for filament formation. Particularly, the viscose and the lyocell processes seem appropriate due to their wide spread industrial application [9, 10]. Other less common methods, e.g. dissolution in ionic liquids or NaOH/urea may be used as well, but are of less interest due to non-industrial scale [11, 12].

Depending on the manufacturing method, different variations of the resulting bead structure may be observed. Applying the lyocell process, particles with a distinctive shell-core structure are generated, implying the localization of the functionalization agent primarily on the surface [13]. Employing functionalization reagents with different degrees of hydrophilicity leads to varying diffusion paths within the spheres. As a result, different substituent distribution within the cellulose bead may occur. Therefore, determination of the substitution pattern within the structure is essential for the pinpointing of potential applications.

Fourier transform infrared (FTIR) spectroscopy is a nondestructive, versatile, and label-free technique for chemical analysis of a wide range of samples. It offers attractive features such as fast sample preparation, sound sensitivity, and the capacity for comprehensive qualitative as well as accurate quantitative analysis. This spectroscopic technique has been successfully applied for the characterization of cellulosic fibers [14-17].

In this work, cellulosic beads manufactured by dissolving pulp in N-methylmorpholine-N-oxide (NMMO) and regenerating the so produced dope were used as raw material for functionalization. Alcenyl succinic anhydrides are commonly used sizing agents increasing the hydrophobicity of paper, whereas citric acid is a small hydrophilic molecule enabling cellulose cross-linking due to two reactive groups. Application of the two different functionalization agents allowed the investigation of diffusion depending on the reagent properties and the treatment conditions. The analyses of the treated beads were performed using FTIR microscopy.

Materials & Methods

Materials

Cellulose II beads were obtained by Lenzing AG and were produced by regeneration of cellulose in water, using a device that enabled the formation of spherical particles during the regeneration step. Previously, the pulp was dissolved in NMMO [13]. The obtained beads with a diameter of ca. 2.5 mm, were washed NMMO free and air dried.

Unless otherwise specified, all the chemicals used were obtained by commercial suppliers (purity grade at least lab quality). 1-octenylsuccinylanhdyride (OSA), commonly used as a surface active agent, was kindly provided by Miliken Chemicals.

Functionalized Bead Preparation

For preparation of the cross-linked beads, a solution containing 19.23 g citric acid (CA) and 5.62 g of KH_2PO_4 was prepared in deionized H_2O in a 50 ml volumetric flask. 0.98 g of the beads were suspended in 14 ml of the solution and left unstirred for 30 minutes to swell. Subsequently, the beads were filtered off and dried at 160 °C in vacuum to start the cross-linking reaction, due to ester formation of the citric acid and the cellulose hydroxyl groups. After 15 minutes, the material was washed with warm deionized water and air dried.

For functionalization with OSA, an initial solvent exchange was necessary to remove water, as a non-aqueous solvent was necessary for the reaction. Therefore, beads with 6.44 g dry cellulose content were suspended in acetone that was replaced by acetone once and twice by toluene. After the solvent exchange procedure the beads were stirred in 250 mL toluene containing 15 mL pyridine at 60 °C for one hour under argon atmosphere. Subsequently, 31.74 g OSA were dropwise added and the suspension was further stirred at 90 °C for 18 hours under argon. After the reaction time, the functionalized beads were filtered, washed with acetone and air dried [18].

Sample Preparation for Analysis

Air dried cellulose beads that were functionalized with citric acid (CA) and 1-octenylsuccinylanhdyride (OSA) were cryo-cut at approx. -15°C to expose the center of the bead so that the cross section could be investigated by FTIR microscopy (Figure 1). The obtained hemispheres were glued to a microscope slide.



Figure 1: Cellulose beads before (a) and after (b) the functionalization reactions; (b) left: a cut bead prepared for FTIR analysis.

FTIR Microscopy

FTIR microscopic measurements were performed using a Bruker Hyperion 3000 IR microscope (Bruker, Ettlingen, Germany) equipped with a liquid nitrogen cooled

HgCdTe (mercury cadmium telluride, MCT) detector, connected to a Bruker Tensor 37 FTIR spectrometer. Attenuated total reflection (ATR) microscopy spectra were acquired using a Ge-ATR 20x objective. For all measurements, spectra were recorded as the co-addition of 100 scans with a spectral resolution of 4 cm^{-1} . Instrument control and spectrum acquisition were performed with OPUS 7.2 software (Bruker, Ettlingen, Germany). In one measurement run, IR microscopic measurements of the bead cross section were performed beginning at the center and continuing outwards with a distance between measurements of approx. $80\text{ }\mu\text{m}$ (Figure 2). After every measurement run, the Ge-ATR crystal was cleaned with water and ethanol.

For evaluation of the penetration depth of the substrates, areas of the substrate bands were normalized with an IR band attributed to the cellulose chain. The obtained ratios were then normalized to values between 0 and 1. These normalization steps were necessary to account for differences in the IR absorbance due to unequal pressure and contact between the ATR crystal and the cellulose bead surface.

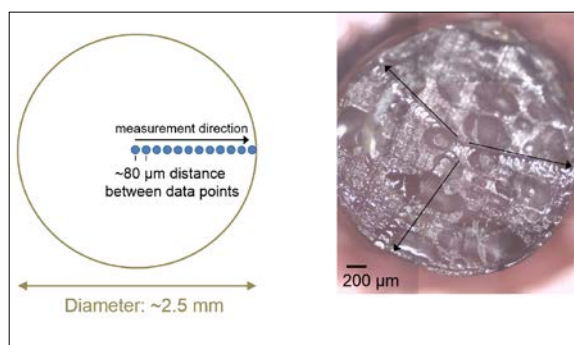


Figure 2: left: Schematic of measurement procedure. ATR-IR microscopic measurements were performed on the bead cross section, starting in the center. right: Picture of the bead cross section after performing multiple measurement runs. The indents of the ATR crystal are visible on the bead surface.

Results & Discussion

In this paper, cellulosic beads after cross-linking with citric acid and 1-octenylsuccinylhydride are described. In both investigated cases, a change of color was observed after the reaction completion, which may indicate a surface functionalization as well as the formation of cellulose degradation products and other co-products and their adsorption at the surface. Yellowing of cellulosic materials after a citric acid treatment has been described in the literature before [7]. The experiments were performed once and no optimization of the reaction conditions was made, since the work was part of a project dealing with screening and evalua-

tion of suitable functionalization agents. On that account, rather low mass increases were observed, suggesting fairly low degrees of substitution (Table 1). Nevertheless, detectable bands in the FTIR spectra were sufficient to indicate a successful functionalization and enabled to create diffusion profiles of the reagents.

Table 1: Yields after functionalization reactions

| Functionalization agent | m_{initial} [g] | m_{final} [g] | Δm [g] | Δm [%] |
|--------------------------------|-----------------------------|---------------------------|-------------------|-------------------|
| Citric acid (CA) | 0.98 | 1.03 | 0.05 | 5.1 |
| 1-Octenylsuccinylhydride (OSA) | 6.44 | 6.48 | 0.04 | 0.6 |

* o.d. beads

FTIR microscopy was performed on the bead cross sections revealed by cryo-cutting. ATR-IR microscopic spectra were measured at a distance of approx. $80\text{ }\mu\text{m}$, resulting in 15-16 measurement points across the bead radius. On one cross section, multiple measurement runs were performed (Figure 2). The IR spectra of the untreated and modified cellulose beads are shown in Figure 3 and show characteristic bands of cellulosic material [16].

Furthermore, the modified beads feature IR bands at 1600 cm^{-1} (OSA) and 1580 cm^{-1} (CA), which have been attributed to the carboxylate group of functionalized cellulose [19, 20]. The IR spectra were analysed for evaluation of the penetration depth of the substrates into the cellulosic beads. Figure 4 shows the normalized IR intensities of the IR bands attributed to OSA and CA. Absorbance values of OSA rapidly decline within the exterior $400\text{ }\mu\text{m}$ of the cellulose beads. In contrast, IR band intensities of CA drop slowly until reaching a plateau at approx. $1000\text{ }\mu\text{m}$ within the cellulose bead. The general decrease of substrate moieties towards the bead center seems reasonable, since derivatization of the hydroxyl group within the bead interior is limited by diffusion, while the outmost hydroxyl groups of the beads are readily accessible. The relative density of the functional groups, however, differs between OSA and CA. In this context, the C8 group of OSA may limit further diffusion into the bead and this substrate reacts within the outer layers of the bead. In contrast, the sterically more compact CA diffuses and reacts further into the cellulose bead, even though this reagent possesses two reactive groups for cross-linking.

As citric acid could be found throughout the entire bead, it could be used to enhance the stability of the cellulosic spheres. The cross-linking affects the cellulose hydroxyl groups and may prevent degradation reactions to a certain extent, as the cellulose molecules are connected after the reaction resulting in decreased accessibility [21]. A similar effect on wood was

demonstrated by Bischof Vuksic [8]. The stability of wood samples after CA treatment was enhanced due to prevented swelling, further increasing the micro-tensile strength. These results suggest a stabilizing effect on the treated beads, however, additional experiments would be necessary to confirm the assumption.

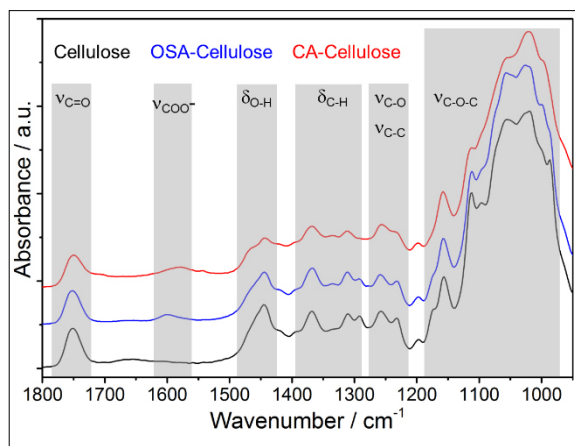


Figure 3: IR spectra of cellulose beads (black) without functionalization, and modification with (blue) OSA and (red) CA.

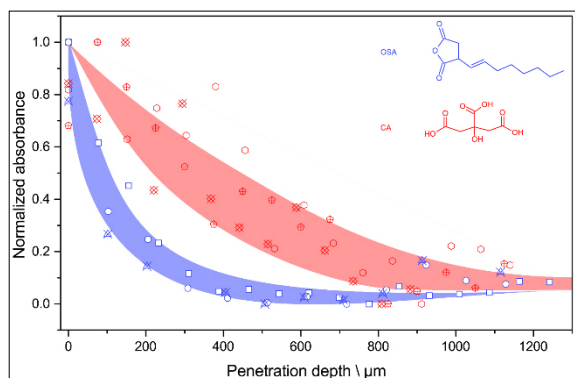


Figure 4: Normalized IR intensities of characteristic bands of (blue) OSA and (red) CA plotted versus the penetration depth within the cellulose bead.

Conclusions

In this report we demonstrate for the first time that FTIR microscopy is an excellent method for determination of functionalization patterns within cellulose beads of sufficient size, providing the presence of IR-active groups in the reagent. In our case, the influence of the reagent structure and size on the penetration depth was shown. Citric acid was detected almost throughout the entire bead, whereas the highest concentrations of 1-octenylsuccinylanhydride were found closer to the surface.

Acknowledgements

Financial support was provided by the Austrian government, the provinces of Lower Austria, Upper Austria, and Carinthia as well as by Lenzing AG. We also express our gratitude to the Johannes Kepler University, Linz, the University of Natural Resources and Life Sciences (BOKU), Vienna, and Lenzing AG for their in-kind contributions.

A.S., K.W. and B.L. gratefully acknowledge financial support by the Austrian research funding association (FFG) under the scope of the COMET programme within the research project “Industrial Methods for Process Analytical Chemistry – From Measurement Technologies to Information Systems (impACTs)” (contract #843546).

References

- [1] Gericke, M., J. Trygg, and P. Fadim, Functional Cellulose Beads: Preparation, characterization, and applications. *Chem Rev*, 2013. 113: p. 4812-4836.
- [2] Rogowin, S.A., Neue Erfolge auf dem Gebiet der chemischen Modifizierung von Zellulose. *Lenzinger Ber*, 1970. 30: p. 16-25.
- [3] Dimow, K., et al., Ionen austauschende Fasern auf Cellulosebasis. *Lenzinger Ber*, 1978. 45: p. 60-65.
- [4] Mais, U., et al., Functionalization of cellulose. *Lenzinger Ber*, 2000. 79: p. 71-76.
- [5] Morales, A., et al., Adsorption and releasing properties of bead cellulose. *Chinese J Polym Sci*, 2004. 22(5): p. 417-423.
- [6] Ishimura, D., Y. Morimoto, and S. Hidenao, Influences of chemical modifications on the mechanical strength of cellulose beads. *Cellulose*, 1998. 5(2): p. 131-151.
- [7] Xun, H. and X. Zhou, Mechanism of citric acid crosslinking in cotton fabrics. *J China Textile University*, 1999. 16(2): p. 16-20.
- [8] Bischof Vuksic, S., et al., Polycarboxylic acids as non-formaldehyde anti-swelling agents for wood. *Holzforschung*, 2006. 60: p. 439-444.
- [8] Weber, H., Overview on latest developments in viscose industry. *Lenzinger Ber*, 2005. 84: p. 8-16.
- [10] Fink, H.P., et al., Structure formation of regenerated cellulose materials from NMMO-solutions. *Progress in polymer science*, 2001. 26(9): p. 1473-1524.

- [11] Trygg, J., et al., Physicochemical design of the morphology and ultrastructure of cellulose beads. *Carbohydr Polym*, 2013. 93: p. 291-299.
- [12] De Oliveira, W. and W.G. Glasser, Hydrogels from polysaccharides. II. Beads with cellulose derivatives. *Journal of Applied Polymer Science*, 1996. 61(1): p. 81-86.
- [13] Häubl, M., J. Innerlohinger, and C. Schirk, Three-dimensional cellulose moulded body, method for the production and use of the same. 2015. WO2015054711 (A2).
- [14] Garside, P. and P. Wyeth, Identification of cellulosic fibres by FTIR spectroscopy. *Stud Conserv*, 2003. 48: p. 269-275.
- [15] Carillo, A., et al., Structural FTIR analysis and thermal characterisation of lyocell and viscose type fibres. *Eur Polym J*, 2004. 40: p. 2229-2234.
- [16] Comnea-Stancu, I.R., et al., On the identification of Rayon/Viscose as a Major Fraction of Microplastics in the Marine Environment: Discrimination between Natural and Man-made Cellulosic Fibers by Fourier Transform Infrared Spectroscopy. *Appl Spectrosc*, 2017. 71(5): p. 939-950.
- [17] Fan, M., D. Dai, and B. Huang, Fourier Transform Infrared Spectroscopy for Natural Fibres, in *Fourier Transform – Materials Analysis*, S.M. Salih, Editor. 2012, InTech: China.
- [18] Belhafaoui, B., et al., Succinate-bonded cellulose: A regenerable and powerful sorbent for cadmium-removal from spiked high-hardness groundwater. *J Hazard Mater*, 2009. 169: p. 831-837.
- [19] McSweeney, J.D., R.M. Rowell, and S.-H. Min, Effect of Citric Acid Modification of Aspen Wood on Sorption of Copper Ion. *J Nat Fibers*, 2006. 3(1): p. 43-58.
- [20] Quellmalz, A. and A. Mihranyan, Citric Acid Cross-Linked Nanocellulose-Based Paper for Size-Exclusion Nanofiltration. *ACS Biomater Sci Eng*, 2015. 1(4): p. 271-276.
- [21] Schramm, C. and B. Rinderer, Application of Polycarboxylic Acids to Cotton Fabrics under mild curing Conditions. *Institute of Textile Chemistry and Textile Physics*, 2006. 40(9-10): p. 799- 804.

Key Aspects of the Bleaching of Industrially Found Cellulosic Chromophores

Nele Sophie Zwirchmayr¹, Ute Henniges^{1,4}, Thomas Röder², Antje Potthast¹, and Thomas Rosenau^{1,3*}

¹ Division of Chemistry of Renewable Resources, Department of Chemistry, University of Natural Resources and Life Sciences, Muthgasse 18, A-1190 Vienna, Austria

² Lenzing AG, Werkstraße 2, 4860 Lenzing, Austria

³ Johan Gadolin Process Chemistry Centre, Åbo Akademi University, Porthansgatan 3, Åbo/Turku FI-20500, Finland

⁴ Conservation of Works of Art on Paper, Archival and Library Materials, State Academy of Art and Design Stuttgart, Höhenstraße 16, 70736 Fellbach, Germany

* Contact: thomas.rosenau@boku.ac.at

Abstract

The cellulosic chromophores 2,5-dihydroxy-[1,4]-benzoquinone, 5,8-hydroxy-[1,4]-naphthoquinone, 2,5-dihydroxyacetophenone and 2,6-dihydroxyacetophenone, main contributors to cellulose discoloration, were bleached with H₂O₂, O₃ and ClO₂ at conditions resembling the corresponding sequence in industrial pulp bleaching (P, Z, or D-stage). Measurement of reaction kinetics allowed conclusions on activation energy, reaction mechanism, activation parameters and the presence of colored intermediates. Final degradation products were determined; small carboxylic acids form the major part of them.

Keywords: cellulosic chromophores, P-stage, Z-stage, D-stage, 2,5-dihydroxy-[1,4]-benzoquinone, 5,8-hydroxy-[1,4]-naphthoquinone, hydroxyacetophenones

Introduction

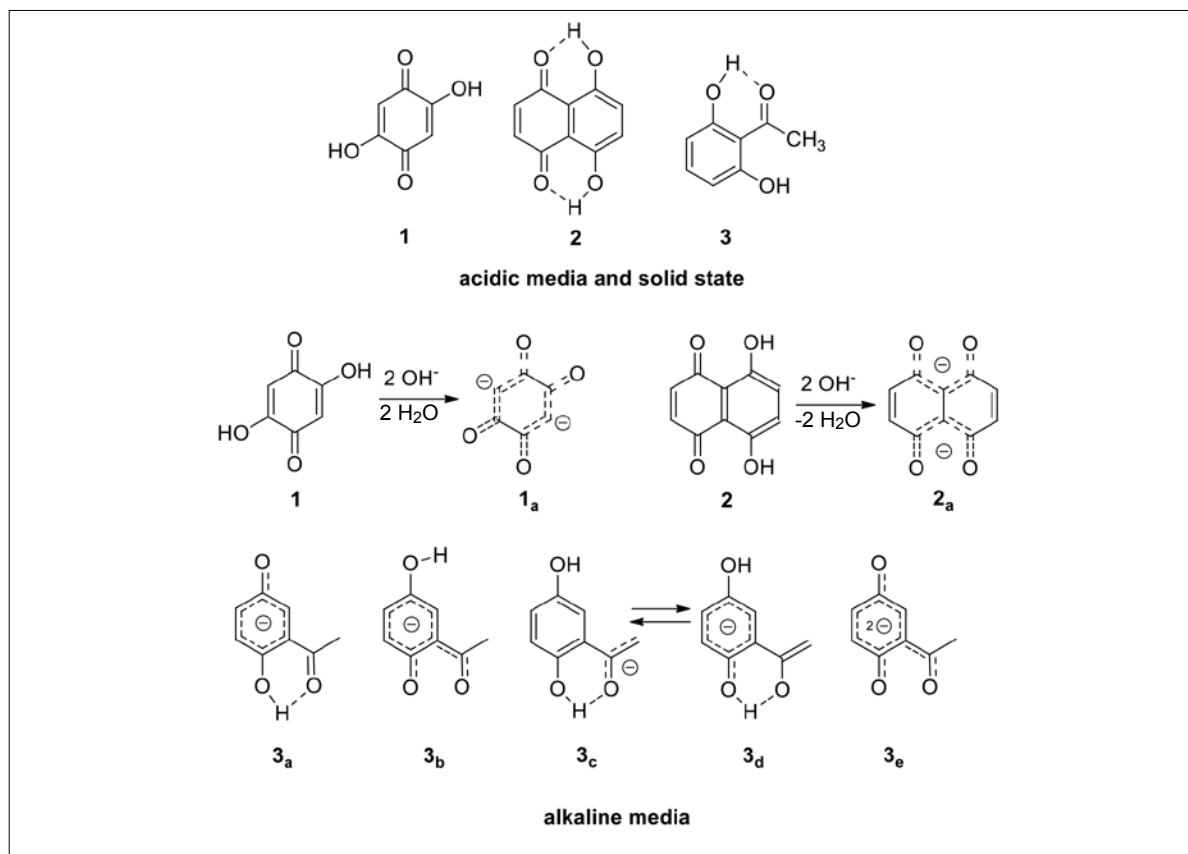
As a million tons per year industry, the pulp and paper industry is a key player in European economies and holds the potential for the development of environmentally benign and sustainable consumer products. For the industry highest product brightness is the goal, ensured by extensive bleaching. Cellulose-based products are also supposed to stay white over time and show as little ageing (yellowing) as possible. However, maximum brightness comes with a downside: oxidative, hydrolytic and thermal stress inflicted on the polysaccharide raw material, caused by the extensive use of bleaching chemicals. The connection between damages in the polysaccharide and the formation of colored molecules that reduce brightness was established in the seventies by Theander and his co-workers. The group described how chemical stress can cause aliphatic carbohydrates to form aromatic structures even without the presence of any lignin [1,2,3,4,5,6,7]. Some of these aromatics have a yellow tint themselves,

and further oxidation leads to additional chromophoric compounds. Recently, the link between the chromophore precursor hexeneuronic acid (4-deoxy-β-L-threo-hex-4-enopyranosiduronic acid, HexA) found in glucuronoxylan-containing cellulosic pulps (hardwood) and cellulosic key chromophores was established [8,9,10].

To reveal the nature of chromophores commonly found in pulp and paper, the chromophore release and identification method (CRI) was developed. CRI is therefore an analytical method specifically targeting cellulosic chromophores. The CRI method is based on application of a Lewis acid and a reductant (BF₃·2 HOAc/Na₂SO₃) by which chromophores can be released from pulp and separated by common analytical techniques. Typically, these chromophores are present in remarkably low amounts which range from ppm to ppb. Although present in such small amounts, their high extinction coefficients in the VIS region is the reason they give a

yellow tint to cellulose products that is immediately recognizable by the human eye. The CRI method has been applied to a manifold of cellulose products, among them lignin free cellulosic materials, such as aged cotton or aged bacterial cellulose. CRI revealed that cellulosic chromophores belong to three compound classes: hydroxy-[1,4]-benzoquinones, hydroxy-[1,4]-naphtho-

quinones, and hydroxy-acetophenones. Within these three classes, three structures were isolated that together make up about 80% of the total chromophore mass (Scheme 1): 2,5-dihydroxy-[1,4]-benzoquinone (1), 5,8-hydroxy-[1,4]-naphthoquinone (2), and 2,5-dihydroxyacetophenone (3). These three compounds are thus regarded as key chromophores [11,12,15].



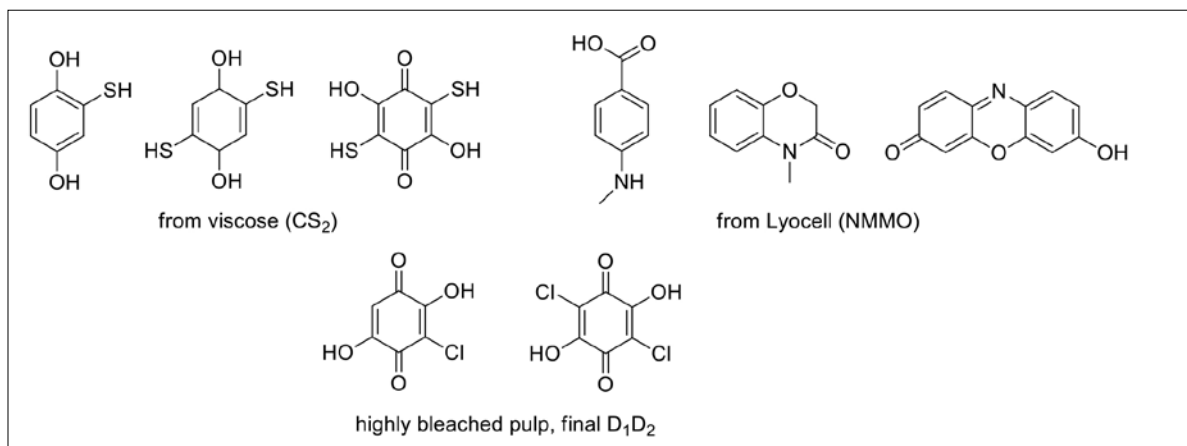
Scheme 1: The key chromophores 2,5-dihydroxy-[1,4]-benzoquinone (1), 5,8-hydroxy-[1,4]-naphthoquinone (2), and 2,5-dihydroxyacetophenone (3). Hydrogen bonds present in solid state and acidic media are formed between carbonyl oxygens and the H-atom in OH moieties are marked by dashed lines. In alkaline media, deprotonation results in the anions **1a** from **1**, **2a** from **2** and **3a-3e** from **3**.

Chromophores found in pulp and paper can be subdivided into primary chromophores and secondary chromophores. A primary chromophore is formed from the polysaccharide by oxidative and hydrolytical stress during bleaching or aging (see Scheme 1); in secondary chromophores, however, part of the solvent or process chemicals are found incorporated into the chromophore. From that we can conclude that secondary chromophores are dependent on the underlying process; for example, in chromophores found in the spinning bath of viscose solutions, sulfur atoms originating from CS₂ can be found, as well as motifs from the solvent NMMO, or chlorine atoms after a D-stage; see Scheme 2 for details [13,14,15,53].

Although the CRI method allowed to identify the most common cellulosic key chromophore, its down-

side is the large amount of sample needed and its inability to be automated. Improvements in the analysis of cellulosic chromophores have been made by implementing the ambient ionization techniques DESI (desorption electrospray ionization), PS (paper spray), and derivatization methods simpler than the CRI method that allow detection by GC-ECD (electron capture detection) and EI-GC-MS (electron ionization) with limits of detection as low as 60 ng chromophore/g cellulose [16,17].

Besides their strong color, further important characteristics of cellulosic chromophores are their high stabilization that roots in H-bonding in acid and solid state and resonance stabilization in alkaline media (Scheme 1) [18,19,20]. The latter impedes an attack at a double bond, the mode of action of many oxidizers.



Scheme 2: Various types of secondary chromophores where functional groups of solvent molecules can be found incorporated into the chromophores (CS_2 or NMMO). The same is possible for the bleaching chemical, as in the presented case of ClO_2 bleaching.

Bleaching studies using the neat chromophores in set-ups mimicking industrial bleaching are a powerful tool to optimize bleaching sequences and the use of bleaching chemicals, and to achieve the economically and environmentally most sustainable product bright-

ness. Bleaching studies were performed with the key chromophores DHBQ, DHNQ, 2,5-DHAP, and 2,6-DHAP (4) and the most used bleaching agents H_2O_2 , O_3 and ClO_2 . An overview of the bleaching scheme is given in Figure 1.

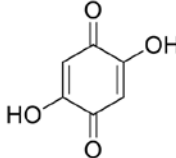
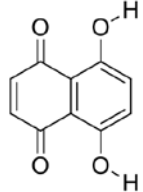
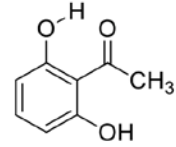
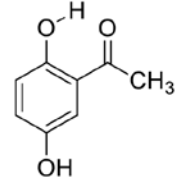
| |  |  |  |  |
|--|---|---|--|---|
| | DHBQ (1) | DHNQ (2) | 2,5-DHAP (3) | 2,5-DHAP (4) |
| H_2O_2 | pH 10, UV/VIS kinetics, GC-MS and NMR for degradation product analysis | | | |
| O_3 | pH 2 mixture of $\text{H}_2\text{O}/\text{MeOH}$, chromophores dissolved*, UV/VIS kinetics, GC-MS and NMR for degradation product analysis | | | |
| ClO_2 | pH 3, wherever possible UV/VIS kinetics [†] , GC-MS and NMR for degradation product analysis | | | |
| *as opposed to high shear mixing as applied in the industrial Z-stage | | | | |
| [†] measuring UV/VIS kinetics is impeded by the similar VIS absorption of ClO_2 and chromophore in some cases (2,5-DHAP, 2,6-DHAP) | | | | |

Figure 1: Overview of the bleaching experiments performed with the chromophores 1-4 and the bleaching agents H_2O_2 , O_3 , and ClO_2 .

Results and discussion

Peroxide bleaching

Hydrogen peroxide (H_2O_2) is applied in P-stages in industrial bleaching. Among its advantages are its easy storability and its harmless decomposition products, water and oxygen. When H_2O_2 bleaching, corresponding to an industrial P-stage was applied to the chromophores 1-4, the observed kinetics were of pseudo first order throughout (linear correlation of $\ln[c]$ vs. time) [23,21,22]. Typical degradation curves obtained from

H_2O_2 bleaching with large excesses of peroxide (see Table 1 for details) are presented together with Arrhenius plots in Figure 2 [23]. Arrhenius plots are constructed from temperature variation while keeping the peroxide content constant and are needed to calculate activation energy E_a , activation parameters and the reaction constant k . E_a and k are crucial when investigating the bleaching behavior of chromophores. E_a represents how “hindered” or “approachable” a chemical reaction is, as it is the energy barrier that has to be overcome in order for the reaction to take place.

As a rule of thumb, chemical reactions with activation energies >25 kcal/mol are not likely to take place at room temperature and would need catalysis or heating of the reaction mixture. In our case, the observed activation energies were below this threshold. The reaction rate constant k , on the other hand, is a parameter that represents the speed at which a chemical reaction takes place. It is temperature dependent, thus for

industrial bleaching we should keep in mind that the higher the temperature and the higher k , the faster the reaction; a fact that we also observed in our H_2O_2 bleaching experiments.

Reaction conditions, activation parameters, activation energy $E_a(\text{exp})$ as calculated from Arrhenius plots of the peroxide bleaching of DHBQ, DHNQ, 2,5-DHAP, and 2,6-DHAP are presented in Table 1.

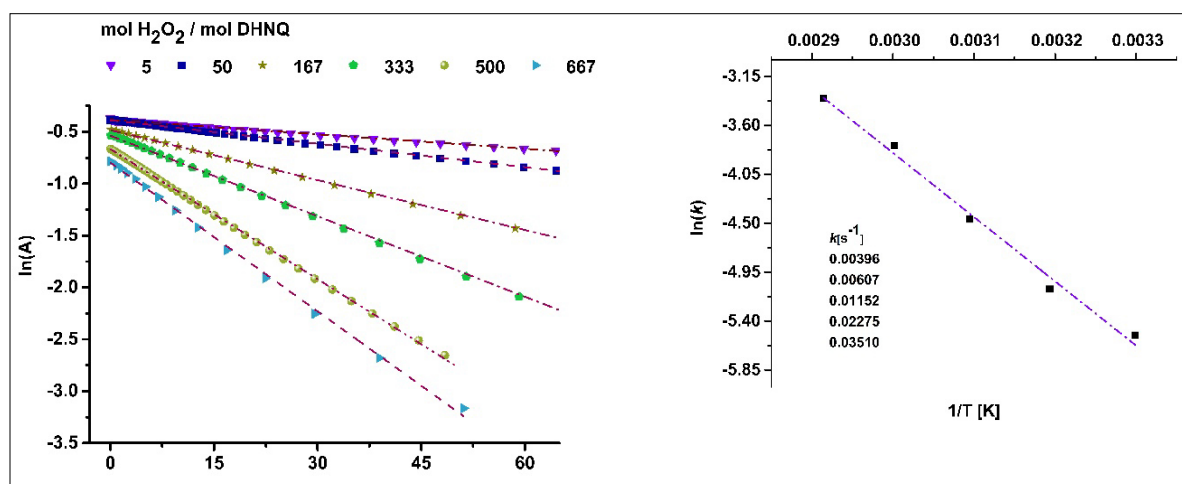


Figure 2: H_2O_2 degradation of DHNQ. Left: $\ln(A)$ vs. time with various excesses of peroxide. The dashed line represent the linear fit. Right: Arrhenius plot constructed from the data obtained by temperature variation from 30 °C to 70 °C while keeping the excess peroxide constant at 100 mol H_2O_2 / 1 mol DHNQ. k -values correspond to the temperatures 30-70 °C. Graphs adapted from reference [23].

Table 1: Parameters of bleaching experiments performed with the chromophores DHBQ, DHNQ, 2,5-DHAP, and 2,6-DHAP and H_2O_2 [23,21].

| Chromophore | Molar excess of peroxide relative to chromophore | Activation energy [kcal / mol] | k [s ⁻¹] and temperature range [°C] |
|-------------|--|--------------------------------|---|
| DHBQ | 257 | 16.1 | 0.00064-0.0261 5-50 |
| DHNQ | 5-667 | 11.7 | 0.00396-0.0351 30-70 |
| 2,5-DHAP | 100 -1100 | 8.79 | 0.0011-0.0060 36-80 |
| 2,6-DHAP | 100 -1100 | 10.60 | 0.0034-0.0245 36-80 |

Ozone bleaching

Ozone is used increasingly in the pulp and paper industry. Although ozone is harmful for most organisms, the environmental concerns over its use are still lower than in the case of chlorine-based bleaching agents. That is mainly due to its harmless degradation product oxygen. Ozone's reaction with double bonds has been the subject of many studies. First suggestions on the mechanism by Criegee were followed by extensive computational and analytical studies on the complexes and ozonides formed during ozonolysis [25,26,27,28, 29,30,31,32,33,34,35,36,37,38,39,40]. In pulp bleaching, the formation of different radical species and other oxidative species, for example $\bullet OH$ and H_2O_2 , have to be taken into account. Radicals like $\bullet OH$ can damage the polysaccharide and result in lower

viscosity. This process is dependent on the pH applied and other factors, such as temperature and metal ions present. These chemical reactions can be used to one's advantage, as they allow to tailor the viscosity of a cellulose product according to purpose [24,41,42,43, 44,45,46,47]. The reactivity of ozone towards polysaccharide-derived key chromophores 1-4 was investigated by dissolving them at pH 2 with the aid of co-solvent (MeOH), sampling before and during the bleaching and subsequent VIS measurements. Degradation products were analyzed by GC-MS and NMR measurements. The ozone load was 0.021 g O_3 /l and the gas flow of 50 l/h, bleaching was performed at room temperature. An overview of the bleaching conditions applied is given in Table 2.

Table 2: Chromophore amounts, solvent composition and volumes of chromophore solutions used in ozone bleaching experiments, as well as total bleaching time until decoloration.

| Chromophore | Amount [mg] | Concentration [mmol/l] | H ₂ O (pH 2, H ₂ SO ₄) [ml] | MeOH [ml] | Total bleaching time [s] |
|-------------|-------------|------------------------|---|-----------|--------------------------|
| 1 | 184 | 4.378 | 290 | 10 | 480 |
| 2 | 52 | 0.912 | 200 | 100 | 900 |
| 3 | 187 | 4.083 | 200 | 100 | 360 |
| 4 | 185 | 4.026 | 300 | 50 | 480 |

Ozone bleaching results were promising: Although in some cases the formation of a colored intermediate was observed (DHNQ, 2,6-DHAP), all chromophores could be fully degraded – see Figure 3 for degradation curves obtained from VIS measurements. As visible from the curves of the O₃ degradation of chromophores,

there is no defined reaction order immediately derivable from the graphs. In this case, the activation energy E_a cannot be calculated from VIS measurements. Although the activation energies of O₃ could not be calculated, it was possible to compare the chromophores among each other, as presented in Table 3.

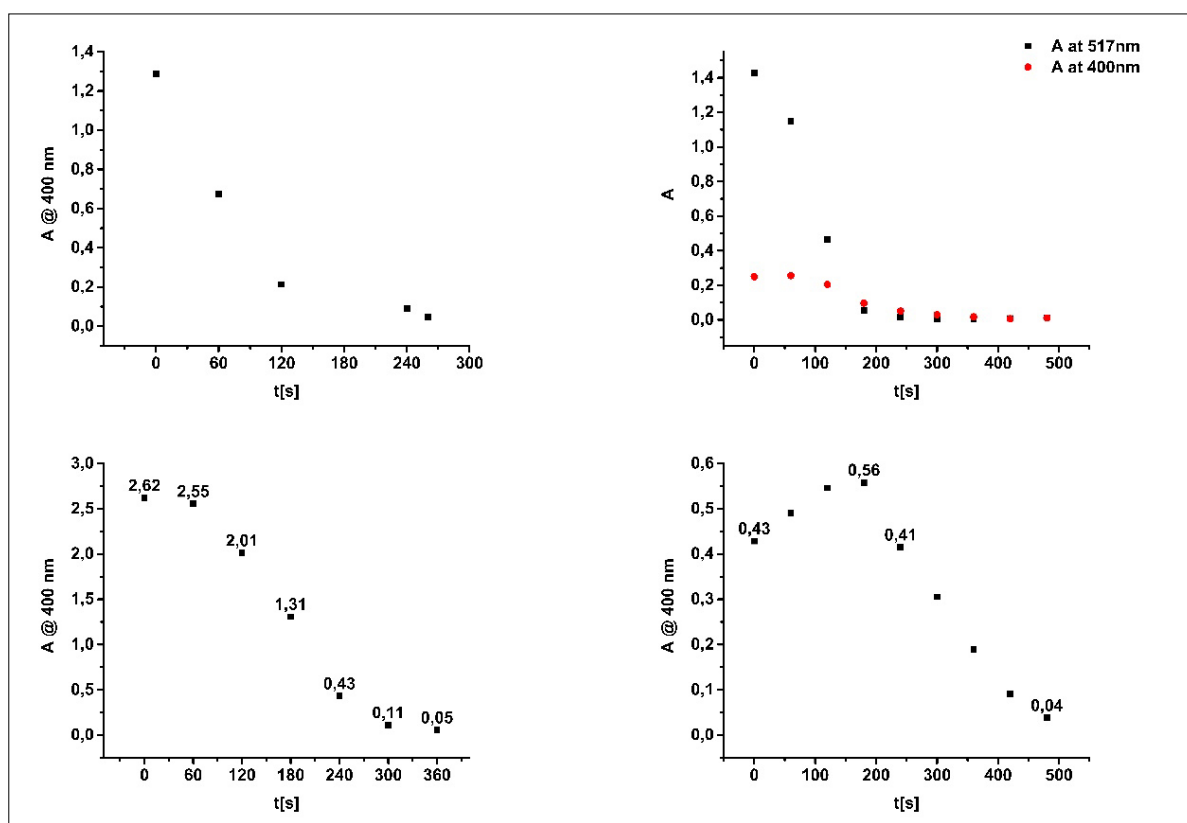


Figure 3: Kinetic analyses from ozone bleaching experiments of the cellulosic chromophores DHBQ, DHNQ, 2,5-DHAP, and 2,6-DHAP. The absorption at 400 nm is displayed and in case of DHNQ additionally also at 517 nm where the formation of a colored intermediate was observed in the full spectra from 200 to 700 nm.

Table 3: Comparison of the time until full decoloration of chromophore solutions in ozone bleaching.

| | | | |
|-------------|-------|-------------|-------|
| Chromophore | t [s] | Chromophore | t [s] |
| 2-OH-NQ | 203 | DHBQ | 386 |
| 2,5-HAP | 293 | DHNQ | 1843 |
| 2,6-HAP | 367 | | |

DHNQ and DHBQ showed to be the most resistant to ozone bleaching, an observation that matches their chemical behavior: in H_2O_2 , these two chromophores had the highest activation energies (16.1 and 11.7 kcal / mol, respectively) [21,23]; their high thermodynamic stability is discussed in references 18 and 19.

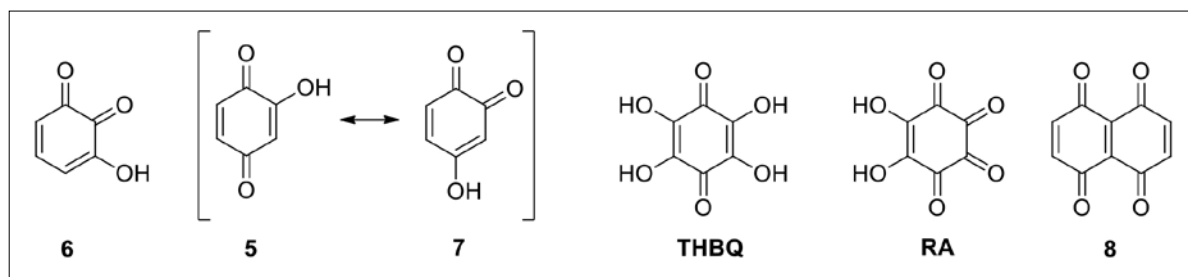
Chlorine dioxide

Although chlorine dioxide is a very strong oxidant and known for its high reactivity [48,49,50,51,52] and selectivity – it leaves the polysaccharide largely unharmed but targets lignin – in pulp bleaching its behavior towards chromophores showed to be less “straightforward” than for example it is the case with H_2O_2 . When the reactivity of ClO_2 with the key chromophore DHNQ was assessed, VIS measurements revealed that DHNQ is re-formed in the case of the reaction of ClO_2 molar equivalents (referring to moles DHNQ) are less than 5. A peculiar behavior is also reported from ClO_2 and DHBQ, where several colored intermediates are formed in the course of the oxida-

tion reaction. Colored intermediates are found in most bleaching reactions, although sometimes we can only speculated about their nature.

Colored intermediates

In ozone bleaching, VIS measurements revealed the formation of colored intermediates for some chromophores (DHNQ and 2,6-DHAP); similar observation were made in H_2O_2 and ClO_2 bleaching. These intermediates can have VIS absorptions comparable to or higher than the parent chromophore. Their structure is not always known, and usually, colored intermediates are degradable by the bleaching agent that initially caused their formation; however, the fact that they exist also emphasizes the importance of at least 200 molar excesses in peroxide bleaching and > 5 molar excessed for ClO_2 (in case of O_3 no such description can be made) and also points out the importance of adequate mixing during the bleaching process. Examples for such colored intermediates are presented in Scheme 3.



Scheme 3: Quinones 5, 6 and 7 from 2,6-DHAP and 2,5-DHAP from peroxide bleaching, respectively; tetrahydroxy benzoquinone (THBQ) and rhodizonic acid (RA) from the ClO_2 bleaching of DHBQ, 1,4,5,8-naphthalenetetrone (8) from P-stage bleaching of DHNQ as examples for chromophore intermediates formed during pulp bleaching [53].

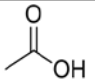
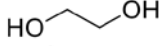
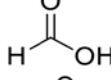
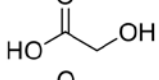
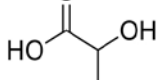
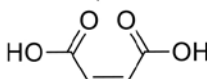
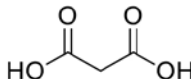
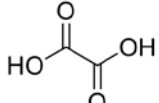
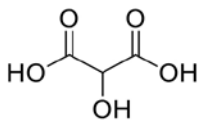
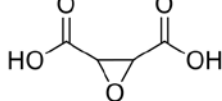
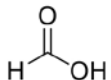
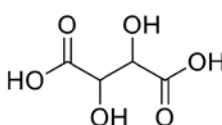
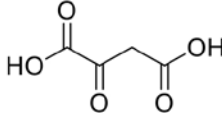
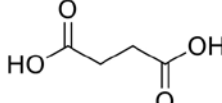
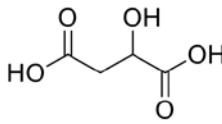
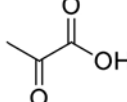
Final degradation products found in chromophore bleaching

When bleaching chromophore solutions, the application of H_2O_2 , O_3 , or ClO_2 results in large similar degradation products, which are the gaseous CO_2 and carboxylic acids. Table 4 gives an overview of the found degradation products and the bleaching methods applied.

We were pleased to observe that, besides the formation of colored intermediates, all found final degra-

dation products were colorless. The substances were in good agreement with literature reports on similar experiments. Additionally, it should be pointed out that the small amounts of carboxylic acids generated from chromophore degradation should not cause any fluctuation of pH, scaling or sedimentation. If that is the case during industrial processes, other causes than the chromophore degradation should be considered.

Table 4: Overview of carboxylic acids found in chromophore bleaching as determined by GC-MS and NMR measurements of the reaction mixtures.

| Structure | Substance name | Found in (bleaching method) |
|---|-------------------------------|---|
|  | Acetic acid | O ₃ , H ₂ O ₂ , ClO ₂ |
|  | Ethylene glycol | O ₃ |
|  | Formic acid | O ₃ |
|  | Glycolic acid | O ₃ , ClO ₂ |
|  | Lactic acid | O ₃ |
|  | Maleic acid | O ₃ , H ₂ O ₂ , ClO ₂ |
|  | Malonic acid | O ₃ , H ₂ O ₂ |
|  | Oxalic acid | O ₃ , H ₂ O ₂ , ClO ₂ |
|  | Tartronic acid | O ₃ , ClO ₂ |
|  | 2,3-Oxirane dicarboxylic acid | O ₃ , H ₂ O ₂ |
|  | Formic acid | H ₂ O ₂ |
|  | Tartaric acid | H ₂ O ₂ |
|  | Oxaloacetic acid | H ₂ O ₂ |
|  | Succinic acid | H ₂ O ₂ , ClO ₂ |
|  | Malic acid | ClO ₂ |
|  | Pyruvic acid | ClO ₂ |

Conclusions

Experimental investigations of chromophore bleaching were performed under conditions similar to industrial bleaching using H_2O_2 , O_3 , and ClO_2 and the cellulosic chromophores DHBQ, DHNQ, 2,5-DHAP, and 2,6-DHAP. In all cases it was possible to fully degrade the chromophores, but colored intermediates were observed in most bleaching reactions. To avoid chromophore (re)formation, the molecular excess of the bleaching agent should be around 200 molar equivalents referring to chromophore for H_2O_2 bleaching and at least 5 molar equivalents in the case of ClO_2 bleaching (for O_3 no values can be given) and the importance of homogeneity and adequate mixing is pointed out. We observed that for H_2O_2 temperatures above room temperature – we investigated up to 80 °C – are beneficial for the bleaching process. O_3 bleaching was performed in solution at room temperature. Literature states that O_3 bleaching benefits from lower temperatures due to the reduced formation of competing radical that damage the polysaccharide, but the temperature applied industrially certainly has to be a compromise of desired molecular weight of the final product and energy efficiency, as cooling and heating are energy demanding processes. Finally, all observed degradation products were colorless carboxylic acids or CO_2 .

Acknowledgements

The authors would like to thank the Austrian Research promotion Society (FFG, project 829443) for financial support.

References

- [1] Popoff, T.; Theander, O., Formation of aromatic compounds from carbohydrates. I. Reaction of D-glucuronic acid, D-galacturonic acid, D-xylose, and L-arabinose in slightly acidic, aqueous solution. *Carbohydr. Res.* 1972, 22 (1), 135-49.
- [2] Popoff, T.; Theander, O., Formation of aromatic compounds from carbohydrates. Part III. Reaction of D-glucose and D-fructose in slightly acidic, aqueous solution. *Acta Chem. Scand., Ser. B* 1976, B30 (5), 397-402.
- [3] Olsson, K.; Pernemalm, P. A.; Popoff, T.; Theander, O., Formation of aromatic compounds from carbohydrates. V. Reaction of D-glucose and methylamine in slightly acidic, aqueous solution. *Acta Chem. Scand., Ser. B* 1977, B31 (6), 469-74.
- [4] Olsson, K.; Pernemalm, P. A.; Theander, O., Formation of aromatic compounds from carbohydrates. VII. Reaction of D-glucose and glycine in slightly acidic, aqueous solution. *Acta Chem. Scand., Ser. B* 1978, B32 (4), 249-56.
- [5] Theander, O.; Westerlund, E., Formation of aromatic compounds from carbohydrates. VIII. Reaction of D-erythrose in slightly acidic, aqueous solution. *Acta Chem. Scand., Ser. B* 1980, B 34 (10), 701-5.
- [6] Theander, O.; Nelson, D. A.; Hallen, R. T., Formation of aromatic compounds from carbohydrates. X. Reaction of xylose, glucose, and glucuronic acid in acidic solution at 300°C. *Prepr. Pap. – Am. Chem. Soc., Div. Fuel Chem.* 1987, 32 (2), 143-7.
- [7] Nelson, D. A.; Hallen, R. T.; Theander, O., Formation of aromatic compounds from carbohydrates. Reaction of xylose, glucose, and glucuronic acid in acidic solution at 300°. *ACS Symp. Ser.* 1988, 376 (*Pyrolysis Oils Biomass*), 113-18.
- [8] Rosenau, T.; Potthast, A.; Zwirchmayr, N. S.; Hettegger, H.; Plasser, F.; Hosoya, T.; Bacher, M.; Krainz, K.; Dietz, T., Chromophores from hexeneuronic acids: identification of HexA-derived chromophores. *Cellulose (Dordrecht, Neth.)* 2017, 24 (9), 3671-3687.
- [9] Rosenau, T.; Potthast, A.; Zwirchmayr, N. S.; Hosoya, T.; Hettegger, H.; Bacher, M.; Krainz, K.; Yoneda, Y.; Dietz, T., Chromophores from hexeneuronic acids (HexA): synthesis of model compounds and primary degradation intermediates. *Cellulose (Dordrecht, Neth.)* 2017, 24 (9), 3703-3723.
- [10] Zwirchmayr, N. S.; Hosoya, T.; Hettegger, H.; Bacher, M.; Krainz, K.; Dietz, T.; Henniges, U.; Potthast, A.; Rosenau, T., Chromophores from hexeneuronic acids: chemical behavior under peroxide bleaching conditions. *Cellulose (Dordrecht, Neth.)* 2017, 24 (9), 3689-3702.
- [11] Rosenau, T.; Potthast, A.; Krainz, K.; Hettegger, H.; Henniges, U.; Yoneda, Y.; Rohrer, C.; French, A. D., Chromophores in cellulose, XI: isolation and identification of residual chromophores from bacterial cellulose. *Cellulose (Dordrecht, Neth.)* 2014, 21 (4), 2271-2283.
- [12] Rosenau, T.; Potthast, A.; Milacher, W.; Hofinger, A.; Kosma, P., Isolation and identification of residual chromophores in cellulosic materials. *Polymer* 2004, 45 (19), 6437-6443.
- [13] Adorjan, I.; Potthast, A.; Rosenau, T.; Sixta, H.; Kosma, P., Discoloration of cellulose solutions in N-methylmorpholine-N-oxide (Lyocell). Part 1: Studies on model compounds and pulps. *Cellulose (Dordrecht, Neth.)* 2005, 12 (1), 51-57.
- [14] Rosenau, T.; Potthast, A.; Milacher, W.; Adorjan, I.; Hofinger, A.; Kosma, P., Discoloration of cel-

- lulose solutions in N-methylmorpholine-N-oxide (Lyocell). Part 2: Isolation and identification of chromophores. *Cellulose (Dordrecht, Neth.)* 2005, 12 (2), 197-208.
- [15] Korntner, P.; Hosoya, T.; Dietz, T.; Eibinger, K.; Reiter, H.; Spitzbart, M.; Roeder, T.; Borgards, A.; Kreiner, W.; Mahler, A. K.; Winter, H.; Groiss, Y.; French, A. D.; Henniges, U.; Potthast, A.; Rosenau, T., Chromophores in lignin-free cellulosic materials belong to three compound classes. *Chromophores in cellulose, XII. Cellulose (Dordrecht, Neth.)* 2015, 22 (2), 1053-1062.
- [16] Schedl, A.; Korntner, P.; Zweckmair, T.; Henniges, U.; Rosenau, T.; Potthast, A., Detection of Cellulose-Derived Chromophores by Ambient Ionization-MS. *Anal. Chem. (Washington, DC, U. S.)* 2016, 88 (2), 1253-1258
- [17] Schedl, A.; Zweckmair, T.; Kikul, F.; Bacher, M.; Rosenau, T.; Potthast, A., Pushing the limits: Quantification of chromophores in real-world paper samples by GC-ECD and EI-GC-MS. *Talanta* 2018, 179, 693-699.
- [18] Hosoya, T.; French, A. D.; Rosenau, T., Chemistry of 5,8-dihydroxy-[1,4]-naphthoquinone, a key chromophore in aged cellulose. *Mini-Rev. Org. Chem.* 2013, 10 (3), 302-308.
- [19] Hosoya, T.; French, A. D.; Rosenau, T., Chemistry of 2,5-dihydroxy-[1,4]-benzoquinone, a key chromophore in aged cellulose. *Mini-Rev. Org. Chem.* 2013, 10 (3), 309-315.
- [20] Hosoya, T.; French, A. D.; Rosenau, T., Chemistry of 2,5-dihydroxyacetophenone, a Key Chromophore in Cellulosic Substrates. *Mini-Rev. Org. Chem.* 2015, 12 (1), 88-95.
- [21] Hosoya, T.; Rosenau, T., Degradation of 2,5-Dihydroxy-1,4-benzoquinone by Hydrogen Peroxide under Moderately Alkaline Conditions Resembling Pulp Bleaching: A Combined Kinetic and Computational Study. *J. Org. Chem.* 2013, 78 (22), 11194-11203
- [22] Hosoya, T.; Rosenau, T., Degradation of 2,5-Dihydroxy-1,4-benzoquinone by Hydrogen Peroxide: A Combined Kinetic and Theoretical Study. *J. Org. Chem.* 2013, 78 (7), 3176-3182.
- [23] Zwirchmayr, N. S.; Hosoya, T.; Henniges, U.; Gille, L.; Bacher, M.; Furtmueller, P.; Rosenau, T., Degradation of the Cellulosic Key Chromophore 5,8-Dihydroxy-[1,4]-naphthoquinone by Hydrogen Peroxide under Alkaline Conditions. *J. Org. Chem.* 2017, 82 (21), 11558-11565.
- [24] Ragnar, M. On the Importance of Radical Formation in Ozone Bleaching, *Kungliga Tekniska Högskolan*, 2000.
- [25] Gillies, J. Z.; Gillies, C. W.; Lovas, F. J.; Matsuura, K.; Suenram, R. D.; Kraka, E.; Cremer, D., Van der Waals complexes of chemically reactive gases: ozone-acetylene. *Journal of the American Chemical Society* 1991, 113 (17), 6408-6415.
- [26] Gillies, C. W.; Gillies, J. Z.; Suenram, R. D.; Lovas, F. J.; Kraka, E.; Cremer, D., Van der Waals complexes in 1,3-dipolar cycloaddition reactions: ozone-ethylene. *Journal of the American Chemical Society* 1991, 113 (7), 2412-2421.
- [27] Epstein, S. A.; Donahue, N. M., Ozonolysis of Cyclic Alkenes as Surrogates for Biogenic Terpenes: Primary Ozonide Formation and Decomposition. *J. Phys. Chem. A* 2010, 114 (28), 7509-7515.
- [28] Chuong, B.; Zhang, J.; Donahue, N. M., Cycloalkene Ozonolysis: Collisionally Mediated Mechanistic Branching. *Journal of the American Chemical Society* 2004, 126 (39), 12363-12373.
- [29] Vayner, G.; Addepalli, S. V.; Song, K.; Hase, W. L., Post-transition state dynamics for propene ozonolysis: Intramolecular and unimolecular dynamics of molozonide. *J. Chem. Phys.* 2006, 125 (1), 014317/1-014317/16.
- [30] Wheeler, S. E.; Ess, D. H.; Houk, K. N., Thinking Out of the Black Box: Accurate Barrier Heights of 1,3-Dipolar Cycloadditions of Ozone with Acetylene and Ethylene. *J. Phys. Chem. A* 2008, 112 (8), 1798-1807.
- [31] Kuczkowski, R. L., The structure and mechanism of formation of ozonides. *Chemical Society Reviews* 1992, 21 (1), 79-83.
- [32] Bernatek, E.; Moeskeland, J.; Valen, K., Ozonolysis of phenols. II. Pyrocatechol, resorcinol, and quinol. *Acta Chem. Scand.* 1961, 15, 1454-60.
- [33] Bernatek, E., Ozonolyses in the Naphthoquinone and Benzofuran Series. *Oslo Univ. Press*: 1960; p 144 pp.
- [34] Bernatek, E., Ozonolysis of naphthoquinones. I. Ozonolysis of 1,4-naphthoquinone in chloroform. *Tetrahedron* 1958, 4, 213-22.
- [35] Bernatek, E., The ozonization of p-benzoquinone. *Acta Chem. Scand.* 1954, 8, 1943.
- [36] Bernatek, E.; Straumsgard, K. A., Ozonolysis of p-benzoquinone. II. *Acta Chem. Scand.* 1959, 13, 178-85.
- [37] Pillar, E. A.; Guzman, M. I., Oxidation of Substituted Catechols at the Air-Water Interface: Production of Carboxylic Acids, Quinones, and Polyphenols. *Environmental Science & Technology* 2017, 51 (9), 4951-4959.
- [38] Geletneky, C.; Berger, S., The Mechanism of Ozonolysis Revisited by 17O-NMR Spectroscopy. *European Journal of Organic Chemistry* 1998, 1998 (8), 1625-1627.

- [39] Criegee, R., Mechanism of Ozonolysis. *Angewandte Chemie International Edition in English* 1975, 14 (11), 745-752.
- [40] Ragnar, M.; Eriksson, T.; Reitberger, T.; Brandt, P., A new mechanism in the ozone reaction with lignin-like structures. *Holzforschung* 1999, 53 (4), 423-428.
- [41] Pi, Y.; Zhang, L.; Wang, J., The formation and influence of hydrogen peroxide during ozonation of para-chlorophenol. *J. Hazard. Mater.* 2007, 141 (3), 707-712.
- [42] Buehler, R. E.; Staehelin, J.; Hoigne, J., Ozone decomposition in water studied by pulse radiolysis. 1. Perhydroxyl (HO_2)/hydroperoxide (O_2^-) and HO_3/O_3^- as intermediates. *The Journal of Physical Chemistry* 1984, 88 (12), 2560-2564.
- [43] Gierer, J., Formation and involvement of superoxide (O_2^-/HO_2) and hydroxyl ($\text{OH}\cdot$) radicals in TCF bleaching processes. A review. *Holzforschung* 1997, 51 (1), 34-46.
- [44] Chirat, C.; Lachenal, D., Effect of Hydroxyl Radicals in Ozone Bleaching. *Holzforschung* 1997, 51 (2), 147-154.
- [45] Pouyet, F.; Lachenal, D.; Das, S.; Chirat, C., Minimizing viscosity loss during totally chlorine-free bleaching of hardwood kraft pulp. *Bio Resources* 2013, 8 (1), 238-249, 12 pp.
- [46] Chirat, C.; Lachenal, D., Effect of ozone on pulp components. Application to bleaching of kraft pulps. *Holzforschung* 1994, 48 (Suppl.), 133-9.
- [47] Chirat, C.; Lachenal, D., Other ways to use ozone in a bleaching sequence. *Tappi J.* 1997, 80 (9), 209-214.
- [48] Leigh, J. K.; Rajput, J.; Richardson, D. E. Kinetics and Mechanism of Styrene Epoxidation by Chlorite: Role of Chlorine Dioxide. *Inorg. Chem.* 2014, 53, 6715-6727.
- [49] Aguilar, C. A. H.; Narayanan, J.; Singh, N.; Thangarasu, P. Kinetics and mechanism for the oxidation of anilines by ClO_2 : a combined experimental and computational study. *J. Phys. Org. Chem.* 2014, 27, 440-449.
- [50] Lehtimaa, T.; Kuitunen, S.; Tarvo, V.; Vuorinen, T., Reactions of aldehydes with chlorous acid and chlorite in chlorine dioxide bleaching. *Holzforschung* 2010, 64, 555-561.
- [51] Napolitano, M. J.; Green, B. J.; Nicoson, J. S.; Margerum, D. W., Chlorine Dioxide Oxidations of Tyrosine, N-Acetyltyrosine, and Dopa. *Chem Res Toxicol* 2005, 18, 501-508.
- [52] Hull, L. A.; Davis, G. T.; Rosenblatt, D. H.; Williams, H. K. R.; Weglein, R. C., Oxidations of amines. III. Duality of mechanism in the reaction of amines with chlorine dioxide. *J. Am. Chem. Soc.* 1967, 89, 1163-70.
- [53] Hettegger, H.; Hosoya, T.; Rosenau, T., Chemistry of the Redox Series from Hexahydroxybenzene to Cyclohexanehexanone. *Curr. Org. Synth.* 2016, 13 (1), 86-100.

Cellulose Carboxylate/Tosylate Mixed Esters: Dependence of their Physicochemical Properties on the Degree of Carboxylate Substitution

Daniela C. Ferreira,^{1,2} Gustavo S. Bastos,¹ Annett Pfeiffer,³ Denise F. S. Petri,² Thomas Heinze,^{3*} and Omar A. El Seoud^{2*}

¹ Institute of Chemistry, the University of São Paulo, Prof. Lineu Prestes Av., 748, 05508-000, São Paulo, SP; * Contact: elseoud.usp@gmail.com

² Institute for Technological Research of the State of São Paulo S.A., Laboratory of Pulp and Paper, Prof. Almeida Prado Av., 532, 05508-901, São Paulo, SP, Brazil

³ Centre of Excellence for Polysaccharide Research, Institute of Organic and Macromolecular Chemistry, Friedrich Schiller University of Jena, Humboldtstraße 10, D-07743, Jena, Germany; * Contact: Thomas.Heinze@uni-jena.de

Abstract

The dependence of the physicochemical properties of cellulose carboxylate/tosylate mixed esters on their molecular structures is reported. The esters employed have a constant degree of substitution (DS) of the tosyl group, $DS_{Tosyl} = 0.98$ and variable DS of the ester group, DS_{Acyl} (ester = acetate, butanoate, hexanoate). These mixed esters do not exhibit glass transition temperatures and decompose before melting. Using perichromic dyes and contact angle measurements of their films, the dependence of the following properties on DS_{Acyl} were investigated: empirical polarity, Lewis acidity and basicity, and hydrophobicity. Most of these properties display a simple dependence on DS_{Acyl} , which reflects the conversion of the hydroxyl- into ester group. These mixed esters were regenerated as uniform microspheres from their solutions in acetone; their adsorption of methylene blue and Sudan IV dyes was studied, and the dye adsorption data correlate with the Lewis basicity and the dispersive component of surface energy.

Keywords: cellulose mixed ester; cellulose carboxylate/tosylate, thermal analysis, perichromic indicator, contact angle; microspheres, dye absorption.

Introduction

The impetus for studying cellulose derivatives with mixed functionalities is that their properties are different, sometimes better compared to the corresponding derivatives with one functionality. For example, mixed carboxylic esters, e.g., cellulose acetate/propionate, acetate/butanoate, and acetate/phthalate have properties (luster, hardness) better than simple esters, e.g., cellulose acetate, propionate and phthalate, probably because of the juxtaposition of both acyl moieties in the same anhydro-glucose unit (AGU). Cellulose mixed esters are employed in sheeting, molding plastics, film products, lacquer and melt dip coatings, and controlled drug release [1-3].

Most research was carried out on mixed esters of C₂-C₄ carboxylic acids. Cellulose carboxylate/tosylate mixed esters (Cell-carboxylate/tosylate) carry strongly dipolar groups (C=O and S=O) with different basicities and a polarizable aromatic ring. Additionally, introduction of sulphur as a substituent into cellulose decreases the decomposition temperature of the derivative, and suppresses its flaming combustion by reducing the amount of flammable volatile products produced on thermal degradation [4].

It is expected that the presence of different functionalities and the control of the degree of substitution (DS) allows the modulation of physicochemical properties

of Cell-carboxylate/tosylate. This increases their potential use in applications where acid-base and hydrophobic interactions are important, e.g., immobilization of biomacromolecules by adsorption. The fact that the tosylate is a good leaving group allows the preparation of novel deoxy-cellulose derivatives containing halogen atoms [5] or amino groups [2]. Moreover, some of these mixed esters can be processed by extrusion from the melt; form films by casting from their solutions in organic solvents; and microspheres by precipitation in water [6,7].

Recently, we synthesized a series of Cell-carboxylate/tosylate mixed esters by acylation of cellulose tosylate with carboxylic acid anhydrides (acetic-, butanoic- and hexanoic anhydride) as shown in Figure 1. The starting cellulose tosylate had a (fixed) $DS_{Tosyl} = 0.98$ and the final mixed esters had $DS_{Ac} = 0.37-1.50$ (acetates), $DS_{Bu} = 0.39-0.92$ (butanoates), and $DS_{Hx} = 0.26-1.05$ (hexanoate). We casted these mixed esters as films; determined their empirical polarity by a perichromic

dye, and regenerated them from acetone solutions as microspheres with narrow size distribution [7].

In the present work, we examined in details some physicochemical properties of these esters that are relevant to applications. In particular, we wanted to correlate the above-mentioned properties with the structural variable across the series, i.e., DS_{Acy} , and between the three esters series (acetates, butanoates, and hexanoates) at comparable DS_{Acy} . We determined Lewis acidity and basicity of their films by using perichromic dyes, *vide infra*, and extracted information about film hydrophobicity and surface energy from contact angle measurements. All examined properties showed simple dependence (linear or not) on DS_{Acy} . The properties of the films are affected by the acid-base affinity of carbonyl ($RCO-$), modulated by steric effects of the alkyl group ($RCO-$). We found that dye adsorption efficiency by microspheres of these mixed esters is related to their Lewis basicity and the dispersive component of surface energy.

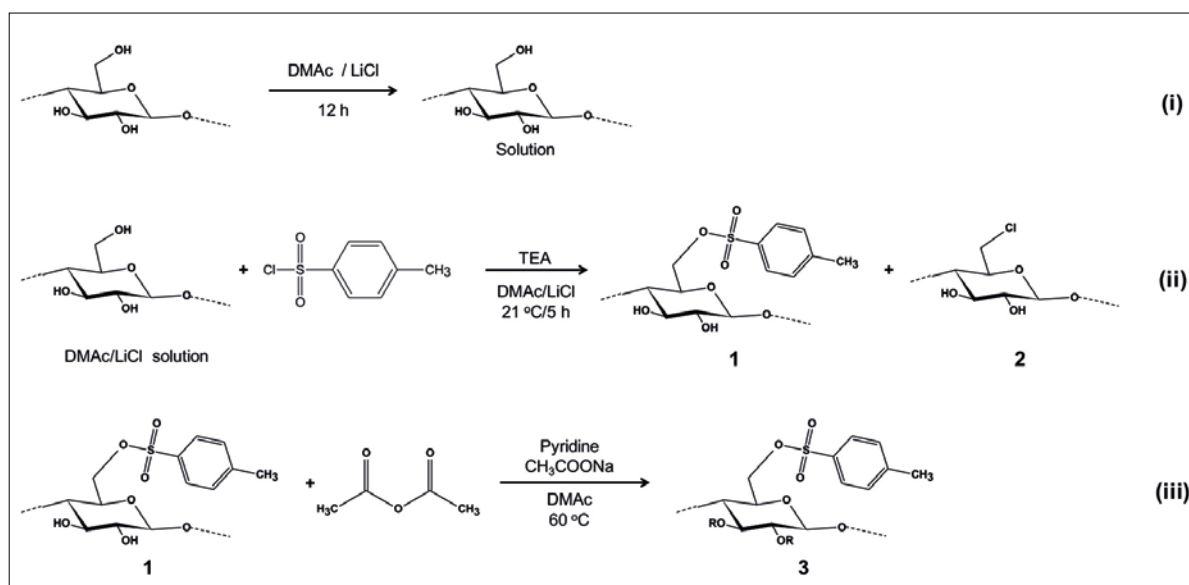


Figure 1: Scheme of cellulose acetate/tosylate synthesis: (i) microcrystalline cellulose (MCC) dissolution in *N,N*-dimethylacetamide (DMAc)/LiCl; (ii) tosylation of cellulose, and (iii) acetylation of cellulose tosylate, where $R = H$ in unsubstituted hydroxyl or CH_3CO in cellulose acetate/tosylate. We depict: 1 = cellulose tosylate; 2 = cellulose deoxy-chloro (side product $DS_{Cl} = 0.03$ to 0.07), and 3 = cellulose acetate/tosylate [7].

Experimental

Chemicals

The chemicals were purchased from Sigma-Aldrich or Merck and were purified as recommended elsewhere [8]. The compounds 5-nitroindoline (NI); β -carotene, methylene blue (MB), and Sudan IV (SU-IV) are commercial. The perichromic probes 2,6-dichloro-4-(2,4,6-triphenylpyridium-1-yl) (WB), *o*-*tert*-butylstilbazolium betaine (TBSB), *o,o'*-di-*tert*-butylstilbazolium betaine

(DTBSB), 1-methyl-5-nitroindoline (MNI) and 2-(*N,N*-dimethylamino)-7-nitro-9-*H*-fluorene (DMANF) were available from previous studies [9,10]. The molecular structure of the dyes employed in the present work is shown in Figure 2.

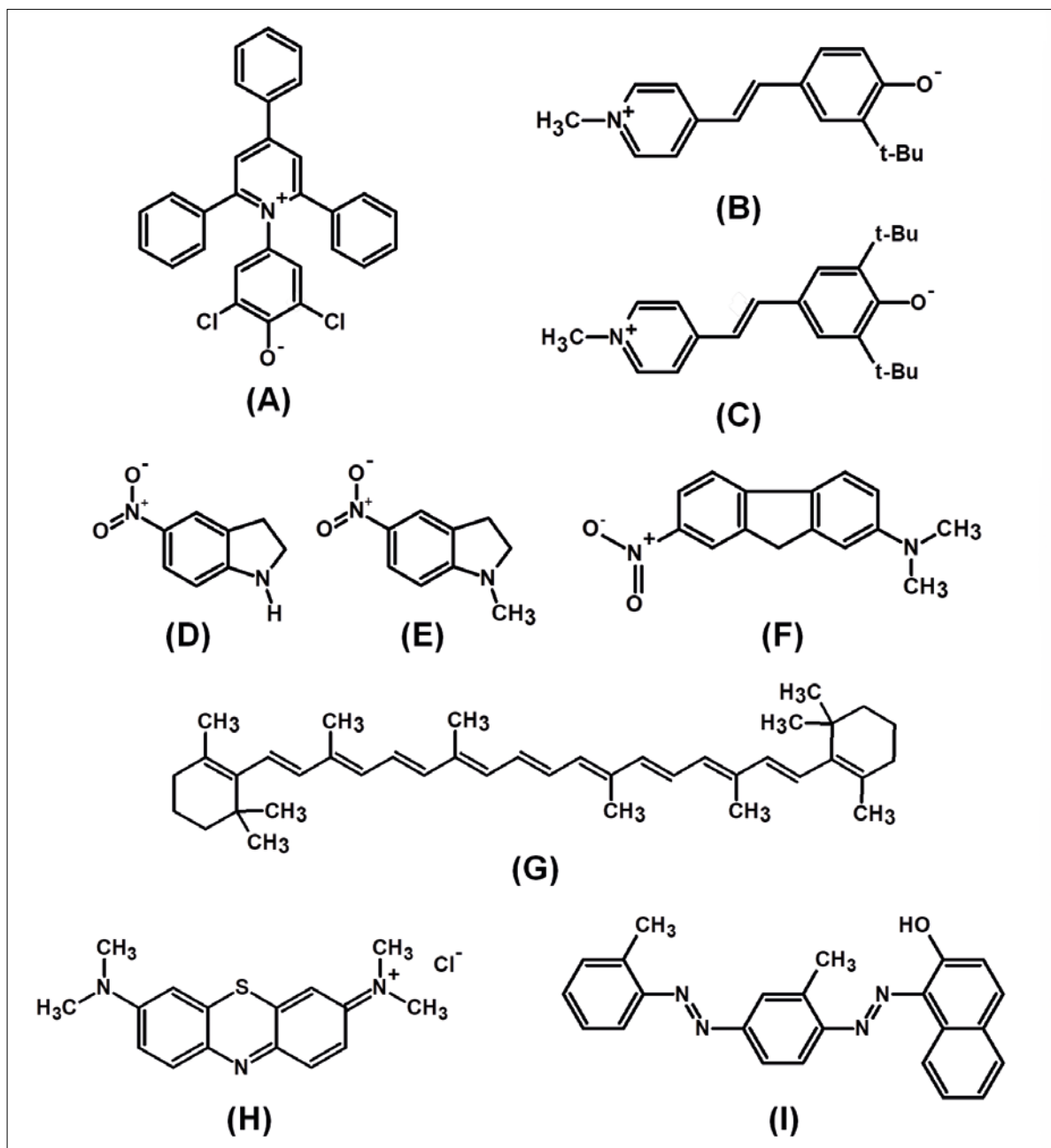


Figure 2: Molecular structures of perichromic probes and dyes employed in the present work. (A) 2,6-dichloro-4-(2,4,6-triphenylpyridinium-1-yl)phenolate (WB); (B) *o*-*tert*-butylstilbazolium betaine (TBSB); (C) *o,o'*-*di-tert*-butylstilbazolium betaine (DTBSB); (D) 5-nitroindoline (NI); (E) 1-methyl-5-nitroindoline (MNI); (F) 2-(*N,N*-dimethylamine)-7-nitro-9*H*-fluorene (DMANF); (G) β -carotene; (H) methylene blue and (MB); (I) Sudan IV (SU-IV).

Cellulose Carboxylate/ Tosylate Mixed Esters

The cellulose carboxylate/tosylate mixed esters that we employed were those available from our previous study, see Figure 1 [7].

Equipments

The following equipment were employed: UV-VIS reflectance spectra of cellulose mixed ester films, Shimadzu UV-2550, UV-VIS spectrophotometer equip-

ped with model IST-204A reflectance accessory; TGA curves, TA instruments Q50 thermo-balance; DSC curves, TA Instruments Q20; TG-MS, Netzsch STA 490 PC Luxx thermo-analyzer coupled to Aëlos QMS 403C mass-spectrometer; contact angle, Surface Electro Optics, model Phoenix-i.

Measurements

Thermal Analysis

To obtain the DSC curves of cellulose mixed esters, we weighted ca. 3 mg of each sample in a sealable aluminum crucible; the latter was sealed and heated at 10 K/min, under a dynamic nitrogen atmosphere (100 mL/min). First, we annealed each sample by heating from 25 °C to 220 °C; cooled it to 25 °C, then heated it again. The DSC cell was calibrated by using Indium (*m.p.* 156.6 °C; $\Delta H_{\text{fusion}} = 28.42 \text{ J/g}$) and Zinc (*m.p.* 419.6 °C; $\Delta H_{\text{fusion}} = 112.0 \text{ J/g}$).

For recording the thermogravimetric curves we heated ca. 5 mg sample contained in a platinum crucible from 25 °C to 400 °C, at heating rate of 10 K/min, under a dynamic nitrogen atmosphere, 50 mL/min. We calculated the decomposition temperature (T_{Decomp}) from the first derivative of thermogravimetric curve, and analyzed the gases liberated during sample decomposition by mass spectrometry.

Determination of Surface Properties of Cellulose Mixed Esters Films by Perichromic Probes

Films of cellulose tosylate and Cell-carboxylate/tosylate containing the perichromic dyes shown in Figure 2 were prepared as describe previously [7]. Briefly, cellulose mixed ester solutions (0.1 g/mL) were prepared in acetone containing the appropriate perichromic probe (concentration = 10^{-3} mol/L for probes B, C and F, 10^{-4} mol/L for probes D, E and G, depicted in Figure 2). We prepared films of cellulose tosylate and Cell-carboxylate/tosylate manually by drop casting on clean glass plates, followed by solvent evaporation under reduced pressure at room temperature.

The reflectance spectra of cellulose tosylate and Cell-carboxylate/tosylate films were recorded at room temperature, under the following conditions, against BaSO_4 as white reference: scanning rate = 140 nm/min; slit width = 1.0 nm; spectral resolution = 0.5 nm. The reflectance spectra were converted into the corresponding absorption curves by the Kubelka-Munk function [11] as implemented in version 2.21 of Shimadzu UV-probe program. The values of λ_{max} were calculated from the first derivative of the absorption spectra; the uncertainty in λ_{max} was $\pm 1 \text{ nm}$.

The perichromic properties, empirical polarity ($E_T(WB)$); Lewis acidity (SA), Lewis basicity (SB), dipolarity (SD) and polarizability (SP) were calculated from the λ_{max} of the intramolecular charge transition band of appropriated perichromic probe. The calculations are shown in Supporting Information, SI.

Contact Angle and Surface Energy of Cell-Carboxylate/Tosylate Films

We prepared Cell-carboxylate/tosylate films by casting from their solutions (0.1 g/mL) in DMSO on clean silicon dishes, and evaporated the solvent under reduced pressure at 40 °C to allow the formation of smooth films [12].

In order to determine the surface energy of the polymers (γ_s), contact angle (θ) measurements were performed with diiodomethane (θ_{DIM}) and distilled water (θ_W) at $(24 \pm 1) \text{ }^\circ\text{C}$ by the sessile drop method [13], the droplet volume used for the measurements was 10 μL . At least three samples of the same material were analyzed.

The surface energy (γ_s) of the cellulose mixed ester films and its polar (γ_s^p) and dispersive (γ_s^d) components were calculated using the Owens-Wendt's equation [14], also known as the geometric mean equation. Values of θ_W and θ_{DIM} , were measured and the γ_s^p and γ_s^d components of the surface tension of diiodomethane ($\gamma_L = 50.8 \times 10^{-3} \text{ J/m}^2$; $\gamma_L^p = 50.8 \times 10^{-3} \text{ J/m}^2$) and water ($\gamma_L = 72.8 \times 10^{-3} \text{ J/m}^2$; $\gamma_L^p = 51.0 \times 10^{-3} \text{ J/m}^2$ and $\gamma_L^d = 21.8 \times 10^{-3} \text{ J/m}^2$) were taken from the literature [15].

The advancing (θ_a) and receding (θ_r) contact angles were measured at $(24 \pm 1) \text{ }^\circ\text{C}$ for water droplets. θ_a and θ_r were determined employing droplet volume of 10 μL and 5 μL , respectively. The contact angle hysteresis ($\Delta\theta$) was calculated as the difference between θ_a and θ_r values [13]. At least three samples of the same material were analyzed.

We employed one-way analysis of variance (ANOVA) with post hoc (p) test to evaluate the differences of data among groups, and considered $p < 0.05$ as significant difference.

Dye Adsorption Test by Cellulose Mixed Ester Microspheres

Cell-carboxylate/tosylate samples (each with $DS_{\text{Acyl}} \approx 0.4$ and 1.0) were shaped into microspheres by drop technique as described elsewhere [7]. The influence of DS_{Acyl} on dye adsorption capacity of Cell-carboxylate/tosylate microspheres was tested using MB and SU-IV.

Cell-carboxylate/tosylate (5 mg) were shaped into spheres resulting in 2.5 mL of acetone/water suspension (20% of acetone in water). To this suspension of spheres, we added 0.5 mL of MB solution (430 mg/L); stirred the suspension for 24 h ($25 \pm 1 \text{ }^\circ\text{C}$); removed microspheres by centrifugation (10 000 g), and determined the UV-VIS absorbance of the supernatant. Because of insolubility of SU-IV in water, we employed a protocol similar to that employed for MB, except for the solvent employed for microsphere formation and

dye adsorption (pure 2-propanol) and dye concentration (206 mg/L). The dye removal efficiency by the microspheres was calculated as recommended elsewhere, see the Supporting Information [16].

Results and Discussion

Note: The calculations of all cellulose mixed ester parameters are given in Supporting Information.

Dependence of the Thermal Properties of Cell-Carboxylate/Tosylate on DS_{ACYL}

Thermogravimetric Analysis

Typical TGA curves of cellulose tosylate and Cell-carboxylate/tosylate with $DS_{Acyl} \approx 1.0$ and their parameters are shown in Figure SI 1A and Table SI 1. All TGA curves showed two-stage weight loss starting for the mixed esters at 185 ± 3 °C ($T_{Decomp1}$) and at

221 ± 4 °C ($T_{Decomp2}$) in agreement with literature [17,18].

We gain information about the thermal decomposition of these mixed esters from analysis of sample weight loss, and m/z of the gases evolved during their heating; these results are depicted in Figure SI 2 and Table 1. The relevant information is that during $T_{Decomp1}$ we observed peaks at $m/z = 18$ (water) and 44 (CO_2), characteristic of cellulose decomposition, and the peak at $m/z = 60$ due to McLafferty rearrangement of the acyl moiety. During $T_{Decomp2}$ we observed peaks at $m/z = 64$ (SO_2) and $m/z = 91$ (tropylium cation, $C_7H_7^+$), attributed to the degradation of the sulfonate moiety. For all Cell-carboxylate/tosylate mixed esters, however, the characteristic peak of 4-toluenesulfonic acid at $m/z = 173$ was not observed. Our mass spectroscopy data indicate, therefore, that the first reactions that occurs during thermal decomposition of the mixed esters is their deacylation.

Table 1: Values of m/z and the corresponding fragments produced by thermal decomposition of cellulose tosylate and Cell-carboxylate/tosylate

| m/z | Fragment | Decomposition stage | | | |
|-----|---|---------------------|----------------------------|------------------------------|------------------------------|
| | | Cellulose tosylate | Cellulose acetate/tosylate | Cellulose butanoate/tosylate | Cellulose hexanoate/tosylate |
| 18 | H ₂ O | $T_{Decomp1}$ | $T_{Decomp1}$ | $T_{Decomp1}$ | $T_{Decomp1}$ |
| 44 | CO ₂ | $T_{Decomp1}$ | $T_{Decomp1}$ | $T_{Decomp1}$ | $T_{Decomp1}$ |
| 55 | [O≡CCH=CH ₂] ⁺ | - | - | $T_{Decomp1}$ | $T_{Decomp1}$ |
| 60 | [HOC(OH)=CH ₂] ⁺ | - | $T_{Decomp1}$ | $T_{Decomp1}$ | $T_{Decomp1}$ |
| 64 | SO ₂ | $T_{Decomp2}$ | $T_{Decomp2}$ | $T_{Decomp2}$ | $T_{Decomp2}$ |
| 73 | [HOC(O)CH ₂ CH ₂] ⁺ | - | - | $T_{Decomp1}$ | $T_{Decomp1}$ |
| 87 | [HOC(O)CH ₂ CH ₂ CH ₂] ⁺ | - | - | - | $T_{Decomp1}$ |
| 91 | Tropylium cation, [C ₇ H ₇] ⁺ | $T_{Decomp2}$ | $T_{Decomp2}$ | $T_{Decomp2}$ | $T_{Decomp2}$ |

The influence of DS_{Acyl} on decomposition temperatures of cellulose mixed esters is shown in Figure 3. It was found that the two initial decomposition temperatures (IDT) of Cell-carboxylate/tosylate show a simple dependence on DS_{Acyl} ; IDT increase with the increasing DS_{Acyl} . The results of the corresponding regression analysis are listed in Table 2. The dependence of IDT-1 on DS_{Acyl} is an ascending exponential as observed for pure cellulose acetate [9], which is in agreement with the TG-MS data that indicates the scission of acyl units during the first decomposition stage.

Differential Scanning Calorimetry (DSC)

Typical DSC curves of cellulose tosylate and Cell-carboxylate/tosylate are shown in Figure SI 1B, one exothermic and one endothermic peaks (Table SI 2) are presented in curves of all samples. The maximum temperature of exothermic peak (T_{exo}) of all samples shows a linear correlation with $T_{Decomp1}$ (Figure 3C, entry 8-10 in Table 2), indicating that the exothermic peak correspond to the biopolymer decomposition, in agreement with the second heating DSC curve, where no events are observed Figure SI 1C.

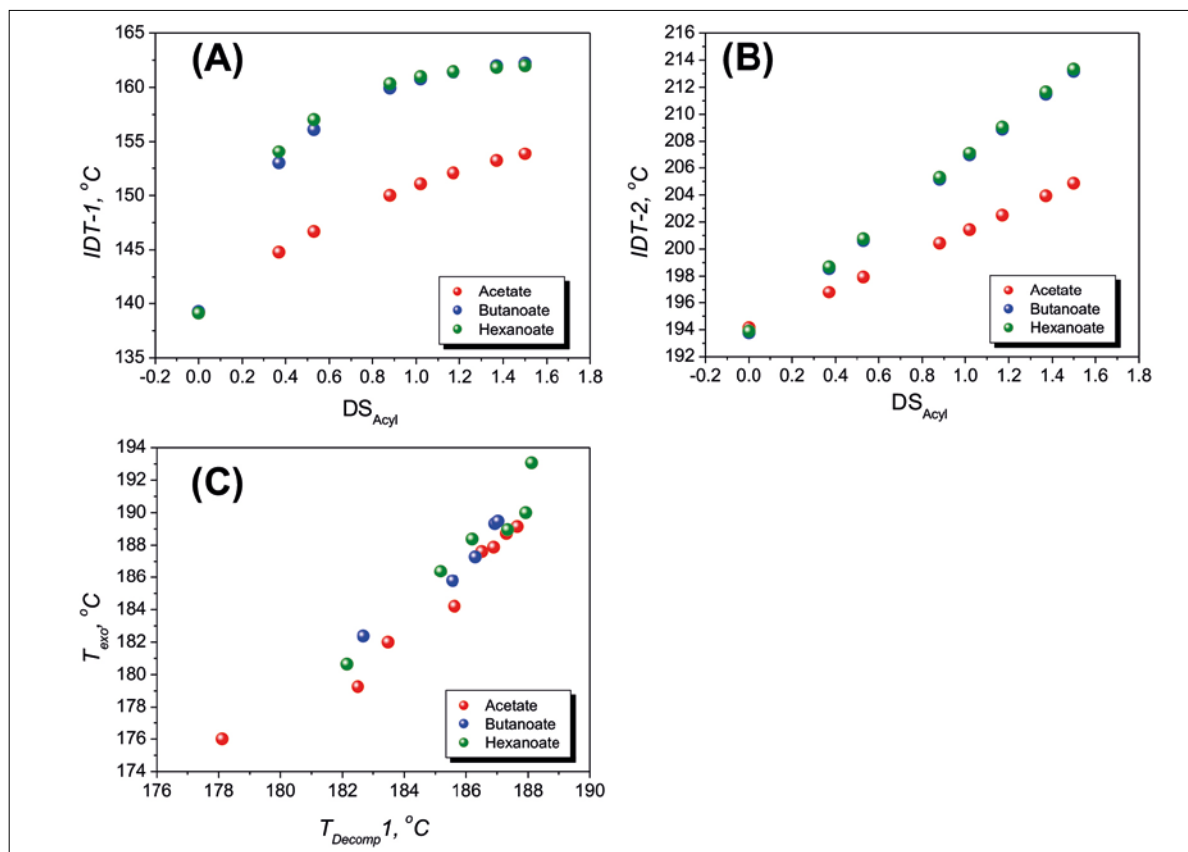


Figure 3: Dependence of the initial decomposition temperatures (IDT) on DS_{Acyl} of Cell-carboxylate/tosylate. (A) First decomposition stage and (B) second decomposition stage. (C) Correlation between DSC and TGA data.

In summary, we conclude the following about the thermal properties of Cell-carboxylate/tosylate: (i) substitution of the hydroxyl groups of AGU by carboxylic ester group produces increase in the corresponding decomposition temperatures; these are correlated with DS_{Acyl} by simple equations; (ii) scission of the acyl group occurs first; (iii) the glass transition- and melting temperatures of these mixed esters are higher than their decomposition temperatures, as is observed for cellulose proper.

Influence of DS_{ACYL} on Surface Properties of Cell-Carboxylate/Tosylate Mixed Esters: Use of Perichromic Probes and Contact Angle Measurement

A successful approach to describe the effect of medium on chemical phenomena is to use a linear combination of medium descriptors, e.g., as shown in Equation (1) [19, 20].

$$\text{Effects of the medium} = a SA + b SB + d SD + p SP \quad (1)$$

where, SA , SB , SD , and SP refers to Lewis acidity, Lewis basicity, dipolarity, and polarizability of the medium, respectively; a , b , d , and p are the correspond-

ing correlation coefficients. A version of Equation (1), applied for a perichromic empirical polarity probe, e.g., WB ($E_T(WB)$) is:

$$E_T(WB) = a SA + b SB + d SD + p SP \quad (2)$$

where $E_T(WB)$ is the surface empirical polarity.

We are interested in understanding and quantifying solute-cellulose derivative interactions. Previously we studied cellulose carboxylic esters [9] and cellulose ethers [21]. To our knowledge, this is the first study on mixed esters.

The effects of the structure of the mixed esters on the properties of the corresponding films (Lewis acidity, Lewis basicity, etc.) are due to the presence of both tosyl and acyl moieties. We attribute the response of the perichromic dyes to the latter moiety because DS_{Tosyl} is constant through the series. Previous data on the same mixed esters showed that the effects of the tosyl and carboxyl moieties are independent. For example, $\hat{v}(\nu_{C=O})$ and $\hat{v}(\nu_{asSO_2})$ are linear functions in DS_{Acyl} [7]. We assume that the same independent contributions to the perichromic parameters are operative for carboxylate/tosylate esters. In other words, we expected a correlation, linear or not, between DS_{Acyl} and

Table 2: Dependence of the thermal properties of Cell-carboxylate/tosylate on the degree of substitution of carboxylate moieties

| Entry | Technique | Regression Equation | Correlation coefficient | Reference |
|-------|-----------|--|-------------------------|--------------|
| 1 | TGA | $IDT-1 = 353.7 - 364.9e^{(-DS_{Ac}/0.831)}$ (for simple Cellulose acetate) ^{a)} | 0.9950 | [9] |
| 2 | TGA | $IDT-1 = 159.067 - 19.861e^{(-DS_{Ac}/1.121)}$ | 0.9965 | Present work |
| 3 | TGA | $IDT-1 = 162.931 - 23.658e^{(-DS_{Bu}/0.426)}$ | 0.9996 | Present work |
| 4 | TGA | $IDT-1 = 162.344 - 23.218e^{(-DS_{Hx}/0.359)}$ | 0.9968 | Present work |
| 5 | TGA | $IDT-2 = 194.149 + 7.143 DS_{Ac}$ | 0.9953 | Present work |
| 6 | TGA | $IDT-2 = 193.769 + 12.932 DS_{Bu}$ | 0.9985 | Present work |
| 7 | TGA | $IDT-2 = 193.895 + 12.962 DS_{Hx}$ | 0.9971 | Present work |
| 8 | TGA-DSC | $T_{Decomp1}(Ac) = -85.006 + 1.458 T_{exo}^{b), c)}$ | 0.9389 | Present work |
| 9 | TGA-DSC | $T_{Decomp1}(Bu) = -110.315 + 1.600 T_{exo}$ | 0.9369 | Present work |
| 10 | TGA-DSC | $T_{Decomp1}(Hx) = -146.553 + 1.797 T_{exo}$ | 0.9248 | Present work |

a) IDT = initial temperature of decomposition. 1 and 2 correspond, respectively, to the first and second decomposition stage observed on TGA curve of Cell-carboxylate/tosylate.

b) $T_{Decomp1}$ = temperature of the first stage of decomposition, determined from DTG curves.

c) T_{exo} = temperature of exothermic peak present in DSC curves.

$E_T(WB)$. We also expected that application of the multi-parameter Equation (2) indicates which film property controls its polarity; a useful information for applications of these mixed properties, e.g., in enzyme immobilization.

The effects of RCO- on the perichromic parameters are due to dipolar and acid/base interactions of RCO-, as well as hydrophobic and steric interactions of RCO-. As a model for the former interactions we use $E_T(WB)$ of ethyl acetate, ethyl butanoate, and ethyl hexanoate: 46.5; 45.3; 44.6 kcal/mol, respectively [22]. The molar volumes (cm^3/mol) of the parent carboxylic acids: 56.1 ± 3.0 ; 89.1 ± 3.0 ; 122.2 ± 3.0 [23] for acetic, butyric and hexanoic acid, respectively, can be used as model for evaluation of the steric interactions. Applying the results of these model compounds to the present cellulose mixed esters, we expect a decrease in $E_T(WB)$ in going from the cellulose acetate/tosylate to cellulose hexanoate/tosylate, probably modulated

by increased hydrophobic interactions and steric hindrance because the preferential conformation of RCO-, e.g., perpendicular or tilted toward the film interface [24]. A similar line of reasoning applies to analysis of the left-hand terms of Equation (2).

$E_T(WB)$

Previously, was showed that $E_T(WB)$ of Cell-carboxylate/tosylate films decrease linearly as a function of increasing DS_{Acy} ; the slopes of the corresponding straight lines increase on going from acetate to hexanoate (Entries 1 to 3 in Table 3) [7]. Consequently, for the same mixed ester series, this decrease is a consequence of replacement of the strongly dipolar OH group by the weaker dipolar RCO-.

Table 3: Dependence of the perichromic properties of Cell-carboxylate/tosylate on the degree of ester substitution

| Entry | Regression Equation | Correlation coefficient | Reference |
|-------|--|-------------------------|--------------|
| 1 | $E_T(WB) = 62.345 - 3.473 DS_{Ac}$ | 0.991 | [7] |
| 2 | $E_T(WB) = 62.453 - 3.861 DS_{Bu}$ | -0.991 | [7] |
| 3 | $E_T(WB) = 62.499 - 4.765 DS_{Hx}$ | -0.989 | [7] |
| 4 | $SA = 0.648 - 0.172 DS_{Ac}$ | -0.9846 | Present work |
| 5 | $SA = 0.638 - 0.244 DS_{Bu}$ | -0.9964 | Present work |
| 6 | $SA = 0.628 - 0.195 DS_{Hx}$ | -0.9976 | Present work |
| 7 | $SB = 0.934 - 0.791 DS_{Ac} + 0.405 DS_{Ac}^2$ | 0.9986 | Present work |
| 8 | $SB = 0.931 - 1.346 DS_{Bu} + 1.191 DS_{Bu}^2$ | 0.9944 | Present work |
| 9 | $SB = 0.931 - 1.194 DS_{Hx} + 0.901 DS_{Hx}^2$ | 0.9989 | Present work |

Lewis Acidity and Lewis Basicity

The values calculated of SA and SB are listed in Table SI-3 and are plotted in Figure 4 and 5. The dependence of SA on DS_{Acyl} is linear (Entries 4 to 6 in Table 3). For the same series of mixed esters, the decrease of SA as a function of increasing DS_{Acyl} results

from the substitution of the hydroxyl groups, hydrogen bond donor, by acyl moiety, hydrogen bond acceptor. The Lewis acidity dependence on RCO^- shows the following order: acetyl > hexanoyl > butanoyl reflecting the above-mentioned acid-base character of RCO^- , probably coupled with steric effects of RCO^- .

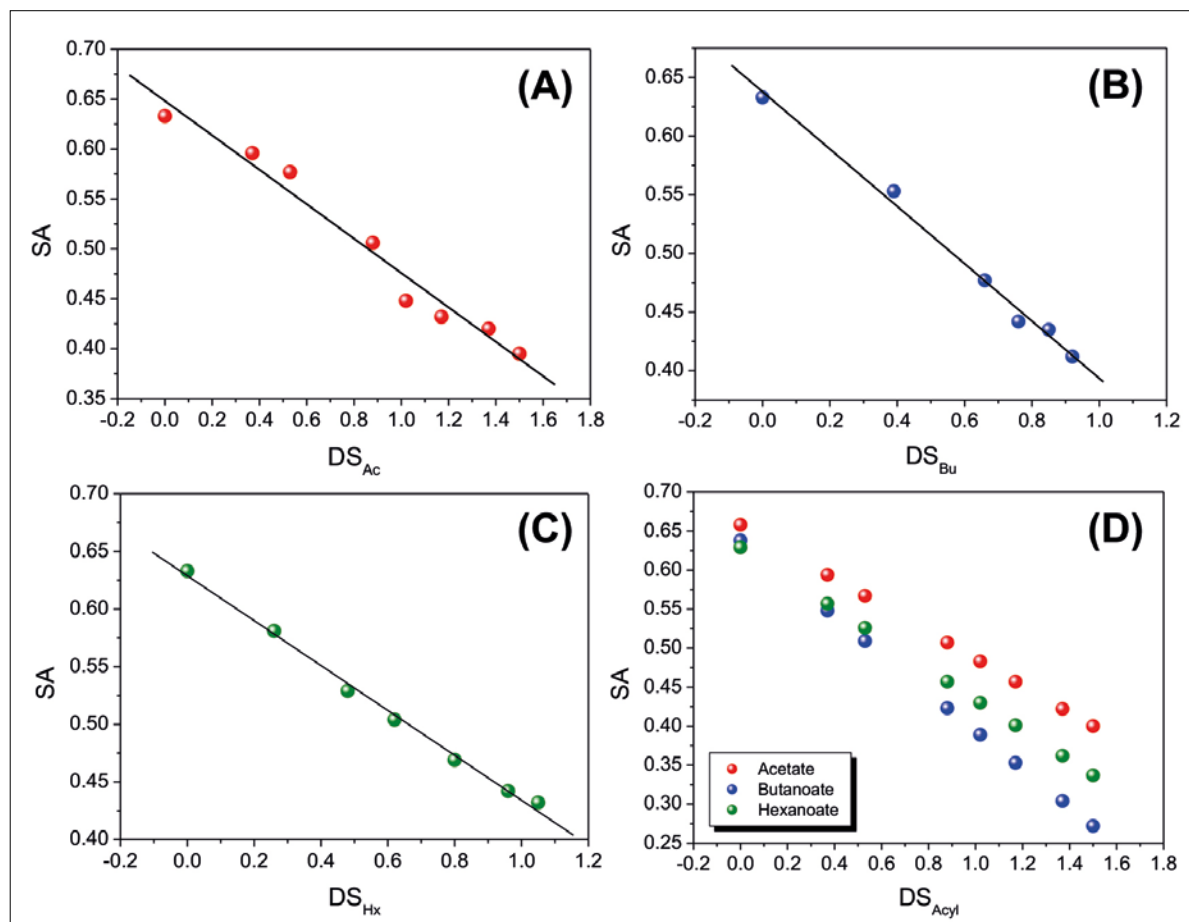


Figure 4: Dependence of Lewis acidity of cellulose carboxylate/tosylate films on the degree of substitution of carboxylate unit. Parts A, B and C refer to acetate/tosylate, butanoate/tosylate and hexanoate/tosylate, respectively. For comparison with the acetate/tosylate series, we calculated the dependence of SA on $DS_{Acyl} > 1.0$ for the butanoate/tosylate and hexanoate/tosylate shown in part D- from the regression equations of Table 3.

The interplay between acid-base character of RCO^- and steric effects of RCO^- is also evident in the correlation of SB with DS_{Acyl} (Figure 5), being a second order polynomial with minimum at $DS_{Acyl} \approx 0.8$ for all mixed ester series, (Entries 7 to 9 in Table 3). As can be seen from part D of Figure 5, the effect of the

length of RCO^- on SB is evident only after the minimum is reached, with the following order: cellulose butanoate/tosylate > cellulose hexanoate/tosylate > cellulose acetate/tosylate; again reflecting the interplay between acid/base character and steric interactions.

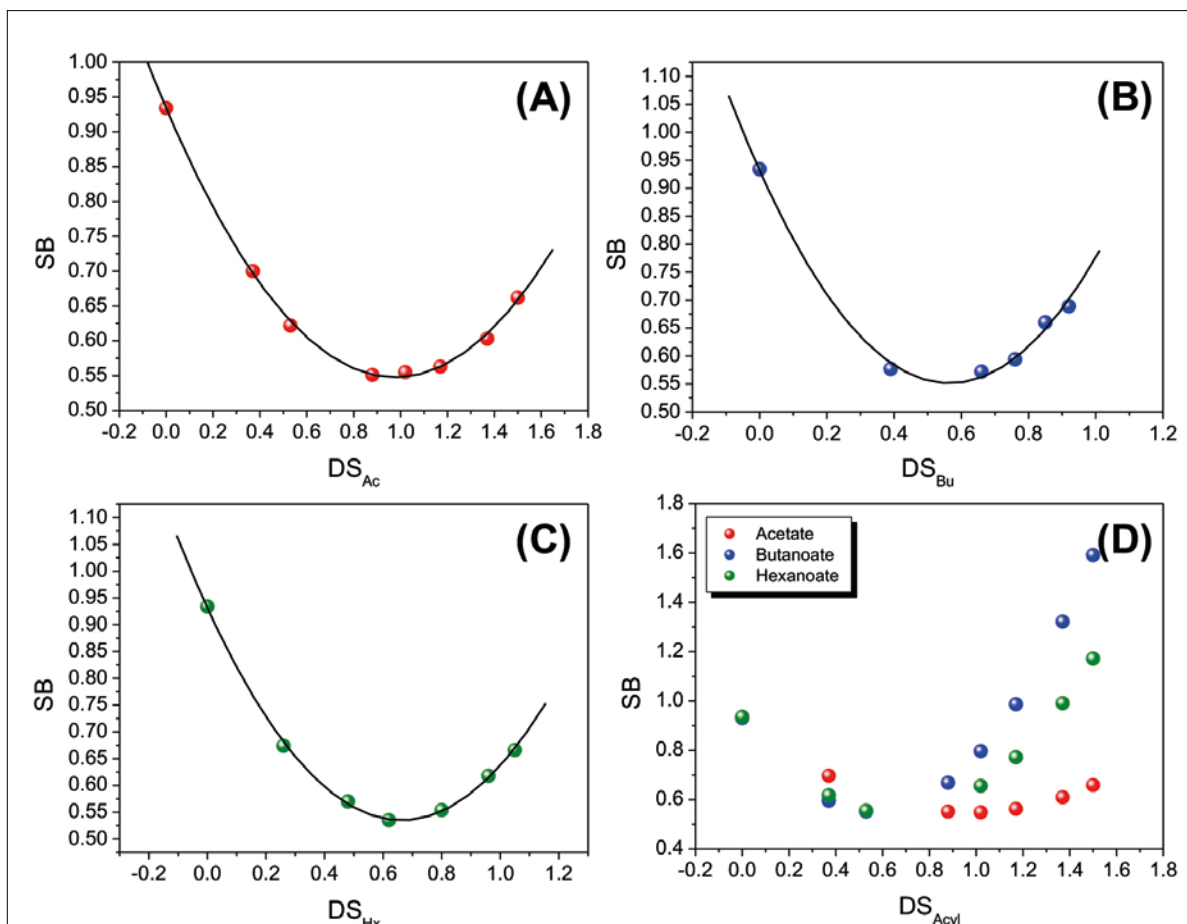


Figure 5: Dependence of Lewis basicity of cellulose carboxylate tosylate films on degree of substitution of carboxylate unit. Parts A, B and C refer to cellulose acetate/tosylate, cellulose butanoate/tosylate and cellulose hexanoate/tosylate, respectively. For comparison with the acetate/tosylate series, we calculated the dependence of SB on $DS_{Acyl} > unity$ for the butanoate/tosylate and hexanoate/tosylate – shown in part D – from the regression equations of Table 3.

Dipolarity and Polarizability

The remaining medium descriptors of Equation (2) are SP and SD. It was not feasible to calculate these descriptors from the spectra of the perichromic probes β -carotene and 2-(N,N-dimethylamine)-7-nitrofluorene (Figure 2), as indicated elsewhere [25, 26]. The reason is the small value ΔSP (= SP cellulose acetate/tosylate – SP cellulose hexanoate/tosylate), ca. 0.03 at $DS_{Acyl} \approx 1.0$. This small variation agrees with the $\Delta SP = 0.04$, calculated for model compounds ethyl acetate and ethyl hexanoate [26]. Consequently, the variation of SP as a function of DS_{Acyl} , or the length of RCO^- is within experimental uncertainty. The correlation of film dipolarity (SD) with the same structural variables

will be similarly affected because we use λ_{max} of β -carotene for calculation of SD, as given elsewhere [26]. Consequently, we thought information regarding these two descriptors from contact angle measurements as indicated below.

Contact Angle and Surface Energy

The contact angle (θ) of a liquid droplet on a surface results from the equilibrium of three forces, namely, the liquid–air (γ_L), liquid–solid (γ_{SL}), and solid–air (γ_S) interfacial tensions, as proposed by Young [27]:

$$\gamma_S = \gamma_{SL} + \gamma_L \cos\theta \quad (3)$$

The work of adhesion (W_{SL}) between the liquid and the surface can be determined by the Young-Dupré equation [27-29]:

$$W_{SL} = \gamma_L (1 + \cos\theta) \quad (4)$$

The Owens-Wendt geometric mean equation allows calculation of WSL from the geometric mean of polar (γ^p) and dispersive (γ^d) components of the surface and liquid:

$$\gamma_L (1 + \cos\theta) = 2 \left(\sqrt{\gamma_S^d \gamma_L^d} + \sqrt{\gamma_S^p \gamma_L^p} \right)$$

Generally two liquids with known γ_L^d and γ_L^p components are used for the contact angle measurements and (γ_S^d) and (γ_S^p) determination. Those parameters indicate the contribution of each type of interaction (dipolar or van der Waals interactions) between solid and liquid to reduce the interfacial tension. High values of γ_L^p indicate that the surface is enriched by hydrophilic groups, whereas the γ_S^d component includes forces between permanent dipoles, permanent dipole and a corresponding induced dipole, and induced dipoles. Therefore, we employed the surface energy method as an alternative to the perichromic approach to evaluate the dipolar- and van der Waals contributions of the

acyl groups to surface properties of Cell-carboxylate/tosylate films.

The θ_W values determined for water are a direct measurement of films hydrophobicity; the larger the θ_W value, the more hydrophobic is the surface. The values are summarized in Table 4. Our data show that the hydrophobicity of Cell-carboxylate/tosylate decreased in the following order: cellulose hexanoate/tosylate > cellulose butanoate/tosylate > cellulose acetate/tosylate. This result agrees with the expected effect of increasing the length of (hydrophobic) RCO-. With few exceptions, an increase of DS_{Acyl} for the same mixed ester series results in an increase θ_W , due to the substitution of OH by RCO.

The γ_S^d and γ_S^p components of the surface energy (γ_S) of Cell-carboxylate/tosylate films (Table 4) were calculated from the values of θ_W and θ_{DIM} values using Equation (5). Although the values of γ_S , γ_S^d and γ_S^p for cellulose acetate/tosylate films are higher than the other Cell-carboxylate/tosylate esters the difference is, however, small. The contribution of γ_S^d to γ_S was the largest regardless of the length of RCO. A similar result was observed for cellulose acetate and cellulose mixed carboxylic esters (cellulose acetate/propionate and acetate/butanoate) [30].

Table 4: Values of θ calculated for water (W) and diiodomethane (DIM) droplets on cellulose ester films and the corresponding polar (γ_S^p) and dispersive (γ_S^d) components of the surface energy (γ_S)

| Sample | DS_{Acyl} | θ_W [°] | θ_{DIM} [°] | γ_S^p [J/m ²] | γ_S^d [J/m ²] | γ_S [J/m ²] |
|------------------------------|-------------|-------------------|-----------------------|-------------------------------------|-------------------------------------|-----------------------------------|
| Cellulose acetate/tosylate | 0.37 | 61 ± 3 | 29 ± 1 | 10.4 ± 0.5* | 44.2 ± 0.4 | 54.6 ± 0.9 |
| | 0.88 | 67 ± 2 | 22 ± 5 | 6.9 ± 0.2 | 47 ± 2 | 54 ± 2 |
| | 1.17 | 69.0 ± 0.1 | 19 ± 1 | 5.82 ± 0.02* | 47.6 ± 0.3 | 53.4 ± 0.3 |
| | 1.50 | 66 ± 6 | 23 ± 1 | 7 ± 1 | 46.4 ± 0.3 | 53 ± 1 |
| Cellulose butanoate/tosylate | 0.39 | 71 ± 1 | 31 ± 3 | 6.0 ± 0.2 | 43 ± 1 | 49 ± 1 |
| | 0.66 | 69 ± 4 | 28.5 ± 0.5 | 6.6 ± 0.4 | 44.4 ± 0.2 | 51.0 ± 0.6 |
| | 0.85 | 73 ± 3 | 32 ± 1 | 5.3 ± 0.3 | 42.9 ± 0.4 | 48.1 ± 0.7 |
| | 0.92 | 75 ± 2 | 33 ± 3 | 4.6 ± 0.3 | 43 ± 1 | 48 ± 1 |
| Cellulose hexanoate/tosylate | 0.26 | 79 ± 5 | 29 ± 3 | 3 ± 1 | 45 ± 1 | 48 ± 2 |
| | 0.48 | 84 ± 3 | 31 ± 2 | 1.7 ± 0.2 | 43.8 ± 0.8 | 45.5 ± 1 |
| | 0.80 | 78 ± 1 | 32 ± 4 | 3.4 ± 0.3 | 43 ± 2 | 46 ± 2 |
| | 1.05 | 87 ± 2 | 40 ± 3 | 1.6 ± 0.4 | 40 ± 1 | 42 ± 1 *a) |

a) The symbol (*) indicates that the data are statistically different ($p < 0.05$), in the corresponding data set.

The dependence of γ_s^d on RCO- follows the order acetyl > butanoyl > hexanoyl, as expected for the contribution of alkyl chain of acyl groups and is opposite to hydrophobicity tendency. The γ_s^d values presented no statistically significant variation on RCO- or DS_{Acyl} , in agreement with perichromic results for SP and SD. Therefore, both techniques (contact angle and perichromism) are not sensitive enough to evaluate the dependence of the dispersive force on DS_{Acyl} .

We note that the homogeneity of Cell-carboxylate/tosylate films was adequate for the surface energy determination, because the mean contact angle hysteresis ($\Delta\theta$) values for most samples was $(16 \pm 4)^\circ$, as shown in Table SI 4, indicating that the films presented smooth homogeneous surfaces.

Dependence of Dye Adsorption on DS_{Acyl} of Cell-Carboxylate/Tosylate

As given by Equation (1), the effect of medium (cellulose derivative) on a phenomenon of interest (adsorption) depends on adsorbate-surface specific and non-specific interactions. As an example, we tested the adsorption of two distinct dyes, water-soluble, cationic MB and oil-soluble, neutral SU-IV by these mixed esters. We used cellulose acetate/tosylate, cellulose butanoate/tosylate and cellulose hexanoate/tosylate with $DS_{Acyl} \approx 0.4$ and 1.0, shaped into microspheres with average diameter of (200 ± 35) nm [7].

The efficiency of Cell-carboxylate/tosylate microspheres (1 wt % of mixed ester in water) to remove the

dyes from solution was calculated from the UV-VIS absorbance spectra (Table 5). Within the same mixed ester series, the removal efficiency (R.E.) of MB increased with increasing DS_{Acyl} , indicating that dye-ester hydrophobic interactions are also operative. Values of R.E. are not significantly different within the three series, for the same DS_{Acyl} , in agreement to the surface energy data.

In case of SU-IV, the values of R.E. are very close for the three Cell-carboxylate/tosylate and practically independent of DS_{Acyl} , which is in agreement with γ_s^d and SP/SD values. It is also possible that dye self-aggregation, [31] contributed to this “leveling” of adsorption within the esters, because dye-dye interactions efficiently competes with dye-microsphere interactions. However, dye self-aggregation is suppressed in aliphatic alcohols, [32] hence stronger interaction of dye-cellulose derivative is expected. Therefore, the low R.E.(SU-IV) values probably reflects the weak dispersive forces as indicated by perichromic and contact angle techniques.

In summary, if MB is taken as a model for charged adsorbates, then it is enough to use members of one carboxylate/tosylate series with different DS_{Acyl} to induce detectable differences in solute adsorption. We intend to test the generality of the previous statement by carrying out additional adsorption experiments with adsorbates whose chemical structures are varied in a systematic way.

Table 5: Dye removal efficiency of Cell-carboxylate/tosylate microspheres

| Sample | DS_{Acyl} | Removal efficiency [%] | |
|------------------------------|-------------|------------------------|-------|
| | | MB | SU-IV |
| Cellulose acetate/tosylate | 0.37 | 42.3 | 15.3 |
| | 1.02 | 70.6 | 16.8 |
| Cellulose butanoate/tosylate | 0.39 | 45.6 | 15.4 |
| | 0.92 | 72.6 | 16.3 |
| Cellulose hexanoate/tosylate | 0.26 | 38.7 | 14.3 |
| | 1.05 | 70.9 | 15.5 |

Conclusions

A series of cellulose carboxylate/tosylate mixed esters with a constant DS_{Tosyl} and variable DS_{Acyl} , with increasing hydrophobicity of the carboxylate moiety (acetate, butanoate, hexanoate) were characterized regarding thermal behavior and surface properties. The cellulose carboxylate/tosylate showed two temperatures of decomposition where scission of the acyl moiety occurs before that of the tosyl counterpart. These mixed esters did not exhibit glass transition- or melting temperatures. Consequently, they can only be regenerated from solution, i.e., not by extrusion from the melt. Surface properties, including empirical polarity, Lewis acidity and Lewis basicity were calculated from the UV-Vis spectra of perichromic probes. Their values are modulated by dipolar and steric effects of the RCO- group, and showed simple dependences on DS_{Acyl} . The small effects of DS_{Acyl} on the spectra of the appropriate perichromic dyes precluded calculation of SD and SP of the films. We sought this information from contact-angle measurements; this technique also indicated the small magnitude of these two descriptors. Finally, we used (water-soluble) MB and (oil-soluble) SU-IV to probe adsorption by cellulose carboxylate/tosylate microspheres. Adsorption of (ionic) MB increases as a function of increasing DS_{Acyl} , whereas this structural variable has practically no effect on adsorption of (nonionic) SU-IV. Adsorption efficiency of both dye agrees with the results of perichromism and contact angle measurements.

Acknowledgements

D. C. Ferreira thanks FIPT for PDCE fellowship for her stay at Friedrich Schiller University of Jena. O. A. El Seoud and Denise F. S. Petri thank CNPq for research productivity fellowships Grants 307022/2014-5 and 305178/2013-0, respectively; and FAPESP for financial support (2014/22136-4). T. Heinze gratefully acknowledged financial support from German Ministry of Food and Agriculture based on an enactment of the German Bundestag. The authors also thanks to L. S. Galvão from IPT for the TGA and DSC measurements, to Prof. V. R. L. Constantino and Dr. R. A. A. de Couto from IQ-USP for the TGA-MS measurements.

References

- [1] K. J. Edgar, C. M. Buchanan, J. S. Debenham, P. A. Rundquist, B. D. Seiler, M. C. Shelton, D. Tindall, *Prog. Polym. Sci.*, 2001, 26, 1605.
- [2] D. Klemm, B. Heublein, H. P. Fink, A. Bohn, *Angew. Chem. Int. Ed.*, 2005, 44, 3358.
- [3] K. J. Edgar, *Cellulose*, 2007, 14, 49-64.
- [4] R. K. Jain, K. Lal, H. L. Bhatnagar, *J. Appl. Polym. Sci.*, 1987, 33, 247.
- [5] G. Siegmund, D. Klemm, *Polym. News*, 2002, 27, 84.
- [6] S. Hornig, T. Heinze, *Biomacromolecules*, 2008, 9, 1487.
- [7] D. C. Ferreira, G. S. Bastos, A. Pfeifer, T. Heinze, O. A. El Seoud, *Carbohydr. Polym.*, 2016, 152, 79.
- [8] W. L. Armarego, C. L. Chai, *Purification of Laboratory Chemicals*, 6th ed. Elsevier Ltd., New York, 2009.
- [9] L. C. Fidale, C. Ißbrücker, P. L. Silva, C. M. Lucheti, T. Heinze, O. A. El Seoud, *Cellulose*, 2010, 17, 937.
- [10] O. A. El Seoud, P. A. R. Pires, C. Loffredo, M. Imran, P. D. Pulcini, M. F. Corrêa, R. Mustafa, *J. Braz. Chem. Soc.*, 2013, 24, 1079.
- [11] M. L. Myrick, M. N. Simcock, M. Baranowski, H. Brooke, S. L. Morgan, J. N. McCutcheon, *Appl. Spectrosc. Rev.*, 2011, 46, 140.
- [12] D. F. S. Petri, G. Wenz, P. Schunk, T. Schimmel, *Langmuir*, 1999, 15, 4520.
- [13] A. W. Adamson, *Physical chemistry of surfaces*, 5th ed., John Wiley & Sons Ltd., Chichester, 1990.
- [14] D. K. Owens, R. C. Wendt, *J. Appl. Polym. Sci.*, 1969, 13, 1741.
- [15] B. Bouali, F. Ganachaud, J.-P. Chapel, C. Pichot, P. Lanteri, *J. Colloid Interface Sci.*, 1998, 208, 81.
- [16] H. Deng, J. Lu, G. Li, G. Zhang, X. Wang, *Chem. Eng. J.*, 2011, 172, 326.
- [17] T. Heinze, K. Rahn, M. Jaspers, H. Berghmans, *J. Appl. Polym. Sci.*, 1996, 60, 1891.
- [18] T. Heinze, K. Rahn, M. Jaspers, H. Berghmans, *Macromol. Chem. Phys.*, 1996, 197, 4207.
- [19] C. Reichardt, T. Welton, *Solvents and Solvent Effects in Organic Chemistry*, 4th ed., Wiley-VCH, New York, 2011.
- [20] L. C. Fidale, T. Heinze, O. A. El Seoud, *Carbohydr. Polym.*, 2013, 93, 129.
- [21] L. C. Fidale, P. M. Lima, L. M. A. Hortêncio, P. A. R. Pires, T. Heinze, O. A. El Seoud, *Cellulose*, 2012, 19, 151.
- [22] R. Casarano, L. C. Fidale, C. M. Lucheti, T. Heinze, O. A. El Seoud, *Carbohydr. Polym.*, 2011, 83, 1285.

- [23] ACD/Labs. Calculated using Advanced Chemistry Development (ACD/Labs) Software V11.02 (© 1994-2017 ACD/Labs).
- [24] M. Wühn, J. Weckesser, C. Wöll, *Langmuir*, 2001, 17, 7605.
- [25] C. Loffredo, P. A. R. Pires, M. Imran, O. A. El Seoud, *Dyes Pigment.*, 2013, 96, 16.
- [26] P. A. R. Pires, M. Imran, C. Loffredo, P. M. Donate, D. Previdi, O. A. El Seoud, *J. Phys. Org. Chem.*, 2013, 26, 280.
- [27] J. K. Berg, C. M. Weber, H. Riegler, *Phys. Rev. Lett.*, 2010, 105, 076103.
- [28] M. K. Chaudhury, *Mater. Sci. Eng.*, 1996, R16, 97.
- [29] P. M. Kosaka, J. Amim Jr, R. S. N. Saito, D. F. S. Petri, in *Model Cellulosic Surfaces – ACS Series* (Ed: M. Roman), American Chemical Society, Washington 2009, 223.
- [30] P. M. Kosaka, Y. Kawano, D. F. S. Petri, *J. Colloid Interface Sci.*, 2007, 316, 671.
- [31] K. Hamada, H. Kubota, A. Ichimura, T. Lijima, S. Amiya, *Ber. Bunsenges. Physik. Chem.*, 1985, 89, 859.
- [32] K. Rohatgi, G. Singhal, *J. Phys. Chem.*, 1966, 70, 1695.

Kinetics of Cellulose Acylation with Carboxylic Anhydrides and N-acylimidazoles in Ionic Liquid/Molecular Solvent Mixtures: Relevance to the Synthesis of Mixed Cellulose Esters

Thais A. Bioni,¹ Naved I. Malek,² and Omar A. El Seoud^{1*}

¹ Institute of Chemistry, the University of São Paulo, Prof. Lineu Prestes Av., 748, 05508-000, São Paulo, Brazil. *Contact: elseoud.usp@gmail.com

² Applied Chemistry Department, S.V. National Institute of Technology, Surat, Gujarat, India.

Abstract

Using conductivity measurements we studied the kinetics of acylation of microcrystalline cellulose (MCC) under homogeneous solution conditions in mixtures of the ionic liquid 1-allyl-3-methylimidazolium chloride (AlMeImCl) and the molecular solvents (MSs) *N,N*-dimethylacetamide (DMAc) and dimethyl sulfoxide (DMSO). The acylating agents were acetic- and propionic anhydride (Ac₂O, Pr₂O, respectively), *N*-acetyl-, *N*-benzoyl- and *N*-propionyl-imidazole (AcIm, BzIm, and PrIm, respectively). Third-order rate constants (k_3) were calculated by dividing the observed rate constants by dividing by the concentrations of the acylating agent and AlMeImCl. We calculated the values of k_3 for the reaction of MCC with each acylating agent, and for the reaction of the biopolymer with their mixtures (Ac₂O+Pr₂O or AcIm + BzIm). These calculations showed that acylation by mixtures of reagents are essentially independent. The dependence of k_3 on the structure of the acylating agent and the nature of the MS were explained by considering the activation parameters. We synthesized the mixed esters under the conditions of the kinetic experiments and used ¹H NMR spectroscopy to calculate the partial degrees of substitution (DS) in each case, e.g., DS_{Acetate} and DS_{Propionate}. The ratio between the individual k_3 , e.g., $k_{3,Ac_2O}/k_{3,Pr_2O}$ and that of the corresponding partial degree of substitution, e.g., DS_{Acetate}/DS_{Propionate} were found to be similar. That is, kinetic data can be successfully employed to predict the product partial degrees of substitution of the mixed esters, if steric effects are not dominant, as in case of the formation of cellulose acetate/benzoate.

Keywords: kinetics, cellulose mixed esters, ionic liquid, molecular solvents

Introduction

Ionic liquids (ILs) dissolve cellulose; the resulting solutions are used for the regeneration and shaping of the biopolymer and its derivatization under homogeneous reaction conditions. Depending on the concentration and characteristics of the dissolved cellulose, the molecular structure of the IL, and the temperature the solutions obtained are anisotropic and very viscous; leading to gel formation at still higher biopolymer concentration. These problems can be attenuated/eliminated by use of molecular solvents (MSs) as diluents for the IL, especially dipolar aprotic ones, e.g., aceto-

nitrile, *N,N*-dimethylacetamide, DMAc, and dimethyl sulfoxide, DMSO [1-3]. The use of MSs as diluents increases heat-transfer, and results in a massive decrease in biopolymer solution viscosity and the energy of viscous flow. According to the Stokes-Einstein diffusion equation, lower viscosity leads to higher diffusion rates of the species present in solution, which corresponds to an increase in mass transfer, hence increase in reaction rate. This expectation was demonstrated experimentally, e.g., for Diels-Alder reactions in pure ILs, [4,5] and their mixtures with MSs [6].

The concentration of the MS in the binary solvent mixture affects important experimental variables, including the concentration of dissolved cellulose and the physico-chemical properties of the resulting biopolymer solution. For example, it was shown that the wt% of dissolved cellulose in IL-DMSO and IL-DMAc shows maxima as a function of the MS mole fraction [7]. The resulting biopolymer solutions were studied by solvatochromic probes. The calculated solvatochromic parameters were found to depend on the nature of the IL and MS, and solution composition. For example, solutions of microcrystalline cellulose (MCC) in IL-MS are more polar and more basic in IL-DMSO than in IL-sulfolane [8]. Favorable solvent properties, e.g., higher polarity and basicity favor cellulose dissolution because of the disruption of the intermolecular hydrogen bonding between biopolymer chains. The same properties favor reactions where there is an increase in polar character between the reactants and transition state, e.g., acyl transfers [9].

A rational use of binary solvent mixtures, however, is not straightforward. The reason is that the dependence of the properties of the binary mixture on its composition is not ideal, i.e., is not linear. This non-ideality applies to macroscopic properties, e.g., density and viscosity, [11, 12] and microscopic ones, e.g., the above-mentioned solvatochromic parameters. Therefore, research is required to understand the mutual interactions of the solvent components as well as their interaction with cellulose. In this regard, kinetic data (rate constants and activation parameters) help in delineating the reason, e.g., for the efficiency of particular combinations of different ILs and MSs.

We studied the kinetics of cellulose uncatalyzed- and imidazole-catalyzed acylation by carboxylic acid anhydrides (acetate to hexanoic) in LiCl-DMAc, pure ILs and IL-MSs [8,12-15]. Here we extend these studies to cover the formation of mixed esters of

aliphatic acids (acetic and propionic) and aliphatic plus aromatic acid (acetic, benzoic, propionic.). Mixed esters with different partial degree of substitution (DS) of each acyl moiety, in particular cellulose acetate/propionate and acetate/butanoate have favorable properties not exhibited by the esters of a single acyl group, probably because of the juxtaposition of both acyl moieties in the same anhydroglucose unit, AGU. These mixed esters are employed commercially on a large scale, e.g., in coating industry, molding plastics, film products, lacquer- and melt dip coatings [16,17]. Industrially, mixed esters are prepared under heterogeneous conditions [18, 19]; few studies reported their synthesis under homogeneous conditions [1,20,21]. To our knowledge, there are no kinetic data on cellulose acylation to form mixed esters under homogeneous reaction conditions.

In the present study, we used conductivity measurements to investigate the simultaneous acylation of dissolved MCC by two acylating agents in mixtures of the IL 1-allyl-3-methylimidazolium chloride (AlMeImCl) with DMAc or DMSO. The acylating agents were acetic- and propionic anhydride (Ac_2O and Pr_2O respectively); N-acetyl-, N-benzoyl- and N-propionylimidazole (AcIm, BzIm, and PrIm, respectively), see Figure 1. Using ^1H NMR spectroscopy, we calculated the partial degree of substitution in each case, e.g., DAcetate and DPropionate for the reaction with $(\text{Ac}_2\text{O} + \text{Pr}_2\text{O})/\text{IL-MS}$. The ratio between the individual third-order rate constants k_3 , e.g., $k_{3,\text{Acetate}}/k_{3,\text{Propionate}}$ and that of the corresponding partial degree of substitution, e.g., $\text{DS}_{\text{Acetate}}/\text{DS}_{\text{Propionate}}$ were similar. That is, kinetic data can be successfully used to predict the partial degrees of substitution of the produced mixed esters. The reaction activation parameters indicated that the observed order of reactivity is due to both enthalpy and entropy.

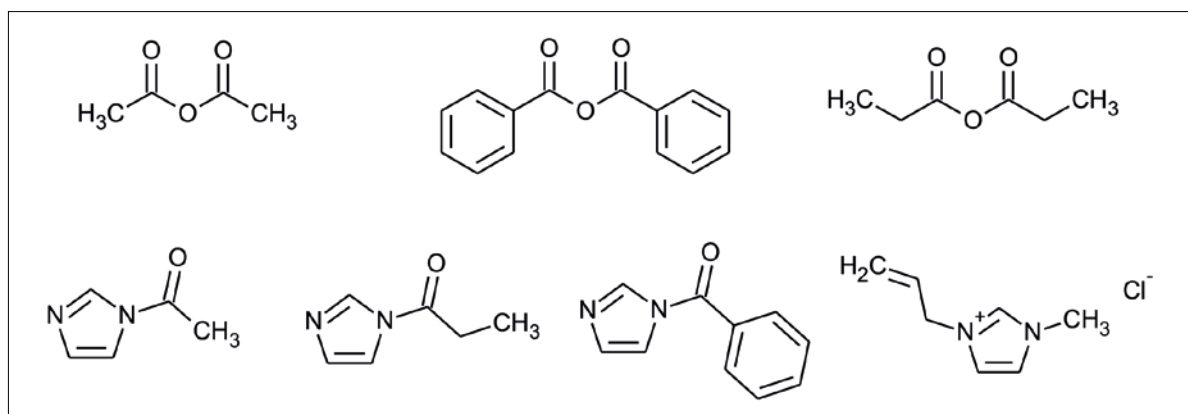


Figure 1: Molecular structures of the substances of interest in the present work; acetic-, benzoic- and propionic anhydride; N-acetyl-, N-propionyl-, N-benzoylimidazole and the ionic liquid 1-allyl-3-methylimidazolium chloride.

Experimental Section

Solvents, reagents and the IL

The MSs and reagents employed were purchased from Alfa Aesar or Merck and were purified according to recommended procedures [22]. Powder MCC (Avicel PH 101) was obtained from FMC BioPolymer, Philadelphia. The viscosity-based degree of polymerization of this cellulose ($DP_v = 175$) was determined by a standard procedure [23], using shear-dilution Cannon-Fenske viscometer (Schott), inserted in Schott AVS 360 automatic viscosity determination equipment. To determine the MCC index of crystallinity (I_c) we used Rigaku Miniflex diffractometer, operating at 30 kV, 15 mA and $\lambda(\text{CuK}\alpha) = 0.154 \text{ nm}$; $0.02^\circ/\text{minute}$ was. I_c was calculated using the peak height method,[24] $I_c = 0.82$.

The IL was synthesized by a microwave-assisted solventless procedure (CEM, model DU-8316), as given elsewhere [7]. Its purity was confirmed by ^1H NMR spectroscopy (Varian Innova-300 NMR spectrometer; 300 MHz for ^1H , reference TMS) Its solution in water showed the absence of acid- or base-impurity (Hanna HI98103 portable pH-meter).

Dissolution of cellulose in binary mixtures of ionic liquid/molecular solvents

MCC (0.35 g, 21.6 mmol) was weighed into a three-necked round-bottom flask fitted with magnetic stirrer and addition funnel (no pressure equilibration tube) containing the appropriate mass of pure IL (20.18 g; 127 mmol). The flask was connected to a vacuum pump (2 mmHg) and heated to 90°C in ca. 2 h. While maintaining the reduced pressure, the IL was slowly introduced, with continuous stirring. The mixture (MCC plus IL) was kept under these conditions for 2 h. After complete dissolution of the MCC, the appropriate mass of the MS (30.4 g of DMAc or 29.82 g of DMSO) was added and the solution stirred for 15 minutes. The compositions of the resulting clear, slightly amber cellulose solutions were, in mol/L: MCC = 0.048; IL = 2.82, MS = 7.75, 8.48 for DMAc and DMSO, respectively. Because of miscibility problem for the reaction with $\text{Ac}_2\text{O}/\text{Pr}_2\text{O}$ in DMAc, we used a more dilute MCC solution, 0.036 mol/L.

Kinetics of acylation of MCC in IL/MSs

For conductivity measurements, we employed PC-controlled Mettler-Toledo S400 SevenExcellence pH/mV meter provided with Mettler InLab 710 conductivity electrode. The latter was inserted into the PTFE cover (fitted tightly with aid of a Viton O-ring) of a double-walled conductivity cell through which water was circulated from a thermostat. We monitored the progress of the acylation reaction by following the

increase in solution conductivity (λ) as a function of time (t), at a constant temperature (T).

The experiment was carried out by introducing the MCC solution in IL-MS into the conductivity cell; thermal equilibration (10 min); addition of the pre-heated solution of the acylating agent in the MS; following the change of (λ) as a function of (t). Acid anhydrides were dissolved in the MS, whereas *N*-acylimidazoles were prepared *in situ* by reacting imidazole with the appropriate acid anhydride in the MS (molar ratio imidazole/acid anhydride 2:1, 30 minutes stirring, room temperature; clear solutions). Table SI-1 (Table 1 of Supplementary Information) shows the final concentrations of MCC, the IL and the acylating agents in the conductivity cell.

The observed rate constants (k_{obs} , s^{-1}) were calculated from the dependence of (λ) on (t), see Figure 2. The second order rate constant (k_2 ; $\text{L mol}^{-1}\text{s}^{-1}$) was calculated from $k_2 = k_{\text{obs}}/[\text{acylating agent}]$. Dividing k_2 by [IL] gave the third order rate constants (k_3 , $\text{L}_2\text{mol}^{-2}\text{s}^{-1}$). The activation parameters were calculated from the dependence of k_3 on T (10 to 70°C), by using standard equations [9].

Synthesis of cellulose mixed esters under conditions of the kinetic experiment

The kinetic experiments were repeated on a larger scale as described elsewhere [20]. Briefly, 0.15 g of MCC was dissolve in 5 mL of 4.24 mol/L IL in the appropriate MS using microwave heating (80°C , 30 min, 30 W), followed by addition of 5 mL of 1.1 mol/L of $\text{Ac}_2\text{O}/\text{Pr}_2\text{O}$ (1:1 molar ratio) or AcIm/BzIm (1: 3 molar ratio) in the MS and heating (80°C , 4 h, 30 W). The produced cellulose mixed ester was precipitated in ethanol, and further purified by suspension several times in hot ethanol. It was filtered and dried for 24 h at 60°C under reduced pressure. Values of the partial DS of the product were calculated from their ^1H NMR spectra (Varian Innova-300 NMR spectrometer), using DMSO-d_6 to which a drop of trifluoroacetic acid was added to displace the signal from the residual OH groups of the AGU. The partial DS values were calculated by comparing the integration the methyl groups of the acetate and propionate moieties, see Figure SI-1 (Figure 1 of Supplementary Information), or the acetate and benzoate groups, see Figure 2.

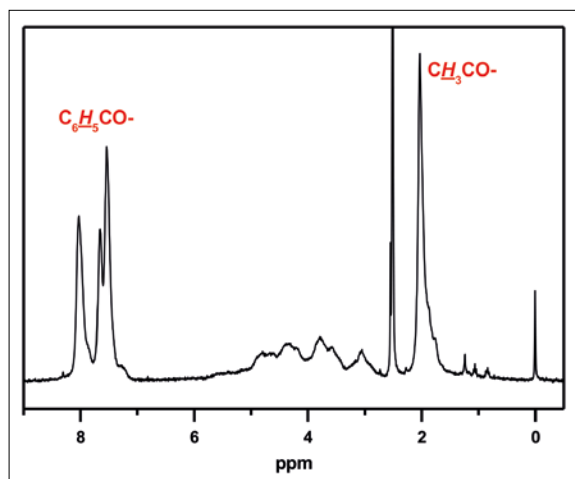


Figure 2: ^1H NMR spectrum in $\text{DMSO-}d_6$ of acetate/benzoate mixed ester synthesized in IL/DMSO (1 *AcIm* + 3 *BzIm*/AGU:). $DS_{Ac} = 1.2$; $DS_{Bz} = 1.08$; $DS_{Ac}/DS_{Bz} = 1.11$. The values $DS_{Acetate}$ and $DS_{Benzoate}$ were calculated by comparing the integrations of $\text{CH}_3\text{CO-}$ (1.9-2.1 ppm) and $\text{C}_6\text{H}_5\text{CO-}$ (7.6-8.2 ppm) peaks.

Synthesis of acetate/benzoate mixed esters of cyclohexylmethanol

This ester was synthesized by reacting mixtures of *N*-acetyl- and *N*-benzoylimidazole in different molar ratios with cyclohexylmethanol (CHM, molar ratio: alcohol:*N*-acylimidazole = 3:1) using microwave heating (60 °C, 2 h, 30 W) in acetonitrile. The relative yields

of the two esters was determined by gas chromatographic analysis using Shimadzu GC-17A equipment, FID, helium carrier gas, flow rate 71 mL/min, injector $T = 250$ °C, column $T = 85$ °C for 3 min and heating ramp of 20 °C/min until 250 °C.

Calculation of the volumes of solvated *N*-acylimidazoles

Calculation of the volumes of *N*-acylimidazoles was done by geometry optimization (gas) using the Orca v. 2.9 software [25]. Molecular volumes of the optimized geometries of *N*-acylimidazoles in DMSO were computed using the Gaussian 09 software [26].

RESULTS AND DISCUSSION

Kinetic data: rate constants and activation parameters

We carried out the kinetic experiments under pseudo first-order conditions; the concentrations of the acylating agents and the IL were in excess relative to [MCC]. Figure 3 shows the variation of solution conductivity as a function of (t). Values of k_{obs} were calculated from (linear) plots of $\ln(\lambda_{\infty} - \lambda_t)$ versus (t), where the “infinity reading” ∞ was calculated by non-linear least square analysis. Second-order rate constants (k_2) were calculated by dividing (k_{obs}) by [acylating agent].

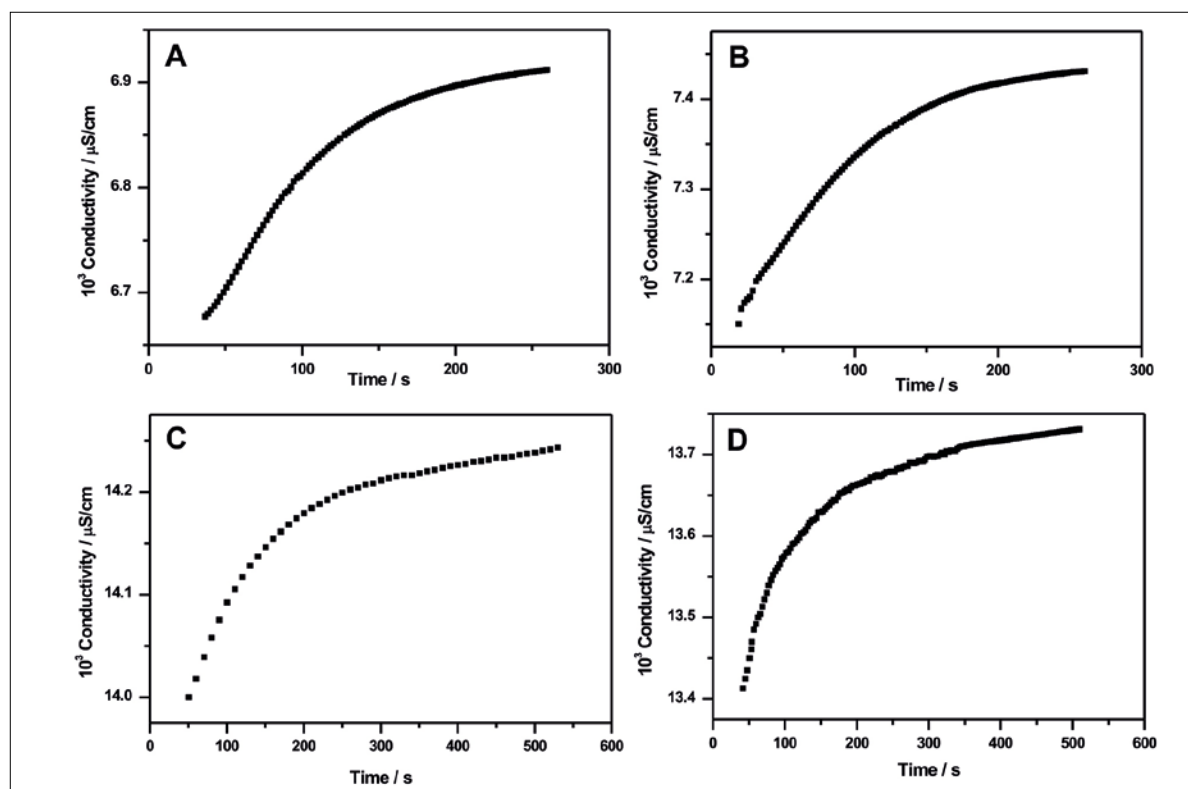


Figure 3: Typical kinetic results showing the dependence on time (t) of solution conductance, employed to calculate the pseudo-first order rate constants (k_{obs}). Part (A) acylation of MCC with pure *AcIm* (40 °C, IL/DMAc); (B) reaction of MCC with *AcIm* + *BzIm* (40 °C, IL/DMAc); (C) reaction of MCC with Ac_2O (50 °C, IL/DMSO); (D) reaction of MCC with $\text{Ac}_2\text{O} + \text{Pr}_2\text{O}$.

Previously we showed that (k_2) increases as a function of increasing [IL] because MCC reacts as a complex (AGU-OH.....IL), so that we calculated the value of (k_3) from: $k_3 = k_2/[IL]$ [8].

The acylating agents used included acid anhydrides and *N*-acylimidazoles. In each case, we ran the reaction

of MCC with each acylating agent alone, and then with a mixture of both acylating agents. The calculated rate constants are listed in Table 1; the corresponding activation parameters are given in Table 2.

Table 1: Calculated third order rate constants (k_3 ; $L^2 \text{ mol}^{-2} \text{ s}^{-1}$) for the acylation of microcrystalline cellulose with carboxylic acid anhydrides in mixtures of 1-allyl-3-methylimidazolium chloride (IL) and the molecular solvents *N,N*-dimethylacetamide (DMAc) and dimethyl sulfoxide (DMSO).^a

| Acylation in IL-DMAc | | | | |
|-----------------------------|--|--|--|--|
| | Ac₂O alone | Pr₂O alone | Mixture Ac₂O + Pr₂O | Ratio; rate constants |
| Temp (°C) | 10⁴ x k_{3,Ac2O} | 10⁴ x k_{3,Pr2O} | 10⁴ (k_{3,Ac2O}+ k_{3,Pr2O}) | k_{3,Ac2O}/k_{3,Pr2O} |
| 40 | 1.76 | 1.58 | 1.64 (-1.8) ^b | 1.11 |
| 50 | 3.39 | 2.91 | 3.10 (-1.6) ^b | 1.16 |
| 60 | 7.27 | 6.19 | 6.62 (-1.7) ^b | 1.17 |
| 70 | 13.28 | 11.72 | 11.83 (-5.7) ^b | 1.13 |
| Acylation in IL-DMSO | | | | |
| | 10³ x k_{3,Ac2O} | 10³ x k_{3,Pr2O} | 10³ (k_{3,Ac2O}+ k_{3,Pr2O}) | k_{3,Ac2O}/k_{3,Pr2O} |
| 30 | 1.37 | 1.20 | 1.29 (0.4) ^b | 1.14 |
| 40 | 2.34 | 1.91 | 2.22 (4.3) ^b | 1.23 |
| 50 | 3.70 | 2.93 | 3.28 (-1.1) ^b | 1.26 |
| 60 | 5.27 | 4.45 | 4.82 (-0.8) ^b | 1.19 |

a - The ratios $DS_{\text{Acetate}}/DS_{\text{Propionate}}$, calculated from the ¹H NMR spectra of the synthesized cellulose mixed esters were 1.1 and 1.3 for the reaction in IL-DMAc and IL-DMSO, respectively.

b - The numbers within parenthesis in the fourth column correspond to % difference between k_3 for the acylation by mixture of anhydrides and the mean of k_3 for the reaction with the individual anhydrides. That is, the value within parenthesis = $\{[k_3(\text{Ac}_2\text{O}+\text{Pr}_2\text{O}) - [(k_3\text{Ac}_2\text{O} + k_3\text{Pr}_2\text{O})/2]] / k_3(\text{Ac}_2\text{O}+\text{Pr}_2\text{O})\} \times 100$.

Table 2: Calculated activation parameters for the acylation of microcrystalline cellulose with carboxylic acid anhydrides in mixtures of 1-allyl-3-methylimidazolium chloride (IL) and the molecular solvents *N,N*-dimethylacetamide (DMAc) and dimethyl sulfoxide (DMSO).^a

| Acylation in IL-DMAc | | | |
|---------------------------------------|--|---|--|
| Acyating agent | Δ^*H (kcal/mol) | $T\Delta^*S$ (kcal/mol) | Δ^*G (kcal/mol) |
| Ac ₂ O alone | 13.97 | -9.45 | 23.42 |
| Pr ₂ O alone | 13.83 | -9.67 | 23.50 |
| Ac ₂ O + Pr ₂ O | 13.67 | -9.79 | 23.46 |
| Acylation in IL-DMSO | | | |
| Ac ₂ O alone | 8.44 | -13.19 | 21.63 |
| Pr ₂ O alone | 8.13 | -13.61 | 21.74 |
| Ac ₂ O + Pr ₂ O | 8.11 | -13.57 | 21.68 |

a- Activation parameters were calculated at 40 °C

The corresponding kinetic data for acylation of MCC by *N*-acylimidazoles in IL-MS are listed in Tables 3 and 4, respectively.

Table 4: Calculated activation parameters for the acylation of microcrystalline cellulose with *N*-acylimidazoles in mixtures of 1-allyl-3-methylimidazolium chloride (IL) and the molecular solvents *N,N*-dimethylacetamide (DMAc) and dimethyl sulfoxide (DMSO).^a

| Acylation in IL-DMAc | | | |
|-----------------------------|--|---|--|
| Acyating agent | Δ^*H (kcal/mol) | $T\Delta^*S$ (kcal/mol) | Δ^*G (kcal/mol) |
| AcIm alone | 3.23 | -17.76 | 20.99 |
| BzIm alone | 3.17 | -17.83 | 21.00 |
| AcIm + BzIm | 3.12 | -17.90 | 21.02 |
| Acylation in IL-DMSO | | | |
| AcIm alone | 3.71 | -17.15 | 20.86 |
| BzIm alone | 3.65 | -17.26 | 20.91 |
| AcIm + BzIm | 3.59 | -17.29 | 20.88 |

a- Activation parameters were calculated at 40 °C

Table 3: Calculated third order rate constants (k_3 in $L^2 \text{ mol}^{-2} s^{-1}$) for the acylation of microcrystalline cellulose with *N*-acylimidazoles in mixtures of 1-allyl-3-methylimidazolium chloride (IL) and the molecular solvents *N,N*-dimethylacetamide (DMAc) and dimethyl sulfoxide (DMSO).^a

| Acylation in IL-DMAc | | | | |
|-----------------------------|---|---|---|---|
| | AcIm alone | BzIm alone | Mixture AcIm + BzIm | Ratio; rate constants |
| Temp (°C) | $10^3 \times k_{3,\text{AcIm}}$ | $10^3 \times k_{3,\text{BzIm}}$ | $10^3 \times (k_{3,\text{AcIm}} + k_{3,\text{BzIm}})$ | $k_{3,\text{AcIm}}/k_{3,\text{BzIm}}$ |
| 20 | 6.85 | 6.69 | 6.71 (-0.9) ^b | 1.02 |
| 30 | 8.67 | 8.73 | 8.50 (-2.4) ^b | 0.99 |
| 40 | 10.65 | 9.99 | 9.94 (-3.8) ^b | 1.07 |
| 50 | 12.62 | 12.53 | 12.36 (-1.7) ^b | 1.01 |
| Acylation in IL-DMSO | | | | |
| | $10^3 \times k_{3,\text{AcIm}}$ | $10^3 \times k_{3,\text{BzIm}}$ | $10^3 (k_{3,\text{AcIm}} + k_{3,\text{BzIm}})$ | $k_{3,\text{AcIm}}/k_{3,\text{BzIm}}$ |
| 20 | 8.31 | 7.33 | 8.19 (4.5) ^b | 1.13 |
| 30 | 10.04 | 10.09 | 9.70 (-3.8) ^b | 1.00 |
| 40 | 13.43 | 12.05 | 12.45 (-2.3) ^b | 1.11 |
| 50 | 16.26 | 14.69 | 15.94 (2.9) ^b | 1.11 |

a - The ratio $DS_{\text{Acetate}}/DS_{\text{Benzoate}}$, calculated from ^1H NMR spectrum (300 MHz) of the synthesized mixed esters were 0.41 (molar ratio AcIm/BzIm = 1:4), 0.91 (AcIm/BzIm = 1:3) for DMAc and 0.71 (AcIm/BzIm = 1:4 BzIm), 1.11 (AcIm/BzIm = 1:3) for DMSO.
b - The numbers within parenthesis correspond to % difference between k_3 for the acylation by mixture of both anhydrides and the mean of k_3 for the reaction with the anhydrides separately. That is, value within parenthesis = $\{[k_3(\text{AcIm} + \text{BzIm}) - ((k_3\text{AcIm} + k_3\text{BzIm})/2)]\} \times 100$.

Regarding these results, the following is relevant:

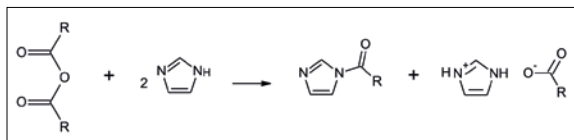
i- First we address acylation by carboxylic acid anhydrides. In both MSs, acylation by pure Ac₂O is faster than by pure Pr₂O by 14 ± 3% (DMAc) and 20 ± 6% (DMSO). This difference in reactivity is probably due to a combination of: (a) slightly higher electrophilicity of the acyl group of former anhydride (pK_a in water = 4.75 and 4.87, for acetic- and propionic acid, respectively) [27]; (b) smaller molar volume of the former anhydride (94.35 cm³/mol) than the latter one (128.99 cm³/mol), i.e., Ac₂O is 73.14% smaller than Pr₂O [27].

ii- The observation that k₃ for the reaction of MCC with the mixture of anhydrides is not far from the mean of the sum of k₃ for the reaction with the individual anhydrides shows that these acylations are practically independent, being affected only by electronic (electrophilicity of the acyl group) and steric factors (volume of the acylating reagent).

iii- The effect of the MS is shown in the activation parameters of Table 2. Here the reaction in IL-DMSO is faster than in IL-DMAc because of gain in Δ[‡]H (Δ[‡]H_{DMSO} < Δ[‡]H_{DMAc} by 5.6 ± 0.1 kcal/mol) not completely compensated by loss in the entropy term (|TΔ[‡]S|_{DMSO} > |TΔ[‡]S|_{DMAc} by 3.8 ± 0.1 kcal/mol).

iv- The ratios between k₃Ac₂O/k₃Pr₂O in both MSs are between 1.11 and 1.26 whereas the DS_{Acetate}/DS_{Propionate}, calculated from the ¹H NMR spectra of the synthesized cellulose mixed esters were 1.1 and 1.3, for DMAc and DMSO, respectively. That is, kinetic data can be employed to predict the structure of the product. To our knowledge, this is the first time that this use is shown, at least for derivatization under homogeneous reaction conditions.

To expand the scope of our investigation, we studied the acylation by *N*-acylimidazoles because these are more reactive than the corresponding acid anhydride and, unlike acyl chlorides, no HCl is produced. *N*-acylimidazoles were generated *in situ*, as shown in Scheme 1:



Scheme 1: Generation *in situ* of *N*-acylimidazole by the reaction of the diazole with acid anhydride.

As shown in Scheme 1, the acylation solution contains imidazolium carboxylate side product that may, in principle, catalyze the acylation reaction by acid-base catalysis. Previously we showed, however, that imidazolium acetate is inert in acylation, i.e., the rate constants ob-

tained using pure *N*-acylimidazole and that prepared *in situ* are essentially the same [14].

Regarding acylation by *N*-acylimidazoles the following is relevant:

v- The (theoretically) calculated molar volumes of *N*-acylimidazoles solvated in DMSO are 78.25, 105.37, 126.49 cm³/mol, giving relative volumes of 1: 1.35: 1.62 for AcIm, PrIm, BzIm, respectively. The pK_a of benzoic acid in water is 4.2 [27], i.e., the acyl group of BzIm is somewhat more electrophilic than that of the aliphatic *N*-acylimidazoles. Based on this factor alone, for AcIm/BzIm of 1:1, we expected DS_{Acetate}/DS_{Benzoate} ≤ 1; this was not the case. Therefore, relative to AcIm the reactivity of BzIm, hence DS_{Acetate}/DS_{Benzoate} is determined by the balance between favorable reactivity of BzIm and unfavorable steric factor due to its larger volume and rigid structure. Steric effects are important in cellulose derivatization because cellulose dissolved in ILs is present as aggregates [28,29]. Consequently, the diffusion of BzIm into these aggregates is expected to be slower than that of AcIm, leading to DS_{Acetate}/DS_{Benzoate} > 1, for AcIm/BzIm molar ratio of unity.

vi- To assess the relative importance of these opposing factors we synthesized esters by reacting CHM (a model for C6-OH of the AGU) with mixtures of *N*-acylimidazoles in IL-MSs, see Table 5. In this reaction, two esters are produced, namely, CHM-based (acetate + propionate) and/or (acetate + benzoate). Because CHM is monomeric we expected, *in principle*, CHM-acetate/CHM-second ester ≈ 1.

vii- Entries 1 and 2 of Table 5 indicate that the ratios of the esters prepared in IL-MSs are close to unity (1.1, 1.3 for DMAc and DMSO, respectively). That is, the nature of the acylating agent (aliphatic anhydride or *N*-acylimidazole with aliphatic acyl group) apparently does not affect the relative ratios between the esters. Entries 3 to 8 show, however, that this is not the case for the reaction of CHM with (AcIm + BzIm), where the former is clearly favored. Thus, the above-mentioned steric retarding effect is also operative for a simple molecule like CHM; ester ratio ≈ 1 is obtained *only* when BzIm is used in excess, e.g., entry 5.

viii- As expected, the reaction with *N*-acylimidazoles is faster than that with the corresponding anhydride. As shown in Tables 2 and 4 the reason is a large decrease in reaction enthalpy (ca. 10 kcal/mol) not completely compensated by the TΔ[‡]S term (ca. 8 kcal/mol). The reaction rates in the molar polar DMSO are 14 to 29% faster than in DMAc due to subtle differences in the activation parameters.

Table 5: Conditions for- and results of the microwave-assisted synthesis of cyclohexylmethanol-based esters by reaction with *N*-acylimidazoles in IL-MSs.^a

| Entry | AcIm/RCOIm molar ratio | Reaction Conditions | Ester ratio |
|-------|--|---|-------------|
| 1 | Ac ₂ O/Pr ₂ O; 1:1 | IL-DMAc; 4h; 30W; 80°C; 6 acylating agents/AGU | 1.1 |
| 2 | AcIm/PrIm; 1:1 | IL-DMSO; 4h; 30W; 80°C; 6 acylating agents/AGU | 1.3 |
| 3 | AcIm/BzIm; 1:1 | IL-DMSO; 30W; 80°C; 6 acylating agents/AGU | 5.0 |
| 4 | AcIm/BzIm; 1:2 | IL-DMSO; 30W; 80°C; 6 acylating agents/AGU | 3.7 |
| 5 | AcIm/BzIm; 1:3 | IL-DMSO; 30W; 80°C; 6 acylating agents/AGU | 1.1 |
| 6 | AcIm/BzIm; 1:3 1:3 | IL-DMAc; 30W; 80°C; 6 acylating agents/AGU | 0.9 |
| 7 | AcIm/BzIm; 1:4 | IL-DMSO; 30W; 80°C; 6 acylating agents/AGU | 0.7 |
| 8 | AcIm/BzIm; 1:4 | IL-DMAc; 30W; 80°C; 6 acylating agents/AGU | 0.5 |

a - Ester ratio refers to the ratio between the two esters produced simultaneously (always relative to acetate). E.g., for the reaction of CHM with (AcIm + PrIm) the result of entry 1, column 4 means that the yield cyclohexylmethyl acetate/ cyclohexylmethyl propionate = 1.1.

Conclusions

Using a simple technique, conductivity, we studied the formation of mixed esters, namely acetate/propionate and acetate/benzoate obtained by the reaction of MCC with mixtures of acid anhydrides and/or *N*-acylimidazoles. This is the first report on the kinetics of formation of mixed esters under homogeneous reaction conditions. The composition of the produced esters can be predicted from the kinetic data, if steric factors are not dominating. This is the case for flexible acylating agents, e.g., Ac₂O and Pr₂O. The reactivity of rigid acylating agents, e.g., BzIm is controlled by steric effects more than by the electrophilicity of its acyl

group. The use of kinetic data to predict product composition eliminates the labor involved optimizing the reaction conditions to obtain mixed esters with targeted partial DS values.

Acknowledgements

Thais Bioni thanks CAPES pre-doctoral research fellowship, O. A. El Seoud thanks CNPq and FAPESP for research productivity fellowships (grant 307022/2014-5), and financial support (grant 2014/22136-4). Naved I. Malik thanks FAPESP for a postdoctoral research fellowship (grant 2013/18008). We thank Dr. Paulo A. R. Pires for carrying out the theoretical calculations.

References

- [1] M. Gericke, P. Fardim, T. Heinze, *Molecules*, 2012, 17, 7458.
- [2] M. Kostag, K. Jedvert, C. Achtel, T. Heinze, O. A. El Seoud, *Molecules*, 2018, 23, 511.
- [3] T. Heinze, O. A. El Seoud, A. Koschella, *Cellulose derivatives: Synthesis, structure, and properties*, 1a Ed., Springer, Cham, 2018.
- [4] K. Baba, E. Ono, S. Itoh, K. Utoh, T. Noda, K. Usui, M. Ishihara, H. Inamo, D. Takagi, T. Asano, *J. Chem. Eur.*, 2006, 12, 5328.
- [5] S. Tiwari, A. Kumar, *J. Phys. Chem. A*, 2012, 116, 1191.
- [6] N. D. Khupse, A. Kumar, *J. Phys. Chem. A*, 2011, 115, 10211.
- [7] T. A. Bioni, E. P. G. Arêas, L. G. Couto, G. Favarin, O. A. El Seoud, *Nordic Pulp*, 2015, 30 (1), 105.
- [8] H. Nawaz, P. A. R. Pires, E. P. G. Arêas, N. I. Malek, O. A. El Seoud, *Macromol. Chem. Phys.*, 2015, 216, 2368.
- [9] E. V. Anslyn, D. A. Dougherty, *Modern Physical Organic Chemistry*, University Science Books, Sausalito, 2006, 355.
- [10] N. D. Khupse, A. Kumar, *J. Solution Chem.*, 2009, 38, 589.
- [11] M. Tariq, K. Shimizu, J. M. S. S. Esperança, J. N. C. Lopes, L. P. N. Rebelo, *Phys. Chem. Chem. Phys.*, 2015, 17, 13480.
- [12] P. A. R. Pires, N. I. Malek, T. C. Teixeira, T. A. Bioni, H. Nawaz, O. A. El Seoud, *Industrial Crops and Products*, 2015, 77, 180.
- [13] H. Nawaz, P. A. R. Pires, T. A. Bioni, E. P. G. Arêas, O. A. El Seoud, *Cellulose*, 2014, 21, 1193.
- [14] H. Nawaz, P. A. R. Pires, O. A. El Seoud, *Carb. Poly.*, 2013, 92, 997.
- [15] H. Nawaz, R. Casarano, O. A. El Seoud, *Cellulose*, 2012, 19, 199.
- [16] P. Carrolo, B. Grospietro, *Plastic Materials Macromol. Symp.*, 2004, 208, 335.
- [17] K. J. Edgar, C. M. Buchanan, J. S. Debenham, P. A. Rundquist, B. D. Seiler, M. C. Shelton, D. Tindall, *Prog. Polym. Sci.*, 2001, 26, 1605.
- [18] R. T. Bogan, R. J. Brewer, *Cellulose esters*, organic. In: J. I. Kroschwitz, M. Bickford, A. Klingsberg, J. Muldoon, A. Salvatore, (eds) *Encyclopedia of polymer science and engineering*. Wiley, NY, 1985, 158.
- [19] L. C. Treece, G. I. Johnson, *Chem. Ind.*, 1993, 49, 241.
- [20] S. Possidonio, L. C. Fidale, O. A. El Seoud, *J. Poly. Sci. Part A: Poly. Chem.*, 2010, 48, 134.
- [21] L. C. Fidale, S. Possidonio, O. A. El Seoud, *Macromol. Biosci.*, 2009, 9, 813.
- [22] W. L. F. Armagero, C. L. L. Chai, *Purification of Laboratory Chemicals*, 5th ed., Elsevier Ltd, New York, 2003.
- [23] ASTM, D 1795-94, *Standard test methods for intrinsic viscosity of cellulose*, 2001.
- [24] G. Buschlediller, S. H. Zeronian, *J. Appl. Polym. Sci.*, 1992, 45, 967.
- [25] F. Neese, U. Becker, D. Ganiouchine, S. Koßmann, T. Petrenko, C. Riplinger, F. Wennmohs, *Orca package v, 2.9*, University of Bonn, 2011.
- [26] Gaussian, Inc., Wallingford CT, 2016.
- [27] *CRC Handbook of Chemistry and Physics*, ed. D. R. Lide, CRC Press, Boca Raton, USA, 85th edn, 2004.
- [28] P. C. Trulove, W. M. Reichert, H. C. De Long, S. R. Kline, S. S. Rahatekar, J. W. Gilman, M. Muthukumar, *ECS Trans.*, 2009, 16, 111.
- [29] O. Kuzmina, E. Sashina, S. Troshenkowa, D. Wawro, *Fibers Text East Eur.*, 2010, 18, 32.

Lignocellulosic Multicomponent Fibers Spun from Superbase-Based Ionic Liquids

Michael Hummel*, Yibo Ma, Anne Michud, Shirin Asaadi, Annariikka Roselli, Agnes Stepan, Sanna Hellstén, and Herbert Sixta*

Department of Bioproducts and Biosystems, Aalto University, P.O. Box 16300, FI-00076 Aalto, Finland

*Contact: michael.hummel@aalto.fi, herbert.sixta@aalto.fi

In memoriam

Mag. Dr. Gerhard Laus († 2017)

Abstract

Recently, the list of solvents for cellulose dissolution and fiber spinning was extended with so-called ionic liquids, which bear great potential in terms of environmental and technical aspects. Herein, we report on 1,5-diazabicyclo[4.3.0]non-5-ene-1-ium acetate – a non-imidazolium, super-base-based ionic liquid – as excellent solvent for a wide set of lignocellulosic solutes to prepare composite fibers of cellulose, hemicellulose, and lignin. The solutions are processed in a Lyocell-type dry-jet wet spinning procedure, which allows for a filament draw in the air gap. The effect of the draw was dependent on the solute composition. With a high share of cellulose, a small draw led already to high tensile strength and modulus. All fibers showed high mechanical properties even when containing a high share of non-cellulosics.

Keywords: lignocellulose, multicomponent fibers, ionic liquids, spinning, fibers

Introduction

In 2005, Lenzinger Berichte published the first report on man-made cellulosic fibers spun from ionic liquids (ILs). [1] This seminal study by Laus and Schottenberger was motivated by an earlier publication of the Rogers group in 2002, when they reported the dissolution of cellulose in imidazolium-based ionic liquids and postulated shaping processes such as filament spinning. [2] ILs consist entirely of ions with a defined melting point below 100 °C. Through the combination of sterically demanding organic cations (mostly with a delocalized charge) and organic or inorganic anions the fluid state is favored in terms of enthalpy and entropy, giving those salts their characteristic low melting points. Amongst the virtually infinite number of ILs accessible through the combination of cations and anions [3], only few have been identified as cellulose solvents. Most of them are still based on an imidazolium cation and have anions such as halides, carboxylates, or phosphates to name only the most prominent ones. [4] Shortly after the discovery of

cellulose-dissolving ILs, some of those were also identified as suitable solvents for the secondary wood polymers, hemicellulose and lignin, either as isolated polymers or jointly in form of the entire wood matrix. Extensive reports and reviews on cellulose and wood dissolving ILs are meanwhile available. [5-10] Following the aforementioned report of Laus et al. in Lenzinger Berichte, numerous studies have investigated spinning of different cellulosic solutes in various, almost exclusively imidazolium-based ILs. A detailed review was given earlier. [4] In two extensive studies, the miscibility and processability of polysaccharide-polysaccharide mixtures in [emim]OAc was compared to NMMO and caustic solution. [11-12] Natural polymers were found to have a strong affinity to cellulose and gave homogeneous multicomponent fibers. Contrary, only few reports address lignocellulosic composite fibers. [13] Fink and coworkers have produced continuous filaments by dissolving hemp entirely [14] and have shown that cellulose can be co-processed with

lignin added to the cellulose solution. [15]

The vast majority of the studies describing IL-based fiber spinning are based on imidazolium halide or carboxylate ILs and used rather simple extrusion equipment which yielded filaments with diameters of 100 μm or higher. Unfortunately, they bear little potential to advance from proof-of-concept extrusion trials to industrial spinning processes as several limitations and drawbacks have been identified during the past decade. Already in the initial Lenzinger Berichte [1,16], severe polymer degradation was observed, when cellulose was processed in imidazolium-based ILs. Evidently, thermal stability and inertness towards the solute at the required processing temperatures are indispensable for feasible fiber spinning. Excessive degradation of the IL and biopolymer does not only limit the economy of the solvent but also complicates the solvent recovery and recycling substantially. Mainly for this reason, halide-containing ILs seem to have little potential for upscaling. They require comparatively high dissolution and processing temperatures at which the IL decomposes [17-18] and cellulose is depolymerized severely even if stabilizers are added. [1,16,19] Carboxylate-based ILs could bypass this problem to some extent. [20] However, the imidazolium moiety can initiate side reactions leading to cellulose modification [21] such as depolymerization [22-23] or acetylation through trans-acylation.[24]

Thermal and chemical stability represent only one criteria for an industrially applicable spinning process. The resulting ionic liquid-polymer solutions must show distinct visco-elastic properties to be suitable for fiber spinning. Many proof-of-concept studies demonstrate the extrusion of filaments with a large diameter through syringe-type devices but do not address the complexity of reducing the diameter to a level of $<20 \mu\text{m}$ which is needed for textile or technical applications. A key-feature of dry-jet wet spinning (cf. Lyocell process) is the draw of the fluid filament in the air gap. The generated elongational stress on the polymer solutions causes the cellulose chains to align along the fiber axis. The highly oriented structure is preserved upon coagulation, resulting in filaments with high mechanical strength and modulus characteristic for Lyocell-type fibers. The filament draw, however, also leads to a substantial decrease of the fiber diameter and is essential as the diameter of the spinneret orifices can only be reduced to a certain extent. A set of complex breaching mechanisms that can be observed in the air gap set a lower limit to the initial filament diameter. [25-26] If the filament is too thin at its exit-point it will break in the air gap and impede spinnability. Thus, the drawability of an initially thick filament is a key feature in the dry-jet wet spinning process to yield thin and strong

fibers. The archetypical IL, [emim]OAc, has been promoted as excellent cellulose solvent due to its low viscosity. However, filaments extruded from [emim]OAc-cellulose solutions can only be stretched to a limited extent because they lack the required elasticity. Also, the coagulation mechanism has to favor the rapid development of a solid polymer filament to prevent breaches in the spin bath. [27] Choosing wet spinning for IL-biopolymer solutions allows to use smaller spin capillaries with smaller diameter as subsequent draw forces are noticeably smaller, preventing aforementioned filament breaks. However, the lack of draw also limits the mechanical properties of the resulting fibers. Polymer alignment is mostly confined to shear-induced orientation in the spin capillary, which is only moderate compared to draw-induced alignment. Stretching of the filament in the spin or washing bath as it is done for advanced viscose fibers such as tire cord or to a smaller extent for Modal fibers is also only possible within limits. The chemical re-generation of viscose-type can be retarded through different additives to the dope or spin bath. The physical coagulation of cellulose-IL solution, however, is assumed to proceed via spinodal decomposition [28] which cannot be retarded to such an extent as in the viscose process. Thus, dry-jet wet spinning is the more promising technique for processing of ionic liquid-biopolymer solutions and, consequently, suitable visco-elastic properties are mandatory.

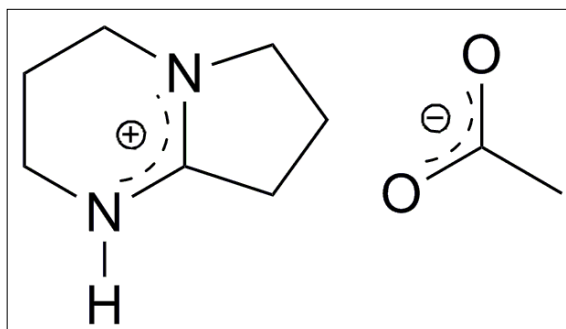


Figure 1: Chemical structure of 1,5-diazabicyclo[4.3.0]non-5-ene-1-ium acetate ([DBNH]OAc) used as solvent in this study.

In 2013, we found that the superbase-based ionic liquid 1,5-diazabicyclo[4.3.0]non-5-ene-1-ium acetate [DBNH]OAc (Figure 1) is an excellent solvent for lignocellulosic material. [29] Although solid at room temperature, [DBNH]OAc shows a very low viscosity of ca. 23 mPa s at its melting point of 65 $^{\circ}\text{C}$. This facilitates handling and favors the kinetics of polymer dissolution. The resulting cellulose solutions are characterized by visco-elastic properties that allow for dry-jet wet spinning at moderate temperatures of

70-85 °C with very high draw applicable, resulting in fibers with excellent mechanical properties. [DBNH]OAc proved to be a robust solvent to spin a broad variety of lignocellulosics. Besides various dissolving pulps [30], cellulose in combination with hemicellulose and/or lignin such as paper-grade kraft pulp, mildly refined birch wood [31], waste paper and cardboard [32], newsprint [33], and cellulose-lignin mixtures [34] were successfully spun into high-performance fibers as reported earlier. Herein, we provide a comprehensive summary of those fibers and establish a relationship between the non-cellulosic part and their influence on the properties of the resulting fibers.

Materials and Methods

Materials

Eucalyptus (*Eucalyptus urugrandis*) prehydrolysis kraft pulp ($[\eta] = 468$ ml/g, DP = 1026, $M_n = 79.8$ kDa, $M_w = 268.6$ kDa, polydispersity 3.4, Bahia Speciality Cellulose, Brazil), birch (*Betula pendula*) prehydrolysis kraft pulp ($[\eta] = 476$ ml/g, DP = 1133, $M_n = 65.9$ kDa, $M_w = 269.3$ kDa, polydispersity 4.1, Enocell Speciality Cellulose, Finland), birch ECF kraft pulp ($[\eta]: 1025$ ml/g; DP = 3100, $M_n = 53.3$ kg/mol, $M_w = 625.5$, polydispersity 11.7, Stora Enso – Imatra mill), and cotton wastes in form of hospital bed sheets (452 ml/g, DP = 1053, $M_n = 151.6$ kg/mol, $M_w = 348.4$ kg/mol polydispersity 2.29, Uusimaa Hospital Laundry – Uudenmaan sairaalapesula Oy, Finland) were used as cellulosic solute. A4 copy paper sheets of 80 g/m²

grammage were used as fine paper. Cuttings residues from a Finnish fluting board mill were used as cardboard source. Newsprint (Helsingin Sanomat) was collected from a local recycling station in Espoo, Finland. Birchwood (*Betula pendula*) chips were provided by Metla, Finland. Beechwood organosolv lignin (OS) was gratefully received from Fraunhofer Institutes, Germany. [34]

Details of the respective refining procedure of the birch wood [31], waste paper and cardboard [32], and newsprint [33] were described earlier. If necessary, the DP was adjusted through sulphuric acid treatment or E-beam irradiation.

[DBNH]OAc was prepared from 1,5-diazabicyclo [4.3.0]non-5-ene (99%, Fluorochem, UK) and acetic acid (glacial, 100%, Merck, Germany) as reported previously. [4]

Pulp dissolution and spinning

[DBNH]OAc was liquefied at 70 °C before the (ligno-) cellulosic solute was dispersed in the IL. The mixture was transferred to a vertical kneader system as described previously [10] and typically dissolved in 90 min or less. Multi-filaments were spun on a customized laboratory piston spinning system (Fourné Polymertechnik, Germany) as described earlier (Figure 2). [4] The spin solutions were extruded at 60-75 °C through spinnerets of 36 or 200 holes with a capillary diameter of 100 µm and a length to diameter ratio (L/D) of 0.2. The filaments were drawn in a ca. 1 cm air gap, coagulated in a water bath (15 °C), washed in hot water (60 °C), and air dried.

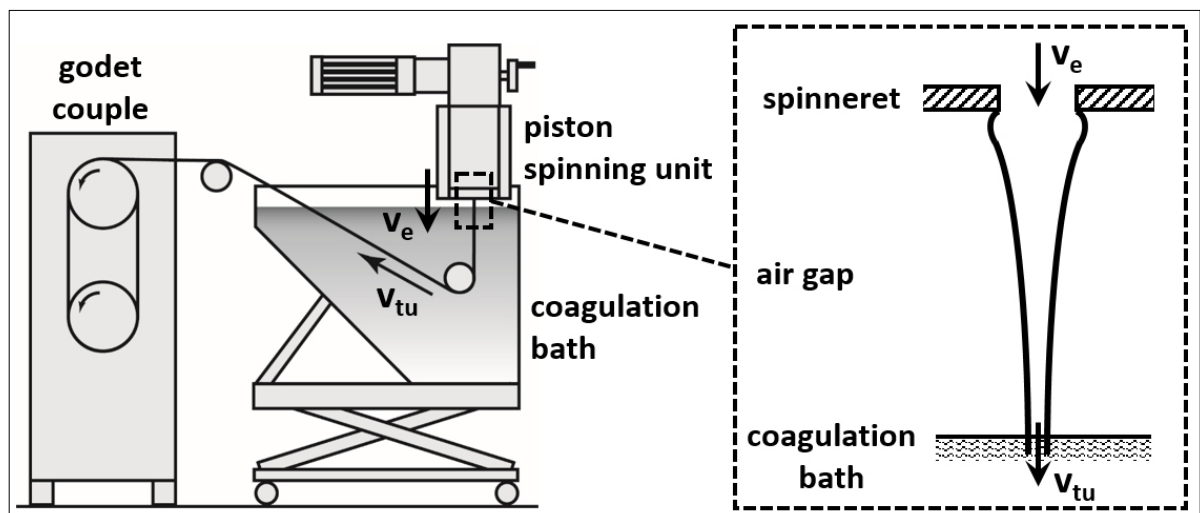


Figure 2: Left: schematic depiction of the customized laboratory piston spinning system (v_e = extrusion velocity, v_{tu} = take-up velocity); right: liquid filament in the air gap. After exiting the spinneret capillary the polymer solution shows dye swelling (exaggerated depiction) before the filament diameter decreases rapidly due to the draw force exerted by the increased take-up velocity. The draw ratio is defined as $DR = v_{tu} / v_e$. [4, 32]

Analytical methods

Methods for the assessment of the rheological properties, chemical composition and molar mass distribution are reported elsewhere. [31] Linear density (dtex), tenacity (cN/tex) and elongation at break (%) were determined according to DIN 53816 in both conditioned (23°C, 50% RH) and wet states using a Vibroskop-Vibrodyn system (Lenzing Instruments GmbH & Co KG, Austria) as described earlier. [33] The Young's modulus of the spun fibers was calculated from the slope of the entire elastic region of the stress-strain curves with a Matlab script according to ASTM standard D2256/D2256M.

Results and Discussion

Lignocellulosic solutes

In several earlier reports we have presented different sets of fibers spun from cellulose with or without hemicellulose and lignin.[30-35] An overview of the various raw materials and their composition is given in Table 1. Cotton taken from waste hospital bed sheets consisted of pure cellulose and had practically no other non-cellulosic constituents. [35] Two hardwood prehydrolysis kraft (PHK) dissolving pulps consisted of ca. 95% cellulose. [30] The hardwood kraft pulp sample had ca. 25% hemicelluloses. Pulps with a lignin content of 10-50% were prepared through

addition of organosolv (OS) lignin to eucalyptus PHK pulp. [34] Feedstock with both hemicellulose and lignin was included via paper and cardboard samples that were refined stepwise to increase the cellulose content gradually. [32] Also, waste newsprint pretreated with an alkaline glycerol pulping process [33] and unbleached birch kraft pulps [31] served as mixed-polymer solute. Both feedstock were pretreated with varying intensity to tailor the non-cellulosic polymer content.

All obtained pulps were adjusted to a target intrinsic viscosity of 400-500 ml/g either by sulfuric acid treatment or E-beam irradiation. The latter did not alter the composition of the feedstock. This particular viscosity level is typical for pulps used in the NMMO-based Lyocell process and proved also suitable for Ioncell spinning. However, the adjustment to the target intrinsic viscosity does not guarantee spinnability. In a systematic study, pulps with varying molar mass distribution were prepared and their spinnability correlated to the macromolecular features of the respective solutes.[36] It was found, that a share of 20-30% of cellulose chains with a $DP \geq 2000$ and an intermediate polydispersity index of around 3-4 were necessary to provide the visco-elastic properties that allow for a high draw ratio in the air gap. Accordingly, the pulps described in Table 1 were adjusted to meet those requirements.

Table 1: Composition of raw material and fibers spun from [DBNH]OAc.

| | | Pulp | | | | Fiber | | | |
|-------------------|-----------|---------------------|----------------|---------------------|-------------|-----------|----------------|---------------------|-------------|
| | | Viscosity [ml/g] | Cellulose % | Hemi-cellulose % | Lignin % | Dope % | Cellulose % | Hemi-cellulose % | Lignin % |
| eucalyptus PHK | | 424 | 95.8 | 2.6 | - | 13 | n/a | n/a | - |
| birch PHK | | 476 | 94.3 | 5.6 | - | 13 | n/a | n/a | - |
| paper | P1 | 470 | 75.5 | 24.1 | 0.4 | 11.5 | 75.9 | 23.2 | 0.98 |
| | P2 | 428 | 88.1 | 11.4 | 0.6 | 13 | 87.8 | 11.1 | 1.13 |
| cardboard | B1 | 500 | 80.2 | 16.6 | 2.9 | 11.5 | 80.8 | 16.4 | 1.13 |
| | B2 | 470 | 88.3 | 9.8 | 1.9 | 13 | 88.8 | 9.7 | 1.44 |
| | B3 | 353 | 89.6 | 9.7 | 0.8 | 13 | 89.4 | 9.6 | 1.01 |
| | B4 | 436 | 82.4 | 16.7 | 0.9 | 13 | 82.4 | 16.4 | 1.22 |
| newsprint | NP 170/3 | 443 | 75.4 | 21.0 | 3.6 | 13 | 77.2 | 19.9 | 2.9 |
| | NP 180/1 | 508 | 73.8 | 20.3 | 5.9 | 12 | 73.6 | 21.5 | 4.7 |
| lignin blends | 10 wt% OS | | 86.6 | 3.3 | 10.1 | 13 | 89.1 | 2.4 | 8.5 |
| | 15 wt% OS | | 81.3 | 3.7 | 15.0 | 13 | 85.4 | 2.3 | 12.3 |
| | 20 wt% OS | | 75.9 | 4.0 | 20.1 | 13 | 82.2 | 2.0 | 15.8 |
| | 30 wt% OS | | 65.2 | 4.9 | 29.9 | 13 | 72.3 | 2.3 | 25.4 |
| | 50 wt% OS | | 46.9 | 5.0 | 48.1 | 20 | 51.9 | 1.9 | 46.2 |
| recycl. cotton | | 452 | 100.0 | - | - | 13 | 100.0 | - | - |
| comm. birch kraft | CBK | 439 | 74.9 | 25.1 | - | 13 | n/a | 21.2 | - |
| lab. birch kraft | BK H25 | | 53.7 | 22.4 | 23.9 | 13 | 55.8 | 20.2 | 24.0 |
| | BK H50 | | 56.4 | 21.8 | 21.8 | 13 | 57.9 | 21.7 | 20.4 |
| | BK H200 | 361 | 75.1 | 9.8 | 15.1 | 13 | 75.2 | 6.1 | 18.7 |
| | BK H500 | 390 | 83.6 | 7.9 | 8.5 | 13 | 85.9 | 5.2 | 8.9 |
| | BK H800 | 367 | 84.6 | 10.4 | 5.0 | 13 | 88.5 | 6.9 | 4.6 |
| | BK H1000 | 403 | 85.0 | 10.2 | 4.8 | 15 | 88.1 | 8.0 | 3.9 |
| | BK H1200 | 351 | 85.9 | 9.8 | 4.3 | 15 | 87.8 | 7.2 | 5.0 |

Fiber spinning

After proper tuning of the rheological properties through polymer DP adjustment, variation of solute concentration and selection of the spin temperature all presented solutes showed good spinnability. As mentioned earlier, spinnability is defined by stable conti-

nuous extrusion and potential to draw the fluid filament in the air gap. [37] Herein, a draw ratio of >10 was considered as good spinnability, which was exhibited by all samples (see Table 2). All solutions could be spun at 60-75 °C.

Table 2: Properties of fibers spun from 13% solutions of the various solutes at the indicated draw ratio (spin capillary diameter in all cases: 100 µm). The pulp code is given in Table 1.

| pulp | draw ratio | conditioned | | | | | | | | wet | | | | | | | |
|-------------------------|------------|--------------|------|-------------------|-----|---------------|-----|----------|-----|-------------------|-----|---------------|------|----------|-------|-------------------|-------|
| | | Titer [dtex] | ± | Tenacity [cN/tex] | ± | Modulus [GPa] | ± | Elong. % | ± | Tenacity [cN/tex] | ± | Modulus [GPa] | ± | Elong. % | ± | Total orientation | ± |
| euca. PHK | 17.7 | 1.21 | 0.14 | 50.5 | 4.8 | 26 | 3.1 | 8.8 | 0.8 | 43.4 | 5.2 | | 9.6 | 1.1 | 0.727 | 0.007 | |
| birch PHK | 15.0 | 1.33 | 0.17 | 52.3 | 3.7 | 23 | 2.4 | 8.9 | 0.9 | 43.4 | 3.8 | | 11.8 | 1.7 | 0.740 | 0.030 | |
| P1 ¹⁾ | 14.1 | 1.34 | 0.23 | 37.6 | 1.7 | 22 | 2.9 | 8.6 | 0.9 | 28.7 | 4.2 | 17 | 1.8 | 9.3 | 1.6 | 0.713 | 0.067 |
| P2 | 16.8 | 1.36 | 0.12 | 43.2 | 1.4 | 24 | 1.4 | 9.4 | 0.5 | 34.0 | 2.3 | 18 | 1.1 | 34.0 | 2.3 | 0.700 | 0.040 |
| B1 ¹⁾ | 15.9 | 1.22 | 0.09 | 44.4 | 2.3 | 23 | 1.5 | 8.0 | 2.3 | 38.3 | 2.7 | 21 | 1.7 | 9.7 | 1.2 | 0.688 | 0.057 |
| B2 | 17.8 | 1.23 | 0.09 | 51.4 | 4.0 | 28 | 2.3 | 8.0 | 0.9 | 43.3 | 3.7 | 24 | 3.0 | 9.6 | 1.3 | 0.738 | 0.068 |
| B3 | 15.9 | 1.22 | 0.22 | 51.1 | 4.9 | 24 | 4.4 | 8.2 | 1.1 | 43.7 | 5.1 | 23 | 2.6 | 10.0 | 1.6 | 0.676 | 0.099 |
| B4 | 14.1 | 1.66 | 0.11 | 45.8 | 2.5 | 24 | 1.3 | 7.5 | 0.5 | 37.4 | 3.4 | 19 | 3.0 | 10.2 | 1.4 | 0.724 | 0.082 |
| NP 170/3 | 18.0 | 0.87 | 0.08 | 37.0 | 1.7 | 16 | 2.8 | 8.7 | 0.9 | 36.9 | 2.3 | | 9.6 | 0.8 | 0.675 | 0.119 | |
| NP 180/1 ²⁾ | 18.0 | 0.76 | 0.12 | 43.9 | 3.5 | 14 | 3.0 | 8.0 | 0.6 | 37.5 | 3.2 | | 8.5 | 1.2 | 0.713 | 0.033 | |
| 10 wt% OS | 15.0 | 1.30 | 0.10 | 42.7 | 1.8 | 24 | 3.8 | 9.2 | 1.2 | 36.0 | 1.2 | 24 | 1.9 | 9.4 | 0.9 | 0.692 | 0.057 |
| 15 wt% OS | 14.1 | 1.50 | 0.20 | 39.2 | 1.8 | 22 | 4.4 | 9.1 | 1.3 | 33.1 | 2.5 | 23 | 2.4 | 8.8 | 1.0 | 0.642 | 0.043 |
| 20 wt% OS | 10.6 | 2.00 | 0.30 | 34.0 | 1.9 | 15 | 1.8 | 11.0 | 1.1 | 29.7 | 2.1 | 18 | 1.3 | 11.5 | 0.9 | 0.686 | 0.058 |
| 30 wt% OS | 12.4 | 1.60 | 0.20 | 30.1 | 3.6 | 12 | 4.4 | 10.6 | 2.3 | 20.0 | 2.5 | 18 | 1.3 | 9.0 | 0.9 | 0.456 | 0.050 |
| 50 wt% OS ³⁾ | 14.1 | 2.10 | 0.20 | 25.7 | 2.6 | 11 | 2.2 | 15.6 | 3.8 | 16.6 | 2.2 | 15 | 0.3 | 11.8 | 1.6 | 0.350 | 0.061 |
| recycl. cotton | 14.1 | 1.40 | | 58.4 | 3.1 | 28 | 4.1 | 7.9 | 1.3 | 52.4 | 3.0 | | 10.2 | 0.8 | 0.745 | | |
| CBK | 12.5 | 1.70 | | 33.6 | 3.3 | 15 | 2.8 | 7.4 | 0.9 | 30.8 | 2.3 | | 9.9 | 2.8 | 0.710 | | |
| BK H25 | 9.7 | 2.02 | 0.24 | 23.0 | 2.1 | 13 | | 8.1 | 0.8 | 11.1 | 1.9 | | 7.7 | 1.5 | 0.507 | 0.055 | |
| BK H50 | 9.7 | 2.14 | 0.36 | 24.4 | 2.2 | 12 | | 7.4 | 0.7 | 13.7 | 1.3 | | 7.0 | 0.4 | 0.554 | 0.062 | |
| BK H200 | 14.1 | 1.56 | 0.13 | 32.1 | 2.4 | 12 | 1.1 | 9.5 | 0.7 | 22.2 | 2.4 | | 9.3 | 0.7 | 0.549 | 0.076 | |
| BK H500 | 12.4 | 1.78 | 0.13 | 38.1 | 2.4 | 18 | 2.1 | 9.0 | 1.1 | 26.1 | 2.9 | | 9.2 | 0.9 | 0.608 | 0.084 | |
| BK H800 | 15.9 | 1.52 | 0.21 | 40.2 | 3.6 | 17 | 0.6 | 8.8 | 0.8 | 27.5 | 1.4 | | 9.6 | 0.6 | 0.676 | 0.099 | |
| BK H1000 ⁴⁾ | 14.1 | 1.59 | 0.19 | 37.3 | 3.3 | 23 | 7.8 | 8.9 | 0.7 | 25.2 | 2.4 | | 8.9 | 0.7 | 0.678 | 0.041 | |
| BK H1200 ⁴⁾ | 8.8 | 2.74 | 0.30 | 32.9 | 4.1 | 15 | 5.9 | 9.2 | 1.7 | 19.9 | 5.0 | | 9.4 | 2.6 | 0.645 | 0.098 | |

¹⁾ spun from 11.5 wt% solution; ²⁾ spun from 12 wt% solution; ³⁾ spun from 20 wt% solution; ⁴⁾ spun from 15 wt% solution

Due to the mild processing conditions and high inertness of the ionic liquid the lignocellulosic solutes did not undergo significant depolymerization as reported for other ILs. [1,16,20] The molar mass distributions of the holocellulosic constituent were virtually identical for the original solute and the spun fiber. [4, 32] Compositional analysis revealed that a very small share of hemicelluloses was not recovered in the spun fiber and lost in the spin bath. It was shown earlier that low molecular weight hemicelluloses can be solubilized by IL-water mixtures. [38-39] Also, in the case of fibers with added beech lignin, lignin was not entirely recovered and a small amount was detected in the spin bath. Consequently, the cellulose content of the fibers is slightly higher than in the original solute (Table 1). Stress-strain curves of some selected samples and of commercial Lyocell and regular viscose fibers are plotted in Figure 3. Viscose as the only wet spun fiber plotted in Figure 3 shows the lowest slope in the initial elastic part, the highest elongation, and lowest tenacity. All Ioncell fibers show a similar elongation between

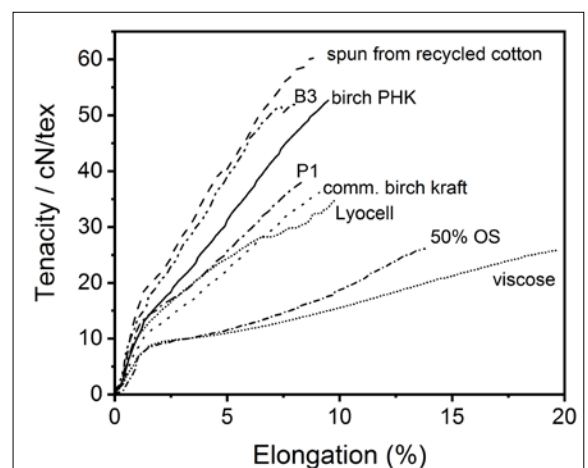


Figure 3: Stress-strain curves of selected samples produced at highest DR. For comparison, commercial Lyocell and viscose fibers were included.

8-10% typical for Lyocell-type fibers but higher tenacity than the commercial NMMO-Lyocell fiber. At 50% organosolv lignin content, the fibers show a

reduced tenacity, which is still higher than that of a commercial viscose fiber. At the same time, the elongation was extended to about 16%.

Fiber properties

As the draw ratio is getting higher, the lateral orientation of the polymer chains increases. This has a pronounced effect on the mechanical properties of the resulting fibers. Figure 4 illustrates the development of the tenacity as a function of the draw ratio. All solutions could be drawn to a high extent, virtually independent of the cellulose content. As the draw is getting higher, the tenacity starts to level off approaching a plateau

value which depends on the solute composition. In Figure 4, the lignocellulosic materials are roughly grouped according to their cellulose content. With lignin and hemicellulose being comparatively short biopolymers, the tensile properties are governed by the cellulosic constituent. With increasing cellulose content higher fiber tenacities are accessible with cotton as 100% cellulose and the 50/50 cellulose-lignin fibers representing the upper and lower limits, respectively. This relationship between the cellulose content and the tensile strength is known and used for commercial technical fibers such as tire cords, which are derived from high purity dissolving pulps.

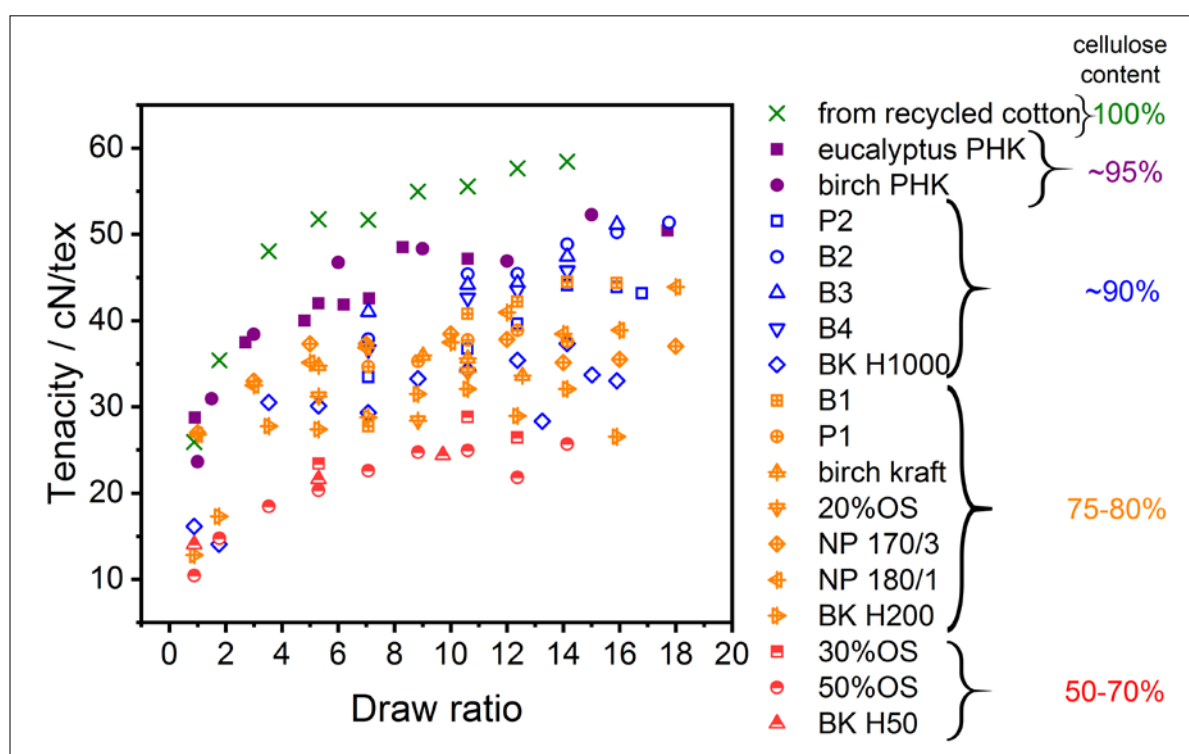


Figure 4: Development of the conditioned tenacity with increasing draw ratio. The lignocellulosic solutes are grouped according to their cellulose content (green, closed symbols: ca. 95% cellulose; blue, open symbols: ca. 90%; orange, +centered symbols: ca. 75-80%; red, half-filled symbols: ca. 50-70%).

Remarkably, the draw required to approach the plateau value depends on the share of non-cellulosic constituents. Filaments based on cotton, i.e. 100% cellulose, develop tenacity very quickly and already at a moderate draw of 5.3 they reach 90% of their final tensile strength of 58 cN/tex (at DR 14.1). As the cellulose content decreases, the tenacity-vs-draw curves flatten out and the tenacity is only developing slowly. A similar behavior was observed in a previous study when varying the concentration of dissolving pulp. The tenacity developed much faster when a 17% solution was spun as compared to 10% cellulose concentration, where the fibers gained strength only slowly with increasing draw ratio. [29]

The Young's moduli of the spun fibers – deduced from the initial elastic part of the stress-strain curve – show a similar trend as observed for the tenacity. Evidently, as the share of cellulose polymer chains and their orientation increase the resulting matrix is gaining in rigidity, reflected by an elevated modulus. Non-cellulosic polymers act as softener and reduce the tensile modulus of the composite fibers. For pure cellulose fibers the increase of the modulus can be correlated with an increase in the tensile strength. [40] A similar trend is observed to some extent despite the composite nature of the fibers under investigation (Figure 5). Based on previous interpretations, this relationship might indicate high structural conformity of the multi-component

fibers, that is the polymers are evenly distributed within the fiber forming a homogeneous matrix. However,

some deviation is observed for fibers with a higher share of hemicelluloses.

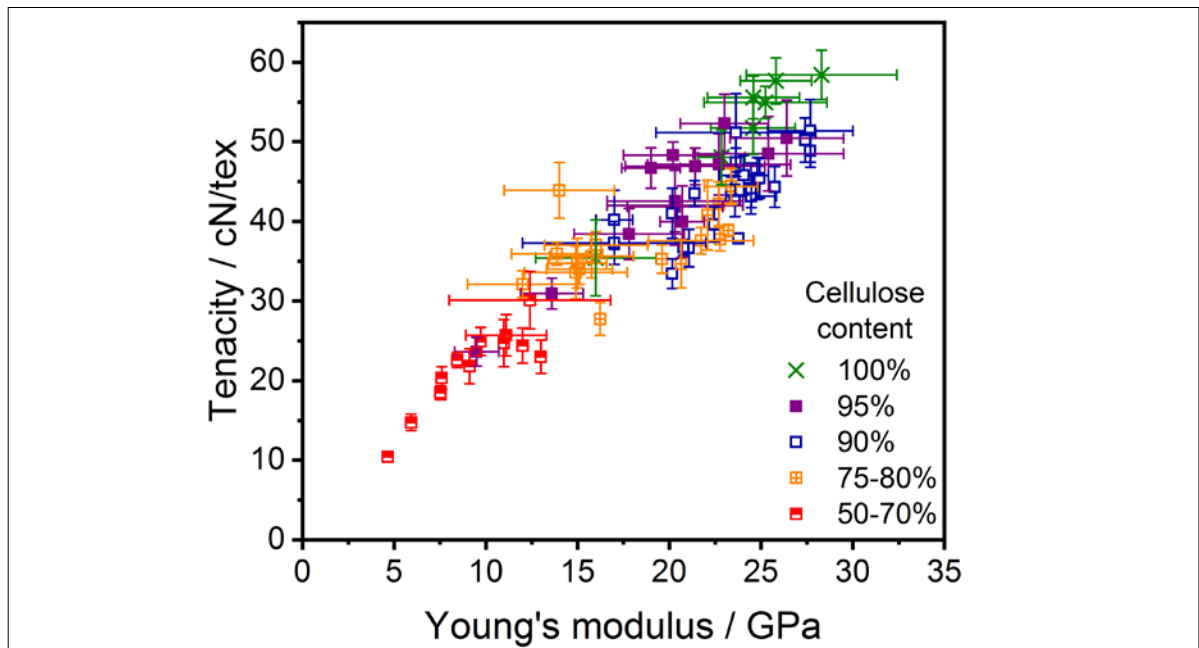


Figure 5: Relationship between tenacity and Young's modulus (in conditioned state) of all presented fibers at different draw ratios.

The elongation at break of regenerated cellulosic fibers is an important parameter in particular when targeting textile applications. The stiffness of the fibers is affecting the resulting yarn and fabrics and might lead to a reduced softness feel of the final garment. This is sometimes perceived as a downside of Lyocell-type filaments and other fibers with a highly oriented structure which are characterized by an elongation at break of <15% in conditioned state. [41] Lenz et al. proposed that the elongation mechanism during lateral fiber deformation is associated with the orientation of the crystalline regions and the straightening of the less ordered amorphous domains in the interstices between the crystallites. [42-44] Thus, the draw ratio also affects the elongation at break. In contrast to the above discussed tensile strength and modulus, the elongation declines for all lignocellulosic solutes as the draw ratio is increased. Non-cellulosic constituents can act as plasticizers and increase the elongation at break.

Summary of the influence of non-cellulosic constituents on the fiber properties

As described above, cellulose is the property-determining constituent in the polymer blend fibers. Owing to its comparably high DP, cellulose governs in particular the mechanical properties. A strength weakening effect of an increasing share of hemicellulose was also reported for viscose and NMMO-Lyocell fibers. [45-46]

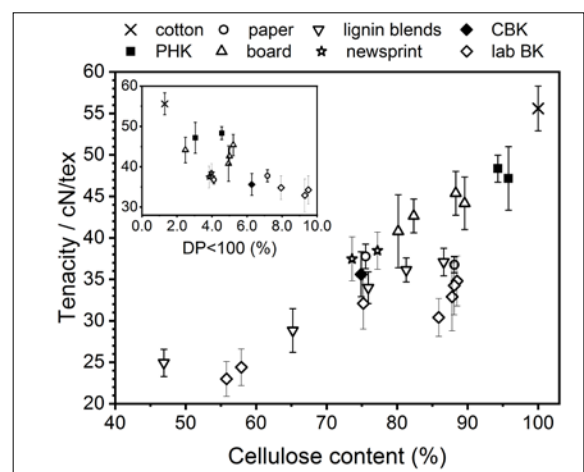


Figure 6: Dependency of the conditioned tenacity of fibers spun at draw ratio of 10 on the cellulose content of the different materials. The inset shows the correlation of the tenacity with the share of low-molecular weight cellulose chains with a DP < 100.

Figure 6 illustrates the tensile strength of all fibers as a function of their cellulose content. In order to minimize draw-induced differences in the cellulose orientation, all depicted values derive from fibers spun at DR 10. The orientation of fibers with non-cellulosic constituents will be reduced nonetheless. As mentioned earlier, the mechanical properties are connected to various structural parameters such as crystallinity, crystallite length and orientation of the amorphous

interstice-domains. [44] Although they are primarily affected by the draw, non-cellulosic parts will obviously influence them as well.

A distinct correlation can be observed, with cotton as pure cellulose yielding the highest strength value. In fact, it is not the chemical nature of hemicellulose that affects the fiber properties but the share of short-chain polymers which is proportional to the presence of hemicellulose. [47] The inset in Figure 6 shows the tenacity of the holocellulose fibers vs. the share of polymers with a DP<100 (cellulose-lignin blend fibers are excluded). As the relative amount of short chains is increasing the fiber tenacity is reduced. This would suggest that narrowly distributed pulps with a high average DP would be most suitable for the production of high-strength fibers. However, this is partly in conflict with the rheological requirements where pulps with a broad molecular weight distribution yield visco-elastic properties that provide better spinnability.

Conclusions

More than 10 years after the seminal publication by Laus and Schottenberger on the potential of ionic liquids for the production of man-made cellulosic fibers, superbase-based ILs seem promising to overcome the obstacles that were identified initially. [DBNH]OAc proved as excellent lignocellulose solvent to produce biopolymer composite fibers for textile and technical applications. The wood constituents cellulose, hemicellulose, and lignin are well soluble and fibers with high mechanical properties could be spun in all cases. A distinct relationship between the cellulose content and tenacity, modulus and elongation at break was identified. Meanwhile, also other groups have picked up and expanded the portfolio of super-base based ILs for fiber spinning. [48] However, more systematic studies are certainly needed to obtain a more conclusive picture on the fiber structure formation. A detailed study of the amorphous and crystalline orientation, including the effects of crystallinity and crystallite dimensions in the context of composite fibers is needed to provide a better understanding of the factors governing the mechanical properties.

Further, the IL recycling concept has to be customized when using multiple solutes. Currently, major efforts are devoted to develop a scalable strategy for a virtually quantitative recovery of the IL for cellulose processing. When using low-molecular weight polymers such as hemicellulose and lignin small shares are lost in the spin bath and have to be removed to avoid accumulation over time. Yet, the unique opportunities offered by ILs should certainly motivate to find also solutions for this challenge.

References

- [1] Laus, G.; Bentivoglio, G.; Schottenberger, H.; Kahlenberg, V.; Kopacka, H.; Roeder, H.; Roeder, T.; Sixta, H., Ionic liquids: current developments, potential and drawbacks for industrial applications. *Lenzinger Ber.* 2005, 84, 71-85.
- [2] Swatloski, R. P.; Spear, S. K.; Holbrey, J. D.; Rogers, R. D., Dissolution of Cellulose [sic] with Ionic Liquids. *J. Am. Chem. Soc.* 2002, 124 (18), 4974-4975.
- [3] Welton, T., Room-Temperature Ionic Liquids. Solvents for Synthesis and Catalysis. *Chem. Rev.* 1999, 99 (8), 2071-2083.
- [4] Hummel, M.; Michud, A.; Tantt, M.; Asaadi, S.; Ma, Y.; Hauru, L. J.; Parviainen, A.; King, A. T.; Kilpeläinen, I.; Sixta, H., Ionic Liquids for the Production of Man-Made Cellulosic Fibers: Opportunities and Challenges. *Adv. Polym. Sci.* 2015, 1-36.
- [5] Pinkert, A.; Marsh, K. N.; Pang, S.; Staiger, M. P., Ionic Liquids and Their Interaction with Cellulose. *Chem. Rev.* 2009, 109 (12), 6712-6728.
- [6] Maeki-Arvela, P.; Anugwom, I.; Virtanen, P.; Sjoeholm, R.; Mikkola, J. P., Dissolution of lignocellulosic materials and its constituents using ionic liquids-A review. *Ind. Crops Prod.* 2010, 32, 175-201.
- [7] Wang, H.; Gurau, G.; Rogers, R. D., Ionic liquid processing of cellulose. *Chem. Soc. Rev.* 2012, 41 (4), 1519-1537.
- [8] Brandt, A.; Grasvik, J.; Hallett, J. P.; Welton, T., Deconstruction of lignocellulosic biomass with ionic liquids. *Green Chem.* 2013, 15 (3), 550-583.
- [9] Singh, S.; Simmons, B. A. In *Ionic liquid pre-treatment: mechanism, performance, and challenges*, John Wiley & Sons Ltd.: 2013; pp 223-238.
- [10] Hauru, L. K. J.; Ma, Y.; Hummel, M.; Alekhina, M.; King, A. W. T.; Kilpeläinen, I.; Penttilä, P. A.; Serimaa, R.; Sixta, H., Enhancement of ionic liquid-aided fractionation of birchwood. Part 1: autohydrolysis pre-treatment. *RSC Adv.* 2013, 3, 16365-16373.
- [11] Wendler, F.; Meister, F.; Wawro, D.; Wesolowska, E.; Ciechanska, D.; Saake, B.; Puls, J.; Le Moigne, N.; Navard, P., Polysaccharide blend fibres formed from NaOH, N-methylmorpholine-N-oxide and 1-ethyl-3-methylimidazolium acetate. *Fibres Text. East. Eur.* 2010, 18, 21-30.
- [12] Wendler, F.; Persin, Z.; Stana-Kleinschek, K.; Reischl, M.; Ribitsch, V.; Bohn, A.; Fink, H.-P.; Meister, F., Morphology of polysaccharide blend fibers shaped from NaOH, N-methylmorpholine-N-oxide and 1-ethyl-3-methylimidazolium acetate. *Cellulose* 2011, 18, 1165-1178.

- [13] Sun, N.; Li, W.; Stoner, B.; Jiang, X.; Lu, X.; Rogers, R. D., Composite fibers spun directly from solutions of raw lignocellulosic biomass dissolved in ionic liquids. *Green Chem.* 2011, 13, 1158-1161.
- [14] Lehmann, A.; Bohrisch, J.; Protz, R.; Fink, H.-P. Method for preparing lignocellulose spinning solution and spin regenerated fibers from it without any initial pretreatments. WO2013144082A1, 2013.
- [15] Lehmann, A.; Ebeling, H.; Fink, H.-P. Method for economical production of lignin-containing precursor fibers for use in further production of carbon fibers. WO2012156441A1, 2012.
- [16] Bentivoglio, G.; Roeder, T.; Fasching, M.; Buchberger, M.; Schottenberger, H.; Sixta, H., Cellulose processing with chloride-based ionic liquids. *Lenzinger Ber.* 2006, 86, 154-161.
- [17] Kosmulski, M.; Gustafsson, J.; Rosenholm, J. B., Thermal stability of low temperature ionic liquids revisited. *Thermochim. Acta* 2004, 412 (1-2), 47-53.
- [18] Meine, N.; Benedito, F.; Rinaldi, R., Thermal stability of ionic liquids assessed by potentiometric titration. *Green Chem.* 2010, 12, 1711-1714.
- [19] Gazit, O. M.; Katz, A., Dialkylimidazolium Ionic Liquids Hydrolyze Cellulose Under Mild Conditions. *ChemSusChem* 2012, 5 (8), 1542-1548.
- [20] Michud, A.; Hummel, M.; Haward, S.; Sixta, H., Monitoring of cellulose depolymerization in 1-ethyl-3-methylimidazolium acetate by shear and elongational rheology. *Carbohydr. Polym.* 2015, 117 (0), 355-363.
- [21] Ebner, G.; Schiehser, S.; Potthast, A.; Rosenau, T., Side reaction of cellulose with common 1-alkyl-3-methylimidazolium-based ionic liquids. *Tetrahedron Lett.* 2008, 49 (51), 7322-7324.
- [22] Dorn, S.; Wendler, F.; Meister, F.; Heinze, T., Interactions of ionic liquids with polysaccharides - 7: Thermal stability of cellulose in ionic liquids and N-methylmorpholine-N-oxide. *Macromol. Mater. Eng.* 2008, 293, 907-913.
- [23] Wendler, F.; Todi, L.-N.; Meister, F., Thermostability of imidazolium ionic liquids as direct solvents for cellulose. *Thermochim. Acta* 2012, 528, 76-84.
- [24] Zweckmair, T.; Hettegger, H.; Abushammala, H.; Bacher, M.; Potthast, A.; Laborie, M.-P.; Rosenau, T., On the mechanism of the unwanted acetylation of polysaccharides by 1,3-dialkylimidazolium acetate ionic liquids: part 1 — analysis, acetylating agent, influence of water, and mechanistic considerations. *Cellulose* 2015, 22 (6), 3583-3596.
- [25] Ziabicki, A.; Takserman-Krozer, R., Mechanism of breakage of liquid threads. *Kolloid-Z.u.Z. Polymere* 1964, 198 (1-2), 60-65.
- [26] Ziabicki, A.; Takserman-Krozer, R., Effect of rheological factors on the length of liquid threads. *Kolloid-Z.u.Z. Polymere* 1964, 199 (1), 9-13.
- [27] Hauru, L. K. J.; Hummel, M.; Nieminen, K.; Michud, A.; Sixta, H., Cellulose regeneration and spinnability from ionic liquids. *Soft Mat.* 2016, 12 (5), 1487-1495.
- [28] Biganska, O.; Navard, P., Morphology of cellulose objects regenerated from cellulose-N-methylmorpholine N-oxide-water solutions. *Cellulose* 2008, 16 (2), 179.
- [29] Sixta, H.; Michud, A.; Hauru, L. K. J.; Asaadi, S.; Ma, Y.; King, A. W. T.; Kilpeläinen, I.; Hummel, M., Ioncell-F: A High-strength regenerated cellulose fibre. *Nord. Pulp Pap. Res. J.* 2015, 30 (1), 43-57.
- [30] Michud, A.; Tantt, M.; Asaadi, S.; Ma, Y.; Netti, E.; Kääriäinen, P.; Persson, A.; Berntsson, A.; Hummel, M.; Sixta, H., Ioncell-F: ionic liquid-based cellulosic textile fibres as alternative to viscose and Lyocell. *Text. Res. J.* 2016, 86 (5), 543-552.
- [31] Ma, Y.; Stubb, J.; Kontro, I.; Nieminen, K.; Hummel, M.; Sixta, H., Filament spinning of unbleached birch kraft pulps: Effect of pulping intensity on the processability and the fiber properties. *Carbohydr. Polym.* 2018, 179, 145-151.
- [32] Ma, Y.; Hummel, M.; Maattanen, M.; Sarkilahti, A.; Harlin, A.; Sixta, H., Upcycling of waste paper and cardboard to textiles. *Green Chem.* 2016, 18, 858-866.
- [33] Ma, Y.; Hummel, M.; Kontro, I.; Sixta, H., High performance man-made cellulosic fibres from recycled newsprint. *Green Chem.* 2018, 20 (1), 160-169.
- [34] Ma, Y.; Asaadi, S.; Johansson, L.-S.; Ahvenainen, P.; Reza, M.; Alekhina, M.; Rautkari, L.; Michud, A.; Hauru, L.; Hummel, M.; Sixta, H., High-Strength Composite Fibers from Cellulose-Lignin Blends Regenerated from Ionic Liquid Solution. *ChemSusChem* 2015, 8 (23), 4030-4039.
- [35] Asaadi, S.; Hummel, M.; Sixta, H. In Regenerated cellulosic fiber from ionic liquid-waste cotton solution by dry-jet wet spinning, ACS spring meeting, Denver, American Chemical Society: Denver, 2015; pp CELL-138.
- [36] Michud, A.; Hummel, M.; Sixta, H., Influence of molar mass distribution on the final properties of fibers regenerated from cellulose dissolved in ionic liquid by dry-jet wet spinning. *Polymer* 2015, 75, 1-9.

- [37] Hauru, L. J.; Hummel, M.; Michud, A.; Sixta, H., Dry jet-wet spinning of strong cellulose filaments from ionic liquid solution. *Cellulose* 2014, 21 (6), 4471-4481.
- [38] Froschauer, C.; Hummel, M.; Iakovlev, M.; Roselli, A.; Schottenberger, H.; Sixta, H., Separation of Hemicellulose and Cellulose from Wood Pulp by Means of Ionic Liquid/Cosolvent Systems. *Biomacromolecules* 2013, 14, 1741-1750.
- [39] Roselli, A.; Hummel, M.; Monshizadeh, A.; Maloney, T.; Sixta, H., Ionic liquid extraction method for upgrading eucalyptus kraft pulp to high purity dissolving pulp. *Cellulose* 2014, 21 (5), 3655-3666.
- [40] Northolt, M. G.; den Decker, P.; Picken, S. J.; Baltussen, J. J. M.; Schlatmann, R., The Tensile Strength of Polymer Fibres. In *Polymeric and Inorganic Fibers*, Springer Berlin Heidelberg: Berlin, Heidelberg, 2005; pp 1-108.
- [41] Röder, T.; Moosbauer, J.; Kliba, G.; Schlader, S.; Zuckerstätter, G.; Sixta, H., Comparative characterisation of man-made regenerated cellulose fibres. *Lenzinger Ber.* 2009, 87, 98-105.
- [42] Lenz, J.; Schurz, J., Fibrillar structure and deformation behavior of regenerated cellulose fibers I. Methods of investigation and crystallite dimensions. *Cellul. Chem. Technol.* 1990, 24, 3-21.
- [43] Lenz, J.; Schurz, J., Fibrillar structure and deformation behavior of regenerated cellulose fibers I. Elementary fibrils and deformation. *Cellul. Chem. Technol.* 1990, 24, 679-692.
- [44] Lenz, J.; Schurz, J.; Wrentschur, E., On the elongation mechanism of regenerated cellulose fibers. *Holzforschung* 1994, 48, 72-6.
- [45] Schild, G.; Liftinger, E., Xylan enriched viscose fibers. *Cellulose* 2014, 21 (4), 3031-3039.
- [46] Zhang, H.; Tong, M., Influence of hemicelluloses on the structure and properties of Lyocell fibers. *Polym. Eng. Sci.* 2007, 47 (5), 702-706.
- [47] Treiber, E., Einfluss der Hemicellulosen auf die Weiterverarbeitung von Chemiezellstoffen. *Papier* 1983, 37 (12), 591-600.
- [48] Kuzmina, O.; Bhardwaj, J.; Vincent, S. R.; Wanasekara, N. D.; Kalossaka, L. M.; Griffith, J.; Potthast, A.; Rahatekar, S.; Eichhorn, S. J.; Welton, T., Superbase ionic liquids for effective cellulose processing from dissolution to carbonisation. *Green Chem.* 2017, 19 (24), 5949-5957.

Man-Made Cellulosic Fibers via the Viscose Process – New Opportunities by Cellulose Carbamate

R. Protz, G. Weidel, and A. Lehmann*

Fraunhofer Institute for Applied Polymer Research, Geiselbergstr. 69, 14476 Potsdam, Germany

*Contact: lehmann@iap.fraunhofer.de

Abstract

Viscose fibers have an ever increasing market share with over 5 million tons p.a.. Main application area for viscose fibers is the textile industry. Nevertheless the broad variability of the viscose process allows realizing even technical man-made cellulose fibers, like Supe 3 tyre cord yarn with tenacities of more than 50 cN/tex. This broad variability of fiber qualities is not reached by any other cellulose shaping process.

However since decades there is a strong focus on decreasing the input of highly toxic CS₂ for the viscose fiber manufacturing and keeping the quality of spinning solutions at the same time, which allows the known processing behavior and resulting in a high fiber quality. The cellulose carbamate process is by far the most intense investigated option to substitute the viscose technology. By different reasons this didn't happen up to today, despite the fact that the cellulose carbamate spinning was already shown on industrial scale.

This paper discusses the opportunity of combining both spinning routes, carbamate and viscose. This enables to realize fiber properties known from the viscose process and at the same time a significant lower CS₂ input for so produced man-made cellulose fibers. The paper will give an overview about the technology, different fiber properties and structural characterization of the same by varying the processing conditions.

Keywords: *man-made cellulose filaments, cellulose carbamate, viscose, cellulose*

Introduction

Viscose fibers have an ever increasing market share with over 5 million tons p.a. [1]. Main application area for viscose fibers is the textile industry. This more than 100 year old process discovered by Cross et al. [2] is still the dominating process to transfer the unspinnable wood-based biopolymer cellulose into man-made fibers via the intermediate sodium cellulose xanthate. As this transformation is a very complex process driven by physics and chemistry a broad variety of properties from resulting man-made cellulosic fibers is accessible by varying process parameters like spinning dope composition (cellulose and alkali content, maturity, etc.) and spinning conditions (coagulation conditions, drawing factors, etc.). Despite the fact that the recycling for the resulting sulphur containing by-products in the viscose process became more and more efficient, it is still a fact that much more than 1 million tons per year of the highly toxic carbon disulfide are needed to give an output of 5 million tons of viscose fibers a year.

This fact as well as the discussed cotton-gap in literature [3] is the main driver to look into alternatives for making man-made cellulosic fibers. The processing of cellulose from *N*-Methylmorpholine-*N*-oxide-Monohydrate solution via an air-gap spinning method is the only further industrialized process to manufacture man-made fibers in >200 kt-scale [4], giving man-made cellulose fibers called Lyocell (CLY). Owing to the different dissolution and shaping conditions combined with a non-derivatizing route, the achieved man-made cellulosic fibers differ in their supermolecular structure compared to viscose fiber (CV) leading to different textile-physical properties [5], whereas the property window of CLY-fibers is not as versatile as it is known from CV-fibers. The viscose process allows even to produce technical filament yarns (Super 3), which are mainly used for rubber good reinforcement in particular fast running and run-flat tires.

At least in pilot scale different alternative routes to realize man-made cellulose fibers were investigated and realized. Most of them following a non-derivatizing route, whereas the dissolving pulp (in some cases additionally pre-treated by acid, alkali or enzymes) is dissolved directly in a solvent and the resulting spinning dope is shaped via wet-spinning (e.g. Celsol [6]) or air-gap spinning technique (e.g. Ioncell [7]) to create man-made cellulose fibers. An example for a derivatizing route is the so called CarbaCell® process [8]. Cellulose is modified with urea to result in an alkali soluble cellulose carbamate (CC), which can be shaped very similar to conditions applied for creating man-made cellulose fibers via the viscose route. Despite the fact that cellulose carbamate is a derivative like cellulose xanthate, the main difference is indeed that cellulose xanthate is a polyelectrolyte, whereas cellulose carbamate is a non-ionic cellulose derivative. So the influence of precipitation conditions, especially electrolyte content like salt concentration as well as kind of salt is much less pronounced in the CarbaCell® process compared to the viscose process. As both derivatives are soluble in alkali, we investigated in the present paper the possibility to combine both cellulose derivatives in solution, shaping the same into man-made cellulosic fibers and characterizing the resulting filaments.

Materials and Methods

Raw materials

For performing the investigations a cellulose carbamate with a DP_{Cuoxam} of 254 was used having a nitrogen content of 2.1%. This cellulose carbamate was synthesized by the method described in [9]. For the viscose dope preparation a softwood pre-hydrolysis kraft pulp, having a DP_{Cuoxam} of 611 and an α -cellulose content of 92.3%, was used. For the xanthation reaction carbon disulfide with a quality of 99.9% from Fisher was used.

Methods

Spinning solution preparation

A cellulose content of 8.5 wt.-% and an alkali content of 7 wt.-% was addressed for all prepared spinning solutions by varying the ratio between cellulose carbamate and sodium cellulose xanthate for the spinning dope as well as for shaping cellulose carbamate and sodium cellulose xanthate themselves. The mixed cellulose solutions were prepared by combining cellulose carbamate solution with a cellulose content of 9.5 wt.-% and adjusting the cellulose content in the viscose dope to 8.8 wt.-%, respectively 10.1 wt.-% in appropriate amounts to realize the later discussed ratios (Table 1).

Table 1: Concentration and amounts of cellulose carbamate and sodium cellulose xanthate solutions to adjust the certain ratio in the spinning dope.

| CC:Na-CX | Cellulose carbamate dope | Sodium cellulose xanthate dope |
|----------|--------------------------|--------------------------------|
| 33:67 | 1 part 9.5 wt.-% | 0.7 parts 8.8 wt.-% |
| 67:33 | 1 part 9.5 wt.-% | 2.4 parts 10.1 wt.-% |

Cellulose carbamate based solution

The cellulose carbamate was mixed with water 1:1 by weight and stored over night at 6 °C. The dissolution lye was introduced in a dissolving vessel equipped with rotor/stator geometry and cooled down to -4 °C. After reaching the temperature the cellulose carbamate was given to the dissolution lye under stirring and dissolved for 120 min at 0 °C. The so obtained cellulose carbamate solution had a cellulose content of 9.5 wt.-% and an alkali content of 7 wt.-%.

Sodium cellulose xanthate based solution

The pulp was cut into sheets (18 x 22 cm) and placed into the steeping chamber of a Blaschke plant. Alkali lye of 18 wt.-% in concentration was slowly given from bottom to top into the alkalization chamber. The steeping was performed for 50 minutes at 35 °C. The sheets of alkali cellulose (AC) were then pressed to obtain the press out factor of 2.9. The resulting alkali cellulose consists of 36.9% cellulose and 14.5% alkali and was disrupted by the defibrator of the Blaschke plant. The so prepared alkali cellulose was aged at 35 °C to reach a DP_{Cuoxam} of 340.

Xanthation took place in a so called baratte. Therefore the alkali cellulose was introduced in the baratte and vacuum was applied. Carbon disulfide (28 wt.-% based on the cellulose) was flushed into the de-pressurized reaction chamber, which lead to loss of vacuum. The xanthation took place for 90 min at 28 °C. In that time the pressure decreases again to the starting value, indicating the complete usage of carbon disulfide for the xanthation reaction.

The resulting, yellowish sodium cellulose xanthate had a γ -value of 51.4 and was dissolved by pre-cooling the dissolution lye to 6 °C and introducing the sodium cellulose xanthate to the dissolving equipment (rotor/stator dissolving geometry of 5l volume). After final addition of the sodium cellulose xanthate the further dissolution took place for 120 min at 6-8 °C.

After combining the sodium cellulose xanthate and cellulose carbamate solution in appropriate amounts (Table 1) to realize the addressed ratio, the spinning dope was filtered by a 20 μ m metal fleece filter.

The maturity was realized by storing the spinning dope at 25 °C for 20 hours.

Spinning of filament yarn

For wet-spinning of the resulting spinning solutions the spinning dope was tempered at 20 °C during spinning and transported by a spinning pump (0.6 cm³ per rotation) to the spinning nozzle. As spinning nozzle a spinneret with 128 holes, each hole having a diameter of 70 μm was used. The spinning bath consists of 80 g/l sulfuric acid and 120 g/l sodium sulfate in water at 40 °C. The resulting bundle of never-dried filaments was drawn from the nozzle by a take-up roller, which delivered the yarn to the decomposition bath, which contained 20 g/l sulfuric acid in water at >90 °C, followed by washing the yarn on nelson-type rollers

using demineralized water at 60 °C. The washed yarn was dried under isometric conditions using drying rollers at 80 °C and finally wound on bobbins.

Jet-stretch and draw factor were varied by adjusting the throughput as well as spinning speed to realize the spinning parameters given in Table 2 .

Table 2: Applied jet-stretch and draw factors during the spinning process.

| Jet-stretch | Draw-factor |
|-------------|-------------|
| 0.6 | 1.1 |
| 0.7 | |
| 0.9 | |
| 0.7 | 1.3 |
| | 1.5 |
| | 1.7 |

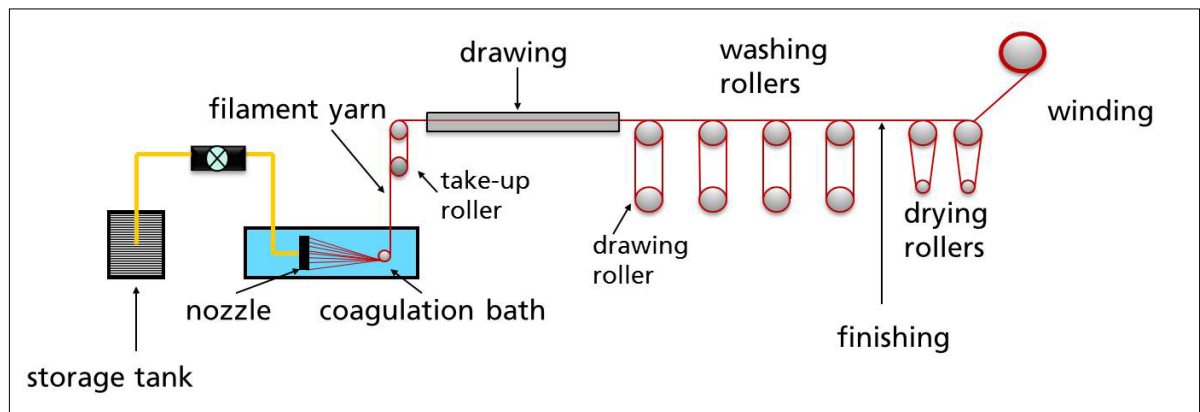


Figure 1: Schematic view of the spinning line for filament yarns at Fraunhofer IAP.

Analytical methods

Rheology

Oscillation rheology of all solutions was measured on an Anton Paar MCR 102 rheometer with a plate and plate geometry. A plate with 50 mm diameter was used and the gap was set to 1 mm. The viscoelastic domain was determined by performing a dynamic amplitude sweep and a strain between 0.1% and 100%. A strain of 1%, which is within the linear viscoelastic regime, was chosen for time sweep measurements. In order to keep the moisture content constant the plate edge was sealed with paraffin oil. The time sweep (frequency 1 Hz and strain amplitude 0.01) was run at 25 °C for 10 hours.

WAXS – Quantitative analysis of the crystalline orientation of cellulose fibers

The fibers were parallel- fixed onto a special sample holder in order to analyze the crystallite orientation. X-ray measurements were carried out by a two-circle D5000 X-ray diffractometer (Bruker-AXS) in symmetrical transmission geometry using CuK α -radiation

($\lambda = 0.15418$ nm) monochromized by a Ge(111)-primary monochromator and operated at 40 kV and 30 mA. Distribution of the (004) lattice plane (chain direction peak) at a diffraction angle 2θ at ~ 34 - 35° was measured by a ϕ -spinner-scan over ϕ -angle range from 60 - 120° with steps of 0.2° and a scanning speed of $0.067^\circ/\text{min}$ (assumed maximum of distribution to be 90°). By following the orientational parameters of the crystallite, the main axis orientation was calculated in order to describe the peak reflex of the (004) plane:

$$OG_{(004)} = \frac{(180^\circ - \text{FWHM})}{(180^\circ)}$$

SEM

The SEM was used to study the morphology of cross sections. The SEM-micrographs were taken by a JSEM 6330F (Jeol, Japan) at an acceleration voltage of 5 kV. Cross sections were prepared by fracturing fibers in liquid nitrogen and finally, a thin Platinum layer (thickness 5 nm) was deposited by sputtering on top of the surface and cross section to avoid electrical charging by the electron beam.

Fiber testing

All produced filaments were stored at 65% relative humidity and 20 °C for at least 24 h for sample conditioning.

Titer determination

The titer of the single filament was determined by a vibroskop (Lenzing) as average value of 20 samples.

Mechanical parameters of filaments

Mechanical properties (tenacity, elongation at break and modulus [sloop in the range of 0.05-0.25% elongation]) of samples were measured using a UNIVERSAL TEST MACHINE ZWICK Z 020. The clamp distance was 20 mm and the testing velocity 10 mm/min by a pre-tension of 0.1 cN. The measurement of 20 samples was averaged.

Results and Discussions

Rheology of spinning dopes

The stability of carbamate and viscose solutions at 25 °C processing temperatures is an important parameter for processability of the corresponding spinning dopes. A substantial difference between cellulose carbamate (CC) and sodium cellulose xanthate is the chemical stability of the CC for months in the dry state [10]. And compared to a sodium cellulose xanthate solution, where the maturity is a very important factor for the resulting fiber properties, a carbamate solution does not require any ripening time [11]. Due to the effects of hydrolysis of the carbamate groups carbamate solutions tend to gelify earlier and therefore should be kept cold [12]. Ongoing changes in the physical and chemical structure in both cases lead to a network build-up up to the point of gelification. Pinnow et al. [13] used this network formation and showed the thermal induced precipitation of CC in order to prepare highly porous materials. As described in literature [12] the addition of zinc oxide (ZnO) is useful to enhance the dissolution and partly to prolong the time before gelation starts. To investigate the effect of the cellulose xanthate and cellulose carbamate ratio in solution on the gelification behavior time sweeps (at 25 °C with strain amplitude 0.01) were conducted and representative results are shown in Figure 2. The carbamate solution shows a cross over point (gel point) of storage modulus G' and loss modulus G'' after 30 minutes, whereas the mixture does not show a significant change in G' and G'' . Due to a partial substitution with viscose a significant increase in solution stability of the mainly cellulose carbamate containing solution can be achieved. This fact enables the storage of spinning dope and a spinning process at room temperature.

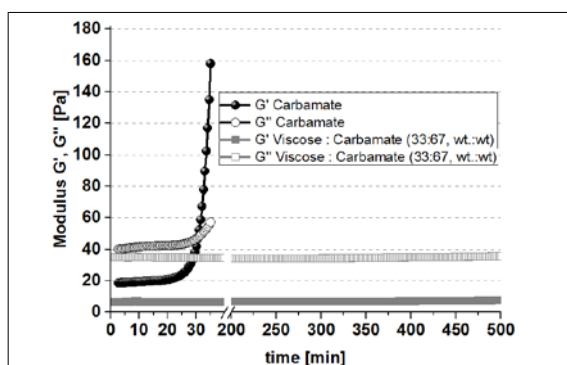


Figure 2: Oscillatory time sweeps at 25 °C for a carbamate solution and a viscose/carbamate-mixture (33/67, wt./wt.) with strain amplitude 0.01 and frequency 1 Hz.

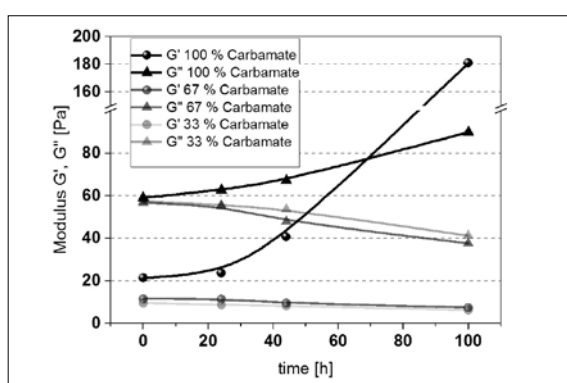


Figure 3: Oscillatory time sweeps at 15 °C for a carbamate solution and viscose/carbamate-mixtures (33/67 and 67/33, wt./wt.) with strain amplitude 0.01 and frequency 1 Hz.

Figure 3 demonstrates the changes in rheology and appearance of mixtures from sodium cellulose xanthate and cellulose carbamate containing different amounts of cellulose carbamate being stored at 15 °C. It can be noticed that initially all solutions are dominantly viscous ($G' < G''$). In case of cellulose carbamate the elastic modulus G' rapidly increases after 24 hours and crosses the loss modulus G'' after 69 hours, whereas the mixtures show constantly a viscous behavior. For the mixtures G' and G'' decrease over time, which can be explained by an ongoing degradation of cellulose chain length (DP decreases) and the cleavage of substituents. The polyelectrolyte sodium cellulose xanthate dilutes (G'' slightly increases with increasing amounts of Na-CX) the cellulose carbamate in solution and seems to hamper or reduce the formation of network-like structures.

Fiber properties

Textile-physical properties

To vary the textile-physical properties of spun filaments the spinning parameters regarding jet-stretch and draw factor were varied in the same way for each

investigated spinning solution. The set of parameters is given in Table 2 (page 79).

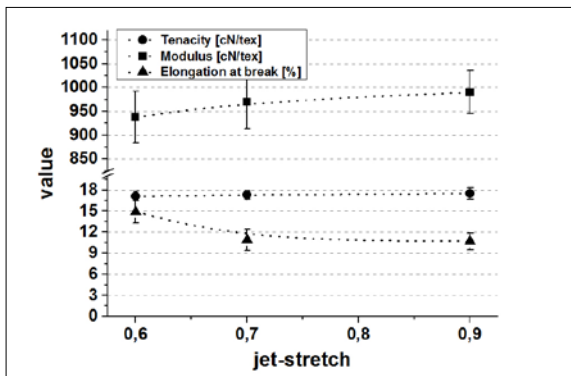


Figure 4: Influence of jet-stretch at a constant draw factor of 1.1 on textile-physical properties for shaping cellulose carbamate and sodium cellulose xanthate at a ratio of 67:33.

At a constant draw-factor, the jet-stretch has a minor influence on the textile-physical properties as shown in Figure 4. The tenacity is nearly not influenced. When the jet stretch becomes higher than 0.6 it can be seen that the value for the modulus increases, whereas the value for the elongation at break decreases.

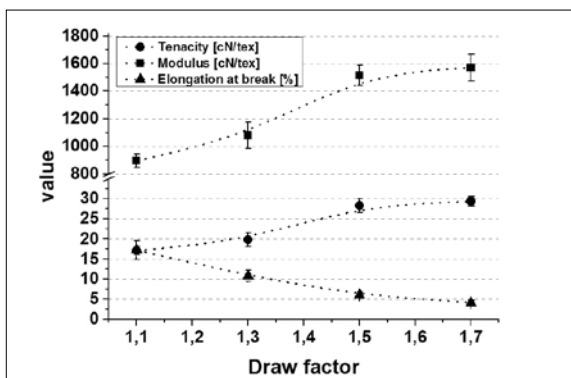


Figure 5: Influence of draw factor at a constant jet-stretch of 0.7 on textile-physical properties for shaping cellulose carbamate and sodium cellulose xanthate at a ratio of 33:67.

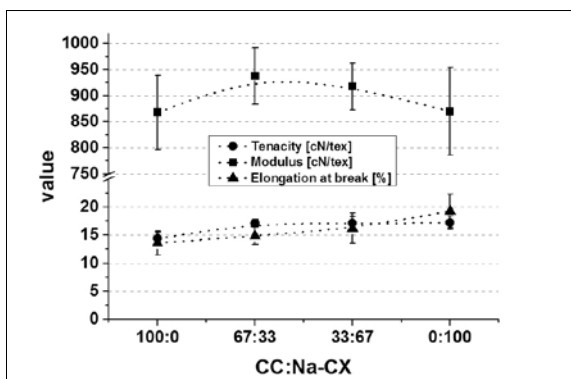


Figure 6: Influence of the ratio of cellulose carbamate (CC) to sodium cellulose xanthate (Na-CX) in the spinning dope for shaping the same at a jet-stretch of 0.6 and a draw factor of 1.1.

A much more pronounced effect on the textile-physical properties for shaping at a ratio of a spinning dope, which consists of a mixture CC:Na-CX of 33:67, can be detected for the draw factor (Figure 5) by keeping the jet-stretch constant. The alignment of the cellulosic polymer chains along the fiber axis is increased by realizing higher draw factors. This results in a higher orientation of the crystalline as well as non-crystalline area of the filaments giving higher values for tenacity and modulus as well as lower values for elongation at break. Despite the fact, that a drawing by factor 1.7 is possible under stable spinning conditions, the further increase in textile-physical properties is limited in comparison to a draw factor of 1.5.

Figure 6 shows an overview of the textile-physical properties of filaments, which were spun by varying the ratio of cellulose carbamate to sodium cellulose xanthate in the spinning dope and shape the same at given spinning parameters. Comparing the shown values for filaments for using cellulose carbamate as derivative for the shaping process lower values for tenacity and elongation at break in comparison for the usage of sodium cellulose xanthate as derivative by using mentioned spinning conditions can be detected, whereas minor differences in modulus are observed.

While the values for elongation at break are increasing by increasing the part of sodium cellulose xanthate in the spinning solution the values for tenacity of resulting filaments are already on the same level like those prepared from a pure viscose based dope by using 1/3 sodium cellulose xanthate and 2/3 cellulose carbamate in the spinning solution. Interestingly there is a slight trend of realizing the highest values for the modulus by using cellulose carbamate and sodium cellulose xanthate at the same time in the spinning dope, independent from the ratio.

By the achieved results it can be clearly seen, that a partly usage of sodium cellulose xanthate in a cellulose carbamate based spinning solution enables a more balanced ratio between the values for tenacity and elongation at break and so mimicking more the textile-physical properties of a viscose based man-made fiber (Figure 7, page 82). To realize this, same spinning bath composition was used and jet-stretch and draw factors had to be adjusted.

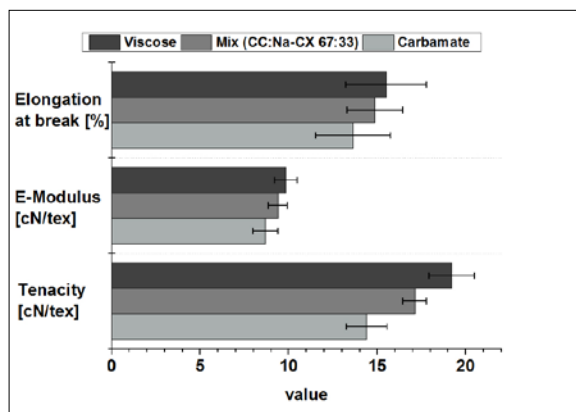


Figure 7: Comparison of textile-physical properties of filaments produced by the viscose and carbamate process as well as the combined process applying the same spinning bath conditions.

Considering an input of 28 wt.-% of carbon disulfide based on cellulose for realizing 1 ton of man-made cellulose fiber (meaning 280 kg CS₂), by using the

composition described in Figure 7 the carbon disulfide input could be decreased down to 9.3 wt.-% (meaning 93 kg CS₂) per ton man-made cellulose fiber and still have the shaping options of a cellulosic polyelectrolyte structure.

Investigation of fiber structure

On filaments produced by spinning under variation of the draw factor and differing in their ratio of used cellulose carbamate to sodium cellulose xanthate some structural parameters by X-ray methods and electron microscopy were estimated.

Orientalional parameters of crystalline phase

As shown in Figure 8 the distribution of the (004) lattice plane (chain direction peak) at a diffraction angle 2θ at ~34-35° by a φ-spinner-scan over φ-angle range from 60-120° for a draw factor of 1.1 (right) and those for a draw factor of 1.5 (left). In Table 3 the values of the corresponding degree of orientation (OG₍₀₀₄₎) are listed.

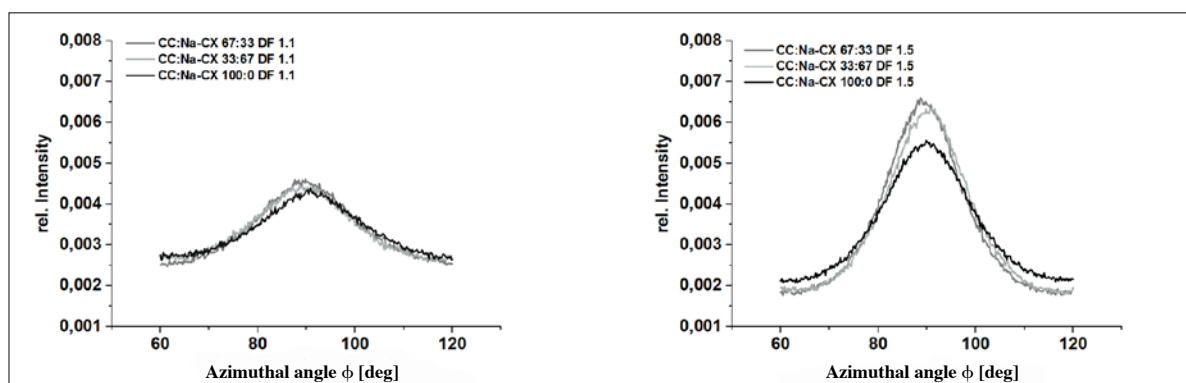


Figure 8: Distribution of the (004) lattice plane of produced filaments as a function of spinning dope composition and draw factor.

For applying a low drawing almost no differences for the values of the OG₍₀₀₄₎ can be detected, which corresponds to the measured E-Moduli (Table 3). By increasing the drawing factor to 1.5 an increase of all

OG₍₀₀₄₎ values was determined. The strongest increase can be seen when cellulose carbamate and sodium cellulose xanthate are combined in the spinning dope and shaped together.

Table 3: Degree of orientation of the (004) lattice plane (OG₍₀₀₄₎) and the corresponding values for the E-Moduli of produced filaments as a function of spinning dope composition and draw factor.

| Filament sample | JS: 0.7 DF: 1.1 | | JS: 0.7 DF: 1.5 | |
|-----------------|---------------------|--------------------|---------------------|--------------------|
| | OG ₍₀₀₄₎ | E-Modulus [cN/tex] | OG ₍₀₀₄₎ | E-Modulus [cN/tex] |
| CC:CV 67:33 | 0.873 | 970 ±83 | 0.901 | 1472 ±96 |
| CC:CV 33:67 | 0.875 | 895 ±47 | 0.897 | 1517 ±72 |
| CC:CV 100:0 | 0.872 | 934 ±38 | 0.888 | 1329 ±85 |

Morphological properties

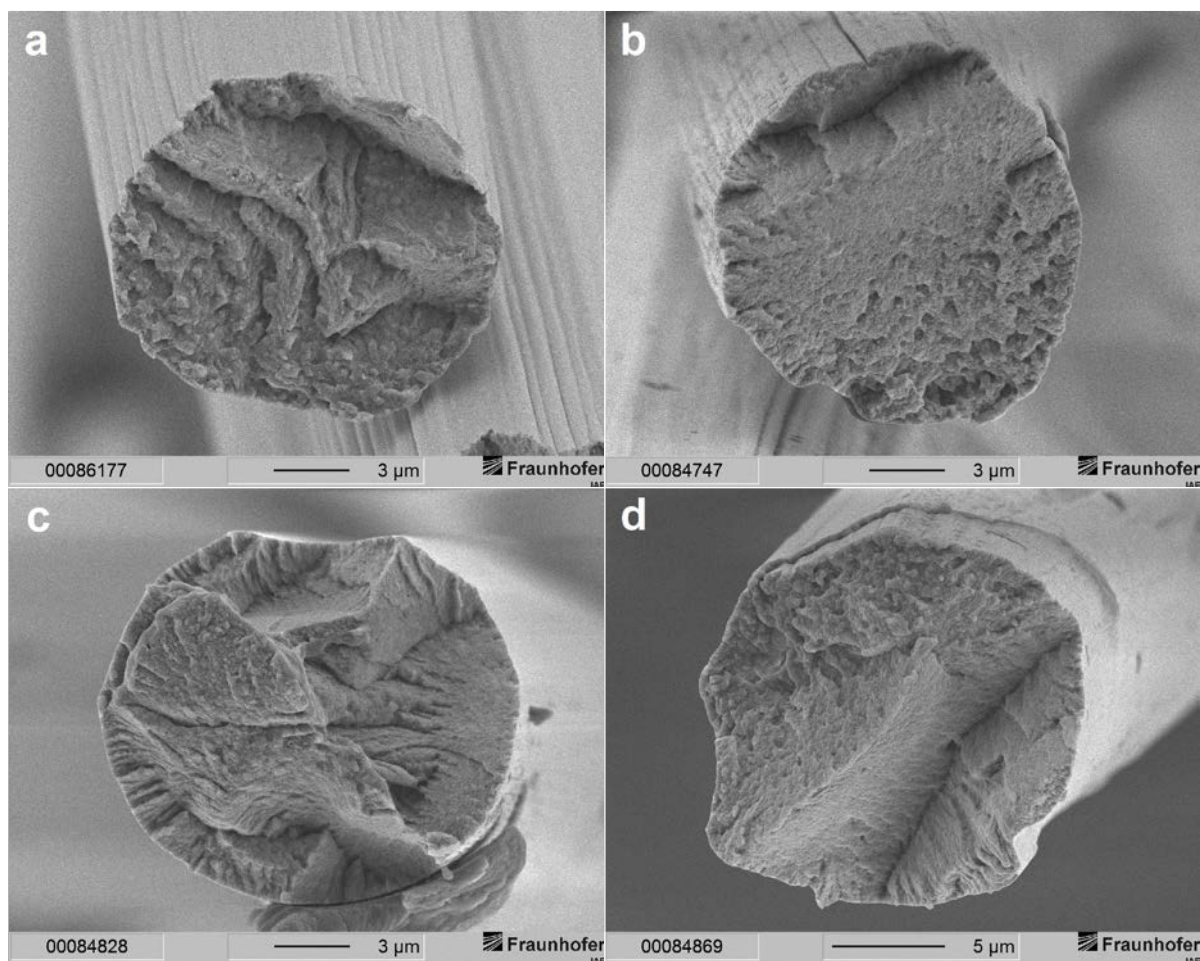


Figure 9: Electron micrographs of cross-section from different cellulosic man-made fibers; a) CC:CV 0:100, b) CC:CV 33:67, c) CC:CV 67:33, d) CC:CV 100:0.

In Figure 9 the picture (a) and (d) depict a cellulose man-made filament according to the viscose process (a) and the cellulose carbamate process (d). From picture (a) a slightly lobulated morphology can be seen, which is dedicated to the structure formation of the polyelectrolyte sodium cellulose xanthate during the precipitation step in the sodium sulfate containing acidic spinning bath. The diffusion of the acid from the spinning bath in the spinning rays of the viscose dope lead to neutralization and finally acidification of the same. During this process sodium sulfate is formed as a by-product of the reaction of the alkali in the spinning dope and the acid in the spinning bath resulting in a dehydration and densification of the sodium cellulose xanthate. Thereby gradients in the concentration of the acid as well as of the salt content in- and outside of the spinning rays causing a centripetal shrinkage of the just formed gel by osmotic and synergetic processes [14], which leads to non-uniform coagulation and so in a lobulated cross-section shape.

In contrast to that such lobulated morphology cannot be detected for a cellulose man-made filament realized via the carbamate route. As cellulose carbamate is not a polyelectrolyte the structure formation during the precipitation step in the spinning bath is less complex and more dedicated to the neutralization of the solvent (alkali lye) by the acidic spinning bath.

Comparing pictures (b) and (c) it can be seen, that as long as sodium cellulose xanthate is the majority of the fiber forming cellulosic polymer in spinning solution, the slightly lobulated morphology can be found in the corresponding filament, too. This lobulated morphology cannot be seen anymore as soon as cellulose carbamate becomes the majority of the cellulosic polymers in the filament (c).

Conclusions

From the found and discussed results it can be concluded, that shaping cellulose carbamate and sodium cellulose xanthate at the same time from alkaline solution is possible. The ratio of both cellulose derivatives can be varied in a broad range. Using the discussed precipitation conditions, filaments with very similar textile-physical properties compared to viscose filaments can be realized. It was found that, in contrast to a cellulose carbamate solution, the solution stability remarkably increases when partly sodium cellulose xanthate is added.

Anyhow, there are not-answered questions like the influence of nitrogen containing by-products in the recycling stream of the sulphur containing by-products in a viscose plant, the origin of cellulose carbamate as well as a deeper investigation on fiber structure and textile-physical properties and further improvement of the same.

Acknowledgements

The authors would like to thank Dr. Andreas Bohn, from Fraunhofer IAP, for performing X-Ray measurement and electron microscopy.

References

- [1] Global and China Viscose Fiber Industry Report, 2013-2016
- [2] C. F. Cross E. T. Bevan C. Beadle; *Berichte der deutschen chemischen Gesellschaft*, 26, 1893
- [3] F. M. Hämmerle; *Lenzinger Berichte*, 89, 2011, 12
- [4] Lenzing AG, Annual Financial Report 2014, 2015
- [5] T. Röder, J. Moosbauer, K. Wöss, S. Schlader, G. Kraft; *Lenzinger Berichte*, 91, 2013, 7
- [6] D. Ciechanka, D. Wawro, W. Steplewski, J. Kazimierzak, H. Struszczyk; *Fibres and Textiles in Eastern Europe*, 13, 2005, 19
- [7] L. K. J. Hauru, M. Hummel, A. Michud, H. Sixta; *Cellulose*, 21, 2014, 4471
- [8] M. Voges, M. Brück, H.-P. Fink, J. Gensrich; *Cellulosic Man-made Fibres in the new Millenium*, Stenungsund, 2000
- [9] US 5,906,926
- [10] H.-P. Fink, J. Ganster, A. Lehmann; *Cellulose*, 21, 2014, 31
- [11] K. Götze; *Chemiefasern nach dem Viskoseverfahren*, Springer-Verlag, Berlin-Heidelberg-New York, 1967
- [12] K. Ekman et al.; *Modification and Hydrolysis in Cellulose Structure*, John Wiley & Sons, New York, 1986, 131
- [13] M. Pinnow et al.; *Macromolecular Symposia*, 262, 2008, 129
- [14] A. Herzog; *Textile Forschung*, 8, 1926, 87

Influence of Carbonization Aids on the Manufacture of Carbon Fibers based on Cellulosic Precursors

Johanna M. Spörl¹, Frank Hermanutz¹, and Michael R. Buchmeiser^{1,2,*}

¹ Deutsche Institute für Textil- und Faserforschung (DITF) Denkendorf, Körschtalstr. 26, D-73770 Denkendorf, Germany

² Lehrstuhl für Makromolekulare Stoffe und Faserchemie, Institut für Polymerchemie, Universität Stuttgart, Pfaffenwaldring 55, D-70550 Stuttgart, Germany

* Corresponding author: Tel. +49(0)711-685 64075, michael.buchmeiser@ipoc.uni-stuttgart.de

Abstract

The application of a new sulfur-based carbonization aid in the manufacture of cellulose-based carbon fibers (CFs) was studied. A process for stabilization was established providing undamaged fibers suitable for continuous carbonization. High mechanical strength cellulose-based CFs were manufactured at comparably low temperatures and in high yield (37% = 83% of theory). Maximum tensile strengths and Young's moduli up to 2 and 84 GPa were obtained at 1400 °C. A well-known phosphorous-based carbonization aid was studied comparatively. Both, the precursor and the CFs were characterized via elemental analysis, wide-angle X-ray scattering (WAXS), scanning electron microscopy (SEM), and tensile testing. Additionally, thermogravimetric analysis coupled with mass spectrometry/infrared spectroscopy (TGA-MS/IR) was used to disclose differences in pyrolysis and structure formation.

Keywords: cellulose; carbon fibers; TGA-MS; TGA-IR; WAXS

Introduction

Cellulose is the oldest known carbon fiber (CF) precursor material. After major research activity on cellulosic precursors in the 1950-1970s, the research in this field was abandoned due to disadvantages such as high production costs at low yields and the much more promising findings with polyacrylonitrile (PAN)-based precursors. Today, interest in cellulosic CF precursors has arisen, for both economic and ecological reasons. [1-8] Man-made regenerated cellulose fibers, like viscose or Lyocell possess well-defined dimensions and high purity. Therefore, they could be used as precursors for high-performance CFs when processed as continuous multi-filaments. The mechanical performance of CFs also strongly depends on controlled processes during pyrolysis and carbonization. The maximum theoretical carbon yield in carbonization of cellulose is 44.4 wt.-%, corresponding to the formal loss of five molecules of water per anhydroglucose unit (AGU). However, due

to degradation reactions and the formation of carbon containing volatiles (like CO₂, CO, alcohols, ketones and other carbon-containing low-molecular-weight substances), the total mass loss might be up to 90%. [1] Different strategies for the stabilization of rayon fibers prior to their carbonization have been reported allowing for carbonization yields of 25-30 wt.-%: the use of low heating rates during pyrolysis up to 400 °C [9-11], oxidative pre-treatment [12-16], the use of a reactive atmosphere [17] or the application of carbonization aids, including catalysts for dehydration (AlCl₃, borax, boronic acid, KHCO₃, NaH₂PO₄, ZnCl₂, NH₄Cl, ammonium phosphates and sulfates) and crosslinking reagents, e.g., urea [5,14,18-27]. We recently reported on an ionic liquid-(IL)derived cellulose phosphonate precursor fiber for CFs, which allows for high carbonization yields of 36% at 1400 °C [28]. An overview of cellulose-based CFs is given in ref.[1] However the

influence of structure formation on mechanical properties of cellulose based CFs was still not fully enlightened. We recently presented a study on Rayon tire cord- (RC-) derived CFs aiming on both, high carbonization yields and good mechanical properties of the final CFs. [29] Therefore, ammonium tosylate (ATS) was tested as new sulfur-based carbonization aid in comparison to the well-known carbonization aid ammonium dihydrogenphosphate (ADHP). Carbonization trials were performed continuously to study the influence of carbonization temperature, dwell time and fiber tension during carbonization and the results were correlated with data obtained from discontinuous processing. In the present work, a closer look is taken on emission gases evolved during pyrolysis and carbonization of untreated and treated cellulose fibers. Furthermore, the influence of the two different carbonization aids on the properties of the resulting CFs is discussed.

Materials and Methods

Materials

A high-strength Rayon fiber RC (Cordenka 700, 1000 filaments, 1840 dtex) was used. According to single filament fineness and tensile testing (own data), the fiber properties were: 18% elongation at break ϵ , 53 cN/tex tenacity σ , 1290 cN/tex Young's modulus E and a fineness T of 2.1 dtex. $(\text{NH}_4)\text{H}_2\text{PO}_4$ was purchased from ABCR GmbH; ammonium tosylate was synthesized by adding 1.3 equiv. of a 25 wt.-% aqueous solution of ammonia to an aqueous solution of p-toluene sulfonic acid, steering the mixture for 1 h and subsequently removing the solvent in vacuo. For comparative analysis, a commercial PAN-based CF T300 (Toray Industries Inc.) was used. The tensile properties (single filament test) were $\epsilon = 1.3\%$, $\sigma = 2.5$ GPa and $E = 190$ GPa.

Application of the carbonization aids

The application of the carbonization aids was accomplished continuously by dipping the fiber in a 0.4 M solution of the respective carbonization agent (retention time: approx. 1.5 s) and subsequently drying the fibers on godets (80 °C) and a heating channel (100 °C). Finally, the fibers were wound on a spool.

Carbonization

For discontinuous carbonization trials, fibers were carbonized under nitrogen in a Gero HTK 8GR/22-1G high-temperature batch type furnace applying a heating rate of 1 K/min below 350 °C and 5 K/min above this temperature. The final carbonization temperature varied from 400 to 2200 °C. For continuous carboniza-

tion trials, a Gero vertical tube furnace was used. Fibers were continuously stabilized under nitrogen at 210 °C (RC/ATS) or 250 °C (RC/ADHP) for 50 minutes. Stabilized fibers were then carbonized at 1400 °C using different dwell times and fiber tensions. In course of these experiments, the preload force on the fiber was increased until the first filaments of the fiber thread broke. For the trials without preload force, the fiber tension was 0.5 cN/tex. Selected fibers were also carbonized in a Gero horizontal tube furnace consisting of two zones, a low temperature zone (carbonization at up to 750 °C, dwell time at $T_{\text{max}} = 4.5$ -5 min) and a high temperature zone (carbonization at 1400 °C, dwell time at $T_{\text{max}} = 3.6$ min).

Characterization

Quantitative phosphorous and sulfur analysis was performed by inductively-coupled plasma-optical emission spectroscopy (ICP-OES) on a Spectro Acros ICP-OES after acidic digestion. Calibration was accomplished with aqueous ICP standards in the concentration range of 1 to 7.5 mg/L at $\lambda = 214.900$ -214.940 nm (base line: $\lambda = 214.784$ -214.813 nm, 214.985-215.022 nm) for phosphorous and $\lambda = 180.714$ -180.762 nm (base line: $\lambda = 180.620$ -180.650 nm, 180.829-180.860 nm) for sulfur.

Scanning electron micrographs (SEM) were recorded on a Zeiss Auriga field emission scanning electron microscope. Samples were sputtered with Pt/Pd prior to analysis.

Mechanical fiber properties were measured according to EN ISO 5079 by a Textechno Favimat tensile tester. Fineness was obtained as weight in g per 10,000 m in length (dtex).

For WAXS measurements, a Rigaku D/Max Rapid II was used at 40 kV and 30 mA with Cu $K\alpha$ radiation ($\lambda = 1.54$ Å). A shine monochromator and an image plate detector were used. The scanning rate was 0.2°/min; the scanning step was 0.1°. All fibers were aligned in a fiber sample holder. Pearson-VII curves were fitted to the crystalline signals and the crystallite size (t) was calculated according to the Scherrer's equation [30]

$$t = \frac{K\lambda}{(B \cdot \cos \theta_b)},$$

where B is the width at half-height of the reflection, K is the Scherrer factor, which depends on the crystallite shape, and θ_b is the Bragg-angle. For CFs, the degree of preferred relative orientation of the crystallites P.O. was calculated according to:

$$\text{P.O.} = \frac{180^\circ - B}{180^\circ}$$

Thermogravimetric analysis coupled to mass spectrometry and IR-spectrometry (TGA-MS/IR) was accomplished in a helium atmosphere at 10 K/min on a NETSCH STA 449 F3 coupled to a QMS 403 C Aelos and a Bruker Tensor 27 FTIR. For all comparisons, identical sample masses were used.

Results and Discussion

Dehydration and stabilization of cellulose with carbonization aids

The fibers were finished with different amounts of ADHP or ATS from aqueous solution, dried and subjected to TGA in comparison to the untreated fiber (Figure 1, Table 1). All thermograms showed a first mass loss around 100 °C which could be attributed to the evaporation of physically absorbed water and a second main mass loss step. The onset temperature of this main mass loss step was at 320 °C for the untreated RC, while it reduced to 224 °C for the fiber treated with ADHP (1 wt.-% P) and 210 °C for the fiber treated with ATS (1 wt.-% S). The residual mass in TGA at 1400 °C increased from 17% for the untreated fiber sample to 38 for the fibers finished with ADHP (1 wt.-% P) and 37% for ATS treated fibers (1 wt.-% S), respectively. This corresponds to 86 and 83% of the theoretical carbon yield and an increase of the carbonization yield of more than 100% compared to untreated fibers. An optimum concentration of ADHP and ATS with respect to the residual mass in TGA was found at 1.0 wt.-% of P or S, respectively (Table 1).

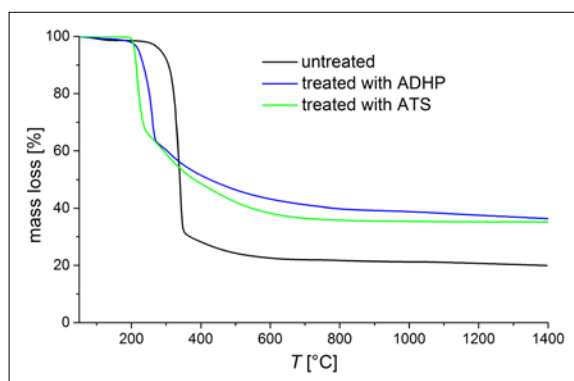


Figure 1: TGA curves of fibers treated with ADHP (1wt.-% P) or ATS (1 wt.-% S) and untreated fibers (rt - 1400 °C, 10 K/min, helium).

It is known for ADHP that it decomposes to NH_3 and H_3PO_4 during heat treatment. Thereby, it can act as a catalyst for dehydration reactions, thus making cellulose less prone to degradation reactions. [31] A similar mechanism is expected for cellulose and ATS, which forms the strong acid p-toluenesulfonic acid ($\text{pK}_a < 1$) during thermal decomposition. This acid can esterify

Table 1: TGA results of untreated fibers and fibers containing different amounts of ADHP and ATS characterized by their phosphorous or sulfur content (rt - 1400 °C, 10 K/min, helium).

| entry | phosphorous [wt.-%] | sulfur [wt.-%] | onset T of decomposition [°C] | residual mass at 1400 °C [%] |
|-----------|---------------------|----------------|-------------------------------|------------------------------|
| untreated | 0 | – | 325 | 17 |
| RC/ADHP1 | 0.6 | – | 239 | 33 |
| RC/ADHP2 | 1.0 | – | 224 | 38 |
| RC/ADHP3 | 1.8 | – | 218 | 34 |
| RC/ATS1 | | 0.4 | 210 | 32 |
| RC/ATS2 | | 1.0 | 210 | 37 |
| RC/ATS3 | | 2.3 | 204 | 35 |

OH-groups of cellulose, resulting in a good leaving group in order to dehydrate the AGU. Thereby cellulose is stabilized. In order to proof this presumption, the emission gases evolved during heat treatment of the fibers were studied by IR spectroscopy in order to gain information on the mechanism of pyrolysis. The emission products H_2O , CO_2 , CO and CH_4 as well as the evolution of gases with functional groups like $\text{C}=\text{O}$, $\text{C}-\text{O}$ and CH_2 could be detected, which belong to decomposition products like aldehydes, ketones, carboxylic ester and alcohols, e. g. (hydroxy)acetaldehyde, acetone, furane derivatives and levoglucosan. The emission gases considered in this study are summarized in Table 2.

Table 2: Evaluation and assignment of emission gases by IR.

| decomposition product / functional group | mode | band range ¹ [cm^{-1}] | baseline ² [cm^{-1}] |
|--|---------------------------|--|--|
| H_2O | ν_s / ν_{as} | 3858-3850 | 3858-3850 |
| CO_2 | ν_{as} | 2396-2265 | 2396-2265 |
| CO | ν_s | 2144-2000 | 2144-2000 |
| CH_4 | ν_s / ν_{as} | 3024-3003 | 3024-3003 |
| $\text{C}=\text{O}$ | ν_s | 1840-1626 | 1840-1626 |
| $\text{C}-\text{O}$ | ν_s | 1209-1143 | 1209-1143 |
| CH_2 | ν_s / ν_{as} | 3002-2859 | 3002-2859 |

¹ band range in the spectrum used for integration,

² baseline for integration.

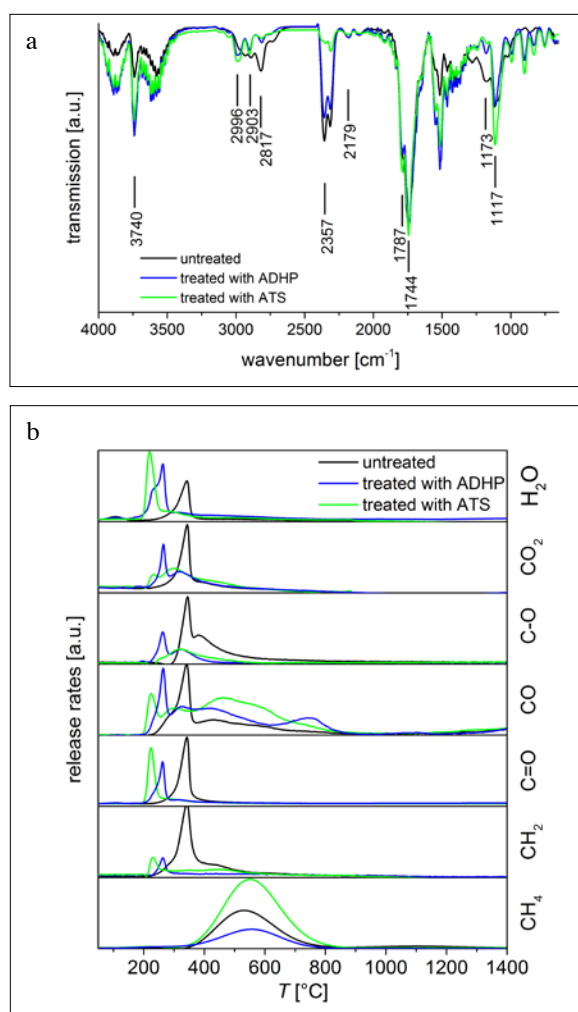


Figure 2: a) Normalized gas phase IR spectra of cellulose fibers (at $T = 339\text{ °C}$) and cellulose fibers treated with ADHP ($T = 246\text{ °C}$) and ATS ($T = 220\text{ °C}$), respectively; b) release rates of selected emission gases during TGA of untreated cellulose fibers and cellulose fibers treated with ADHP and ATS as determined via IR spectroscopy.

Figure 2a depicts the IR spectra taken at the respective main mass loss step of the untreated and treated fibers. For the untreated fiber, the H₂O band was less pronounced whereas the C-H and C-O bands showed a higher intensity than for the treated fibers. Thus it can be seen, that the application of ADHP or ATS acted catalytically in the dehydration reaction [31–35] during pyrolysis resulting in an increased emission of H₂O. Moreover, less CO₂ was formed in the main mass loss step for the fiber treated with ATS.

The release rates of the emission products are depicted in Figure 2b as a function of temperature. The temperatures of maximum release of the gases mostly followed the order of the onset temperatures of the TG signals. For the treated samples, the release of water occurred earlier and in larger amounts than for the untreated fiber sample. Moreover, less CO₂ and less compounds with

C-O functionality were formed. With the ATS additive, release of gas occurred over a longer temperature regime. Compounds with C=O and CH₂ functionalities were formed to a significantly lower extent. The treated samples released more CO, especially in the range 400–800 °C. In contrast to the other emission products, the formation of CH₄ occurred in the range 400–800 °C. The lowest amount of CH₄ was released from the sample treated with ADHP. By contrast, the sample treated with ATS gave rise to the highest emission of CH₄, because CH₄ could also be formed from the additive itself.

In contrast to the formation of tarry products from pure cellulose,[31] even at low temperatures stable fibers formed, which were less prone to decomposition reactions. The suppression of tar formation is not only responsible for the increase of carbonization yield but also has a very positive effect on the final technical implementation because it prevents the fusing of filaments and the contamination of the furnace during carbonization.

For continuous processing, stabilization of the precursor fibers equipped with ADHP (1 wt.-% P) or ATS (1 wt.-% S) was studied by isothermal TGA under N₂ at the respective onset temperature of decomposition. After 55 min, mass losses of 37 and 30% were found at the respective stabilization temperature (Figure 3). Note that the release of three equivalents of H₂O per AGU would correspond to a mass loss of 33%. The formation of small but detectable amounts of CO and CO₂ during stabilization was revealed in both cases by a simultaneous analysis of the evolved gases via MS (Figure 3).

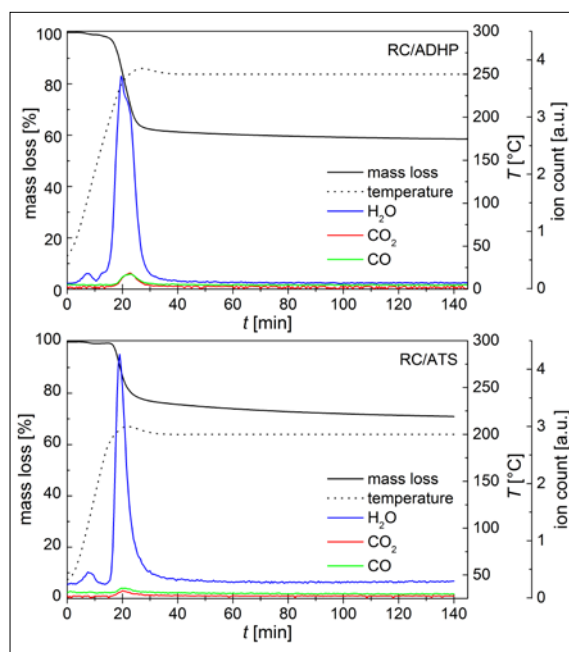


Figure 3: Isothermal TGA-MS of RC/ADHP at 250 °C (top) and RC/ATS at 210 °C (bottom).

Elemental analysis revealed similar C, H and N contents of the stabilized fibers irrespective of the carbonization aid used for impregnation (Table 3). Fibers consisted of almost 60 wt.-% C while about 2 mol of oxygen per AGU remained in the stabilized fiber.

Table 3: Elemental analysis of continuously stabilized fibers derived from RC/ATS and RC/ADHP.

| precursor | EA [wt.-%] | | | |
|-----------|------------|-----|-----|-----|
| | C | H | N | S |
| RC/ATS | 59.8 | 4.5 | 0.5 | 1.2 |
| RC/ADHP | 58.1 | 4.4 | 0.8 | — |

Continuous carbonization at different fiber tensions

Continuous carbonization of an RC fiber containing ATS (1 wt.-% S) and a RC fiber containing ADHP (1 wt.-% P) were performed at 1400 °C. A continuous carbonization of pure RC without any additive was omitted, because in a discontinuous carbonization trial, these fibers already led to very poor mechanical properties and carbon yields. After continuous stabilization

of the precursor fibers carbonization was performed at 1400 °C while applying different amounts of tensile force on to the fiber. A significant enhancement of the mechanical properties, especially Young's modulus, could be achieved by increasing the tensile force (Figure 4). However, for the RC/ATS precursor a higher tensile force could be applied during carbonization experiments, which ultimately resulted in superior mechanical properties in the CF compared to RC/ADHP.

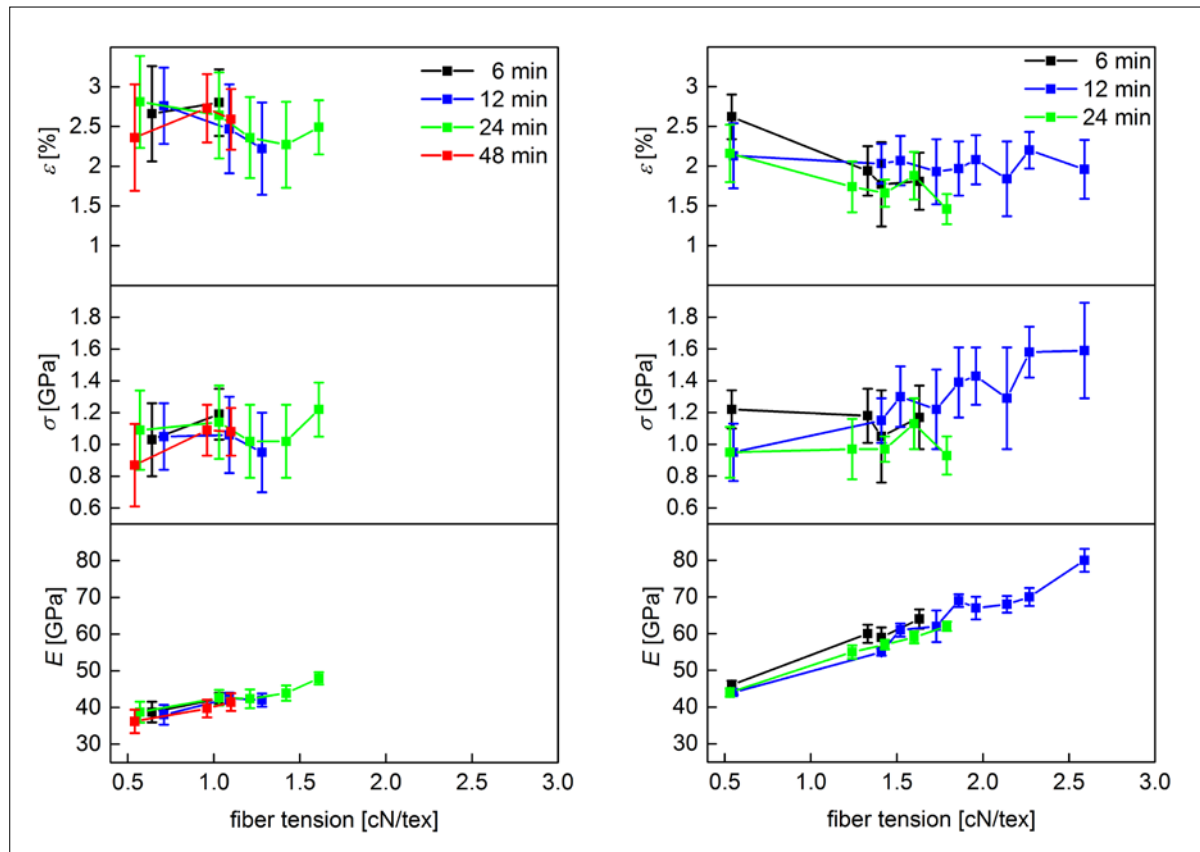


Figure 4: Mechanical properties of RC/ADHP- (left) and RC/ATS derived CFs (right) from continuous carbonization at 1400 °C in dependence of dwell time (6, 12, 24 or 48 min) and fiber tension.

With respect to the maximum tensile force which could be applied before filament breakage the optimum dwell times for carbonization were 12 min for RC/ATS and 24 min for RC/ADHP (Table 4, page 90). RC/ATS resisted a 40% higher tension than RC/ADHP fibers

during processing and thus reached better mechanical properties (Figure 4). Cellulose-based CFs with reasonable mechanical properties (tenacity of 2.0 GPa, Young's modulus of 84 GPa, elongation of 2.4%) were obtained with optimized conditions.

Table 4: Experimental conditions during continuous carbonization at 1400 °C of the stabilized fibers.

| precursor | dwel time [min] | maximum fiber tension ¹ [cN/tex] |
|-----------|-----------------|---|
| RC/ATS | 6 | 1.6 |
| RC/ATS | 12 | 2.6 |
| RC/ATS | 24 | 1.8 |
| RC/ADHP | 6 | 1.2 |
| RC/ADHP | 12 | 1.3 |
| RC/ADHP | 24 | 1.6 |
| RC/ADHP | 48 | 1.1 |

¹maximum fiber tension before filament breakage during carbonization.

Figure 5 depicts the crystalline parameters determined via WAXS analysis of RC/ADHP- and RC/ATS-derived CFs, which were processed at different dwell times, as a function of fiber tension during the continuous carbonization at 1400 °C. Comparable interlayer dis-

tances d002 were found for both precursor types, with slightly lower values for RC/ATS-derived CFs at higher fiber tension. Comparing the two precursor types carbonized at dwell times of 12 and 24 min, the crystallite height L_c was lower for RC/ADHP. The crystallite length L_a increased with the tensile strain applied during carbonization for both precursor types. Although RC/ADHP could only withstand a lower tensile strain than RC/ATS, higher L_a values were reached. However, this did not affect the mechanical properties of RC/ADHP (see Figure 4). The applied force also resulted in an increase of the crystallites' preferred orientation, P.O. In the continuous process without application of tensile force P.O. was about 50%, while with tensile force, a maximum P.O. of 63% for RC/ATS- and 57% for RC/ADHP-derived CFs was reached. This increase in P.O. correlated with the increase in Young's modulus. For comparison, a commercial PAN-based CF T300 (Young's Modulus: 190 GPa, probably carbonized at a temperature of 1200-1400 °C), showed a P.O. value of 81%.

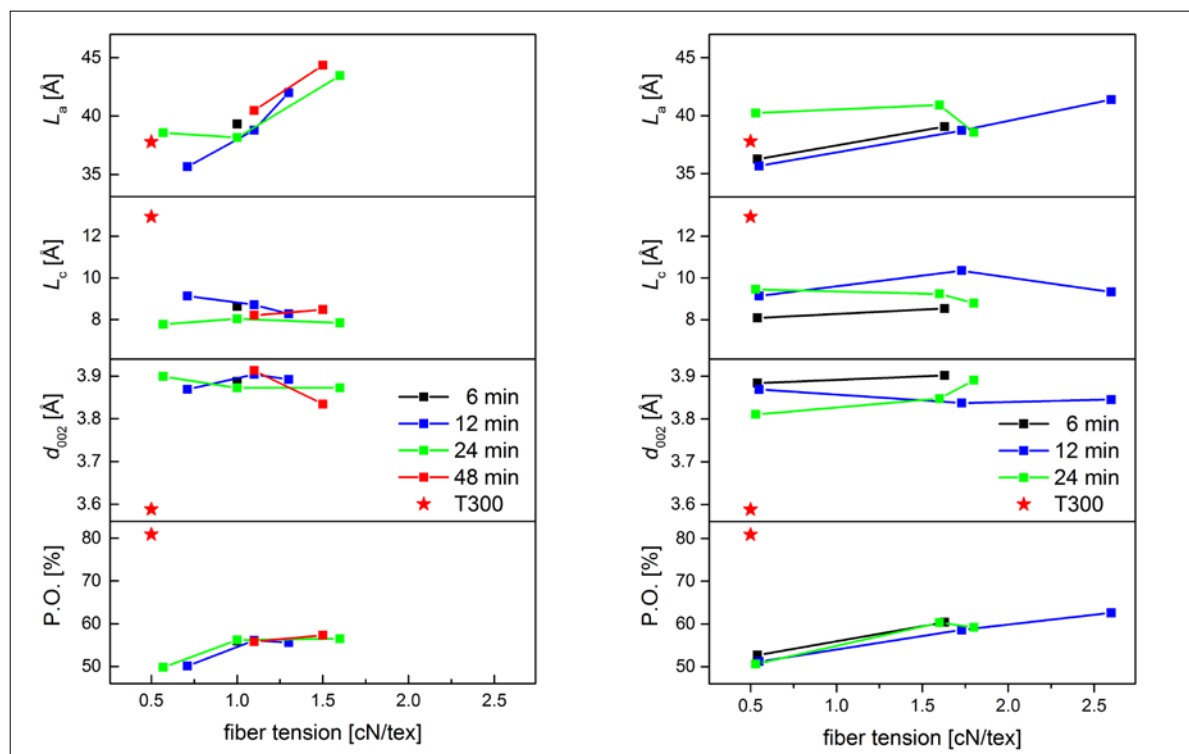


Figure 5: Interlayer distances, crystallite sizes and preferred orientation of RC/ADHP- (left) and RC/ATS-derived CFs (right) from continuous carbonization at 1400 °C and variable dwell times (6, 12, 24 or 48 min) and fiber tensions; T300: values obtained from a commercial PAN-based CF (Toray Industries Inc.).

The elemental composition of the CFs with respect to the dwell time was also considered. Irrespective of the dwell time, higher C contents of ca. 97 wt.-% were found with RC/ATS, in comparison to 92-93 wt.-% for RC/ADHP-derived CFs. Neither S nor H were found, but both CF types contained about 1 wt.-% N.

In graphite-like structures elements other than carbon and hydrogen usually tend to accumulate between the graphite layers rather than to become incorporated into the layer. Therefore phosphorous and oxygen in RC/ADHP-based CFs seem to interfere with layer stacking, thus leading to smaller L_c values. The growth of L_a is instead favored already at low fiber tension.

Fiber morphology and fiber shape

SEM images of RC-derived CFs from continuous carbonization are depicted in Figure 6. After carbonization, the fibers retain the varying and irregular cross-sections, which stem from the viscose manufacturing process. For the RC/ADHP-derived CFs, irrespective of the dwell time, several meso- and some macropo-

res with diameters of up to 75 nm were visible at high image resolution, and yet, ultimate tensile strengths of more than 1 GPa were reached. No pores were found in high resolution images at dwell times of 6 and 12 min for the RC/ATS-derived CFs, whereas at 24 min, a few mesopores with diameters of 20–40 nm were found.

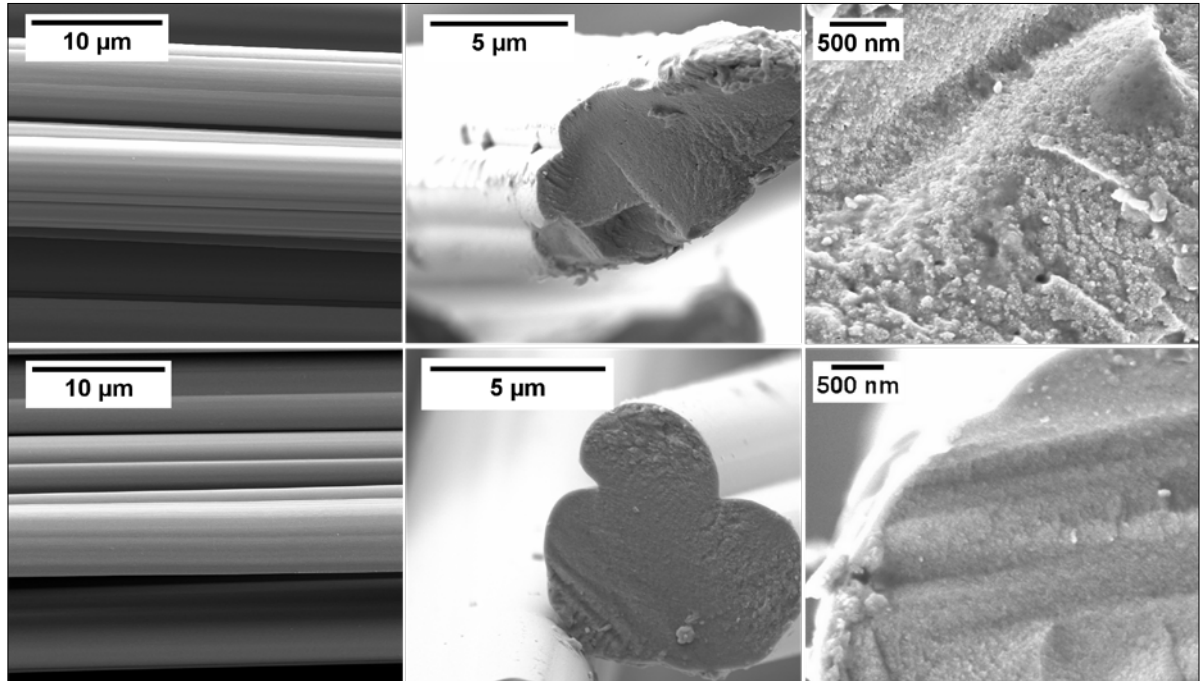


Figure 6: SEM pictures of CFs obtained via continuous carbonization at 1400 °C, top: RC/ADHP-derived CFs, 24 min; bottom: RC/ATS-derived CFs, 12 min.

Structural differences revealed by discontinuous carbonization experiments

In order to gain a better understanding of the differences between the two precursors in carbonization, structure formation of RC/ADHP- and RC/ATS-based CFs was studied in more detail. Precursor fibers containing 1 wt.-% of P and S, respectively, were carbonized under nitrogen in a batch furnace at different temperatures in the range 400–2200 °C. Beside of tensile testing, the resulting CFs were studied via elemental analysis and WAXS. The mechanical properties of discontinuously prepared CFs did not reach the good level of mechanical properties found in continuous carbonization experiments. Fibers, which were not treated with ADHP or ATS were even too brittle for the testing. CFs from both precursors showed similar mechanical properties with a maximum in tenacity (σ) at carbonization temperatures of 1100–1400 °C (Table 5), despite their dissimilar behavior in continuous carbonization. Via process optimization, a maximum tenacity of 1.3 GPa was reached with the RC/ADHP precursor in discontinuous carbonization. However, the average value for RC/ATS and RC/

ADHP was 0.9 GPa. A slight increase in Young's modulus (E) of 10 GPa was reached at a carbonization temperature of 1800 °C.

Table 5: Mechanical properties of RC/ADHP- and RC/ATS-derived CFs from discontinuous carbonization (average values from 20 single filament tests).

| | Φ [μm] | ϵ [%] | σ [GPa] | E [GPa] |
|---------|--------------------------|----------------|----------------|-------------|
| RC/ADHP | 10 | 2.4 | 0.9 | 39.0 |
| RC/ATS | 10 | 2.4 | 0.9 | 39.6 |

With increasing carbonization temperature, the C content increased to >99 wt.-% at 1800 °C, whereas N and H contents decreased (Figure 7). The delta to 100 wt.-% in the elemental analysis in Figure 7 is due to the presence of small amounts of O, P or S in the carbonized material. Thus, P contents of 2–3 wt.-% were found in RC/ADHP-derived CFs carbonized at 1100 °C, while no S was found in RC/ATS-derived CFs carbonized at this temperature. Furthermore, at 1400 °C, CFs derived from RC/ATS or untreated RC (not shown) already consisted of > 99 wt.-% C, while RC/ADHP-derived

CFs obviously contained substantial amounts of oxygen. At higher temperatures, a release of phosphorous and oxygen from the CF, possibly in the form of phosphorous oxides or gaseous P_2 , [36] is indicated. Notably, the C contents of RC/ADHP-derived CFs were higher after continuous carbonization than after discontinuous carbonization, while the overall dwell time was shorter.

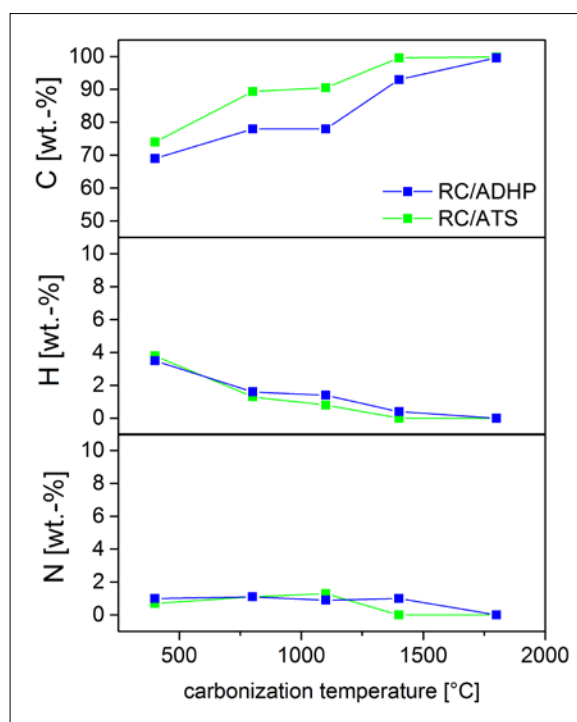


Figure 7: C, H and N contents of RC/ADHP- and RC/ATS-derived CFs obtained via discontinuous carbonization.

Figure 8 depicts the WAXS diffraction patterns of cellulose-based CFs at temperatures between 400 and 2200 °C and shows the growth of the crystallites and the decrease of the interlayer spacing d_{002} , as de-

scribed before. [28–29] From 600 °C to 2200 °C, L_c increased from 9 Å to 14 Å and L_a more than doubled from ca. 25 to 61 Å for both precursors. In the same temperature range, d_{002} decreased from ca. 4.0 Å to 3.6 Å, again for both precursors. This can be attributed to the improvement of the graphitic structure. Up to 1400 °C, RC/ATS-derived CFs tended to smaller d_{002} and larger L_a values than RC/ADHP-derived ones, probably because of the larger amount of heteroatoms present in the structure of RC/ADHP-derived CFs (cf. elemental analysis). The alignment of values above 1400 °C can be explained by the liberation of oxygen and phosphorous at this temperature for RC/ADHP-derived CFs. In relation to continuous carbonization, somewhat higher values for L_a and L_c were found at 1400 °C. This is probably due to the overall dwell time, which was longer for the discontinuous carbonization, mostly because of the long cooling time of the batch furnace. While for RC/ADHP-derived CFs the d_{002} value was similar for continuous and discontinuous processing, a smaller d_{002} value was obtained for RC/ATS-derived fibers in course of discontinuous carbonization. Again, the commercial PAN-based T300 CF, probably carbonized at a temperature of 1200–1400 °C, was used for the comparison of structural properties. In the temperature range 1200–1400 °C, L_a of both RC-derived CFs reached the value of the T300 CF ($L_a = 37.8$ Å). However, L_c and d_{002} reached the values of the T300 CF ($d_{002} = 3.59$ Å, $L_c = 1.29$ nm) only at temperatures above 1800 °C.

For all discontinuous carbonization trials the maximum preferred orientation (P.O.) of the graphite planes (002) reached only 50%, even at high carbonization temperatures. Notably, an increase in orientation of the (002) plane is a fundamental prerequisite for improving Young's modulus [37–38] but requires dynamic tension, as shown before.

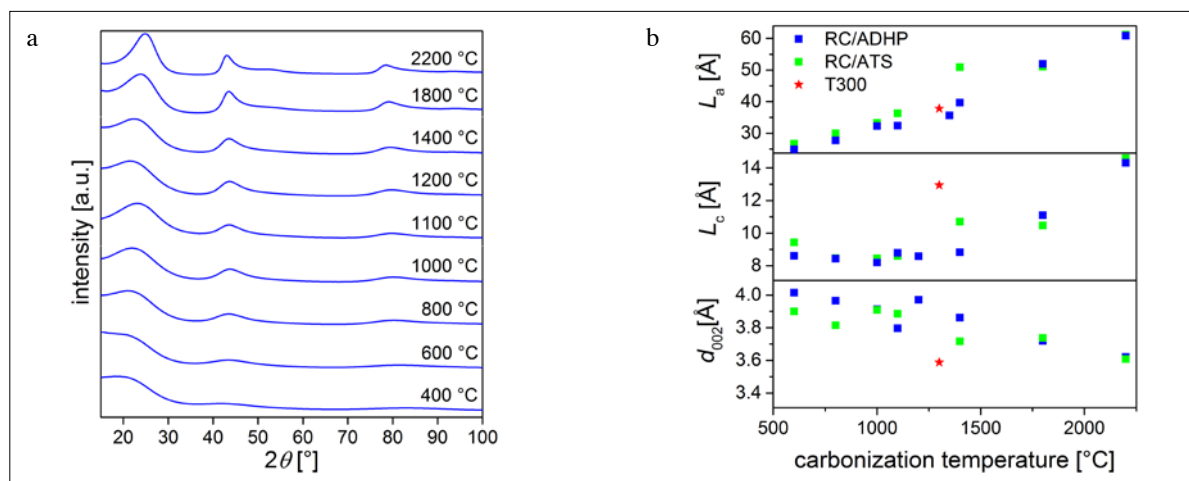


Figure 8: a) Normalized diffraction patterns of RC/ADHP-derived CFs with increasing temperature; b) development of interlayer spacing d_{002} and crystallite dimensions L_a and L_c of RC/ADHP- and RC/ATS-derived CFs with increasing carbonization temperature.

WAXS and elemental analysis revealed differences in the carbon structure of RC/ATS- and RC/ADHP- based CFs. Generally, the phosphorous in RC/ADHP-based CFs impedes structure formation in the material. In the discontinuous process, a difference in L_a was observed rather than in L_c leading towards the conclusion that for layer stacking and thus increase of L_c , also any hindrance in shrinkage is of importance. Phosphorous and oxygen are released at sufficiently high carbonization temperature and structural differences between RC/ATS- and RC/ADHP- based CFs diminish. However, such high temperatures are not favorable for economic reasons and it remains unclear, whether orientation and structure formation at low temperatures could be caught up.

Conclusions

In this study, both, the carbonization yields and the properties of cellulose-based CFs have been considerably improved without the need of an expensive high temperature graphitization. Standard equipment for the carbonization of PAN precursors can be used omitting the special exhaust gas treatment which is needed in case of PAN-based CFs. Commercially available high-strength Rayon fibers equipped with a carbonization aid were used as a precursor fiber. ATS has several advantages over ADHP as a carbonization aid while having the identical effect on carbon yield: Dehydration of cellulose takes place at lower temperatures than with ADHP or without any additive. Concomitantly, carbon loss through carbon-containing volatiles and tar is substantially reduced. Both precursor fibers were suitable for continuous processing with respect to their mechanical stability and resulted in CFs without fusing of single filaments. However, RC/ATS could be processed continuously over a wider range of fiber tension and led to a significant increase in textile mechanical properties, especially in Young's modulus. In case of the RC/ADHP precursor, the incorporation of phosphorous oxides retards the structure formation which is essential for an increase in tensile strength and modulus. The RC/ATS-derived CF show a high carbon content already at low temperatures and the fibers thus withstand higher mechanical tension. Thereby, crystallite growth and orientation are favored. The rather irregular precursor fiber shape was transferred into the CFs. Clearly, a more defined shape and morphology of the precursor should boost the mechanical properties of the resulting CFs. In this respect, Lyocell or IL-spun filament fibers would be promising precursors. Structural changes induced in the CF via the application of a tensile force lead to tunable mechanical properties. They can be further optimized

with regard to processing conditions as well as structure and shape of the precursor fiber in order to substitute PAN-based CFs with a more sustainable cellulose-based CF.

Acknowledgement

The authors would like to acknowledge BASF SE for financing the research and support throughout the project. The authors would also like to thank Cordenka GmbH for supply of the Rayon fibers. Furthermore, the authors would like to thank Dipl.-Geol. Ulrich Hageroth and Sabine Henzler for SEM and Raman measurements.

References

- [1] E. Frank, L. M. Steudle, D. Ingildeev, J. M. Spörl, M. R. Buchmeiser, *Angew. Chem. Int. Ed.* 2014, 53, 5262-5298.
- [2] Q.-L. Wu, S.-Y. Gu, J.-H. Gong, D. Pan, *Synth. Met.* 2006, 156, 792-795.
- [3] H. Zhang, L. Guo, H. Shao, X. Hu, *J. Appl. Polym. Sci.* 2006, 99, 65-74.
- [4] J. K. Park, J. Y. Lee, Y. G. Won, D. H. Cho, Method for manufacturing lyocell based carbon fiber and lyocell based carbon fiber fabric, US2010/0285223A1, 2010.
- [5] G. Bhat, K. Akato, W. Hoffman, in *Proceedings of the Fiber Society Spring Conference*, Empa St. Gallen, Switzerland, 2012.
- [6] X. Zhang, Y. Lu, H. Xiao, H. Peterlik, *J. Mater. Sci.* 2014, 49, 673-684.
- [7] Sohim, <http://www.sohim.by/eng/production/carbon/fibers/>, 2018, aufgerufen am 22.1.2018.
- [8] N. Byrne, M. Setty, S. Blight, R. Tadros, Y. Ma, H. Sixta, M. Hummel, *Macromol. Chem. Phys.* 2016.
- [9] C. E. Ford, C. V. Mitchell, Union Carbide Corporation, Fibrous graphite, US3107152, 1963.
- [10] C. B. Cross, D. R. Ecker, O. L. Stein, Union Carbide Corporation, Artificial Graphite Process, US3116975, 1964.
- [11] P. H. Brunner, P. V. Roberts, *Carbon* 1980, 18, 217-224.
- [12] R. Bacon, in *Chem. Phys. Carbon*, Vol. 9, 1 ed. (Eds.: P. L. Walker, P. A. Throver), Marcel Dekker, Inc, New York [u.a.], 1973, pp. 1-102.
- [13] A. A. Konkin, in *Handbook of Composites Vol. 1: Strong Fibres*, Vol. 1 (Eds.: A. Kelly, Y. N. Rabotnov, W. Watt, B. V. Perov), Elsevier Science Publishers B.V., Amsterdam (The Netherlands), 1985, pp. 275-325.

- [14] I. Karacan, T. Soy, *J. Mater. Sci.* 2013, 48, 2009-2021.
- [15] R. F. Schwenker, E. Pacsu, *Ind. Eng. Chem.* 1958, 50, 91-96.
- [16] S. E. Ross, *Text. Res. J.* 1968, 38, 906-913.
- [17] A. Shindo, Y. Nakanishi, I. Soma, in *Appl. Polym. Symp.*, Vol. 9 (Ed.: J. Preston), Interscience Publ, New York [u.a.], 1969, pp. 271-284.
- [18] P. J. Goodhew, A. J. Clarke, J. E. Bailey, *Mater. Sci. Eng.* 1975, 17, 3-30.
- [19] W. K. Tang, W. K. Neill, *J. Polym. Sci., C Polym. Symp.* 1964, 6, 65-81.
- [20] A. Basch, M. Lewin, *Text. Res. J.* 1975, 45, 246-250.
- [21] J. B. Tomlinson, C. R. Theocharis, *Carbon* 1992, 30, 907-911.
- [22] A. A. Morozova, Y. V. Brezhneva, *Fibre Chem.* 1997, 29, 31-35.
- [23] H. Li, Y. Yang, Y. Wen, L. Liu, *Compos. Sci. Technol.* 2007, 67, 2675-2682.
- [24] Q. Wu, N. Pan, K. Deng, D. Pan, *Carbohydr. Polym.* 2008, 72, 222-228.
- [25] Q. Liu, C. Lv, Y. Yang, F. He, L. Ling, *J. Mol. Struct.* 2005, 733, 193-202.
- [26] S. Son, K. Massonne, F. Hermanutz, J. M. Spörl, M. R. Buchmeiser, R. Beyer, BASF SE, Method for production of carbon fibers from cellulose fibers, WO2015173243, 2015.
- [27] N. Byrne, J. Chen, B. Fox, *J. Mater. Chem. A* 2014, 2, 15758-15762.
- [28] J. M. Spörl, A. Ota, S. Son, K. Massonne, F. Hermanutz, M. R. Buchmeiser, *Mater. Today Commun.* 2016, 7, 1-10.
- [29] J. M. Spörl, R. Beyer, F. Abels, T. Cwik, A. Müller, F. Hermanutz, M. R. Buchmeiser, *Macromol. Mater. Eng.* 2017, 302, 1700195.
- [30] P. Scherrer, *Gött. Nachr.* 1918, 98-100.
- [31] B. K. Kandola, A. R. Horrocks, D. Price, G. V. Coleman, *J. Macromol. Sci. Polym. Rev.* 1996, 36, 721-794.
- [32] S. Gaan, P. Rupper, V. Salimova, M. Heuberger, S. Rabe, F. Vogel, *Polym. Degrad. Stab.* 2009, 94, 1125-1134.
- [33] R. K. Jain, K. Lal, H. L. Bhatnagar, *J. Appl. Polym. Sci.* 1985, 30, 897-914.
- [34] J. Scheirs, G. Camino, W. Tumiatti, *Eur. Polym. J.* 2001, 37, 933-942.
- [35] D. Radlein, J. Piskorz, D. S. Scott, *J. Anal. Appl. Pyr.* 1991, 19, 41-63.
- [36] A. F. Holleman, E. Wiberg, N. Wiberg, *Lehrbuch der anorganischen Chemie*, 102. ed., de Gruyter, Berlin; New York, 2007.
- [37] F. R. Barnet, M. K. Norr, *Composites* 1976, 7, 93-99.
- [38] D. Crawford, D. J. Johnson, *J. Microsc.* 1971, 94, 51-62.

Continuous Alkali Treatments of Lyocell. Effects of Alkali Concentration, Temperature and Fabric Construction.

Ján Široký^{1,2}, Avinash P. Manian², Barbora Široká², Richard S. Blackburn¹,
and Thomas Bechtold^{*2}

¹ Sustainable Materials Research Group, Centre for Technical Textiles, University of Leeds,
Leeds LS2 9JT, UK

² Research Institute of Textile Chemistry and Textile Physics, University of Innsbruck, Höchsterstraße 73,
A-6850, Dornbirn, Austria.

* Corresponding author: Research Institute of Textile Chemistry and Textile Physics, University of Innsbruck,
Tel: +43 (0) 5572 28593, Fax.: +43 (0) 5572 28629. E-mail: textilchemie@uibk.ac.at.

Abstract

Continuous alkali treatment under varying NaOH concentration, temperature, and fabric construction; has a substantial influence on dimensional and mechanical properties as well as on morphological, molecular and supramolecular properties of lyocell fabrics causing changes in their structure and performance. Physico-mechanical properties and structural changes of NaOH treated fabrics were examined by dimensional changes, flexural rigidity (in dry and wet state), mass per area, water retention, physico-mechanical tests, and applying ATR-FTIR spectroscopy to evaluate changes in crystallinity indices. Maxima of TCI, LOI, shrinkage, flexural rigidity, and minima for HBI, water retention, crease recovery, tensile strength and elongation at break, were observed at concentrations of 3.33 and 4.48 mol dm⁻³ NaOH and at temperature of 25 °C and 40 °C. Further, it was observed that treatment temperature of 40 °C have a substantially lower impact on treated fabric properties. The cellulose II-based fabrics with different construction did not show uniform behaviour in studied properties after undergoing alkali treatment, despite they are made of the same material.

Keywords: Alkali; Fibres; Textiles; Swelling; Mechanical Properties; FT-IR; Crystallinity

Introduction

The focus of the work was to examine the effect of process variables and fabric construction in the treatment of lyocell with NaOH in a continuous process. Woven lyocell fabrics of three different constructions: plain, sateen and twill, were treated with NaOH solutions of different concentrations, at two temperatures (25°C and 40°C), in a pilot-scale open-width washing range, to simulate commercial processing operations. Previously [1-3], we have reported on the influence of treatment process variables on the mechanical and physico-chemical properties of plain-woven fabrics. In this paper, we examine the interaction effects of process variables with weave type.

Materials and Methods

Materials

Plain- (1/1 weave), twill- (3/1 weave) and sateen-woven (5/1 weave), desized, scoured lyocell fabrics (Tencel®, 140 g m⁻², comprised of 50/1 Nm staple yarn) used for this observation were kindly supplied by Lenzing AG, Austria. Technical grade NaOH (ca. 50% w/w) was used in formulating the alkali solutions in treatments, with Lyogen MC (Clariant, Basel, Switzerland) added as wetting agent. Analytical grade acetic acid was used in formulating the neutralization liquor.

Evaluation of changes in crystallinity and hydrogen bonding intensity by ATR-FTIR

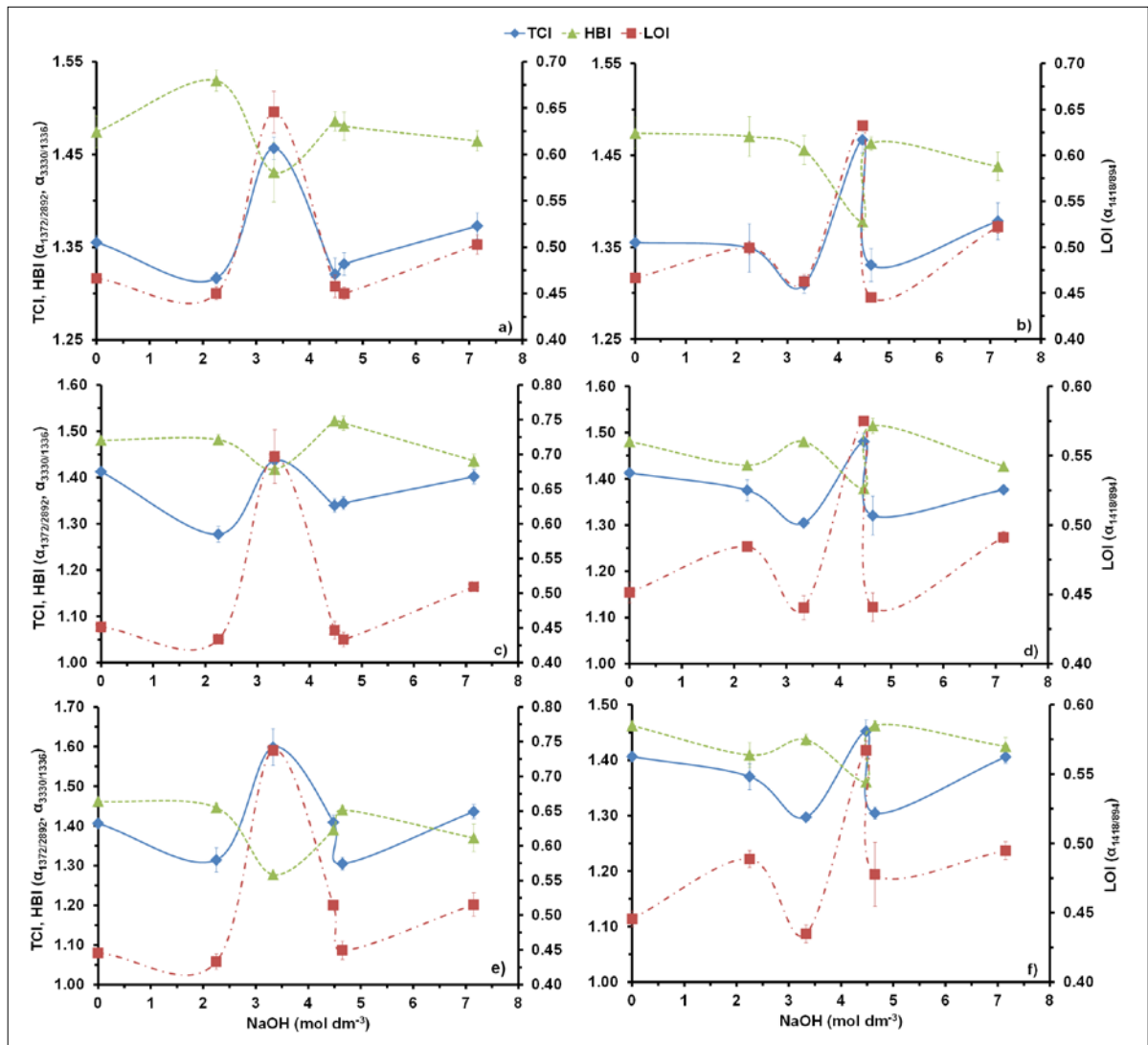


Figure 2: Total crystallinity index (TCI, blue diamond), lateral order index (LOI, red square) and hydrogen bonding intensity (HBI, green triangle) of plain (a, b), twill (c, d) and sateen (e, f) with increasing NaOH concentration, under constant tension (147 N m^{-1}) and varying temperature (25°C for a, c and e, or 40°C for b, d and f) in treatment stage of continuous NaOH treatment.

The evaluations are based on indices, which are ratios of absorbance intensities at two wavenumbers. These include Total Crystallinity Index (TOI), Lateral Order Index (LOI), and Hydrogen-Bond Intensity (HBI) [1, 5-9]. The TCI represents the overall degree of order in cellulose and is given by the ratio of absorbance at 1364 cm^{-1} (C–H deformation in cellulose II) to 2892 cm^{-1} (C–H stretch in cellulose II). LOI reflects the ordered regions perpendicular to the chain direction, and is the ratio of the band at 1418 cm^{-1} (CH_2 scissoring at C(6) in cellulose II) to 894 cm^{-1} (C–O–C valence vibration of β -glycosidic linkage). The HBI is the ratio of absorbance bands at 3336 cm^{-1} to 1336 cm^{-1} , and is closely related to the well ordered crystalline phase and the degree of intermolecular regularity.

The crystallinity changes in the lyocell fabrics subjected to alkali treatment, obtained by using ATR-FTIR method, are shown in Figure 2. In general, TCI and LOI show parallel behaviour over the whole range of alkali concentrations and treatment temperatures, although the absolute values differ. The higher magnitude for LOI occurred due to fact that LOI represents the ordered regions perpendicular to the chain direction, which is greatly influenced by chemical processing of cellulose [6]. Two peaks are observed for TCI and LOI at a concentration of 3.33 mol dm^{-3} NaOH for fabrics treated at 25°C , and at a concentration of 4.48 mol dm^{-3} NaOH for fabrics treated at 40°C . These maxima may have been most probably influenced by several factors. The known maximum of uptake

(about 3.00 mol dm⁻³) and degree of swelling, which at its maximum (between 3.00 and 3.75 mol dm⁻³) decreases with increasing temperature of the treatment liquor [10]. Also, the rate of fibre swelling has an influence which decreases with increasing concentration of alkali, attributed to increasing viscosity and surface tension in the treatment liquor and a reduction in the rate of alkali diffusion within substrates [1]. Another influence may be an increase of fibre orientation due to applied tension to softened – fully swollen substrate at maximum swelling (crystalline conversion to less ordered structure via breaking inter- and partly intra-hydroxyl groups within cellulose unit). Therefore, the maxima of crystallinity indices were achieved at higher NaOH concentration as it is observed when pad-batch process is applied. However, the differences in magnitude for TCI, LOI or HBI among used constructions revealed some trends which may have been influenced by their weaving and thus, different accessibility to alkali. The similar magnitude for TCI was observed when fabrics were treated under both treatment temperatures 25 °C or 40 °C. Whilst the LOI increased in order plain < twill < sateen as the weaving became loose at treat-

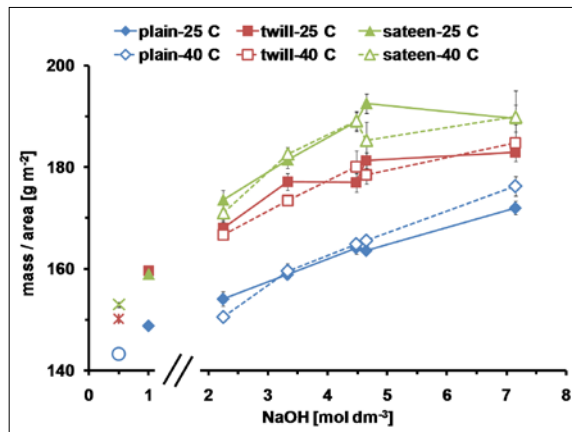


Figure 3: Mass per area vs. NaOH concentration in the fabrics: untreated plain (white circle), twill (red snowflake) or sateen (green cross); control plain (blue diamond), twill (red square) or sateen (green triangle), and fabrics treated with different alkali concentrations (2.25-7.15 mol dm⁻³) and temperatures (25°C with full markers and lines; 40°C with white markers and dashed lines) in treatment stage.

ment temperature of 25 °C, when treated with 40 °C rose in order plain < twill ≈ sateen. When comparing

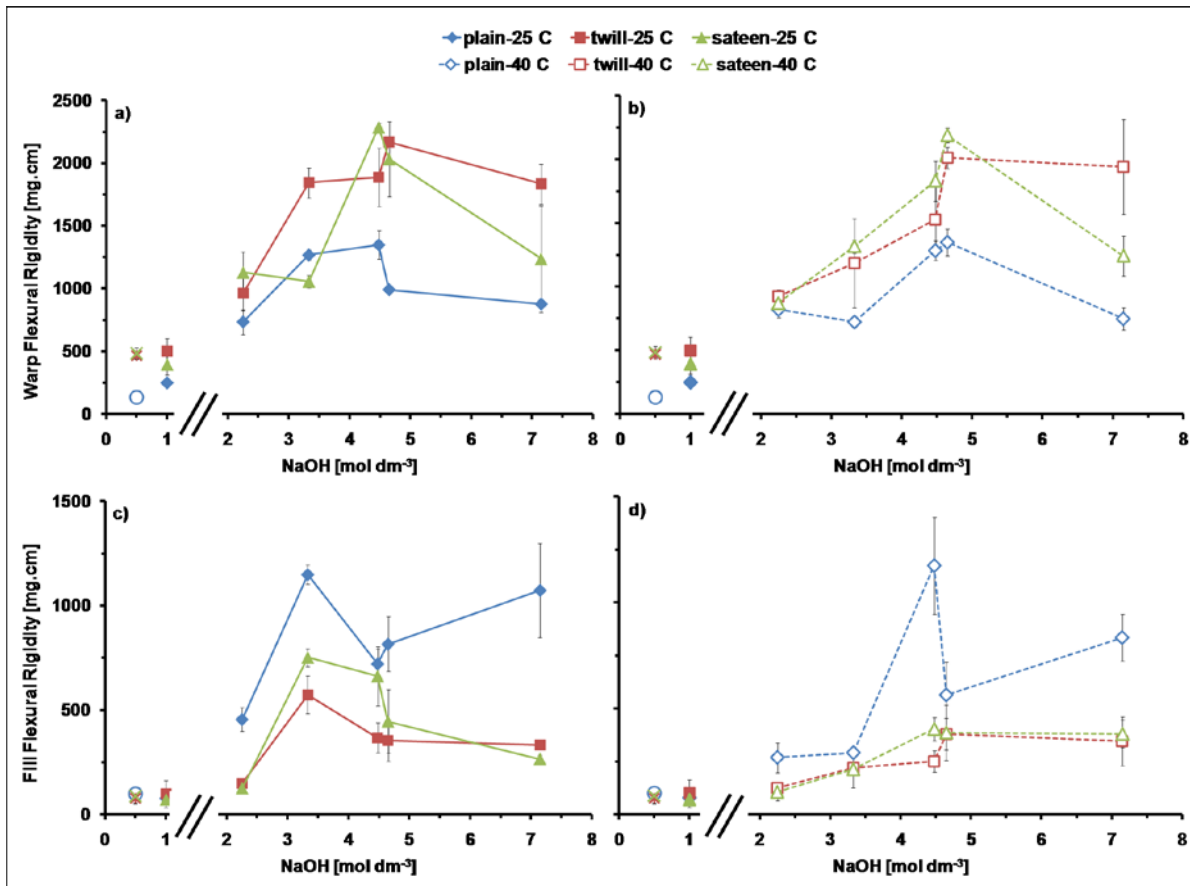


Figure 4: Flexural rigidity of the dry-state (a-b) warp and (c-d) weft in the fabrics: untreated plain (white circle), twill (red snowflake) or sateen (green cross); control plain (blue diamond), twill (red square) or sateen (green triangle), and fabrics following the alkali-treatment (2.25-7.15 mol dm⁻³), tension and temperatures (a-c; with full markers and lines) 147 N m⁻¹ / 25°C and (b-d; with white markers and dashed lines) 147 N m⁻¹ / 40°C.

the HBI for both temperatures, the magnitudes are more or less the same for all examined constructions. When the comparison of TCI or LOI with HBI is made, a “mirror effect” is observed, while TCI or LOI show maxima at particular concentration, HBI exhibit minima. This was previously attributed to changes with bulk density as well as with symmetry of cellulose II [1] due to its close relation to the well-ordered system and the degree of intra- and inter-molecular regularity of hydrogen bonds [11].

Dimensional change

In general, the mass/area (Figure 3) increased with a rise of NaOH pre-treatment concentration for plain, whereas twill and sateen levelled off between 4.48-7.15 mol dm⁻³. However, substantial differences were noted when comparing the various constructions: mass/area increased in the order plain < twill < sateen. Treatment temperature showed either very little or no difference. Increase in control substrate in all examined constructions can be seen in comparison to the un-treated substrates, indicating a degree of overall fabric shrinkage upon treatment with water [2]. In the comparison of

control with those treated with lowest NaOH concentration, the 2.25 mol dm⁻³, only the plain construction did not show substantial difference.

Dimensional change in all fabrics examined upon treatment with water (control) or NaOH treatment was related to fibre swelling, wherein the yarns increase in diameter by about 35% [12], and thus, a warp thread has to take a longer path around the swollen weft thread [13], which, in turn, will cause contraction [2,10,14-17]. The overall effect of the swelling mechanism on fabric dimensional stability is highly dependent on the tightness of the weave [15], and, as a result, the swollen material becomes very compact and tight, and inter-yarn space decreases [13]. In addition, it is known that the degree of fibre swelling and its effect on fabric dimension is influenced by factors such as NaOH concentration, temperature and mechanical restrictions imposed on fibres [2,10,14-17]. Also, the mass/area indicates a significant influence of fabric construction upon solution uptake/swelling and its effect on fabric dimensional stability. As the fabric weave becomes more free, plain < twill < sateen, the swelling and the mass/area rises, and propensity to shrink increases.

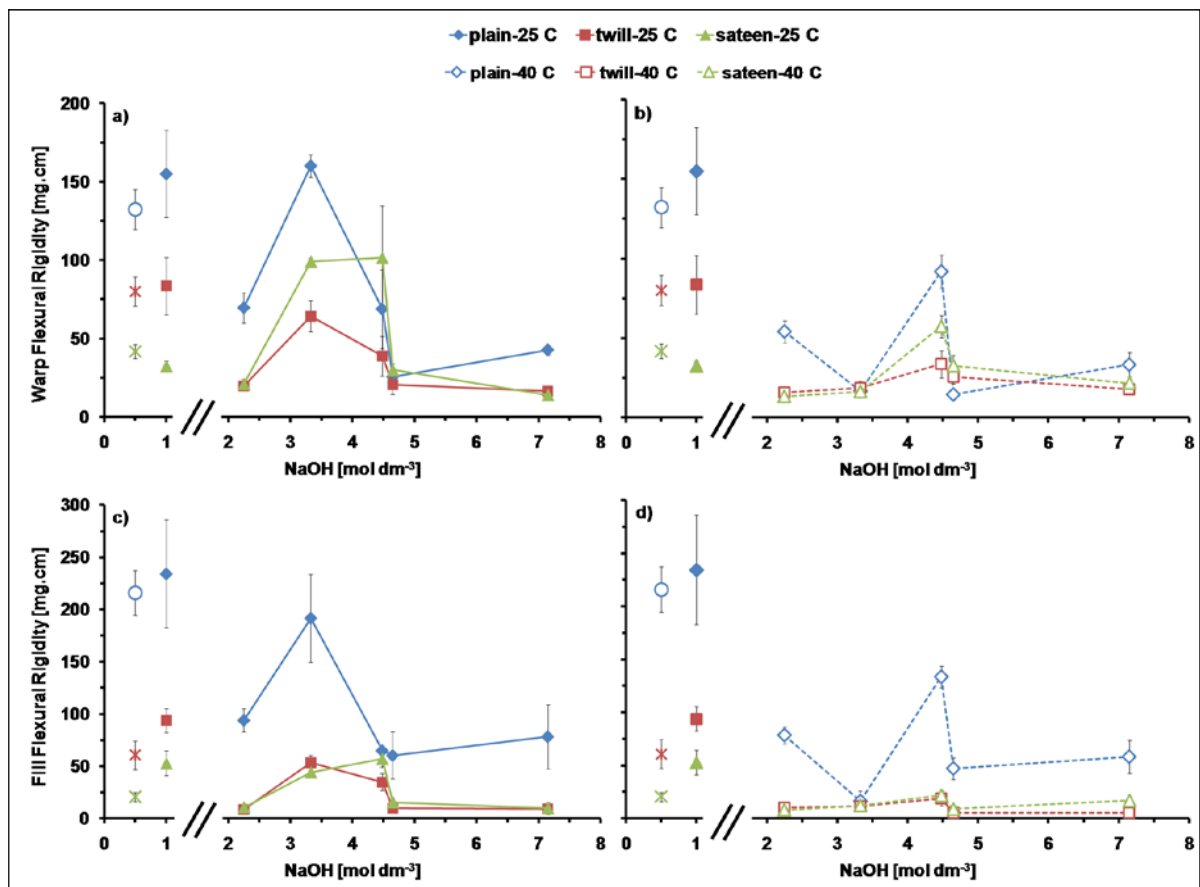


Figure 5: Flexural rigidity of the wet-state (a-b) warp and (c-d) weft in the fabrics: untreated plain (white circle), twill (red snowflake) or sateen (green cross); control plain (blue diamond), twill (red square) or sateen (green triangle), and fabrics following the alkali-treatment (2.25-7.15 mol dm⁻³), tension and temperatures (a-c; with full markers and lines) 147 N m⁻¹ / 25°C and (b-d; with white markers and dashed lines) 147 N m⁻¹ / 40°C.

The obtained results from measurement of flexural rigidity in all studied fabrics are shown in Figure 4 and Figure 5 in the dry-state and wet-state in both warp and weft directions. The dry flexural rigidity, Figure 4, was greater in the NaOH treated fabrics compared to untreated or control fabrics. The control plain fabric exhibited higher value than that untreated along the warp direction, but similar values were observed along the weft direction. In the case of twill and sateen fabrics such a difference was not observed, the un-treated and control fabrics were similar in both directions. Among NaOH treated fabrics, the warp dry flexural rigidity peak was observed at 4.48 mol dm^{-3} NaOH at $25 \text{ }^\circ\text{C}$, and at 4.65 mol dm^{-3} at $40 \text{ }^\circ\text{C}$, respectively. It was also observed that two maxima occur for weft dry flexural rigidity at a concentration of 3.33 mol dm^{-3} NaOH for samples treated at $25 \text{ }^\circ\text{C}$, and at a concentration of 4.48 mol dm^{-3} NaOH for samples treated at $40 \text{ }^\circ\text{C}$, apart from the twill fabric treated at $40 \text{ }^\circ\text{C}$ where the maximum was at concentration of 4.65 mol dm^{-3} .

Wet flexural rigidity, Figure 5, was generally lower in alkali treated fabrics, apart from the warp sateen fabric treated at temperature of $25 \text{ }^\circ\text{C}$, compared with the untreated or control fabrics. There were no observed significant differences between untreated and control fabrics along the warp direction, but different values were detected for twill or sateen fabrics along the weft direction. Two peaks, dependent on the treatment temperature, were observed in both warp and weft wet flexural rigidity of alkali treated fabrics, at a concentration of 3.33 mol dm^{-3} NaOH for fabrics treated at $25 \text{ }^\circ\text{C}$, and at concentration of 4.48 mol dm^{-3} NaOH for fabrics treated at $40 \text{ }^\circ\text{C}$. Obviously, twill fabrics at lower treatment temperature showed an exception to this observation where the peak is marginally towards concentration of 4.48 mol dm^{-3} NaOH, however, increased error bar needs to be considered.

Flexural rigidity is influenced by the physical structure of the fabrics, with therefore different interlacements or cross-over points in the fabric weave. Mobility of the yarns within fabrics is influenced by the compactness of the yarns; close contact among the yarns reduces mobility and enhances the flexural rigidity, in contrast, inter-yarn spaces enhance the mobility and reduce the flexural rigidity. Therefore, the aqueous solution pick-up differs and it is strongly influenced with swelling. The high dry flexural rigidities obtained herein for alkali treated fabrics may have been due to alkali treatment under tension which after neutralization and drying leads generally to high dry flexural rigidity [18]. Those increased values resulted from the temporary fabric settings. Also, the fabric flexural rigidity can be influenced by the rigidity of the yarns, great swelling in alkali solutions affects and forms the

shape of fibres [19, 20] as they became wedged against each other within yarns and led to its close packing. This close packing of fibres within the yarns led further to increase yarn and fabric flexural rigidity. These discussed effects may have been interconnected with the obtained peaks in flexural rigidity of the fabrics treated at a concentration of 3.33 mol dm^{-3} NaOH for fabrics treated at $25 \text{ }^\circ\text{C}$, and at a concentration of 4.48 mol dm^{-3} NaOH for fabrics treated at $40 \text{ }^\circ\text{C}$. Upon re-wetting in water, the degree of yarn swelling did not reach the levels attained during alkali treatment and thus, inter-yarn spaces were maintained at the cross-over points, and the wet flexural rigidity was reduced [2].

Water retention values (WRV)

WRV gives a quantitative indication of the spatial changes in the non-crystalline regions of the fibres. Due to the relation between swelling properties and fine structure of cellulose fibre, WRV might be an indicator of the changes in supramolecular structure such as degree of crystallization, amorphous and void regions. WRV strongly correlates with the volume and structure of pore [21], and it is inversely related to crystallinity. However, WRV values include not only water from pores but also bound water and surface water as well.

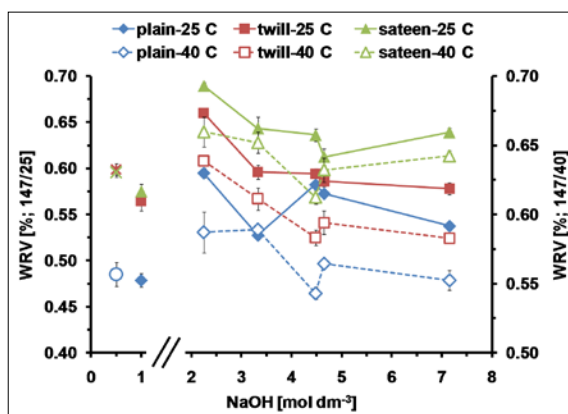


Figure 6: Water retention in the fabrics: untreated plain (white circle), twill (red snowflake) or sateen (green cross); control plain (blue diamond), twill (red square) or sateen (green triangle), and fabrics following the alkali-treatment (2.25 - 7.15 mol dm^{-3}), tension and temperatures (a-c; with full markers and lines) $147 \text{ N m}^{-1} / 25^\circ\text{C}$ and (b-d; with white markers and dashed lines) $147 \text{ N m}^{-1} / 40^\circ\text{C}$. white markers and dashed lines) in treatment stage.

WRVs (Figure 6) were higher for NaOH treated fabrics compared to untreated and control fibres for the same construction, which is as a result of increases in capillary spaces caused by changes to fibre conformation within the yarns as well as structural reorganization in the course of swelling, de-swelling or degree of swelling.

Over the range of NaOH concentrations used, a gradual decrease was detected at both temperatures (25 °C and 40 °C), as well as clear order of plain < twill < sateen. Two minima were observed for fabrics treated at 25 °C; first at 3.33 mol dm⁻³ NaOH for plain fabric, and second at 4.65 mol dm⁻³ for twill, but sateen levelled off between 3.33-7.15 mol dm⁻³. While, treatment temperature of 40 °C led to sharp minimum at 4.48 mol dm⁻³ for all treated fabrics. The minimum in WRV at 4.65 mol dm⁻³ NaOH may imply a maximum swelling or reaching maximum swelling at the higher NaOH concentration in comparison with plain fabric due to fabric construction differences. Differences between fabric constructions are associated with different interlacements within each fabric construction and, thus, the disparate aqueous NaOH uptake and kinetics apply herein [13] as well as the greatest reorganization in amorphous and quasi-crystalline structure observed previously.[1] When the effect of temperature is considered, the elevated temperature exhibited lower WRV for all studied constructions and thus, more expressive effect of structure can be expected.

Abrasion resistance.

From mass loss in the abrasion resistance tests shown in Table 1, it was observed that the alkali treated fabrics showed enhanced abrasion resistance compared to the control fabric, and the process conditions, alkali concentration and treatment temperature exerted significant influence on the abrasion resistance. Significant improvements in abrasion among NaOH treated fabrics were observed at 3.33 mol dm⁻³ NaOH for 25 °C, and at 4.48 mol dm⁻³ NaOH for 40 °C. However, an exception is found for plain fabric treated with 3.33 mol dm⁻³ at 25°C where there is a marginal improvement in abrasion among NaOH treated fabrics, in fact, minimum in mass loss was observed at 7.15 mol dm⁻³ NaOH. In general, probably as a result of the decrease of inter-yarn spaces at cross-over points in the treated fabrics as the mass/area increased (see Figure 4), and therefore, treated fabrics became packed together. This leads to a greater propensity in the treated fabrics for the dissipation of applied stress.

In addition, the abrasion resistance of the control sateen fabric was similar to that sateen fabric treated with 2.25 mol dm⁻³. However, with additional increase of NaOH concentration (3.33 mol dm⁻³), exceptional improvement in abrasion resistance is observed, 51% increase in abrasion resistance in comparison to control sateen fabric. It is believed that at this particular process conditions at which sateen fabric reaches kind of “optimum” treatment towards enhancement of this property.

Tensile strength and elongation.

Values of tensile strength and elongation at break are also presented in Table 1. In general, twill and sateen fabrics exhibited higher tensile strength in comparison with plain fabric. Treatment temperature does not show significant influence on tensile strength of the same type of fabric. Compared to the control fabric, only twill showed a distinct increase in tensile strength (3.0-11.6% for 25 °C; 0.3-10.0% for 40 °C) over the whole range of alkali concentrations and temperatures used. In contrast, sateen fabric exhibited lower values over the whole range of alkali concentrations and temperatures used. From the alkali treated plain fabric, only 2.25 mol dm⁻³ NaOH for both temperatures exhibited higher values in comparison with the control fabric; other alkali concentrations applied to plain fabric displayed lower or the same values.

Opposite trends were observed for flexural rigidity, wherein maxima for flexural rigidities were detected at the same points associated with minimum tensile strength; this is associated to fabric embrittlement caused by NaOH treatment. In all examined process conditions and different constructions, the highest elongation at break was observed in fabrics subjected to 7.15 mol dm⁻³ NaOH, with very little or no difference between treatments at 25 °C and 40 °C. Compared to the control fabric, elongation at break for plain fabric increased by 27.9%, twill by 30.0% and sateen by 18.8% (average values between two temperatures), which may have been influenced by an increase in yarn crimp and, thus, fabric tends to elongate the most. Overall, fabric elongation at break decreased with increasing alkali concentration in the range of 2.25-4.65 mol dm⁻³ NaOH; however, some differences between fabric construction and treatment temperature were detected. In the fabrics treated at 25 °C, elongation at break decreased continuously with alkali concentration up to either 4.48 mol dm⁻³ NaOH for plain fabric and 3.33 mol dm⁻³ NaOH for twill and sateen fabrics, increasing thereafter. Conversely, elongation at break of fabrics subjected to 40 °C reduced gradually with alkali concentration up to 4.65 mol dm⁻³ NaOH, but sharp increase was observed in fabrics treated at a concentration of 4.48 mol dm⁻³. The height of the particular peaks is reduced in order plain > twill > sateen.

Crease recovery

The alkali concentration range of 2.53-7.15 mol dm⁻³ NaOH, and treatment temperature 25 °C or 40 °C, did not exhibit a significant influence on the crease recovery (shown in Table 1 as crease recovery angle; CRA) between different fabric constructions. Fabrics treated at elevated temperature (40 °C) displayed substantially greater crease recovery than those treated at lower temperature (25 °C). A sharp minimum at a concentration of 3.33 mol dm⁻³ NaOH was observed for all examined fabrics treated at 25 °C, however, at 40 °C a minimum at 4.48 mol dm⁻³ NaOH for plain fabric was observed, and at 4.65 mol dm⁻³ NaOH for twill fabric; no distinguishing minimum for sateen fabric was observed. Fabric crease recovery is inversely related to the rigidity and directly related to the elastic recovery in fabrics [2], as was observed herein.

Conclusions

In this work, it was demonstrated that the most substantial changes occur at certain alkali concentrations and temperatures when tension of 147 N m⁻¹ is applied; at 3.33 mol dm⁻³ NaOH concentration for fabrics treated

at 25 °C, and at 4.48 mol dm⁻³ NaOH concentration for fabrics treated at 40 °C. These treatment parameters, which are required to reach maximum swelling, are markedly higher compared to pad-batch process (without tension). Those maxima are mainly affected by maximum swelling and applied tension, which tends to increase the fibre orientation of already softened substrate due to alkalisation. Under the same conditions, the greatest molecular reorganization in the amorphous and quasi-crystalline structure of examined lyocell fabrics is observed; treated lyocell showed the maxima for TCI and LOI, and minima for HBI. This was evidenced by dimensional and mechanical properties; peaks of fabric shrinkage and flexural rigidity (in dry and wet state), and minima in WRV, crease recovery, tensile strength and elongation at break.

Degree of swelling increases as temperature decreases [10,22], and has a substantial effect on examined fabrics performance such as accessibility, flexibility, softness, and extensibility of the treated substrate in comparison to, for example, the pad-batch process. Overall, the temperature of 25 °C has a significantly higher influence in comparison with treatment at 40 °C. Therefore, the elevated treatment temperature (40°C) in conjunction with NaOH concentration of 4.48 mol dm⁻³ have a substan-

Table 1: Mechanical properties.

| Treatment ^a | Temperature [°C] ^b | Mass loss [%] ^c | | | Tensile strength [N] ^d | | | Elongation [%] ^d | | | CRA(W+F) [°] ^e | | |
|------------------------|-------------------------------|----------------------------|------|------|-----------------------------------|-----|-----|-----------------------------|------|------|---------------------------|-----|-----|
| | | P | T | S | P | T | S | P | T | S | P | T | S |
| 0.0 | 25 | 9.3 | 12.4 | 11.6 | 838 | 893 | 948 | 18.1 | 13.5 | 11.2 | 191 | 200 | 242 |
| 2.53 / 0.73 | 25 | 5.8 | 9.0 | 11.4 | 900 | 997 | 929 | 17.3 | 13.1 | 12.4 | 175 | 172 | 194 |
| 3.33 / 1.08 | 25 | 5.5 | 7.0 | 5.9 | 727 | 938 | 868 | 16.2 | 7.5 | 6.2 | 100 | 99 | 111 |
| 4.48 / 1.18 | 25 | 6.1 | 9.3 | 7.2 | 748 | 927 | 878 | 14.7 | 13.2 | 11.2 | 137 | 119 | 125 |
| 4.65 / 1.48 | 25 | 6.4 | 9.0 | 7.7 | 833 | 920 | 896 | 16.5 | 15.4 | 11.4 | 153 | 138 | 129 |
| 7.15 / 2.15 | 25 | 5.2 | 9.1 | 8.8 | 830 | 921 | 908 | 22.6 | 17.6 | 13.1 | 146 | 147 | 158 |
| 2.53 / 0.73 | 40 | 6.8 | 9.8 | 11.6 | 885 | 982 | 933 | 15.5 | 12.2 | 11.2 | 188 | 198 | 181 |
| 3.33 / 1.08 | 40 | 6.6 | 10.6 | 11.0 | 763 | 928 | 917 | 14.0 | 12.1 | 11.6 | 172 | 171 | 158 |
| 4.48 / 1.18 | 40 | 5.0 | 8.7 | 8.9 | 812 | 896 | 908 | 19.6 | 14.8 | 12.3 | 146 | 144 | 148 |
| 4.65 / 1.48 | 40 | 5.8 | 11.5 | 9.5 | 800 | 963 | 877 | 13.5 | 11.6 | 11.2 | 156 | 125 | 145 |
| 7.15 / 2.15 | 40 | 5.9 | 9.2 | 9.5 | 792 | 931 | 869 | 23.7 | 17.5 | 13.5 | 162 | 161 | 154 |

a Alkali concentrations [mol dm⁻³] in treatment / stabilization liquors.

b Temperature of treatment liquor; stabilization liquor temperature was maintained at 60°C in all experiments.

c Mass loss observed after 7000 abrasion cycles in tests.

d Measurements along warp direction in fabrics.

e CRA after 30 min of recovery; sum of values obtained along warp and weft directions.

tially less negative impact on treated fabric properties and crystallinity indices, except the dimensional change, which is more pronounced. Additionally, at treatment condition of 4.48 mol dm⁻³ NaOH and temperature of 40 °C, the elongation showed increase between 8-10% for all studied constructions compared to that control fabric, in other words, they became more extensible. Distinguished differences in swelling and overall performance of lyocell fabrics with different construction, but consisting of the same type of cellulosic fibre and of similar mass per area were observed. These changes can point out the significance of taking them on account particularly in the course of the end use, e.g. in fabric drape, softness or roughness, dyeing and finishing, etc.

Acknowledgements

The authors thank The University of Leeds and Lenzing AG for the provision of a scholarship to Mr. Široký, and we are grateful to the Versuchsanstalt-Textil and HTL-Dornbirn for the use of their facilities, the Amt der Vorarlberger Landesregierung, Europäischer Fonds für Regionale Entwicklung (EFRE), and COMET K-project “Sports Textiles” project number 820494 funded by Die Österreichische Forschungsförderungsgesellschaft (FFG), for their provision of the financial support. The authors would also like to acknowledge Dr. Mohammad Abu-Rous and Dr. Jörg Schlangen for their assistance, help with experimental work, and also for fruitful discussion of the results.

References

- [1] Široký, J., et al., Attenuated total reflectance Fourier-transform Infrared spectroscopy analysis of crystallinity changes in lyocell following continuous treatment with sodium hydroxide. *Cellulose*, 2010. 17(1): p. 103-115.
- [2] Široký, J., et al., Alkali Treatments of Lyocell in Continuous Processes. I. Effects of Temperature and Alkali Concentration on the Treatments of Plain Woven Fabrics. *Journal of Applied Polymer Science*, 2009. 113(6): p. 3646-3655.
- [3] Široký, J., et al., Continuous alkali treatment process of plain woven lyocell fabrics: Effect of alkali concentration. *Itc&Dc: 4th International Textile Clothing & Design Conference, Book of Proceedings*, 2008: p. 453-458.
- [4] Široká, B., J. Široký, and T. Bechtold, Application of ATR-FT-IR Single-Fiber Analysis for the Identification of a Foreign Polymer in Textile Matrix. *International Journal of Polymer Analysis and Characterization*, 2011. 16(4): p. 259-268.
- [5] Corgié, S.C., H.M. Smith, and L.P. Walker, Enzymatic transformations of cellulose assessed by quantitative high-throughput fourier transform infrared spectroscopy (QHT-FTIR). *Biotechnology and Bioengineering*, 2011. 108(7): p. 1509-1520.
- [6] Hofmann, D., H.P. Fink, and B. Philipp, Lateral Crystallite Size and Lattice-Distortions in Cellulose-II Samples of Different Origin. *Polymer*, 1989. 30(2): p. 237-241.
- [7] Nelson, M.L. and R.T. O'Connor, Relation of Certain Infrared Bands to Cellulose Crystallinity and Crystal Lattice Type. Part II. A New Infrared Ratio for Estimation of Crystallinity in Celluloses I and II. *Journal of Applied Polymer Science*, 1964. 8(3): p. 1325-1341.
- [8] Hurtubise, F. G. and H. Krassig, Classification of Fine Structural Characteristics in Cellulose by Infrared Spectroscopy – Use of Potassium Bromide Pellet Technique. *Analytical Chemistry*, 1960. 32(2): p. 177-181.
- [9] O'Connor, R.T., E.F. DuPré, and D. Mitcham, Applications of Infrared Absorption Spectroscopy to Investigations of Cotton and Modified Cottons Part I: Physical and Crystalline Modifications and Oxidation. *Textile Research Journal*, 1958. 28(5): p. 382-392.
- [10] Warwicker, J., Swelling of Cotton in Alkalis and Acids. *Journal of Applied Polymer Science*, 1969. 13(1): p. 41-54.
- [11] Široký, J., et al., Alkali treatment of cellulose II fibres and effect on dye sorption. *Carbohydrate Polymers*, 2011. 84(1): p. 299-307.
- [12] Burrow, T., Recent results with lyocell fibres in textiles. *Lenzinger Berichte*, 1998. 78: p. 37-40.
- [13] Široký, J., R.S. Blackburn, and T. Bechtold, Influence of fabric structure on NaOH release from woven lyocell type material. *Textile Research Journal*, 2011. doi:10.1177/0040517511399968.
- [14] Bredereck, K., et al., Alkali- und Flüssigammoniak-Behandlung von Lyocellfasern. *Melliand Textilberichte*, 2003. 84(1/2): p. 58-64.
- [15] Saville, B.P., *Physical testing of textiles*. 1999, Cambridge: Woodhead Publishing.
- [16] Richter, G.A., L.E. Herdle, and I.L. Gage, Accessible Cellulose as Measured by Sorption of Sulfuric Acid. *Industrial and Engineering Chemistry*, 1953. 45(12): p. 2773-2779.
- [17] Neale, S.M., The swelling of cellulose, and its affinity relations with aqueous solutions. Part I – Experiments on the behaviour of cotton cellulose and regenerated cellulose in sodium hydroxide solution, and their theoretical interpretation. *Journal of the Textile Institute Transactions*, 1929. 20(12): p. T373-T400.

- [18] Ibbett, R.N. and Y.L. Hsieh, Effect of fiber swelling on the structure of lyocell fabrics. *Textile Research Journal*, 2001. 71(2): p. 164-173.
- [19] Goswami, P., et al., Dyeing behaviour of lyocell fabric: effect of NaOH pre-treatment. *Cellulose*, 2009. 16(3): p. 481-489.
- [20] Goswami, P., et al., Effect of sodium hydroxide pre-treatment on the optical and structural properties of lyocell. *European Polymer Journal*, 2009. 45(2): p. 455-465.
- [21] Schaumann, W., Properties of Lenzing viscose and Lenzing modal applied to finishing. *Lenzinger Berichte*, 1996. 75: p. 81-90.
- [22] Krässig, H. A., *Cellulose: Structure, Accessibility and Reactivity*. 1993, Gordon and Breach Science Publishers S. A: Yverdon, Switzerland.

Chitin Coated Cellulosic Textiles as Natural Barrier Materials

Auriane Freyburger¹, Yaqing Duan², Cordt Zollfrank², Thomas Röder³,
and Werner Kunz^{1,*}

¹ Institute of Physical and Theoretical Chemistry, University of Regensburg, Regensburg, Germany

² Biogenic Polymers, Technical University of Munich and Straubing Center of Science for Renewable Resources, Straubing, Germany

³ Lenzing AG, Werkstraße 2, 4860 Lenzing, Austria

* Contact: werner.kunz@chemie.uni-regensburg.de

Abstract

The two most abundant biopolymers chitin and cellulose have unique properties suitable for designing renewable materials. Cellulose already plays a significant role in the production of daily materials such as textile fibers while chitin still remains widely less utilized. In this work, new cellulose/chitin composite materials were prepared to study the advantages of a chitin coat on the properties of cellulose-based textiles. Textiles produced from TENCEL[®], Lenzing Viscose[®], Lenzing Modal[®] and cotton fibers were coated by regenerating chitin from a mixture of an ionic liquid (1-butyl-3-methylimidazolium acetate) and a bio-sourced co-solvent (γ -valerolactone). The coat was applied only on one side of the textiles. Structural and morphological analysis demonstrated that a uniform and non-modified chitin film of 10 μm was successfully coated on all type of textiles without damaging their network. The degree of acetylation of the used chitin and the fabricated chitin coating determined by elemental analysis was 95.8% and 91.9%, respectively. The influence of the chitin coat on the textiles properties was characterized by wetting, and gas/water permeability comparative studies of the conventional and coated textiles. The results demonstrated that the presence of chitin decreased the water wettability of the textiles solely on the coated site. Moreover, the chitin layer acted as a promising water and oxygen barrier independently of the nature of the textiles.

Keywords: Chitin coating, water and oxygen barrier, TENCEL[®], Lenzing Viscose[®], Lenzing Modal[®], cotton, textile fibers.

Introduction

Currently, most polymeric materials are manufactured from petrochemical (fossil) resources. In order to reduce the dependence on petrochemical feedstocks and their environmental impacts, the development and the use of polymers from biomass as renewable materials is important to our society [1]. In biomass, the natural polysaccharides cellulose (poly β -(1,4)-D-glucopyranose) and chitin (poly β -(1,4)-2-acetamido-2-desoxy-D-glucopyranose) are the most abundant biopolymer resources. With cellulose being the principal structural component in higher plants, it has an estimated annual production of 10^{12} tons, while chitin is mainly contained in crustacean shells up to 75 000 tons per year [2,3]. In addition to their abundance and bio-

degradability, they have good chemical and mechanical properties suitable for various applications as filtration process, textile, hygienic, packaging and biomedical utilization [2,4,5]. However, being not meltable below their degradation temperature and having rigid bulk structures, the processing of these biopolymers is a real challenge and research on it has been increasing exponentially [2,6].

Cellulose processing has been successfully performed by more or less complex and polluting methods and is mainly industrially used in the production of fibers for textile and nonwoven applications. Among the most prominent man-made cellulose fiber generations one finds viscose, the Modal and Tencel[®] fibers. The first

generation of cellulosic fibers, viscose, is manufactured by derivatization of cellulose pulp with sodium hydroxide and carbon disulfide to cellulose xanthate and subsequent regeneration of the cellulose by solution spinning. Modal is the second generation of regenerated cellulose fibers and produced by a modified viscose process, inter alia, by using a pulp with a higher degree of polymerization. The third generation named Tencel® is manufactured by the Lyocell process, an environmentally friendlier way to produce fibers from cellulose solutions in N-methylmorpholine-N-oxide in presence of water. Besides these man-made fibers, the natural cellulosic fibers from cotton are still the most widely applied raw materials used to produce textiles. [7]

Chitin has not achieved the same commercial value as has cellulose and a large majority of its production (60-70%) is used to produce its de-acetylated derivative chitosan [8]. Chitin is structurally similar to cellulose, but bears an acetamido group at the C₂ position of the glucose units instead of an hydroxyl group. This particularity confers it advantages over cellulose such as excellent antibacterial properties, a less hydrophilic character and water retention/chelate metal ions capacity [4,9]. However, it induces also a more complex inter- and intramolecular hydrogen bonding network, causing a decreased solubility [10]. To date, the only promising environmentally friendly and direct solvents for chitin are ionic liquids (ILs). ILs are salts with a melting point below 100 °C. Imidazolium-based ILs, for instance 1-butyl-3-methylimidazolium acetate (BmimOAc), were described as the most effective solvents without changing drastically the properties of chitin [10-12]. I.e. the chitin can be recovered without deacetylation, which is a prerequisite for maintaining the chitin properties.

The aim of this study is to give new functional properties to four different cellulosic fibers (cotton, viscose, modal and lyocell textiles) applying chitin coatings. For this purpose, 1-butyl-3-methylimidazolium acetate has been used to dissolve chitin in presence of the co-solvent, γ -valerolactone (GVL) obtainable from renewable resources, for facilitating the polymer solution processing. By coating the chitin dope on the textiles, composite materials could be prepared having distinguished properties of each polymer, i.e. cellulose and chitin, on each face. The effect of the regenerated chitin film on the structure and the properties of the textiles were characterized by scanning electron microscopy, infrared spectroscopy, water contact angle measurements and water/gas permeability studies. Furthermore, a method was also used to recycle and reuse the costly ionic liquid at the end of the coating route.

Materials and Methods

Materials

Textiles used in this work were obtained from Lenzing AG (Austria) and produced from four different cellulosic fibers: TENCEL®, cotton, Lenzing Viscose®, and Lenzing Modal®. All textiles were washed and desized by Lenzing AG and dried at 70 °C for 5 days in an oven prior to use.

Chitin solutions were prepared with dried α -chitin powder from shrimp shells purchased from Sigma Aldrich (Germany). Its degree of polymerization and of acetylation were measured to be 1690 and 95.8%, respectively. The solvent system used to dissolve chitin was composed of γ -valerolactone (Reagent Plus®, purity $\geq 99\%$) from Sigma Aldrich (Germany) and 1-butyl-3-methylimidazolium acetate (BmimOAc, purity $\geq 98\%$) from IoLiTec (Germany). The latter was dried using a high vacuum setup (at 10^{-6} mbar) for 5 days, prior to dissolution of the chitin. All other chemicals were used without further purification.

Methods

Chitin solutions were prepared by dissolving α -chitin (2 wt%) in BmimOAc (88 wt%) and GVL (10 wt%) under nitrogen atmosphere at 110 °C. After total dissolution of chitin, a small amount of GVL was added to dilute the highly viscous gel and to facilitate the coating. The final solution was composed of 1.6 wt% chitin, 30 wt% GVL and 68.4 wt% BmimOAc.

Chitin coating was performed by putting one face of the textiles in contact with the chitin solution at 100 °C. Textiles were then moved on the chitin solution surface by a pair of tweezers for 5 minutes to provide a homogeneous chitin layer. Chitin covered textiles were left at room temperature for 2 hours to allow a slow gelation of the chitin. Each material was subsequently soaked in ethanol for 2 days and in deionized water for 2 days in order to remove the solvent residues, i.e. BmimOAc and GVL, and to induce coagulation of the chitin layer. The produced materials were dried between 2 glass plates at room temperature for several days.

Recovery of the ionic liquid BmimOAc was accomplished after the coating procedure using the following method. The ethanol-based coagulation solutions were first filtrated with a 0.2 μm polytetrafluorethylene (PTFE) membrane filter to remove any possible polymer residues. The obtained liquids were dried for two hours under reduced pressure (100 mbar) at 40 °C using a rotary evaporator. Further drying was carried out with a high vacuum setup (10^{-6} mbar) at 40 °C for 5 days. The purity of the recycled BmimOAc was

analyzed by ^1H - and ^{13}C -NMR measurements in dimethyl sulfoxide- d_6 recorded with a Bruker Avance 300 spectrometer (Germany) at 300 MHz.

To characterize the composition of the materials, infrared spectra were measured with a Fourier transform infrared spectroscopy (FTIR) instrument equipped with an attenuated total reflectance (ATR) sampler by pressing the samples against a Smart Diamond ATR sensor (Nicolet 380, Thermo Fisher Scientific, USA). Spectra were recorded in the range from 400 to 4000 cm^{-1} .

Films morphologies were studied by scanning electron microscopy (SEM). Dried samples were placed on carbon tape and coated with Au/Pd. SEM images were obtained with a digital scanning electron microscope (DSM 940 A, Zeiss, Germany) in secondary imaging mode at an acceleration voltage of 10 kV.

The wetting properties of the films were characterized by water contact angle measurements using a goniometer type P1 equipped with a microscope and a back light (Erna Inc., Japan). Measurements were performed at room temperature on both surfaces of the coated films, i.e. on the chitin layer and the untreated textile layer. A 2 μL drop of deionized and sterile filtered water was formed by an automated micrometer pipette (Hamilton Company, USA) and placed on the sample surface. The angle of the tangent formed at the water drop base was recorded as well as the liquid drop absorption time on each material. Overall five drops were placed on various surface locations for each sample.

The ability of water and oxygen to pass the materials was investigated with permeability tests at a constant temperature of 20 ± 1 °C. Water permeability measurements were performed using a setup with two cells allowing the film to be in contact with 8 mL of two different solvents, deionized water and ethyl lactate (EL), through a hole of 3 mm in diameter. For the coated materials, the chitin coat was in contact with the water cell. Both solutions were stirred at 200 rpm for 7 h and 150 μL were collected with an Eppendorf pipette from each cell at the same time at defined time intervals. The water concentration in each cell in function of time was measured by volumetric Karl-Fischer-Titration (870 KF Titrino plus, Metrohm, Switzerland). The water permeability coefficient, $P_{\text{H}_2\text{O}}$ was used to characterize the water barrier property of the films and was determined using Fick's first law as [13]:

$$J_{\text{H}_2\text{O}} = P_{\text{H}_2\text{O}} \times \Delta c_{\text{H}_2\text{O}} \quad (1)$$

where $J_{\text{H}_2\text{O}}$ represents the flow of water per unit area, $\Delta c_{\text{H}_2\text{O}}$ the difference in water concentration between

the ethyl lactate and the water filled cell. The flux $J_{\text{H}_2\text{O}}$ can be also expressed by Equation 2:

$$J_{\text{H}_2\text{O}} = \frac{1}{A} \times \frac{dc_{\text{H}_2\text{O in EL cell}}}{dt} \times V \quad (2)$$

with the permeation area A , the water concentration in the ethyl lactate cell $c_{\text{H}_2\text{O}}$ in EL cell), the volume related to the water concentration V , and the time t . Thus, the water permeability coefficient can be calculated from Equations 1 and 2 by:

$$|P_{\text{H}_2\text{O}}| = \frac{V}{A \times |\Delta c_{\text{H}_2\text{O}}|} \times \frac{dc_{\text{H}_2\text{O in EL cell}}}{dt} \quad (3)$$

Water permeability coefficients were calculated considering only the average of the values between 120 and 420 min. Before 120 min, the difference in water concentration between the two cells could not be precisely determined due to the uncertainty of the water concentration measurements in the pure water cell carried out by Karl-Fischer-Titration.

Oxygen permeation under dry condition was evaluated with an optical measurement conducted by a chemical optical sensor (type PSt6 from PreSens, Germany). The experimental setup consists of a self-developed measurement cell comprising the chemical optical sensor spot inside, read out via a polymer optical fiber (POF-2SMA from PreSens, Germany) connected to a fiber optic oxygen transmitter (Fibox 4 trace from PreSens, Germany). The film was fixed on the top of the permeation cell with a constant volume of 49.38 cm^3 and was in contact with the ambient air through a hole of 5 mm diameter. After flushing the chamber three times with nitrogen, the increase of the oxygen partial pressure over time in the chamber was recorded three times for each sample. The time range was selected from 0 to 13 min, which is the period of time where accurate oxygen partial pressures (from 0 to 52 hPa) could be measured by the sensor spot for the textiles. The permeability of the film was calculated with the oxygen permeability coefficient, P_{O_2} , determined using an adaptation of the ideal gas law (4) and the Fick's first law (5).

$$p_{\text{O}_2} \times V = n_{\text{O}_2} \times R \times T \quad (4)$$

$$J_{\text{O}_2} = -P_{\text{O}_2} \times \Delta c_{\text{O}_2} = \frac{1}{A} \times \frac{dn_{\text{O}_2}}{dt} \quad (5)$$

In Equation 4, p_{O_2} is the partial pressure of oxygen, V the volume of the chamber, n_{O_2} the oxygen amount in moles, R the gas constant, and T the absolute temperature. In Equation 5, J_{O_2} represents the flow of oxygen per unit area, Δc_{O_2} the difference in oxygen concentration between the filled chamber and the outside, and A the

permeation area. By combining these two equations, the oxygen permeability coefficient could be calculated by:

$$|P_{O_2}| = \frac{V}{A \times |\Delta P_{O_2}|} \times \frac{dp_{O_2}}{dt} \quad (6)$$

The oxygen permeability coefficients were calculated considering only the average of the calculated values between 1 and 13 min.

Results and Discussion

Structure of the coated textiles

The studied textiles consist of an ordered structural assembly of cellulosic fibers (TENCEL[®], Cotton, Lenzing Viscose[®], and Lenzing Modal[®]) having a white color. They were produced by interlacing warp fibers (longitudinal) and weft fibers (transversal) so that each warp fiber passes alternately under and over each weft fibers. This structural hierarchy can be well observed in Figure 2 A). After dissolution of the chitin in a mix-

ture composed of the ionic liquid BmimOAc and the co-solvent GVL, a chitin layer was formed on one side of the textiles by promoting its precipitation in ethanol [10]. Once the textiles were coated with chitin, they exhibited a thin transparent shiny film on the chitin side while the untreated side was visually not modified during the coating (Figure 1).

The morphology of the prepared materials was observed with SEM. An example of the obtained SEM images for the coated material viscose performed on the surface of both sides, i.e. chitin and textile layer, and the cross section is presented in Figure 2. On the one hand, it could be observed that the viscose network consisting of interlaced fibers was not damaged by the coating procedure. The chitin side, on the other hand, exhibited a homogeneous and smooth surface without crevices or flaws. The chitin layer covered the pores of the textile without penetrating inside. The cross section of the coated material displayed two distinct layers, i.e. the interlaced fibers representative



Figure 1: Appearance of untreated and chitin coated textiles.

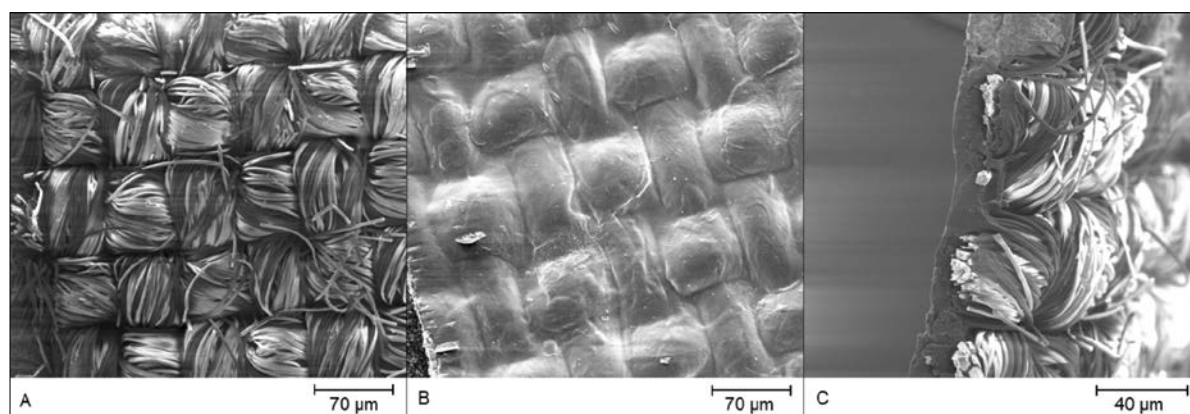


Figure 2: SEM images of the viscose textile coated with chitin obtained from (A) the viscose side, (B) the chitin side, and (C) the cross section.

of the textile side and a thin homogeneous chitin coat. The same observations were made also for all three other coated materials. The thickness of the chitin coat on all materials was estimated to be $10 \pm 2 \mu\text{m}$ as inferred from the cross section SEM images.

To confirm the presence of chitin on the coated side and to exclude degradation of the textiles, all materials were characterized by FTIR in ATR mode. Figure 3 shows the FTIR-ATR spectra of the chitin side for the four coated textiles. The IR curves were shifted by a

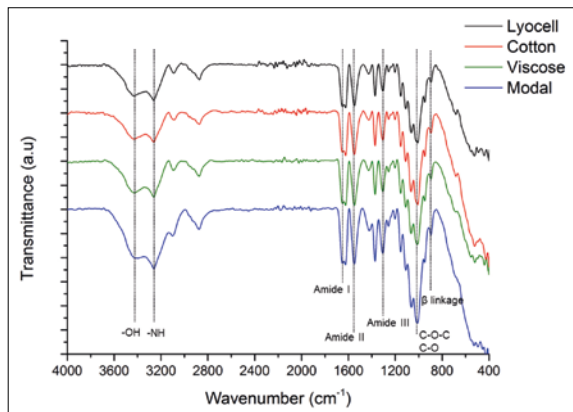


Figure 3: FTIR-ATR spectra of the chitin coated side for the prepared textiles.

constant value self-developed for visual clarity. Firstly, no differences appeared comparing all spectra. Secondly, the specific bands characteristic to chitin such as the amide I doublet band located at 1654 and 1625 cm^{-1} , the amide II band at 1550 cm^{-1} and the amide III band at 1307 cm^{-1} could be detected for all materials. This means that the recovered chitin was not deacetylated. The other bands at 3430 and 3261 cm^{-1} were attributed to the OH and NH stretching, at 3090 cm^{-1} to the CH_3 asymmetric stretching, and at 2875 cm^{-1} to the CH_3 symmetric, CH, and CH_2 stretching [14]. CH deformation and C- CH_3 amide stretching vibrations were assignable to the peaks at 1428 and 1373 cm^{-1} . The intense peaks at 1154–1010 cm^{-1} corresponded to C-O-C and C-O stretching. The last peak at 896 cm^{-1} confirmed the presence of β linkage in the molecule [14,15]. This indicated that chitin was successfully coated on the textiles and no obvious degradation occurred during the preparation.

Each starting material and its corresponding side on the coated textiles are compared by FTIR-ATR curves in Figure 4. Again, IR curves for the coated textiles were shifted for a better display. The spectrum for each textile side was similar to the spectrum for its non-

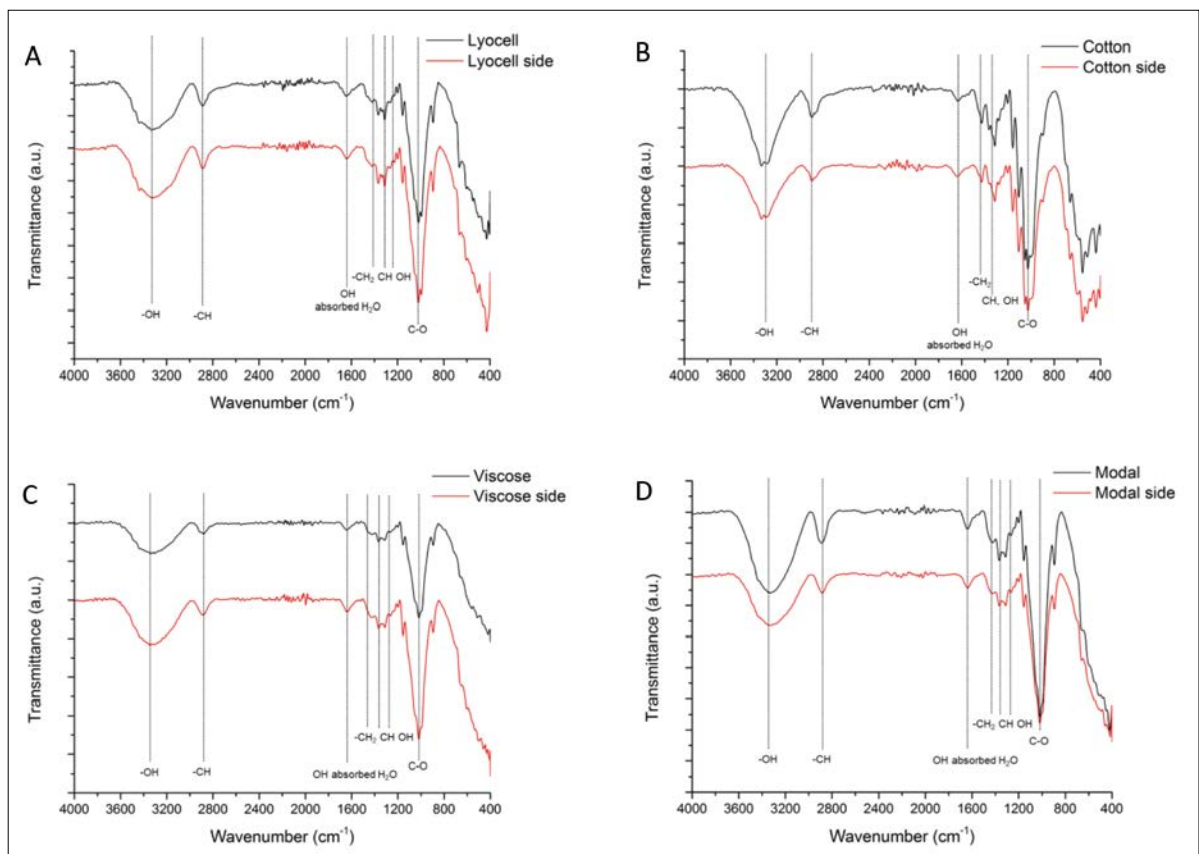


Figure 4: Comparative FTIR-ATR spectra of each reference textile, (A) lyocell, (B) cotton, (C) viscose, and (D) modal with its corresponding untreated side on the coated materials.

coated material independent of its crystalline structure, namely cellulose I for the natural cotton and cellulose II and amorphous cellulose for the man-made lyocell, viscose, and modal textiles. Thus, the cellulosic fibers were not chemically degraded during the coating process. In addition, the absence of the chitin characteristic bands confirmed the presence of chitin solely on the coated side of the prepared material as also observed under SEM.

Evaluation of new functional properties

In order to evaluate the specific properties of these new materials, a comparison of the untreated textiles and the coated ones were performed regarding their wetting and permeation performance.

In a first step, we studied whether the chitin coat can act as a water barrier, since this biopolymer is a major structural component in the exoskeleton of marine crustaceans and contributes to their protection [3]. Therefore, wetting properties of the films were characterized using water contact angles measurements. Typically, contact angles lower than 90° correspond to favorable wetting of the surface (termed hydrophilic), whereas low wettability materials (hydrophobic) induce contact angles higher than 90° [16]. The relation between the water contact angles and the type of textile (coated and non-coated) is illustrated in Figure 5 A). Due to the high hydrophilic behavior of cellulosic fibers and the porous structure of the textiles, no water contact angle could be measured for the non-coated materials as the water drop was immediately absorbed. Only cotton induced a contact angle of $85 \pm 5^\circ$ for a few seconds (10 s), probably due its highly ordered structure (cellulose I). For the coated materials, the water contact angle tended to be identical on almost all chitin sides and was approximately 90° ($90 \pm 4^\circ$ for the coated Lyocell, $91 \pm 3^\circ$ for the coated Cotton, and $90 \pm 4^\circ$ for the coated Viscose). Only the coated modal textile exhibited a slight smaller value of $84 \pm 3^\circ$. These results proved that the chitin layers exhibit a poor degree of wetting towards water. After a long contact period on the surface of the chitin layer, a decrease of the water contact angles were detected and the absorption times were recorded (Figure 5 B). A complete absorption of a $2 \mu\text{L}$ drop on all chitin layers was reached after ca. 20 min (24 ± 3 min for the coated Lyocell, 22 ± 6 min for the coated Cotton, 21 ± 1 min for the coated Viscose, and 19 ± 4 min for the coated Modal). Accordingly, the formed chitin layer is not impermeable to water but significantly retards its infiltration.

Since the textile side of the coated materials immediately absorbed the water drop textile wettability properties were not changed during the process (Figure 5 B). Consequently, the chitin coat affected only the wet-

ting properties on one side of the coated materials, by making the textiles more hydrophobic and by slowing down the water penetration into the textiles, probably by plugging the holes and the reduced wetting angle towards the more hydrophobic chitin.

Table 1: Water permeability coefficient, $P_{\text{H}_2\text{O}}$, with corresponding standard deviations as a function of the type of materials.

| Materials | $P_{\text{H}_2\text{O}}$ ($\times 10^{-7}$ m/s) |
|----------------------------|--|
| Lyocell | 2.0 ± 0.5 |
| Lyocell coated with chitin | 0.6 ± 0.2 |
| Cotton | 1.6 ± 0.4 |
| Cotton coated with chitin | 0.5 ± 0.2 |
| Viscose | 1.7 ± 0.7 |
| Viscose coated with chitin | 0.5 ± 0.2 |
| Modal | 2.9 ± 0.8 |
| Modal coated with chitin | 0.7 ± 0.2 |

To study the influence of chitin on the water diffusion through the materials, water permeability tests for all of the coated and non-coated materials were additionally performed under identical conditions. From these experiments, water permeability coefficients were calculated according to Equation 3 and are reported in Table 1. As expected, the permeability coefficients for all non-coated textiles were higher than the ones for the coated materials, namely by a factor of 3.3, 3.2, 3.4, and 4.1 for Lyocell, Cotton, Viscose, and Modal, respectively. The water transport was faster and easier through the unmodified textiles, because of their porous and hydrophilic nature of the textiles. As shown in Table 1, water permeability values for the coated textiles ranged from 0.5 to 0.7×10^{-7} m/s. This indicated that the chitin coat has the same water barrier properties independently of the nature of the textile and slow down the water permeation.

In order to explore other barrier effects of the chitin layer, gas (i.e. O_2) permeability tests were carried out under dry conditions. Figure 6 (page 112) shows the evolution of the oxygen partial pressure, p_{O_2} , in the measurement cell as a function of time investigated for all materials. Oxygen permeability coefficients were calculated according to Equation 6 considering the quasi linear increase of the oxygen partial pressure and are reported in Table 2. For non-coated textiles, p_{O_2} identically increased from 0 to 51 hPa in 13 minutes. Furthermore, it has to be noticed that this p_{O_2} raise followed the same trend as in the case when no membrane was fixed on the top of the permeation chamber. Independently of the textile nature, all are highly permeable to oxygen

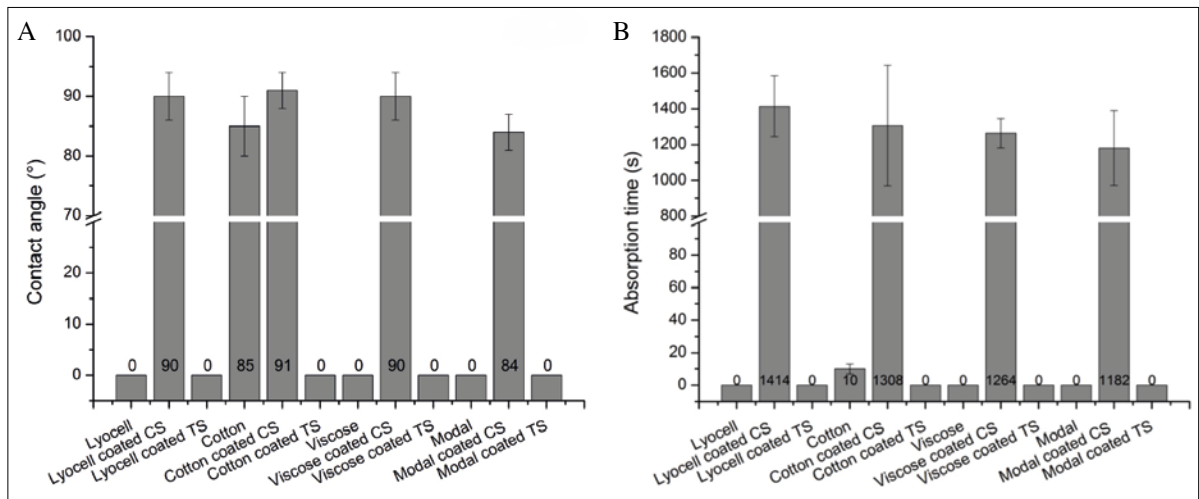


Figure 5: (A) Contact angle and (B) absorption time of a 2 μL water drop on the surface of the textile materials non-coated and coated with chitin (CS stands for Chitin Side and TS for Textile Side).

which can be explained by the presence of open pores. This generated high permeability coefficients for these materials in the range from 9.0 to 9.1×10^{-4} m/s (Table 2). In contrast, the oxygen diffusion through the coated materials was much slower as shown in Figure 6 B). After 13 minutes, p_{O_2} values of 3.1, 3.0, 2.8, and 2.7 hPa were recorded for the coated Lyocell, Cotton, Viscose, and Modal, respectively. As a result, coated textiles show significant lower permeability coefficients, which were ranged from 0.40 to 0.46×10^{-4} m/s. Comparing these values to those obtained for the non-coated textiles, it can be concluded that oxygen respectively permeated through Lyocell, Cotton, Viscose, and Modal 19.8, 19.8, 21.4, and 22.8 times faster than through its corresponding coated materials.

Table 2: Oxygen permeability coefficients, P_{O_2} , with corresponding standard deviations as a function of the type of materials.

| Materials | P_{O_2} ($\times 10^{-4}$ m/s) |
|---------------------|--|
| Without membrane | 9.4 ± 0.4 |
| Lyocell | 9.1 ± 0.3 |
| Lyocell with chitin | 0.46 ± 0.02 |
| Cotton | 9.1 ± 0.4 |
| Cotton with chitin | 0.46 ± 0.02 |
| Viscose | 9.0 ± 0.3 |
| Viscose with chitin | 0.42 ± 0.01 |
| Modal | 9.1 ± 0.3 |
| Modal with chitin | 0.40 ± 0.01 |

To prove that these new functional properties were caused by chitin and not just by the plugging of the textile pores, the same coating procedure was performed

with cellulose instead of chitin. To achieve this, a Lyocell textile was coated with microcrystalline cellulose under the same conditions as previously described. Unfortunately, it was not possible to reproduce a comparably thin $10 \pm 2 \mu\text{m}$ cellulose layer. Therefore a quantitative comparison could not be done, especially for the permeability tests. However, it can be mentioned that cellulose coating induced a lower water contact angle of 54° instead of 90° for the chitin coating. The water drop was also two times faster absorbed by the cellulose layer than by the chitin one. Concerning the gas/water permeability properties of the cellulose coated Lyocell, it seemed that cellulose coating was more permeable to water but slightly less to oxygen than chitin coating. Further work has to be done to confirm these observations.

At the end of the coating process, the recycling of the ionic liquid was attempted for sustainability and profitability interests. Once chitin regenerated, the ethanol-based precipitation solutions were collected and submitted to a drying procedure detailed in the methods. Ethanol could be successfully removed under reduced pressure using a rotary evaporator. However, GVL was still present in the residue due to its remarkable low vapor pressure (0.65 kPa at 25°C and 3.5 kPa at 80°C) [17]. A second step was thus carried out to remove GVL by using a high vacuum setup. Analysis of the obtained extract by ^1H and ^{13}C NMR revealed that BmimOAc remained unaltered and no trace of ethanol or GVL was detected. The recovered IL was reused to dissolve successfully 2 wt% of chitin as described above in the dissolution experiment. Again, BmimOAc was then a second time recovered and reused without appreciable decrease of its efficiency.

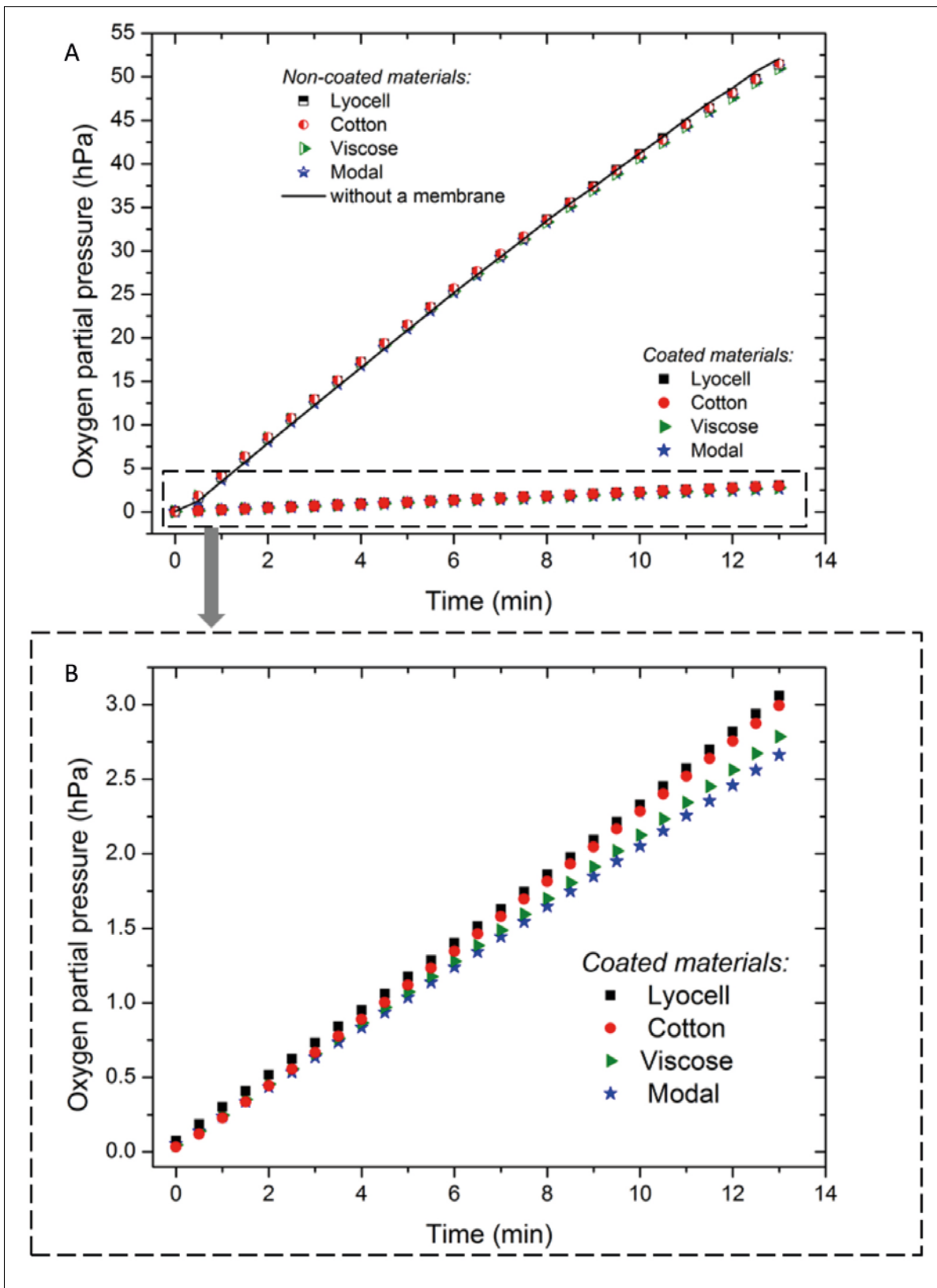


Figure 6: Oxygen partial pressure, p_{O_2} , over time measured in the O_2 permeation chamber for (A) all the textile materials non-coated and coated with chitin and for (B) specific to the coated materials.

Conclusions

Textiles made from TENCEL[®], Lenzing Viscose[®], Lenzing Modal[®] and cotton fibers were coated with chitin, a natural and antibacterial polymer, to produce new functional and renewable materials. The approach used therefore was the chitin regeneration on one surface of the textiles. Chitin was dissolved in the ionic liquid 1-butyl-3-methylimidazolium acetate with a bio-sourced solvent γ -valerolactone and precipitated with ethanol, after being in contact with the starting materials. Transparent chitin coats of 10 μ m thickness were successfully created on the textiles without penetration into the textiles. These new composite materials exhibited the unique properties of chitin on one side without degrading cellulose properties on the other side. The chitin coat influenced the properties of the resulting composite materials by making them more hydrophobic and by slowing down the penetration of water or O₂ into the membrane. Further optimization, as for instance the increase of the thickness of the coat, could improve the barrier properties of these new materials, making them potential candidates for various applications as impermeable textiles for hygiene products. Finally, a procedure to recover the ionic liquid during the process was proposed for sustainable concerns.

Acknowledgements

As part of the project ForCycle, this work was supported by the Bavarian State Ministry of the Environment and Consumer Protection.

References

- [1] Mohanty, A. K.; Misra, M.; Drzal, L. T.: Sustainable Bio-Composites from Renewable Resources: Opportunities and Challenges in the Green Materials World. *Journal of Polymers and the Environment* 2002, 10, 19-26.
- [2] Klemm, D.; Heublein, B.; Fink, H.-P.; Bohn, A.: Cellulose: Fascinating biopolymer and sustainable raw material. *Angew. Chem., Int. Ed.* 2005, 44, 3358-3393.
- [3] Khor, E.: Chapter 5: the sources and production of chitin. In *Chitin: fulfilling a biomaterials promise*; Elsevier, 2014; pp 63-72.
- [4] Ravi Kumar, M. N. V.: A review of chitin and chitosan applications. *Reactive and Functional Polymers* 2000, 46, 1-27.
- [5] Islam, S.; Bhuiyan, M. A. R.; Islam, M. N.: Chitin and Chitosan: Structure, Properties and Applications in Biomedical Engineering. *J. Polym. Environ.* 2016, Ahead of Print.
- [6] Rinaudo, M.: Chitin and chitosan: Properties and applications. *Progress in Polymer Science* 2006, 31, 603-632.
- [7] Shen, L.; Patel, M. K.: Life cycle assessment of man-made cellulose fibers. *Lenzinger Ber.* 2010, 88, 1-59.
- [8] Kurita, K.: Chitin and Chitosan: Functional Biopolymers from Marine Crustaceans. *Mar. Biotechnol.* 2006, 8, 203-226.
- [9] Crini, G.; Guibal, É.; Morcellet, M.; Torri, G.; Badot, P.-M.: Chitine et chitosane. Préparation, propriétés et principales applications. In *Chitine et chitosane, du biopolymère à l'application*; Presses universitaires de Franche-Comté, 2009; pp 19-53.
- [10] Wu, Y.; Sasaki, T.; Irie, S.; Sakurai, K.: A novel biomass-ionic liquid platform for the utilization of native chitin. *Polymer* 2008, 49, 2321-2327.
- [11] Qin, Y.; Lu, X.; Sun, N.; Rogers, R. D.: Dissolution or extraction of crustacean shells using ionic liquids to obtain high molecular weight purified chitin and direct production of chitin films and fibers. *Green Chem.* 2010, 12, 968-971.
- [12] Jaworska, M. M.; Kozlecki, T.; Gorak, A.: Review of the application of ionic liquids as solvents for chitin. *J. Polym. Eng.* 2012, 32, 67-69.
- [13] Evans, D. F.; Wennerström, H.: 6. Bilayer systems. In *The Colloidal Domain: Where Physics, Chemistry, Biology, and Technology Meet*; Wiley, 1999; pp 328-331.
- [14] Pearson, F. G.; Marchessault, R. H.; Liang, C. Y.: Infrared spectra of crystalline polysaccharides. V. Chitin. *J. Polym. Sci.* 1960, 43, 101-16.
- [15] Muzzarelli, R. A. A.; Morganti, P.; Morganti, G.; Palombo, P.; Palombo, M.; Biagini, G.; Mattioli Belmonte, M.; Giantomassi, F.; Orlandi, F.; Muzzarelli, C.: Chitin nanofibrils/chitosan glycolate composites as wound medicaments. *Carbohydr. Polym.* 2007, 70, 274-284.
- [16] Yuan, Y.; Lee, T. R.: Contact Angle and Wetting Properties. In *Surface Science Techniques*; Springer Berlin Heidelberg, 2013; pp 3-34.
- [17] Horvath, I. T.; Mehdi, H.; Fabos, V.; Boda, L.; Mika, L. T.: γ -Valerolactone – a sustainable liquid for energy and carbon-based chemicals. *Green Chem.* 2008, 10, 238-242.

Improvement of Dyeing Performance of Cellulose Fibers by Pre-Treatment with Amino Cellulose

Thomas Heinze^{1,*}, Thomas Wellhöfer¹, Kerstin Jedvert^{1,2}, Andreas Koschella¹, and Hendryk Würfel¹

¹ Institute for Organic Chemistry and Macromolecular Chemistry, Friedrich Schiller University of Jena, Humboldtstraße 10, 07743 Jena, Germany

² Dr. Kerstin Jedvert, Bio-based Fibres, Swerea IVF, P.O. Box 104, SE-431 22 Mölndal, Sweden

* Contact: Thomas Heinze@uni-jena.de

Abstract

Dyeing experiments with differently shaped cellulose fibers (paper samples and pulp fibers) were performed before and after treatment of the samples with amino cellulose in aqueous solution. Surface coating was achieved by simple dipping. A colorimetric assay applying 4,4'-dimethoxytriphenylchloromethane/perchloric acid was used to determine the amino group content on the paper surface, while the surface loading of pulp fibers was measured by fluorescence spectrophotometry. The amino cellulose concentration in the treatment solution can be kept as low as 0.05%. Pulp fibers were coated uniformly. Coating of paper with amino cellulose increased the dyeing performance significantly independent of the amino cellulose type used.

Keywords: adsorption; cellulose and other wood products; dyes/pigments; polysaccharides; textiles

Introduction

Dyeing of cellulose fibers in paper and textiles is strongly connected with the retention of the dye molecules at the fiber surface [1]. With respect to the demand of environmentally benign processes, it is desirable to improve the interaction between the cellulose surface and the dye. In textile dyeing, addition of quaternary ammonium salts has been found to improve the performance of anionic dyes [2]. However, adding various compounds to the dyeing mixture, which might improve the dyeing performance, does not reduce the waste. The effluents must be treated adequately before they can be disposed of [3].

Surface modification prior to the dyeing step is a promising route to increase the interaction between cellulose fiber and dye molecules. 6-Deoxy-6-(ω -aminoalkyl) amino celluloses have been identified as a class of biopolymer derivatives that strongly bind to a wide variety of materials, including metals, glass, and various synthetic polymers, forming stable layers and even monolayers on the surface [4]. Moreover, cationic cellulose derivatives possess a high affinity to the anionic

surface of cellulose [5-7]. Application of cationic cellulose derivatives for modification of pulp fibers has shown to be promising to improve properties of the fiber surface (e.g. wetting and bacteriostatic behavior), while preserving the inherent properties of the fibers, such as high mechanical strength and low density [8].

A major advantage of the treatment using amino cellulose is its simple application, being added from an aqueous solution. The main part of the cationic cellulose remains in the filtrate and can be reused easily. The cationic polysaccharide layer reverses the surface charge from negative to positive and, hence, increases the interaction with negatively charged dye molecules [9,10]. Therefore, it is expected that not particularly reactive dyes can be applied to cellulose fibers and the amount of dyestuff can be reduced.

The accurate determination of surface loading, i.e., the content of amino groups on the surface is of crucial importance for the evaluation of the dyeing performance. Several methods have been described, which are

based on a colorimetric test. Gaur et al. developed a method based on 4,4'-dimethoxytriphenylchloromethane [11-13]. The reagent reacts with the amino groups and the excess of reagent is removed. Subsequently, perchloric acid treatment liberates the 4,4'-dimethoxytriphenylmethyl cation, whose content can be colorimetrically determined at 498 nm. Primary and secondary amines can be identified with nitrophenylisothiocyanate-O-trityl, which is subsequently cleaved by trifluoroacetic acid and determined by colorimetry [14]. The anionic dye Acid Orange 7 (sodium-4-[(2-hydroxy-1-naphthyl)azo]benzenesulfonate) binds at amino groups at a pH value of 3. Excess of dye is removed by washings and the adsorbed dye is desorbed with sodium hydroxide before it is colorimetrically determined at a wavelength of 485 nm [15,16]. Ninhydrin can be used for the quantification of amino groups as well. The colorless reagent reacts with amino groups under formation of Ruhemann's purple, whose concentration is determined by colorimetry at 570 nm [17-19]. Due to the low molar extinction coefficient of $\epsilon = 15,000 \text{ M}^{-1}\text{cm}^{-1}$, a large surface or a high loading is required to obtain reliable results. In the present paper, we wish to report on the ability of amino cellulose derivatives to improve the dyeing performance of different kinds of cellulosic materials by a simple coating treatment with aqueous amino cellulose solutions.

Experimental

Materials

6-Deoxy-6-(2-aminoethyl)amino cellulose (EDA-cellulose, degree of substitution of EDA groups, DS_{EDA} , 0.83 [20] and 6-deoxy-6-(2-(bis(2-aminoethyl)aminoethyl)amino) cellulose (TAEA cellulose, DS of TAEA groups, DS_{TAEA} 0.60 [21] were prepared according to previously published methods by conversion of cellulose *p*-toluenesulfonic acid ester with the corresponding amines.

For adsorption experiments on pulp fibers, two dissolving grade pulps were used: a pre-hydrolysis kraft pulp "Purple grade" from Södra (P1) and a dissolving grade sulfite pulp from Domsjö (P2). The carboxyl groups present in the pulps were transformed into the sodium salt form according to a method published elsewhere [22]. The pulps were treated with an EDA-cellulose marked with 9-(methylaminomethyl)anthracene for fluorescence measurements. The labelled EDA-cellulose was prepared by simultaneous conversion of cellulose *p*-toluenesulfonic acid ester with excess ethylene diamine according to [23] and the fluorescence dye (FD) 9-(methylaminomethyl)anthracene (DS_{EDA} 0.69, DS_{FD} 0.08).

The dyes (see Table A1 in annex), except crystal violet and thymol blue (Acros Organics), were purchased from Sigma Aldrich and used as received for the preparation of 0.1% solution.

The following papers were included in the studies: Kymi-Acacia (coated, paper A), Chanshu-Acacia (coated, paper B), Nordland-Betula (uncoated, paper C), Nordland-Acacia (uncoated, paper D), Yes-Silver multifunction (paper E).

Measurements

UV/Vis-spectra were measured with a Lambda 16 UV/Vis-spectrophotometer (Perkin Elmer) in reflectance mode.

Fluorescence measurements were performed with an LS 50B fluorescence spectrometer (Perkin Elmer).

Methods

Adsorption of Amino Cellulose on Pulp Samples

Amino cellulose marked with 9-(methylaminomethyl)anthracene was dissolved in distilled water with an adjusted pH value of ~ 3.3 (adjusted with 0.1 N HCl). The solution was diluted to a final concentration of 0.01%, (w/w). Adsorption experiments were conducted by adding different amounts (volumes) of the solution to the same amount of pulp. The treatment was carried out on 50 g (dry mass) of pulp for each sample for 20 min at room temperature under vigorous stirring. Subsequently, the solution was removed with a syringe and was filtered through a poly(tetrafluoroethylene) filter (0.45 μm , diameter 30 mm, Genetec), and measured by fluorescence spectroscopy. The fluorescence quantum yields of the labeled amino cellulose derivatives were measured for samples in water-citric acid and diluted hydrochloric acid both at pH value of 3.1. Anthracene and 9,10-diphenylanthracene in ethanol have been used as calibration standards (see annex).

Dyeing of Paper Samples

Dye solutions (0.1%, w/v) were prepared according to Table A1 and placed in test tubes. Paper (1-2 cm^2) samples were added and treated for 10 min under shaking. After decanting the supernatant, the wet paper was washed with 2 mL of the solvent mixture used for the particular dye until no further dye is extracted. The wet paper was carefully removed and air-dried.

Determination of the Amino Group Content with 4,4'-Dimethoxytriphenylchloromethane

Reagent A: 1.694 g 4,4'-dimethoxytriphenylchloromethane, 1.522 g tetrabutylammonium nitrate, and 0.909 g sym-collidine were dissolved in 10 mL dry *N,N*-dimethylformamide (DMF) under exclusion of light.

Reagent B: 26 mL Perchloric acid were mixed with 23 mL methanol.

The sample was covered with reagent A (2 mL) and kept for 35 min at room temperature under exclusion of light. The liquid phase was removed and the sample was thoroughly rinsed with anhydrous DMF and anhydrous methanol under exclusion of moisture. Washing was continued until filtrates remained colorless upon addition of reagent B. After being dried, the sample was covered with reagent B and shortly shaken. The absorbance at 498 nm against reagent B as blind value was measured after 2 min. Calculation of the amino group content was conducted according to equation 1.

$$\frac{n \left[\frac{\text{nmol}}{\text{cm}^2} \right]}{A \left[\text{cm}^2 \right]} = \frac{\text{Abs}_{498\text{nm}} \cdot 2\text{mL}}{0.07\text{mL} \cdot \text{nmol}^{-1} \cdot 1\text{cm} \cdot A \left[\text{cm}^2 \right]} = \frac{\text{Abs}_{498\text{nm}}}{A \left[\text{cm}^2 \right]} \cdot 28.6\text{nmol}$$

Results and Discussion

It was found that amino cellulose interacts very intensively with a variety of materials [4]. In the present work, dyeing experiments of cellulose (paper, pulp fibers) were carried out without and with a prior treatment of the samples applying amino cellulose by dipping or spraying. The surface loading regarding the amino cellulose was determined colorimetrically with 4,4'-dimethoxytriphenylchloromethane.

Adsorption of Amino Cellulose (AC) on Pulp Samples

In a first set of experiments, pulp samples were treated with an aqueous solution of EDA cellulose labeled with 9-(methylaminomethyl)anthracene. The amount of polymer adsorbed was calculated by fluorescence spectroscopy of the remaining solutions, i.e., after the treatment of the pulp was carried out. There is no difference in the amount of AC absorbed for the different pulps, as can be seen in Table 1. It could also be observed that the AC is attached to the pulp fibers by radiation of the samples with UV-light after the treatment (Figure 1).

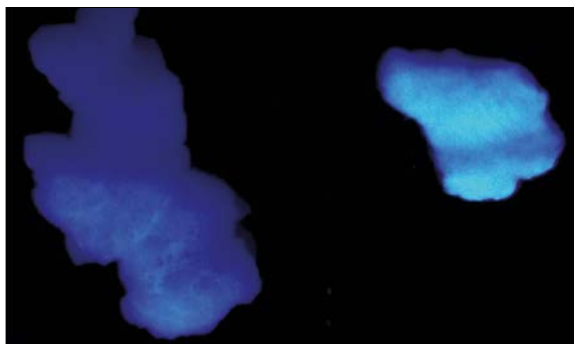


Figure 1: Photography of pulp fibers radiated with UV-light after treatment with amino cellulose marked with 9-(methylaminomethyl)anthracene (samples 1, left and 5, right, see Table 1).

Table 1: Amount of fluorescently labelled 6-deoxy-6-(2-aminoethyl)amino (EDA) cellulose (AC) adsorbed on pulp fibers (treatment at room temperature for 20 min).

| Sample no. | Pulp ^{a)} | Volume of EDA cellulose ^{b)} solution added [mL] | Amount adsorbed of AC on fibers [g] (average of three measurements) |
|------------|--------------------|---|---|
| 1 | P1 | 2 | 2.08 10 ⁻⁴ |
| 2 | P1 | 5 | 4.70 10 ⁻⁴ |
| 3 | P1 | 10 | 9.32 10 ⁻⁴ |
| 4 | P1 | 30 | 2.95 10 ⁻⁴ |
| 5 | P1 | 50 | 5.00 10 ⁻⁴ |
| 6 | P2 | 2 | 2.07 10 ⁻⁴ |
| 7 | P2 | 5 | 4.66 10 ⁻⁴ |
| 8 | P2 | 10 | 9.28 10 ⁻⁴ |
| 9 | P2 | 30 | 2.96 10 ⁻⁴ |
| 10 | P2 | 50 | 5.00 10 ⁻⁴ |

^{a)} P1: pre-hydrolysis kraft pulp "Purple grade" from Södra, P2: dissolving grade sulfite pulp from Domsjö

^{b)} Degree of substitution of 6-deoxy-6-(2-aminoethyl) amino groups DSEDA 0.69, DS of 6-deoxy-6-(9-(methylaminomethyl)anthracene) groups DSFD 0.08

It can be noticed that the fibers are uniformly coated with the fluorescent AC derivative. The different fluorescence intensity reflects the different amounts of AC absorbed on the fiber surface.

Amino Cellulose Coating of Paper Samples

The experiments were carried out with a usual copy paper. Due to the chemical and physical nature of paper as well as the high porosity, high load capacities should be expected compared to other material like, e.g., glass. However, it turned out that the load capacity with respect to the coated surface is difficult to measure because the total surface of the paper accessible for AC cannot be measured and, moreover, swelling processes during both coating and dyeing may influence the surface area. Thus, experiments were performed with uniform samples of constant dimensions. The values summarized in Table 2 shows that a small concentration of the solution of amino cellulose is needed for the coating process.

Table 2: Surface loading of paper (copy paper: Future Multitech, white paper for inkjet, copier, laser, fax, 75 g/m²) with aqueous solution of 6-deoxy-6-(2-aminoethyl)amino cellulose (EDA) cellulose of different concentration.

| | Concentration of EDA cellulose (%) | | |
|--|------------------------------------|-------|-------|
| | 0.025 | 0.050 | 0.100 |
| Sample surface (cm ²) | 2 | 2 | 2 |
| Absorption (diluted to 1:100) | 1.017 | 1.162 | 1.169 |
| Load capacity (mmol/cm ⁻²) | 1.452 | 1.660 | 1.670 |

It became obvious that the concentration of EDA cellulose dissolved in water as low as 0.05% is sufficient to saturate the paper surface with amino cellulose (about 1.6 mmol/cm²). The slight difference of load capacity between a concentration of EDA cellulose dissolved in water of 0.050% and 0.100% is within the error range of the method applied. While the coating is incomplete at concentration below 0.025%, an excess of amino cellulose is rinsed away when applying higher concentrations of AC.

An important question is the reusability of the coating solution. As can be seen in Figure 2, the surface load capacity is almost constant and, hence, independent of the number of cycle. Therefore, the amino cellulose solution can be used repeatedly without loss of activity at least for ten times.

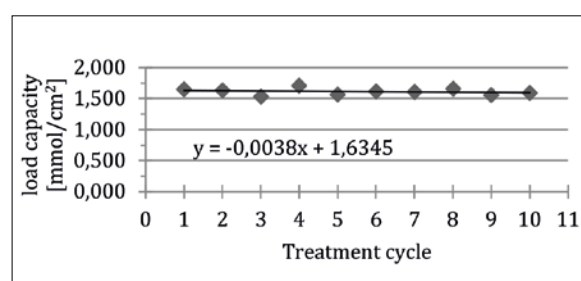


Figure 2: Dependency of surface loading capacity of paper by repeated treatment using the same amino cellulose solution.

Dyeing of Paper

Dyes of different chemical structure were prepared as 0.1% (w/v) solutions (see Table A1). The dye absorption was evaluated by visual inspection and by UV/Vis-spectrometry. The results summarized in Table 3 clearly indicate that surface coating with amino cellulose improves the dyeing performance. Crystal violet, methylene blue, and methyl red are absorbed, while the paper treated with Ruhemann's purple does not show any color. Treatment of the paper samples with EDA leads to an increase of the color intensity in most cases. It became obvious that the color intensity is distinctly influenced by the chemical structure of the dye. Anionic dyes (methyl red, Ruhemann's purple) exhibited a much better binding to the amino cellulose coated surface compared with cationic dyes (crystal violet, methylene blue). It is known that cationic cellulose derivatives possess a high affinity to the negatively charged cellulose surface [6]. The surface is, therefore, charged with cationic moieties, which act as anchor for the anionic dye molecules. A similar observation was reported in the case of amino group containing nanocrystalline cellulose (NCC) [24]. They found that NCC functionalized with amino moieties could be used as an adsorbent to remove anionic dyes in aqueous solution. The highest efficiency was found under acidic conditions.

Table 3: Results of dyeing experiments of paper before and after treatment with amino cellulose derivatives.

| Dye solution ^{a)} | Crystal violet 70% H ₂ O, 30% MeOH | Methylene blue 70% H ₂ O, 30% MeOH | Methyl red 70% H ₂ O, 30% MeOH | Ruhemann's purple 50% H ₂ O, 50% EtOH |
|----------------------------|--|--|--|---|
| Untreated | | | | |
| Coated with EDA-cellulose | | | | |
| Dye solution | Coomassie brilliant blue G250 70% H ₂ O, 20% MeOH, 10% HAc | Congo red 50% H ₂ O, 50% EtOH | Thymol blue 100% EtOH | Eriochrome black T 100% H ₂ O |
| Untreated | | | | |
| Coated with EDA-cellulose | | | | |
| Coated with TAEA-cellulose | | | | |

a) 6-Deoxy-6-(2-aminoethyl)amino cellulose (EDA-cellulose); 6-deoxy-6-(2-(bis(2-aminoethyl)aminoethyl)amino) cellulose (TAEA cellulose)

Coomassie brilliant blue, Congo red, and Eriochrome black T absorb weakly onto the cellulose fibers, Thymol blue did not lead to a visible coloration. Those dyes were selected for more detailed investigations. Treatment of cellulose with both EDA- and TAEA

cellulose led to comparable dyeing efficiency, i.e., the color intensity was remarkably increased and comparable independent of the type of AC. It may be concluded that the number of available amino groups does not increase the coloration. Larger differences
















were observed in the case of dyes without carboxylate moieties. Obviously, the structural features in Thymol blue (hydroxyl groups) and Eriochrome black T (hydroxyl- and sulfonate groups) induce a weaker interaction with the amino group-containing surface. While Thymol blue colored paper exhibited a different color intensity, different colors were observed in case of Eriochrome black T.

The dyeing performance of commercially available textile dyestuffs (reactive dye Benzaktiv HE red and marine) on office papers depending on the AC treatment was also studied in order to check if treatment with AC leads to an increased dyeing effect. The dyeing process was carried out under omission of the dyeing

regime given by the manufacturer. Both Bezaktiv HE dyes (red and marine) were applied as 0.1% (w/v) solutions solely or mixed with marine and red color.

Comparably weak dyeing could be observed in case of all dye combinations if no previous AC treatment was carried out (Table 4). Almost no dyeing could be observed in case of paper A. AC treatment of the paper prior to the dyeing process increased the color intensity remarkably. Obviously, the dyes interact much better with the amino groups compared to the hydroxyl groups. No difference between EDA- and TAEA cellulose could be found. Combination of both dyes led to mixed colors, which were homogeneously distributed.

Table 4: Dyeing of paper samples with reactive dyes with and without amino cellulose treatment.

| Dye ratio (red:marine) / paper ^{a)} | Untreated | Coated with EDA ^{b)} -Cellulose | Coated with TAEA ^{b)} -Cellulose |
|--|---|--|---|
| 1:0 Paper E |  |  |  |
| 2:1 Paper A |  |  |  |
| 1:1 Paper C |  |  |  |
| 1:2 Paper D |  |  |  |
| 0:1 Paper B |  |  |  |

a) Paper A (Kymi-Acacia, coated), paper B (Chanshu-Acacia, coated), paper C (Nordland-Betula, uncoated), paper D (Nordland-Acacia, uncoated), paper E (Yes-Silver Multifunction)

b) 6-Deoxy-6-(2-aminoethyl)amino cellulose (EDA-cellulose); 6-deoxy-6-(2-(bis(2-aminoethyl)aminoethyl)amino) cellulose (TAEA cellulose)

Conclusions

It was shown that amino cellulose can be coated on different cellulose surfaces by a simple dipping technique. A much diluted solution of AC (0.05%) can be used several times without losing activity. Amino cellulose is absorbed on the surface of cellulose fibers and turns the surface charge positive. Therefore, anionic dyes bind better to the positively charged surface and the dyeing performance can be improved. Further studies should be performed to apply this approach to textiles. In this regard it is interesting to examine the resistance of this coating against washing.

Acknowledgements

KJ: The Swedish Research Council Formas is gratefully acknowledged for financial support.

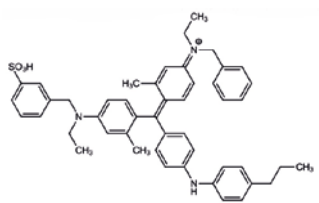
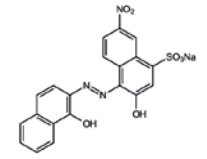
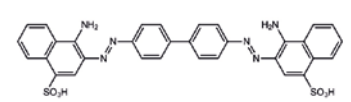
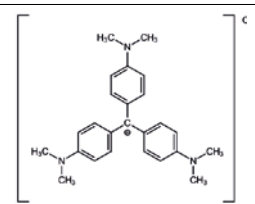
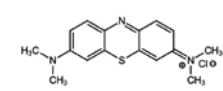
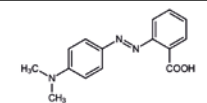
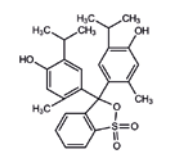
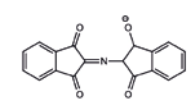
References

- [1] A. Stanislawski, E. Drzewinska, Retention of dyes on cellulose fibres during paper production. *Ann. Warsaw Univ. Life Sci.-SGGW. For. Wood Technol.* 62, 256-259 (2007).
- [2] S. Sharif, S. Ahmad, M. M. Izhar-ul-Haq, Role of quaternary ammonium salts in improving the fastness properties of anionic dyes on cellulose fibres. *Color. Technol.* 123, 8-17 (2007).
- [3] T. Bechtold, E. Burtscher, Y.-T. Hung, Treatment of textile wastes. *Handbook of Industrial and Hazardous Waste Treatment*, Marcel Dekker, 379-413 (2004).
- [4] T. Heinze, M. Siebert, P. Berlin, A. Koschella, Biofunctional materials based on amino cellulose derivatives – A Nanobiotechnological Concept. *Macromol. Biosci.* 16, 10-42 (2016).

- [5] T. Genco, L. F. Zemljč, M. Bračič, K. Stana-Kleinschek, T. Heinze, Characterization of viscose fibers modified with 6-deoxy-6-amino cellulose sulfate. *Cellulose* 19, 2057-2067 (2012).
- [6] O. Grigoriy, H. Wondraczek, A. Pfeifer, P. Fardim, T. Heinze, Fluorescent multifunctional polysaccharides for sustainable supramolecular functionalization of fibers in water. *ACS Sustainable Chem. Eng.* 5, 1794-1803 (2017).
- [7] K. Jedvert, T. Elschner, T. Heinze, Adsorption studies of amino cellulose on cellulose. *Macromol. Mater. Eng.* 302, 1700022 (2017).
- [8] B. Vega, H. Wondraczek, C. S. P. Zarth, E. Heikkilä, P. Fardim, T. Heinze, Charge-directed fiber surface modification by molecular assemblies of functional polysaccharides. *Langmuir* 29, 13388-13395 (2013).
- [9] S. Bratskaya, S. Schwarz, G. Petzold, T. Liebert, T. Heinze, Cationic starches of high degree of functionalization: 12. Modification of cellulose fibers toward high filler technology in papermaking. *Ind. Eng. Chem. Res.* 45, 7374-7379 (2006).
- [10] I. Szilagy, G. Trefalt, A. Tiraferri, P. Maroni, M. Borkovec, Polyelectrolyte adsorption, interparticle forces, and colloidal aggregation. *Soft Matter* 10, 2479-2502 (2014).
- [11] R. Gaur, S. Paliwal, P. Sharma, K. Gupta, A simple and sensitive spectrophotometric method for the quantitative determination of solid supported amino groups. *J. Biochem. Biophys. Meth.* 18, 323-329 (1989).
- [12] R. K. Gaur, K. C. Gupta, A spectrophotometric method for the estimation of amino groups on polymer supports. *Anal. Biochem.* 180, 253-258 (1989).
- [13] R. K. Gaur, P. Sharma, K. C. Gupta, 4, 4'-Dimethoxytrityl chloride: a reagent for the spectrophotometric determination of polymer-supported amino groups. *Analyst* 114, 1147-1150 (1989).
- [14] S. S. Chu, S. H. Reich, NPIT: a new reagent for quantitatively monitoring reactions of amines in combinatorial synthesis. *Bioorg. Med. Chem. Lett.* 5, 1053-1058 (1995).
- [15] S. G. Hu, C. H. Jou, M. C. Yang, Surface grafting of polyester fiber with chitosan and the antibacterial activity of pathogenic bacteria. *J. Appl. Polym. Sci.* 86, 2977-2983 (2002).
- [16] M. Pohl, N. Michaelis, F. Meister, T. Heinze, Biofunctional surfaces based on dendronized cellulose. *Biomacromolecules* 10, 382-389 (2009).
- [17] T. Finlay, V. Troll, M. Levy, A. Johnson, L. Hodgins, New methods for the preparation of biospecific adsorbents and immobilized enzymes utilizing trichloro-s-triazine. *Anal. Biochem.* 87, 77-90 (1978).
- [18] S. Moore, W. H. Stein, A modified ninhydrin reagent for the photometric determination of amino acids and related compounds. *J. Biol. Chem.* 211, 907-913 (1954).
- [19] V. K. Sarin, S. B. Kent, J. P. Tam, R. B. Merrifield, Quantitative monitoring of solid-phase peptide synthesis by the ninhydrin reaction. *Anal. Biochem.* 117, 147-157 (1981).
- [20] M. Zieger, M. Wurlitzer, C. Wiegand, K. Reddersen, S. Finger, P. Elsner, P. Laudeley, T. Liebert, T. Heinze, U.-C. Hipler, 6-Deoxy-6-aminoethyleneamino cellulose: synthesis and study of hemocompatibility. *J. Biomater. Sci., Polym. Ed.* 26, 931-946 (2015).
- [21] L. C. Fidale, M. Nikolajski, T. Rudolph, S. Dutz, F. H. Schacher, T. Heinze, Hybrid Fe₃O₄[@] amino cellulose nanoparticles in organic media – Heterogeneous ligands for atom transfer radical polymerizations. *J. Colloid Interface Sci.* 390, 25-33 (2013).
- [22] T. Köhnke, H. Brelid, G. Westman, Adsorption of cationized barley husk xylan on kraft pulp fibres: Influence of degree of cationization on adsorption characteristics. *Cellulose* 16, 1109-1121 (2009).
- [23] T. Heinze, A. Pfeifer, A. Koschella, J. Schaller, F. Meister, Solvent-free synthesis of 6-deoxy-6-(ω -aminoalkyl) amino cellulose. *J. Appl. Polym. Sci.* 133, DOI: 10.1002/APP.43987 (2016).
- [24] L. Jin, W. Li, Q. Xu, Q. Sun, Amino-functionalized nanocrystalline cellulose as an adsorbent for anionic dyes. *Cellulose* 22, 2443-2456 (2015).

Annex

Table A1: Structure, classification, and solvents for the dyes applied.

| Dye / Classification | Dissolved in | Structure |
|--|--|---|
| Coomassie-Brilliant-Blue G250/ Triphenylmethane | 70% Water 20% Methanol 10% Acetic acid |  |
| Eriochrome black T/ Azo | Water |  |
| Congo red/ Azo | 50% Water 50% Ethanol |  |
| Crystal violet/ Triphenylmethane | 70% Water 3% Methanol |  |
| Methylene blue/ Indamin | 70% Water 30% Methanol |  |
| Thymol blue/ Triphenylmethane | 70% Water 30% Methanol |  |
| Methyl red/ Azo | Ethanol |  |
| Ruhemans purple/ Ninhydrin | 50% Water 50% Ethanol |  |

Fluorescence Measurements

Fluorescence measurements were conducted in water-citric acid buffer and a diluted aqueous hydrochloric acid solution at pH = 3.1. Due to self-quenching initiated by a photoinduced electron transfer the fluorescence dye employed needed to be kept at a low pH value [1]. When the amino anthracene nitrogen becomes protonated, this effect vanishes and the fluorescence of the compound can be measured.

In Figure A1 the slopes for the quantum yield calculations are plotted for the standards and the labeled amino cellulose investigated. The quantum yields can be calculated using equation A1:

$$\phi_x = \phi_{ST} \left(\frac{Grad_x}{Grad_{ST}} \right) \left(\frac{\eta_x^2}{\eta_{ST}^2} \right)$$

Here the subscripts ST and X corresponds to the standard and sample respectively. ϕ is the fluorescence

quantum yield and Grad is the gradient from the integrated fluorescence intensities against the absorbance as seen in the plot (Figure A1), η corresponds to the refractive indices of the solvents used for the measurements [2]. The quantum yields for anthracene and 9,10-di-phenylanthracene are given with $\phi_{\text{anthr.}} = 0.27$ and $\phi_{9,10\text{-diph}} = 0.95$ [3,4].

The average fluorescence quantum efficiency of the labeled amino cellulose in aqueous citric acid and diluted hydrochloric acid at pH = 3.1 is $\phi_{\text{A}_{\text{mcell}}} = 45\%$. Knowing these emission properties, it was possible to directly measure the amount of labeled amino cellulose that was left over in the solution after the absorption experiments with different pulp samples (see Table 1).

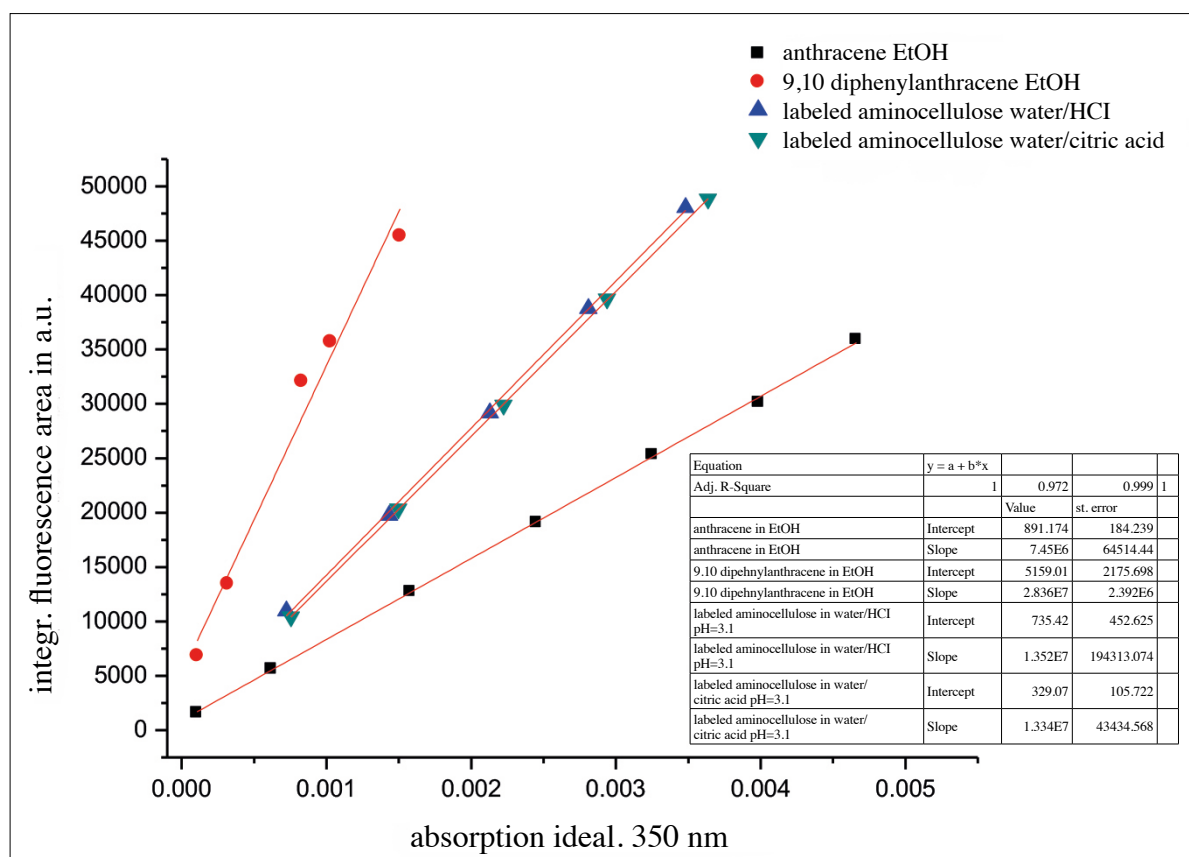


Figure A1: Integrated fluorescence intensities versus the idealized absorptions at 350 nm of two standards (anthracene and 9,10-diphenylanthracene in ethanol, EtOH) and the fluorescence dye labeled 6-deoxy-6-(2-aminoethyl)amino cellulose in water-citric acid and diluted hydrochloric acid solution at pH = 3.1. The resulting gradients can be used in equation A1 to calculate the quantum yields.

References

- [1] R. A. Bissell, E. Calle, A. Prasanna de Silva, S. A. de Silva, H. Q. Nimal Gunaratne, J.-L. Habib-Jiwan, S. L. Annesley Peiris, R. A. D. Dayasiri Rupasinghe, T. K. Shantha, D. Samarasinghe, K. R. A. Samankumara Sandanayake, J.-P. Soumillion, *J. Chem. Soc. Perkin Trans. 2*, 1559-1564 (1992).
- [2] A. T. R. Williams, S. A. Winfield, J. N. Miller, *Analyst*, 108, 1067-1071 (1983).
- [3] W. R. Dawson, M. W. Windsor, *J. Phys. Chem.* 72, 3251-3260 (1968).
- [4] J. V. Morris, M. A. Mahaney, J. R. Huber, *J. Phys. Chem.* 80, 969-974 (1976).

Possibilities for Raw Material Base Expansion for Lyocell Applications by Enzymatic Pulp Treatment

Birgit Kosan^{1,*} and Frank Meister¹

¹ Thüringisches Institut für Textil- und Kunststoff-Forschung e.V., Breitscheidstr. 97
D-07407 Rudolstadt, Germany

* Contact: (+49) 3672 379 220, Fax: (+49) 3672 379 379, e-mail: kosan@titk.de

Abstract

The prospects of an enzymatic modification procedure were studied for adjustment of alternative pulp properties in Lyocell fibres spinning process. Ultimately, an enzymatic treatment was developed which is adaptable to the Lyocell process technology using cellulases with well-defined endo- and exo-activities for an intended reducing of the cellulose DP as well as for an improvement of the pulp solubility in NMMO.

The DP reduction of different tested pulp qualities (paper, viscose and annual plant pulps) was attained between 20 and 25%, with regard to the starting DP of the used pulp sample. Thereby, very small pulp loss was detected. Because of the significant improvement of the pulp solubility by the enzymatic modification, spinning dopes with very good solution states could be received, even when paper grade pulps with lower contents of α -cellulose were applied.

Exemplary for a softwood TCF paper grade pulp, tests for first upscaling in staple fibre and filament preparation could be successfully carried out with integration of the developed enzymatic modification step. The prepared fibre and filament samples showed good textile physical properties.

The developed, innovative enzymatic modification step has a great potential for further expansion of the raw material base in Lyocell process. This could cause to cost savings by applicability of less expensive cellulose raw materials, but it provides also broader possibilities for usage of alternative cellulose sources from recycling materials or annual plants, outside of cotton.

Keywords: *Enzymatic pulp treatment, Lyocell process, pulp base expansion, DP adaption, solution state*

Introduction

Because of the predicted increase of the world textile fibre consumption at simultaneous stagnation of cotton cultivation, the demand for cellulose textile fibres will continue to grow, and it is expected an annual increase of the production of textile fibres of about 3.1% up to the year 2030 [1]. This predicted, disproportionately high increase of the fibre demand by around 2.8 Mio t/a is neither feasible by appropriate improvement of the production of synthetic fibres due to their different moisture management nor by a further increase of the cotton production, because of limitation or reduction of the cultivated amounts in favour of also increasing world food demand as well as comparatively unfavourable farming criteria, i.e. high water consumption or usage of genetically modified seeds and pesticides

at cotton cultivation [2]. The resulting demand is referred to as “cellulose gap”. It opens up the possibility, but also the necessity for a significant improvement of the capacities for production of sustainable cellulosic regenerated fibres [1,3].

The Lyocell process using direct dissolution of cellulose in N-methylmorpholine-N-oxide monohydrate (NMMO) has a special potential for sustainable cellulose fibre processing [4]. The solvent is non-toxic and nearly completely recyclable [5]. However, the Lyocell fibre processing requires the use of special dissolving pulp qualities which were adapted directly for the process. It would be of great interest to extend the range of cellulosic raw materials for Lyocell fibre spinning applications. The usage of low-cost pulp qualities, i.e.

paper grade pulps, cellulose from annual plants [6] or fibre raw material from recycled textile sources could be very interesting on grounds of cost but also from the point of view of a circular flow economy. The paper will report and discuss possibilities of an enzymatic paper pulp treatment, adaptable in the Lyocell process, using suitable cellulases with special ratios of exo-activities for improvement of the accessibility of the cellulose molecules [7] and endo-activities for targeted reduction of their long-chain cellulose parts.

Materials and Methods

The investigations were carried out using softwood TCF paper grade pulp, (NH-P). The determined analytical data of the pulp are listed in Table 1.

Table 1: Analytical data of the used paper grade pulp sample

| Pulp sample | | NH-P |
|-----------------------------|-----------------------|------|
| Cuoxam-DP | | 763 |
| α -cellulose content | [%] | 85.5 |
| Content of carboxyl groups | [$\mu\text{mol/g}$] | 33.2 |
| Content of carbonyl groups | [$\mu\text{mol/g}$] | 27.6 |

The used enzyme samples were cellulase test samples with selected endo and combined exo activities, which were kindly selected and delivered by Biopract GmbH.

N-Methylmorpholine-N-oxide (NMMO) was used as 50% aqueous solution, manufactured and supplied by BASF, without any further pre-treatment.

All other used chemicals were obtained in analytical grade, respectively and were used without any further pre-treatment.

Enzymatic treatment

The enzymatic treatment of the pulp samples was separately carried out before the pulp was admixed to the aqueous NMMO solution and could be smoothly integrated into the existing NMMO technology.

The treatment procedure took place in aqueous medium using the listed enzyme concentrations (see Table 2), referred to cellulose, at pH of 5.5 during 60 minutes treatment time at 50 °C. The treatment was stopped by increase of the pH up to 9. Following, the treated pulp was pressed out from the excess water down to about 30% solid content and introduced in aqueous NMMO for further processing.

For analytical characterisation, the treated pulp samples were washed by deionised water up to neutral pH, pressed out from the excess water and air dried.

Preparation of cellulose dopes

The preparation of cellulose dopes was carried out using a special vertical kneader system, linked with a RHEOCORD 9000 (HAAKE). Temperature, torque moment and revolutions per minute (rpm) vs. time were recorded on-line. The dopes were prepared, starting from an aqueous suspension of the treated pulp in 50% aqueous NMMO, by removal of the excess water at elevated temperatures, higher shearing stress and low pressure during the dissolution processes (80-95 °C mass temperature, 800-40 mbar pressure, 5-20 rpm). 0.5% (w/w) propylgallate, with regard to cellulose, were used for stabilisation of the NMMO solutions. After the finishing of water removal (achieving a NMMO monohydrate state), an after-dissolution step (60 min, 90 °C mass temperature, 250 mbar) followed for homogenisation of the prepared dope.

A first upscaling in 4 kg dope scale was carried out using planetary mixing machine PML 40 (Netzsch-Feinmahltechnik GmbH).

Spinning trials

First spinning tests were carried out by dry-wet spinning experiments for preparation of staple fibres of about 1.7 dtex fineness using a laboratory piston spinning equipment, which is described in former publication. [8] Spinning nozzles, containing 30 holes with capillary diameters of 100 μm were used for all laboratory spinning experiments. The spinning temperatures were selected in each case according to the rheological properties of the used cellulose dopes.

Further semi-technical spinning tests using spinnerets with 6 x 80 capillaries (90 μm outlet diameter) were carried out for investigation of the spinning behaviour and stability. These trials were used for preparation of staple fibres and multifilament samples.

Cellulose characterisation

The virgin and enzymatic treated pulp samples as well as the cellulose samples regenerated from the dopes and from the spinning tests dissolved in Cuoxam were characterised by capillary viscosity for determination of the average degree of polymerisation (Cuoxam-DP). The α -cellulose content was determined by investigation of the pulp amounts which are resistant to 17.5% caustic soda at 20 °C.

The determination of carboxyl group contents has been carried out through complexometric titration of zinc ions after removing of the metal ions from the cellulose at first and adding of zinc acetate solution in a second step.

The carbonyl group contents were analysed by measurement of the absorbance at 530 nm after reaction with 2, 3, 5-triphenyltetrazoliumchloride solution.

The details of this cellulose characterisation were described in former publications. [9,10]

Analytical characterisation of cellulose solutions

Optical characterisation of cellulose solutions was carried out by means of polarisation microscopy (ZEISS Axiolab). Furthermore measurements by laser diffraction (HELOS particle size equipment, SYMPATEC) were used for determination of the particle distribution and particle content of prepared spinning dopes [11]. The determination of the solids contents in the solutions was performed by means of weighing precipitated films, after exhaustive solvent extraction and drying. The rheological measurements were realised as described in the following.

Rheological characterisation

The rheological characterisation of cellulose solutions was performed using a rheometer HAAKE MARS with cone / plate measuring system (4° angle geometry) and electrically heated cone & plate unit with active cone heater.

Zero shear viscosities were calculated from creep attempts in the rotation mode at shear stress of 90 Pa. The determined cellulose solutions showed significant viscoelastic behaviour. A characterisation of the viscoelastic properties was realised in the oscillation mode. Oscillation tests were carried out as frequency sweeps (0.046-14.7 Hz, deformation: 0.07) at different temperatures (60 / 85 / 110°C). WLF-transformation was used for calculation of master curves and relaxation spectra at 85°C reference temperature. This method permits an interpolation of the frequency / angular rate range over several decades and is an evaluated method for the determination of viscoelastic properties of polymer solutions. Details of the rheological dope characterisation had been described in former publications. [9,12]

Fibre characterisation

The textile-physical fibre parameters were determined according to the following methods:

- fineness according to DIN EN ISO 1973,
- tenacity and elongation at break according to DIN EN ISO 5079 and
- loop tenacity according to DIN 53843, part 2.

The filament samples were tested according to:

- yarn fineness according to DIN EN ISO 2060 and
- maximum tensile strength and elongation according to DIN EN ISO 2062.

Results and Discussion

The possibilities of the enzymatic treatment should be exemplary discussed in this paper for the softwood TCF paper grade pulp sample (NH-P). The untreated pulp sample was not suitable for direct use in Lyocell processing because of the comparably high Cuoxam-DP of 763 and the unfavourable dissolution behaviour in NMMO.

The enzymatic treatment of the pulp sample with cellulase samples P1, P4, P10 and P11 containing different mixtures of enzymatic activities resulted in a reduction of the Cuoxam-DP of the pulp sample between 19 and 23%. The attained DP values of the modified pulp samples were between 589 and 619 in an appropriate area for the preparation of Lyocell fibres. The content of carbonyl groups of the pulp sample increases, depending on the DP reduction and the used enzyme type and applied concentration (Table 2). This increase of the carbonyl group contents should indicate the extent of the chain scission and should be significantly influenced by the resulting molecular weight distribution especially on the low molecular amounts.

Table 2: Analytical data of pulp sample NH-P after enzymatic treatment

| Sample / Enzym dosage* | Cuoxam -DP | Reduction of DP | Content of carbonyl groups [μmol/g] |
|--------------------------|------------|-----------------|-------------------------------------|
| NH-P (untreated) | 763 | | 27.6 |
| NH-P / 0,3% P4 | 619 | 18.9 | 61.4 |
| NH-P / 1% P10 | 612 | 19.8 | 51.3 |
| NH-P / 1% P11 | 590 | 22.7 | 48.6 |
| NH-P / 0,5% P1 + 0,3% P4 | 589 | 22.8 | 88.2 |

* Enzyme concentration referred to pulp amount

Dissolution and shaping tests in laboratory scale

The enzymatic modified pulp samples could be used for dope preparation in laboratory scale with cellulose concentrations between 12 and 12.5% (w/w). The microscopic images of the prepared dopes showed a strongly improved solution states without any undissolved fibre residuals. Contrary to this, the dissolution of the unmodified pulp sample resulted in a very bad solution state, even at reduced cellulose concentration of 9% (w/w), containing a lot of undissolved fibre fragments. Figure 1 shows the microscopic images of a 9% dope from the unmodified pulp sample compared to a 12% dope using enzymatic (P11) modified pulp sample. Because of the high particle content with a large number of particles with high aspect ratio, a particle characterisation of the 9% dope with laser diffraction was not possible. In contrast, very small particle contents (< 20 ppm)

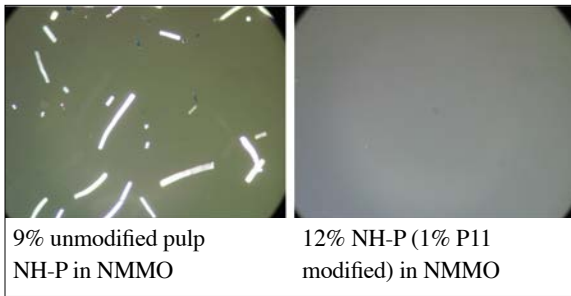


Figure 1: Microscopic images of prepared spinning dopes in NMMO (transmitted light, polarization microscopy, 10x-objective)

with low particle sizes (up to 51 μm in maximum) were detected by laser diffraction at the prepared dopes from enzymatic modified pulp samples.

The rheological properties of the prepared spinning dopes, applying the enzymatic modified pulp samples, are in a well-suitable area for Lyocell process technology. The results of the rheological characterization

are pictured in Table 3 and Figures 1 and 2. The spinning dope which was prepared using the unmodified pulp sample showed lower viscosity and moduli curves, because of the lower cellulose concentration and the incomplete dissolution state.

The dopes were tested regarding their formability to staple fibres using laboratory piston spinning equipment (capillary diameter: 100 μm , 30 capillaries). The applied spinning conditions and achieved fibre properties are listed in Table 4.

Spinning dope 1, prepared by using the unmodified pulp sample, showed a very unstable spinning behaviour. Alongside many capillary breaks, the spinning pressure increased from 32 to 38 bar already during the short time of the laboratory spinning test of about 30 minutes. This pressure increase should be caused by accumulation of particles on the safety filter device because of the worse dope quality containing undissolved fibre residuals or rather gel contents.

Table 3: Results from analytical characterisation of cellulose dopes using pulp sample NH-P

| Sample | | 1 | 2 | 3 | 4 | 5 |
|--|-------|------------|------------|-------------------|------------|------------|
| Pulp treatment | | without | 0.3% P4 | 0.5% P1 / 0.3% P4 | 1% P10 | 1% P11 |
| Cuoxam-DP of applied pulp sample | | 763 | 619 | 589 | 612 | 590 |
| Cellulose concentration | % | 9.1 | 11.8 | 12.5 | 12.2 | 12.0 |
| Zero shear viscosity (85 °C) | Pas | 7,295 | 12,130 | 14,160 | 11,570 | 9,587 |
| Angular velocity (cross over) ¹ | rad/s | 1.27 | 1.37 | 1.34 | 1.68 | 1.88 |
| Storage modulus (cross over) ¹ | Pa | 1,193 | 2,126 | 2,339 | 2,360 | 2,223 |
| Plateau modulus ¹ | Pa | 16,100 | 24,500 | 26,700 | 25,900 | 23,400 |
| Rheological polydispersity | | 4.5 | 4.5 | 4.8 | 4.8 | 4.7 |
| Relaxation time λ_m at H^*m^{-2} | s | >100 | 41 | 87 | 19 | 20 |

¹ calculated from master curves (Figure 2)

² calculated from weighted relaxation time spectra (Figure 3)

Table 4: Spinning conditions and achieved fibre properties using pulp sample NH-P

| Sample | | 1 | 2 | 3 | 4 | 5 |
|----------------------------------|--------|------------|------------|-------------------|------------|------------|
| Pulp treatment | | without | 0.3% P4 | 0.5% P1 / 0.3% P4 | 1% P10 | 1% P11 |
| Cuoxam-DP of applied pulp sample | | 763 | 619 | 589 | 612 | 590 |
| Spinning conditions: | | | | | | |
| Spinning temperature | °C | 87 | 89 | 91 | 89 | 87 |
| Spinning pressure | bar | 32-38 | 29 | 32 | 33 | 23 |
| Spinning speed | m/min | 30 | 30 | 30 | 30 | 30 |
| Spinning behaviour | | unstable | stable | stable | stable | stable |
| Fibre testing: | | | | | | |
| Fineness | dtex | 1.81 | 1.75 | 1.83 | 1.79 | 1.40 |
| Tenacity, cond. | cN/tex | 30.8 | 35.4 | 32.7 | 34.2 | 33.8 |
| Elongation, cond. | % | 12.2 | 14.4 | 14.9 | 13.3 | 13.5 |
| Loop tenacity | cN/tex | 14.7 | 14.7 | 15.3 | 17.3 | 16.0 |
| E-modulus 0.5-0.7% | cN/tex | 795 | 922 | 779 | 882 | 855 |
| Cuoxam-DP fibre | | 703 | 567 | 572 | 560 | 545 |
| Water retention value (WRV) | % | 95.6 | 87.4 | 89.7 | 91.7 | 82.6 |

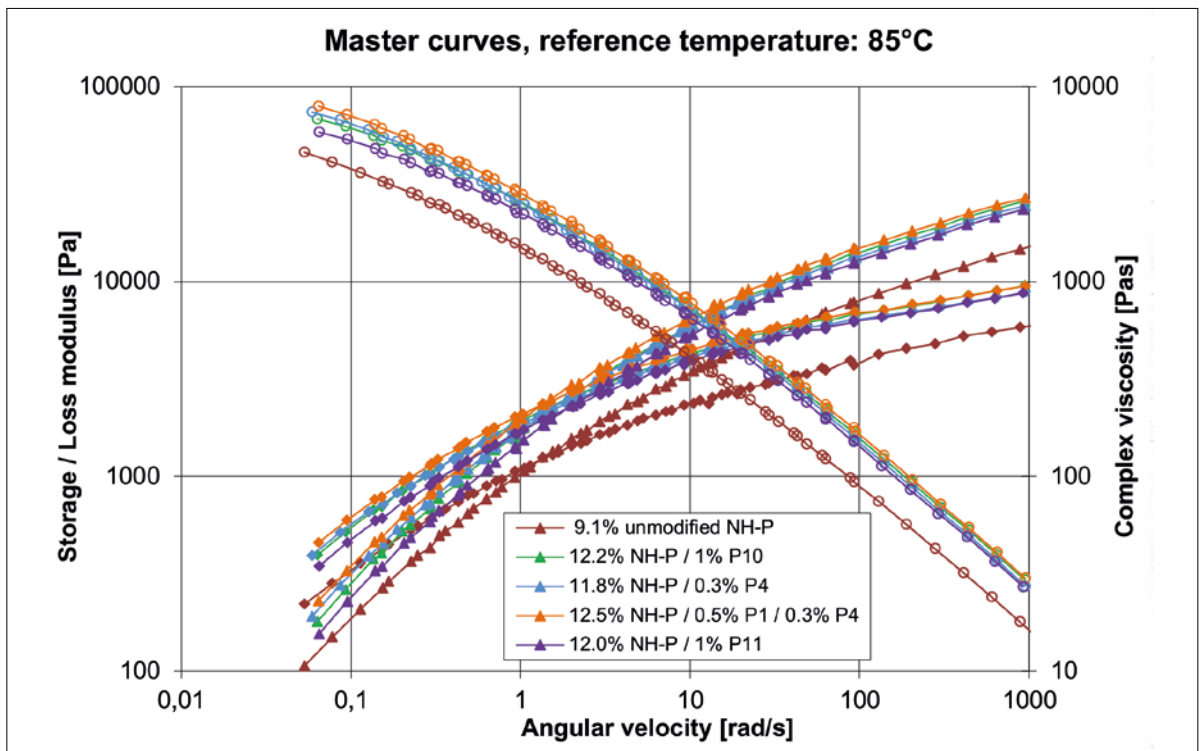


Figure 2: Master curves of spinning dopes using enzymatic treated and unmodified pulp sample NH-P

Triangles: Storage moduli
 Squares: Loss moduli
 Open circles: Complex viscosities

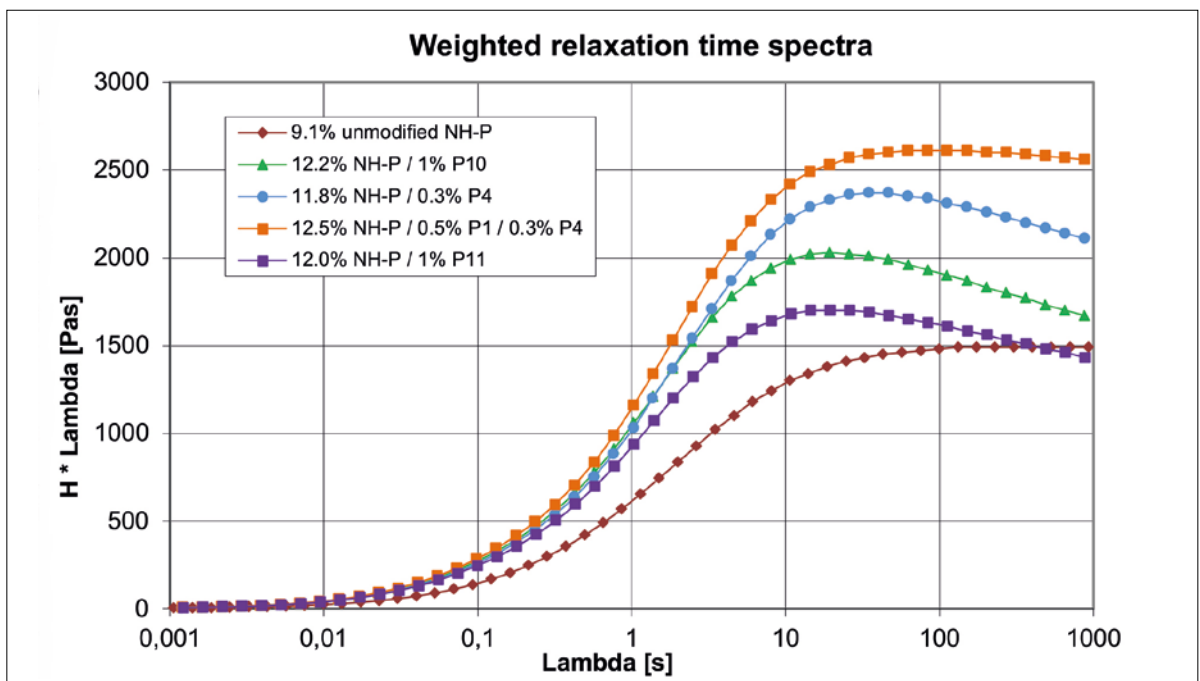


Figure 3: Weighted relaxation time spectra of spinning dopes using enzymatic treated and unmodified pulp sample NH-P

The spinning tests using the dopes from enzymatic modified pulp samples showed a very stable spinning behaviour. The Cuoxam-DP values of the prepared fibres were comparable between 545 and 572. The textile physical properties of the prepared fibres were only

slightly below the level of Lyocell fibres. It illustrates, that the prepared fibres from paper grade pulps showed slightly increased WRV compared with Lyocell fibres, prepared using typical Lyocell pulps. [13]

First upscaling tests

First upscaling tests for the enzymatic treatment (1% P11) of the pulp sample NH-P and following dope preparation were carried out for staple fibre and filament preparation. Both the enzymatic treatment and the dope preparation were carried out firstly with discontinuous batch trials. The preparation of the spinning dopes was possible using dissolution conditions com-

parable to typical Lyocell pulps. Semi-technical spinning tests (6 x 80 capillaries, 90 µm outlet diameter) for investigation of the spinning behaviour and stability as well as the preparation of staple fibres and multifilament yarn were carried out using 12% (w/w) cellulose dopes. The rheological properties of the spinning dopes prepared with these batch trials were comparable to the dopes from the lab tests (Figures 4 and 5).

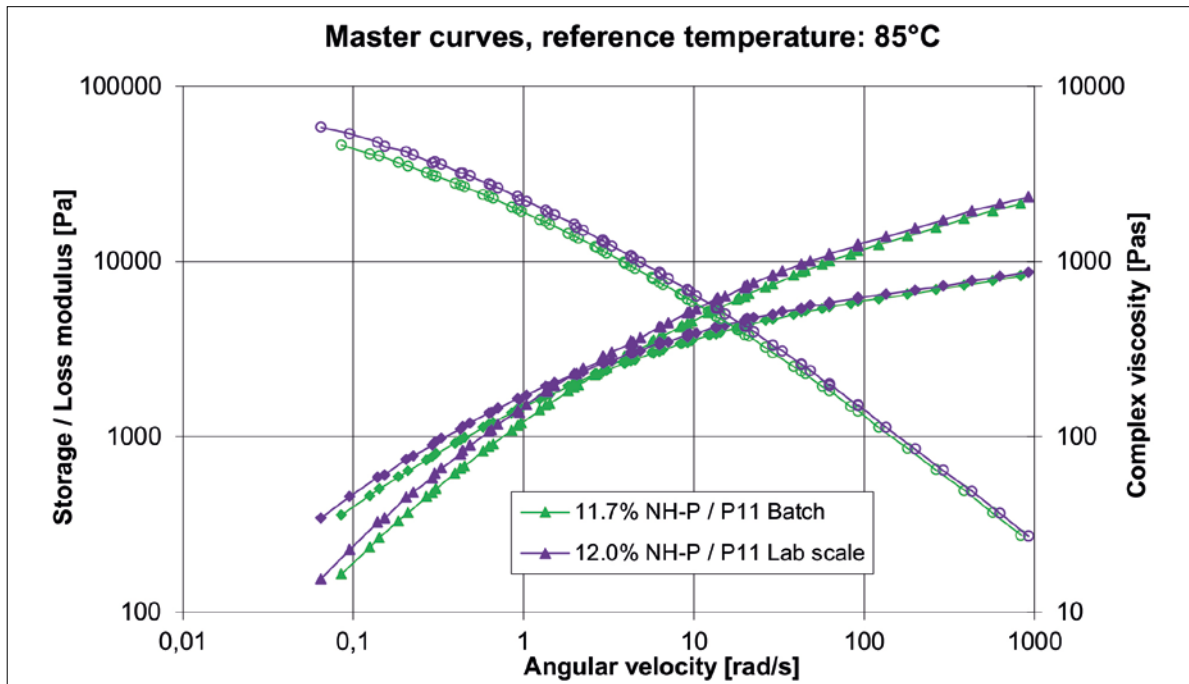


Figure 4: Master curves of spinning dopes comparison of dopes from lab scale and larger batch

Triangles: Storage moduli
 Squares: Loss moduli
 Open circles: Complex viscosities

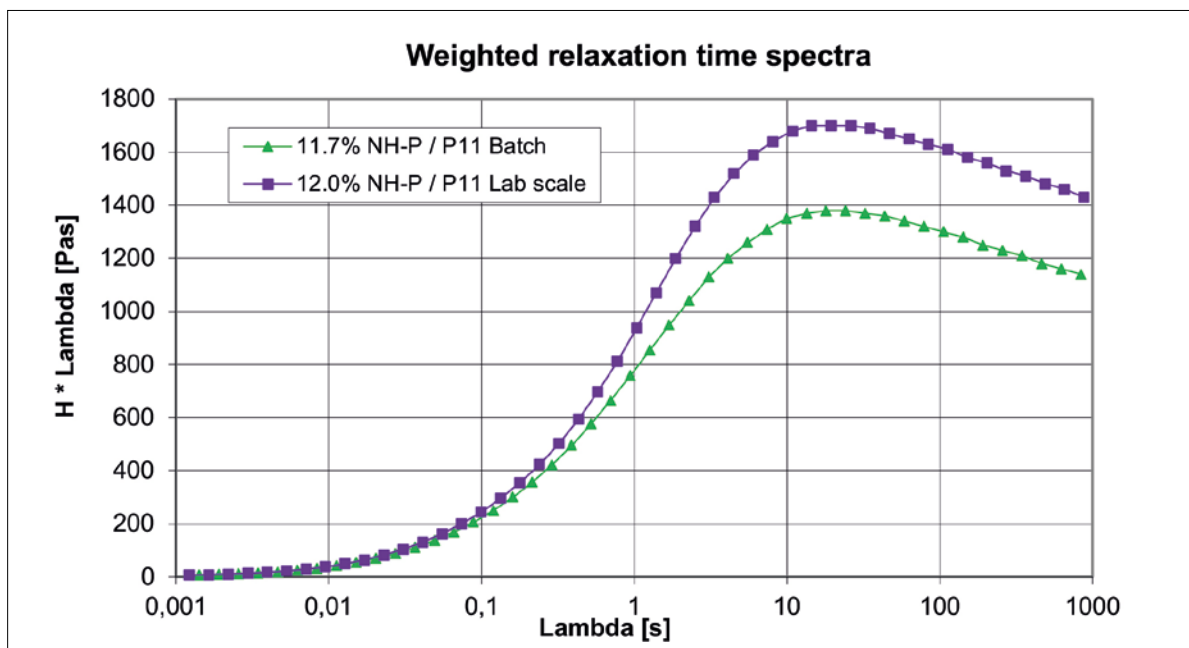



Figure 5: Weighted relaxation time spectra – comparison of dopes from lab scale and larger batch

Tests for staple fibre preparation as well as filament yarn preparation were carried out at spinning speeds of 33 m/min., spinning pressures between 53 and 57 bar, spinning temperatures of 85°C, at typical nozzle service lifetimes without significant improved pressure increase.

The prepared fibres and filaments revealed good textile physical properties. Table 5 illustrates the properties

of the prepared staple fibres as well as the determined single fibre and yarn values of the prepared multifilaments. The detected fibre properties confirm the high potential of the tested enzymatic modification step to adjust alternative cellulose resources for Lyocell applications.

Table 5: Fibre and filament properties from batch trials using pulp sample NH-P (P11 modified)

| | | Fibre properties staple fibres | Fibre properties filaments | Yarn properties filaments |
|---|--------|-----------------------------------|-------------------------------|------------------------------|
| Fineness | dtex | 1.46 | 1.46 | 641 |
| Tenacity, cond. | cN/tex | 38.6 | 41.3 | 40.2 |
| Elongation, cond. | % | 11.8 | 7.6 | 4.7 |
| Loop tenacity | cN/tex | 13.6 | 9.5 | 28.4 |
| E-modulus 0.5-0.7% | cN/tex | 963 | 1,317 | 1,930 |
| Cuoxam-DP fibre | | | 513 | |
|  | | | | |
| Fibre and filament material from batch tests | | | | |

Conclusions

An enzymatic modification using cellulases with adapted exo- and endo-activities is a suitable approach for adjustment of the required average degree of polymerisation and for improved solubility properties of alternative pulp resources for Lyocell fibre spinning. The tested modification step should be adaptable in the Lyocell process. The DP reduction of different tested pulp qualities was detected between 20 and 25%, with regard to the DP of the non-modified pulp sample. Beside the DP reduction, the tested enzyme samples with adjusted exo- and endo-activity surprisingly effected also a significant improvement of the pulp solubility. Therefore, spinning dopes with very good dissolution behaviour were received, even when paper grade pulps with lower contents of α -cellulose are used.

Successful tests for first upscaling for staple fibre and filament preparation could be carried out during application of softwood TCF paper grade pulp (Cuoxam-DP: 763, content of α -cellulose: 85.5%), and integration of the developed enzymatic modification step. The prepared fibre and filament samples showed good textile physical properties for typical Lyocell fibrous regenerates (tenacity in conditioned state: 39-41 cN/tex). The use of such an innovative modification step can significantly extend the raw material base for Lyocell

process technology. It could cause for cost savings when less expensive cellulose raw materials (paper pulps) are applied, but it may provide also broader options for use of pulps extract from recycled cellulose fabrics or from annual plant fibres next to cotton.

Acknowledgements

These works were financially supported by the German Federal Ministry of Economics and Energy (BMW No. MF140191). The authors thank for the granted support.

Furthermore the authors would like to thank Dr. Eng. M. Gerhardt and V. Pelenc (Biopract GmbH) for the assistance and providing of the enzyme samples.

References

- [1] F. M. Hämmerle, The Cellulose Gap (The future of cellulose fibres), *Lenzinger Berichte*, 89, 2011, 12-21
- [2] Gherzi, The future challenges for cotton availability: Chance for Man-made cellulose fibers?, *Allgemeiner Vliesstoff-Report 2 / 2011*
- [3] D. Eichinger, A Vision of the World of Cellulosic Fibers in 2020, *Lenzinger Berichte*, 90, 2012, 1-7

- [4] H. Harms, Potentiale einer neuen Fasergeneration, Lenzinger Berichte, 81, 2002, 27-34
- [5] W. Kalt, B. Zauner, Das Lenzing Lyocell Projekt – Start in ein neues Zeitalter der großtechnischen Zellulosefaserherstellung in Europa, Lenzinger Berichte, 80, 2001, 10-12
- [6] J. Paulitz, I. Sigmund, B. Kosan, F. Meister, Lyocell fibers for textile processing derived from organically grown hemp, Procedia Engineering, 200 (2017) 260-268
- [7] F. Meister, Ch. Michels, H. Kramer, Regenerated Cellulose Moulding and Process for Producing it, WO 1996014451, 1996
- [8] B. Kosan, C. Michels, F. Meister, Dissolution and forming of cellulose with ionic liquids, Cellulose, 15 (2008) 59-66
- [9] B. Kosan, K. Schwikal, F. Meister, Effects of pretreatment and dissolution conditions for improved solution and processing properties of cellulose in ionic liquids, Lenzinger Berichte, 90 (2012) 76-84
- [10] F. Meister, B. Kosan, A tool box for characterization of pulps and cellulose dopes in Lyocell technology, Nordic Pulp & Paper Research Journal 30 (1), 2015, 112-120
- [11] B. Kosan, Ch. Michels, Particle analysis by laser diffraction – application and restrictions in the Lyocell process, Chemical Fibers International, 49, 1999, 50-54
- [12] C. Michels, B. Kosan, Contribution to dissolution state of cellulose in aqueous amine oxide characterized by optical and rheological methods, Lenzinger Berichte, 82, 2003 128-135
- [13] Ch. Michels, B. Kosan, Beitrag zur Struktur von Lyocellfasern, ersponnen aus Aminoxidhydraten bzw. ionischen Flüssigkeiten, Lenzinger Berichte, 86, 2006, 144-153